NATIONAL
URANIUM
TAILINGS
PROGRAM

Energy, Mines and
Resources Canada

Énergie, Mines et
Ressources Canada

Canada

DEMONSTRATION OF THE PROBABILISTIC SYSTEM MODEL FOR ASSESSMENT OF THE LONG-TERM EFFECTS OF ARSENIC/NICKEL-RICH URANIUM MILL TAILINGS DEPOSITS IN CANADA

317pp .

Research Report Prepared for:

NATIONAL URANIUM TAILINGS PROGRAM
ENERGY, MINES AND RESOURCES
GOVERNMENT OF CANADA
OTTAWA, ONTARIO
Contract No. 0SQ85-00207
Req. 15SQ.23241-5-1707

Prepared by:

BEAK CONSULTANTS LIMITED
6870 Goreway Drive
Mississauga, Ontario
L4V 1P1

In Association with:

WHITESHELL NUCLEAR RESEARCH ESTABLISHMENT
ATOMIC ENERGY OF CANADA LIMITED
Pinawa, Manitoba
R0E 1L0

and

CONCORD SCIENTIFIC CORPORATION
2 Tippett Road
Downsview, Ontario
M3H 2V2

Principal Authors

W.J. Snodgrass, P.M. McKee and R.V. Nicholson

Principal Project Personnel

W. Bell
A.J. Chandler
N. Garisto
D. Hart
E. Hodgins
J. Holubeshen
T. Huang
D.L. Lush
J.R. Walker

317pp

August 1986
2250.2

MICROMEDIA

EXECUTIVE SUMMARY

This study, carried out as part of the National Uranium Tailings Program, was conducted to extend and demonstrate the probabilistic modelling approach developed previously (SENES 1985) and to investigate various issues of technical interest to performing and interpreting a probabilistic analysis.

The objective of this study is to demonstrate the application of the probabilistic system model developed by SENES for a generic, non-pyritic, arsenic and nickel-rich tailings, such as typically found in northern Saskatchewan. This has been accomplished by:

- revising the tailings source term model used by SENES in their Phase II assessment (SENES, 1985) to reflect the characteristics of tailings that would be typical of some milling operations in northern Saskatchewan;
- adding other U-238 decay chain radionuclides in addition to the stable elements, arsenic and nickel to the elements considered;
- refining other components of the model framework to better reflect environmental processes;
- establishing parameter values appropriate for an environment that could be considered typical of northern Saskatchewan; and
- running the model for a base case tailings characterized by unflooded conditions impounded by a porous dam, and a scenario characterized by flooded conditions, as expected to occur in a lake disposal situation.

The conditions assumed to apply in this assessment have been selected to be typical of a northern Saskatchewan site. However, site and tailings conditions used here are strictly hypothetical, and are not based on any particular location.

A source term was modelled as a four-layered system consisting of an upper unsaturated zone (two layers) and a lower saturated zone (two layers). For the under-water disposal management case, the four-layered system was treated as completely saturated. To model the geochemical evolution of U, Th-230, Ra-226, Pb-210, Po-210, As and Ni in the tailings, 12 other parameters were considered in the source term.

These parameters were calcium, sulphate, inorganic carbon, manganese, alkalinity, pH, iron, aluminum, lead, barium, dissolved organic carbon and dissolved oxygen. In association with these parameters more than 13 solid phases were considered.

The transport of these five radionuclides and two stable elements was considered through all environmental pathways. Aqueous pathways included transport via surface water, and groundwater. Atmospheric pathways considered exhalation of radon and wind erosion of dust. The deposition of dust upon soil was used to calculate soil concentrations over time. Transport through surface water and groundwater pathways occurred to the first lake of a chain-lake system. The second water body on the chain, an embayment connected to a large lake, was the location of the critical group. Dilution by flow, radiological decay and sediment - water transport controlled the surface water concentrations. Adsorption, radioactive decay, advection and dispersion were the major factors affecting groundwater transport.

The radionuclides contributed to critical group dose through various pathways including inhalation of radon and dust and consumption of vegetables influenced by atmospheric deposition and root uptake of elements from the soil. Consumption of moose which subsist upon contaminated vegetation and water, and consumption of water and fish from the embayment form the other major pathways to man.

Calculations of dose rate to the critical group are presented in the form of total dose, dose by pathway, and dose by radionuclide. The results for the base case suggest that atmospheric pathways, in particular radon transport, may be more important for this type of generic site than previous studies on Elliot Lake area tailings (SENES, 1985) have suggested. The sensitivity analyses for the physical transport model suggest that factors affecting source term concentrations and removal rate from the tailings (e.g., radon emanation coefficient) are in a relative sense the most important parameters. Future work can be directed towards refining the calibration of those source term factors which affect the relative partitioning of transport through atmospheric and surface water pathways.

The model development is reviewed and documented in this report. Code verification techniques are also summarized.

TABLE OF CONTENTS

Page

EXECUTIVE SUMMARY i

1.0 INTRODUCTION 1.1
  1.1 Background 1.1
  1.2 Objectives 1.1

2.0 REFERENCE SITE CHARACTERISTICS 2.1
  2.1 Regional Setting 2.1
  2.2 Local Setting 2.1
  2.3 Tailings Management Options 2.2
  2.4 Description of the Reference Site 2.2

3.0 MODELLING APPROACH 3.1
  3.1 Introduction 3.1
  3.2 Modelling Approach for This Demonstration 3.3
  3.3 Example of the Monte Carlo Simulation Approach 3.3

4.0 SOURCE TERM MODEL 4.1
  4.1 Physical Representation of Tailings 4.1
  4.2 Chemical Substances Considered in Tailings 4.2
  4.3 Calcium, Sulphate, Carbonate and pH 4.3
    4.3.1 Open System 4.4
    4.3.2 Closed System 4.9
    4.3.3 Solution Complexes 4.10
    4.3.4 Ionic Strength Calculations 4.10
  4.4 Mass Balance Calculations 4.11
  4.5 Minor Elements (Fe, Al, Pb, Ba, Mn) 4.12
    4.5.1 Iron Chemistry 4.13
    4.5.2 Aluminum Chemistry 4.14
    4.5.3 Lead Chemistry 4.15

4.5.4 Barium Chemistry 4.16
4.5.5 Manganese Chemistry 4.16
4.6 Toxic Elements (Ni, As) 4.18
4.6.1 Nickel Model 4.18
4.6.2 Arsenic Model 4.20
4.7 Coprecipitation Control Upon Elements 4.22
4.7.1 Elements Controlled by Coprecipitation 4.22
4.7.2 Relevant Aspects of Coprecipitation Theory 4.22
4.8 Uranium Model 4.25
4.8.1 Summary of Uranium Chemistry During Milling 4.26
4.8.2 Chemical Model Used for Uranium 4.27
4.8.3 Analysis of Mathematical Solution for Uranium Model 4.28
4.9 Thorium-230 Model 4.29
4.9.1 Chemistry of Th-230 During Milling 4.29
4.9.2 Chemical Model Used for Th-230 4.30
4.10 Radium 4.34
4.10.1 Chemistry of Radium 4.34
4.10.2 Derivation of Radium Model 4.35
4.11 Lead-210 4.41
4.11.1 Chemistry of Pb-210 4.41
4.11.2 Model for Pb-210 4.42
4.12 Polonium 4.44
4.12.1 Chemistry of Polonium 4.44
4.12.2 Model for Po-210 4.44
4.13 Redox Model 4.44
4.14 Parameter Values and Model Simulation 4.46

5.0 ENVIRONMENTAL PATHWAYS 5.1
5.1 Atmospheric Pathways 5.1
5.1.1 The Dust Source Model 5.1
5.1.2 The Radon Source Model 5.5
5.1.3 The Air Dispersion Component Model 5.7

Page

- 5.2 Soil Deposition 5.8
- 5.3 Groundwater Dispersion 5.9
- 5.4 Surface Water Component Model 5.11
- 5.5 Uptake by Vegetation 5.15
  - 5.5.1 Concentrations in Edible Vegetation from Foliar Deposition (Subroutine VEGDEP) 5.15
  - 5.5.2 Concentrations in Edible Vegetation from Root Uptake (Subroutine (VEGDEP) 5.16
- 5.6 Uptake by Aquatic Biota 5.19
  - 5.6.1 Concentrations of Element i in Edible Portions of Fish (Subroutine AQBIOTA) 5.19
    - 5.6.1.1 Concentrations in Fish 5.19
    - 5.6.1.2 Toxicity Considerations 5.20
  - 5.6.2 Concentrations in Aquatic Plants 5.21
- 5.7 The Forage-Moose Pathway (Subroutine VEGEAT) 5.22
- 5.8 Uptake by Man (Subroutine DOSEIN) 5.27
  - 5.8.1 Introduction 5.27
  - 5.8.2 Ingestion 5.28
    - 5.8.2.1 Vegetation 5.28
    - 5.8.2.2 Moose 5.29
    - 5.8.2.3 Drinking Water 5.30
    - 5.8.2.4 Fish 5.31
  - 5.8.3 Inhalation 5.32
    - 5.8.3.1 Suspended Particulates 5.32
    - 5.8.3.2 Radon and Its Daughters 5.32

6.0 SYSTEM CODE 6.1
- 6.1 Structure 6.1
  - 6.1.1 Review of SENES Code Structure 6.1
  - 6.1.2 Code Structure of this Project 6.2
- 6.2 Software Quality Assurance 6.4
  - 6.2.1 Software Development Process and Standards 6.4

Page

6.2.2 Verification and Testing 6.6
6.2.3 Quality Assurance Summary 6.8

7.0 PROBABILISTIC ASSESSMENT RESULTS 7.1
7.1 Base Case Simulation 7.1
7.2 Management Option Simulation 7.5
7.3 Sensitivity and Uncertainty Analysis 7.6

8.0 TEMPORAL CHARACTERISTICS OF SOURCE MODEL AND AQUATIC PATHWAYS 8.1
8.1 Source Term Characteristics 8.1
8.2 Reviewing Lake Characteristics 8.3

9.0 SUMMARY AND RECOMMENDATIONS 9.1

10.0 REFERENCES 10.1

APPENDIX A: Source Term: Reaction Path Code Calculations
APPENDIX B: Food Chain and Environmental Transport Parameters
APPENDIX C: Sensitivity Analysis of Radon and Dust Pathway Models
APPENDIX D: Output Frequency Distributions, Scenario 1 (Unflooded Tailings)
APPENDIX E: Output Frequency Distributions, Scenario 2 (Flooded Tailings)

1.0 INTRODUCTION

1.1 Background

Energy, Mines and Resources Canada established the National Uranium Tailings Program (NUTP) in 1982 to consolidate previous work on Canadian uranium mill tailings, to fund additional research and to develop approaches to predict the long-term impacts of uranium mill tailings. SENES Consultants Limited (SENES) are developing a probabilistic system model for assessing the long-term environmental effects of uranium mill tailings. By the beginning of this study, they had completed two out of three development phases:

- Phase I: assess long-term impacts under conditions of natural variability and uncertainty in model parameters (SENES, 1984), and
- Phase II: refine the model framework and carry out a preliminary application of the model for radium and radon releases from a generic pyritic tailings site (SENES, 1985).

Over the past decade, there has been a significant amount of uranium discovered in northern Saskatchewan within the Athabasca sandstone basin. Prior to this, most of the uranium development had occurred to the north of the sandstone basin on the Shield where surface showings of uranium and other associated minerals led to the development of several orebodies. Most of the recent large discoveries lie in the southeastern portion of the basin, stretching in a broad band from Wollaston Lake southwest down to the Key Lake area. Within this band, the uranium orebodies, for the most part, lie at the contact between the sandstone and the underlying basement rocks, at depths ranging from very near surface to over 500 m. Over the next decade, the development of several orebodies in this area appears likely. Many of these deposits contain significant quantities of nickel and arsenic, are of a relatively high grade, and tend to be non-pyritic.

1.2 Objectives

The objective of this study is to demonstrate the application of the probabilistic system model developed by SENES for a generic, non-pyritic, arsenic and nickel-rich tailings, such as typically found in northern Saskatchewan. This has been accomplished by:

- developing a new tailings source term model to reflect the characteristics of tailings that would be typical of northern Saskatchewan;
- adding other U-238 decay chain radionuclides, and two stable but potentially toxic elements, arsenic and nickel, to the substances considered in the model;
- revising other environmental pathways, food chain and dose components of the model to better reflect environmental processes;
- revising the data management structure of the systems code;
- establishing parameter values appropriate for an environment that could be considered typical of northern Saskatchewan; and
- running the model for a base case tailings characterized by unflooded conditions impounded by a porous dam, and a scenario characterized by flooded conditions, as expected to occur in a lake disposal situation.

The conditions assumed to apply in this assessment have been selected to be typical of a northern Saskatchewan site. However, site and tailings conditions used here are strictly hypothetical, and are not based on any particular location.

2.0 REFERENCE SITE CHARACTERISTICS

2.1 Regional Setting

The broad band of land along the southeastern edge of the Athabasca sandstone which forms the region considered in this project is covered to varying thicknesses with overburden composed of sandy, bouldery, glacial tills and outwash deposits. The overburden is derived predominantly from the sandstone, but it contains some Shield boulder and sand material. The land is relatively flat and rolling, with some areas of moraine, eskers and other glacial deposits showing a high degree of local relief.

In the immediate post-glacial period, the lake basins in the area received a quantity of silts and clays in glacial runoff, and these silty varved clays are found blanketing the bottoms of most of the lakes. In the post-glacial period, the input of terrestrial organic material from the watershed and the production of organic material internally in each lake have resulted in a layer of organic material blanketing the glacial clays on the bottom of the lakes. The vegetation on the surrounding wateshed is dominated by jack pine in drier areas and by black spruce in the wetter areas. Stands of deciduous trees, such as poplar and birch, are found throughout the area with alder being common along the edges of streams.

2.2 Local Setting

A review of the actual locations of operating uranium mines in northern Saskatchewan has shown that there are often several alternative layouts possible. Site planning by design results, where at all possible, in the placement of the tailings area near the headwaters of a local sub-watershed. The resultant tailings surface area to upstream catchment basin area ratio is usually on the order of 1:10. It has not been deemed prudent in the past to discharge treated tailings effluents directly to a large river or lake which may be used for recreational, commercial or subsistence fishing. Rather, discharge of treated effluent and post-operational seepage is usually designed to enter small, marshy streams or lakes where natural processes remove radionuclides and toxic stable elements, generally by sedimentation. The hydraulic residence time of process discharges in many of the small lake or stream systems is as long as a few months. The hydraulic residence time of seepage into these systems would be much longer because of the considerably reduced flows.

2.3 Tailings Management Options

At present within the model region, there are a wide variety of tailings management practices employed that take advantage of both local site-specific conditions and the particular characteristics of the tailings. The most common management practice is the placement of tailings in a low area bounded by natural topography for a portion of the perimeter and by a retaining dam for another part of the structure. This, however, can vary considerably, depending upon the site conditions present and the nature of the tailings and tailings management practices employed. For example, at the Key Lake site, the tailings management area is completely surrounded by a retaining dyke while at the Rabbit Lake site, the original tailings are bounded on two ends with an engineered dyke and the tailings that are presently produced are placed in the original mined-out pit. The model site baseline condition chosen for this demonstration is a tailings partially contained by natural topography and partially by an engineered dam structure. An alternate management scenario considered as part of a sensitivity analysis is disposal in a deep lake basin.

The northern Saskatchewan sandstone deposits are, in general, of a relatively high grade, typically being milled at concentrations of a few percent uranium. The nature of the associated minerals and the relatively high grade of uranium necessitates the use of a significant quantity of process chemicals per unit of ore processed and tailings produced. The result is a tailings mass with a high percentage of very fine-grained process precipitates. This fine-grained material results in a lower overall permeability than the lower grade tailings typical of Ontario. The higher percentage of relatively soluble process precipitates will also result in differences in long-term geochemical behaviour.

2.4 Description of the Reference Site

Existing tailings sites in northern Saskatchewan are generally located in areas drained by small watesheds. At the Cluff Lake, Key Lake and Rabbit Lake sites, the tailings areas cover 50 to 90 ha and drain into small lakes of about 10 to 150 ha in surface area. These small lakes, in turn, empty into larger waterbodies, either directly through a small stream, or indirectly through a series of streams, small lakes and rivers. The tailings typically cover 5 to 15% of the total watershed area of the first small lake.

The tailings disposal site is taken to occupy a surface area of 50 ha and to have an average depth of 16 m, resulting in a total volume of 8×10^6 m^3. The tailings area is taken to be located in the watershed of a small lake (100 ha) having a total watershed area of 600 ha. This small lake drains into an embayment of a large lake via a stream. The entire watershed area upstream of the point of discharge into the embayment is 750 ha. The embayment has a surface area of 3,300 ha and a mean depth of 15 m. Figure 2.1 provides a schematic representation of the watershed setting of the site.

For the base case, the critical group is assumed to inhabit a site located 4 km from the tailings on the shore of the large embayment. This critical group is assumed to subsist largely on fish caught in the embayment, on fruits and vegetables grown in a garden at the receptor location shown in Figure 2.1, on moose hunted in the local area, and on drinking water derived from the embayment. Figure 2.2 illustrates the pathways considered for releases of radionuclides, arsenic and nickel from the tailings to the receptor.

For the flooded tailings management option, all critical group and environmental parameters are assumed to be unchanged from the base case condition. Only parameters controlling releases from the source term are assumed to be altered by flooding of the tailings.

Under certain circumstances, the critical group may use a well water supply rather than lake water for their drinking water supply. In this study, we have also incorporated the capability of assessing a well water pathway if groundwater transport results in a contaminant plume reaching the critical group during the modelling time frame.

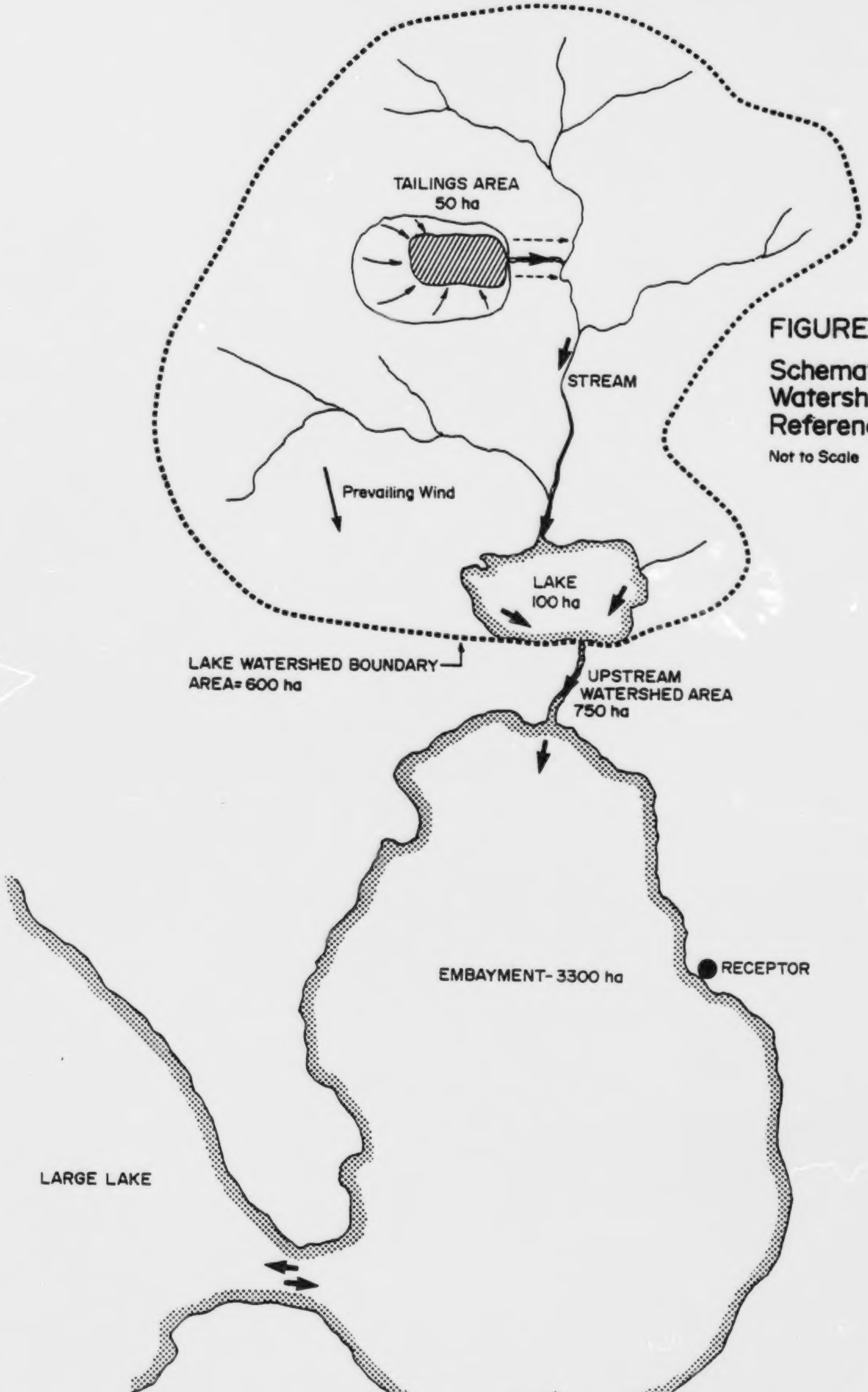
TAILINGS AREA
50 ha
STREAM
Prevailing Wind
LAKE
100 ha
LAKE WATERSHED BOUNDARY
AREA= 600 ha
UPSTREAM
WATERSHED AREA
750 ha
EMBAYMENT- 3300 ha
RECEPTOR
LARGE LAKE

FIGURE 2.1

Schematic Illustration of Watershed Setting for the Reference Tailings Site

Not to Scale

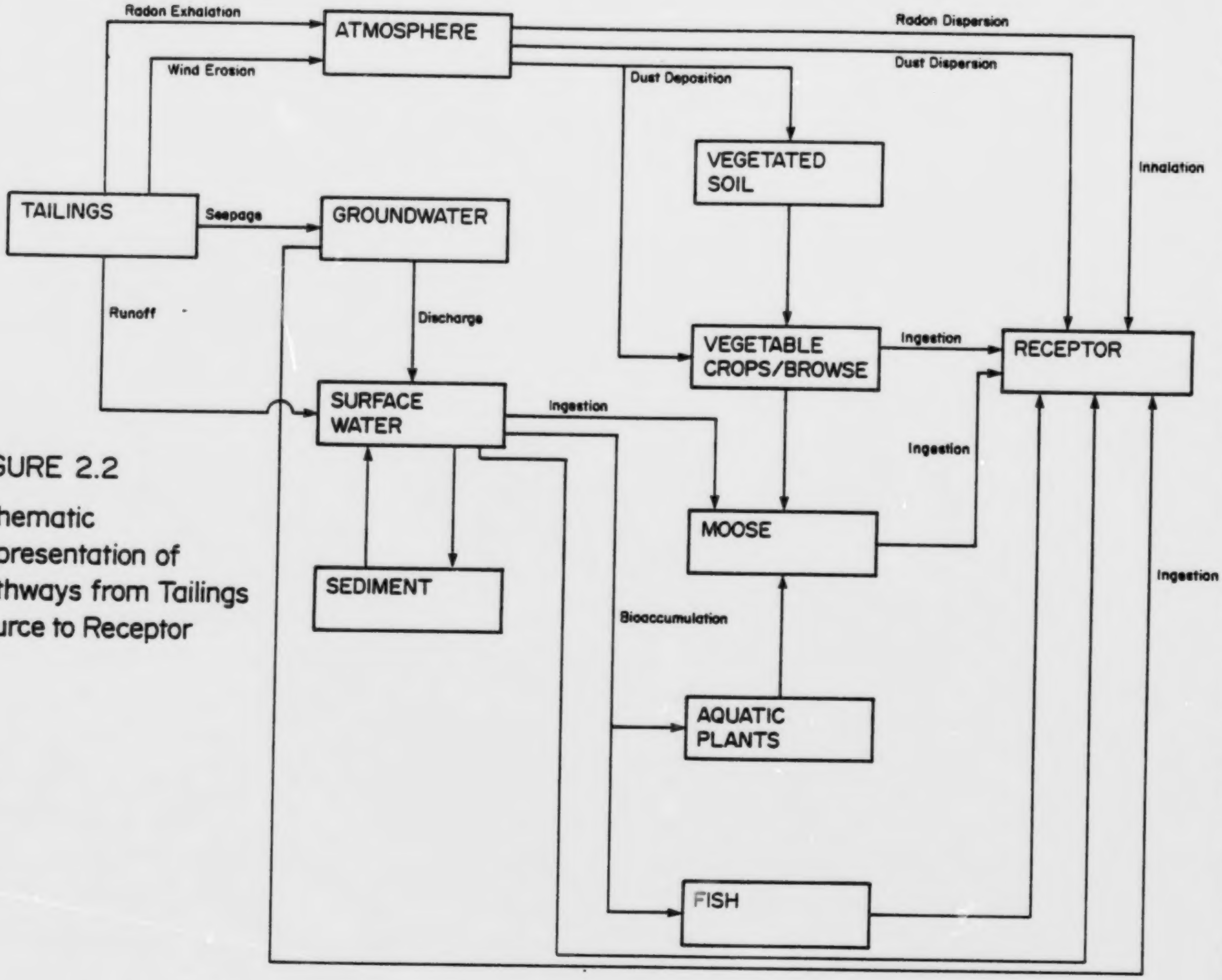
Radon Exhalation
ATMOSPHERE
Wind Erosion
Radon Dispersion
Dust Dispersion
Dust Deposition
VEGETATED SOIL
Inhalation
TAILINGS
Seepage
GROUNDWATER
Runoff
Discharge
VEGETABLE CROPS/BROWSE
Ingestion
RECEPTOR
SURFACE WATER
Ingestion
Ingestion
MOOSE
SEDIMENT
Ingestion
Bioaccumulation
AQUATIC PLANTS
FISH

FIGURE 2.2

Schematic Representation of Pathways from Tailings Source to Receptor

3.0 MODELLING APPROACH

3.1 Introduction

The overall objective of this study is to demonstrate the application of the Uranium Tailings Analysis Program (UTAP) for a non-pyritic, nickel- and arsenic-rich tailings. Considerable refinement and adaptation of specific subroutines in the model, as well as preparation of parameter data input, were required. Although the overall modelling framework and approach of UTAP are detailed in earlier reports by SENES (1984, 1985), a brief review of UTAP and underlying concepts is presented here.

Traditionally, environmental models have been evaluated in a deterministic fashion. That is, a single value is selected for each input parameter in the model. This results in a single estimate of some environmental consequence, such as radiation dose received by an individual in a critical group.

But many parameters in environmental systems models are either imprecisely known or are inherently variable. Probabilistic analysis allows the modeller to incorporate the uncertainty and variability associated with individual model parameters directly into model predictions. In the probabilistic approach, probability distributions rather than single values are specified for input parameters for environmental simulation models. The models are re-evaluated repeatedly, with new values randomly selected from the specified probability distributions of the input parameters. Thus, the results of the model are represented as a frequency distribution. The UTAP model utilizes such a probabilistic approach.

Figure 3.1 illustrates the overall systems structure of the Phase II UTAP probabilistic system model. It consists of "control modules" and "simulation (component) modules". The latter are specific mathematic models used to describe the systems of interest, such as geochemical processes in the tailings source term, generation of dust containing radionuclides from the tailings surface, bioaccumulation of radionuclides by fish, and intake by receptor group individuals. The primary control module, RANSIM, is a computer program designed to perform the iterative probabilistic sampling required for the analysis. The second control module, the Parameter Allocation and Control module (PAC) fulfills an intermediate role between the component modules and RANSIM. The entire systems model is programmed in the FORTRAN-77 language.

FIGURE 3-1

CONCEPTUAL FLOW DIAGRAM
OF SYSTEMS APPROACH

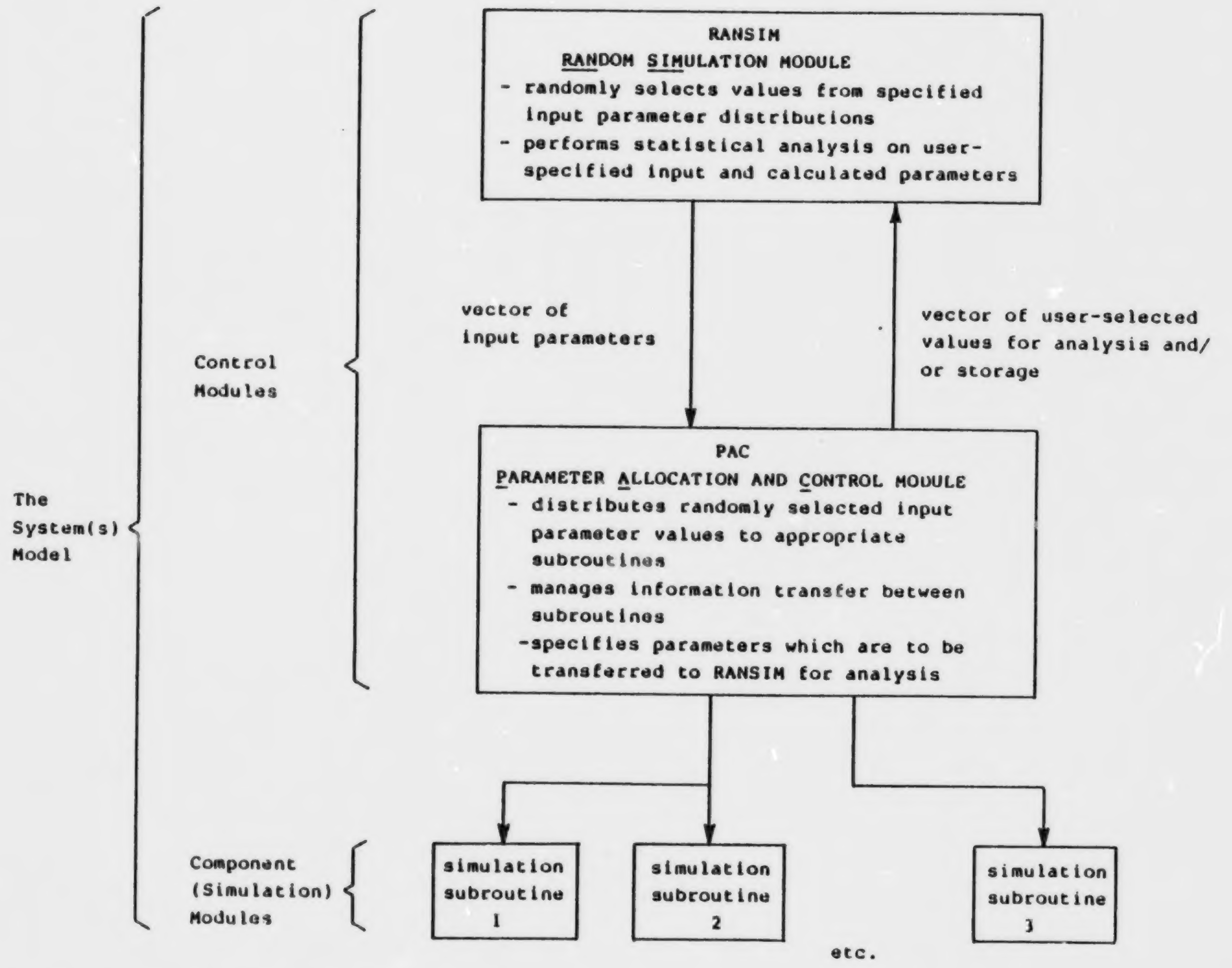
The System(s) Model
Control Modules
Component (Simulation) Modules
RANSIM
RANDOM SIMULATION MODULE
- randomly selects values from specified input parameter distributions
- performs statistical analysis on user-specified input and calculated parameters
vector of input parameters
vector of user-selected values for analysis and/or storage
PAC
PARAMETER ALLOCATION AND CONTROL MODULE
- distributes randomly selected input parameter values to appropriate subroutines
- manages information transfer between subroutines
-specifies parameters which are to be transferred to RANSIM for analysis
simulation subroutine 1
simulation subroutine 2
simulation subroutine 3
etc.

RANSIM is able to sample from a series of nine different statistical distributions for input parameters:

- constant value,
- normal,
- log normal,
- uniform,
- log-uniform,
- triangular,
- beta,
- arbitrary, and
- correlated.

RANSIM also has the capacity to compute a variety of summary statistics on user-specified input parameters or on calculated parameters:

- arithmetic mean,
- arithmetic standard deviation,
- geometric mean,
- geometric standard deviation,
- skewness,
- kurtosis,
- maximum value, and
- minimum value.

PAC accepts input parameter values from RANSIM and passes them on to the appropriate component modules. PAC accesses the component modules in an appropriate sequence and makes intermediate results available where necessary. It also ensures that the appropriate calculated results are transfered back to RANSIM for analysis and (possibly) disk storage.

The component modules are simply the computer coded mathematical models describing specific geochemical or other environmental processes.

3.2 Modelling Approach for This Demonstration

The objective of this study is to demonstrate an application of the UTAP system for releases of U-238 decay chain radionuclides and the stable elements arsenic and nickel from a generic, non-pyritic uranium tailings such as may be found at various locations in northern Saskatchewan. To accomplish this, various component models were either revised or adapted to suit the requirements of this demonstration. The overall system model structure of UTAP, including RANSIM, was retained intact, thus demonstrating the adaptability of the systems model to other types of tailings.

The source term component module of UTAP was re-written in its entirety for this demonstration, since the geochemical processes and input-output parameters of the source term differ drastically from those used for modelling release of radium from pyritic tailings in the SENES Phase II program. All component models were revised to a lesser extent in order to handle new radionuclides and stable elements. New component models were developed to describe new pathways. Additional pathways incorporated into this demonstration include a groundwater pathway (a groundwater component model was in the development stage by SENES at the beginning of this project) and a soil pathway. Parameter values and distributions were selected to be appropriate for an environment in northern Saskatchewan, rather than for an environment near Elliot Lake, Ontario, as in the earlier SENES work. Component models used for this demonstration are detailed in Sections 4 and 5 of this report.

3.3 Example of the Monte Carlo Simulation Approach

A reader not familiar with the Monte Carlo Simulation approach may have difficulty understanding the calculations presented in this report. In this section, an attempt is made to describe the method by which the results are obtained. The overall concept is outlined in Figure 3.2 adapted from SENES (1984).

Consider that there are three variables that influence the dose to man from the discharge of Ra-226 to a lake where a person obtains their drinking water; the discharge rate of Ra-226 (x), the dilution rate in the lake (y), and the dose - conversion factor (z) from the lakewater to man. Specification of an appropriate set of models would allow one to calculate the dose to man for the given discharge rate.

FIGURE 3.2: CONCEPT OF A PROBABILISTIC ANALYSIS

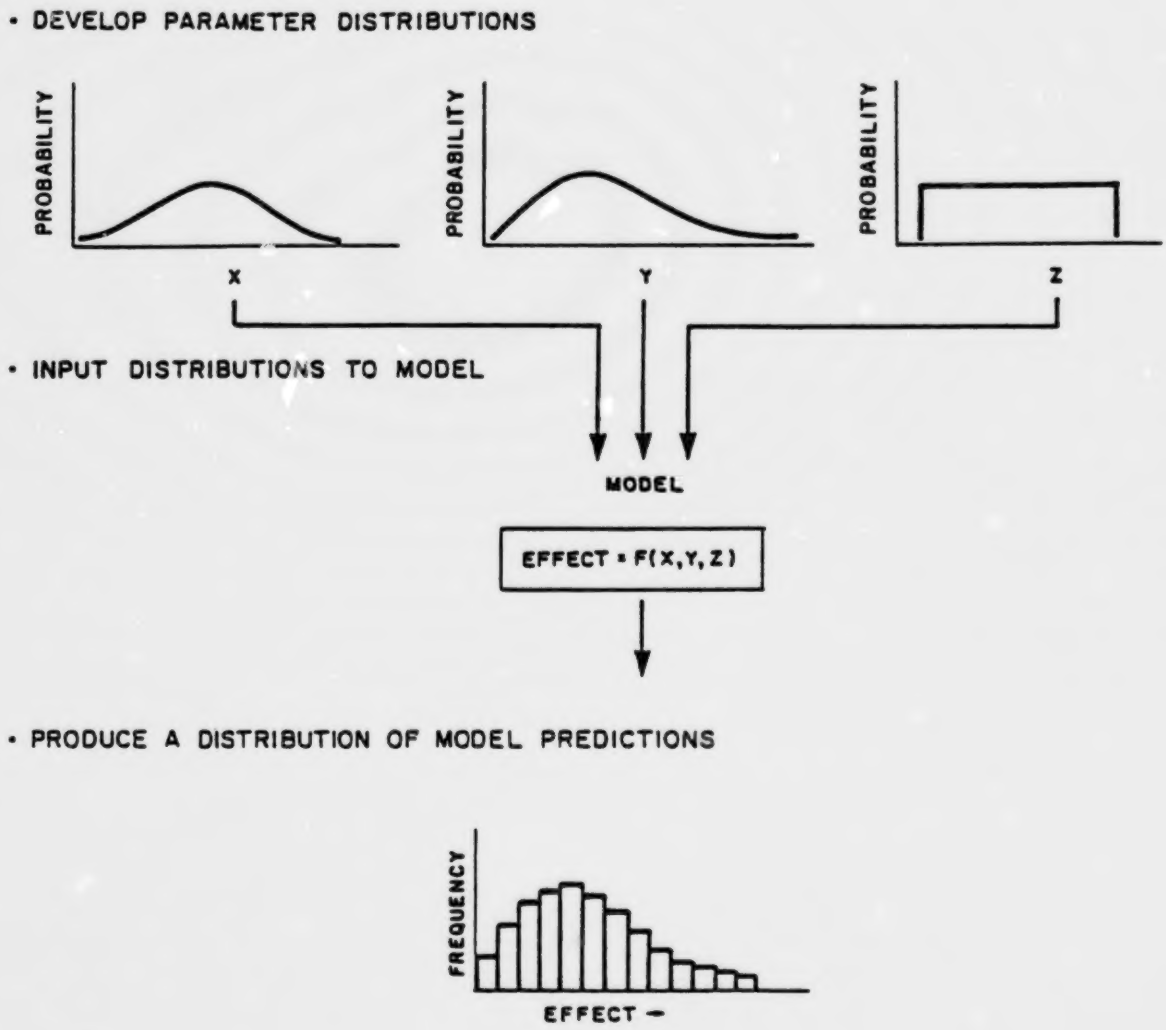
• DEVELOP PARAMETER DISTRIBUTIONS
PROBABILITY
X
PROBABILITY
Y
PROBABILITY
Z
• INPUT DISTRIBUTIONS TO MODEL
MODEL
EFFECT = F(X,Y,Z)
• PRODUCE A DISTRIBUTION OF MODEL PREDICTIONS
FREQUENCY
EFFECT →

But, the numerical values for x, y and z are not known precisely. Rather they each have a mean and a variance associated with them. This is represented in Figure 3.2 by the probability density function for each parameter. To evaluate the effect of the variance of each parameter upon the calculated dose, the Monte Carlo simulation method involves a repeated series of calculations. In the first simulation, a parameter value for each of x, y and z is randomly sampled from within the probable distribution of the parameter and then the dose is calculated. In a second simulation, a new set of parameter values are obtained and the second dose calculation made. This simulation process (sampling for parameters values, calculation of dose) is repeated many times until a stable frequency distribution of calculated values of dose are obtained. For some applications (e.g., reservoir ecosystem simulation), it has been found that 25-40 simulations are sufficient to obtain stable estimates of the mean of the calculated response. But for stable estimates of the entire calculated dose frequency distribution it has been found (SENES, 1984, 1985) that of the order of 400-500 repeated simulations are required.

In addition, various parameters will vary over time. For example, the discharge rate from the tailings will vary over time. Hence, one has a three dimensional set of results to be presented: (i) the frequency, (ii) of a particular dose (iii) over time. The problem presenting this information is illustrated as a 3-D plot on Figure 3.3, showing frequency (f), dose and time, along the three axes of a rectangular coordinate system. For the example presented in Figure 3.2 and assuming that it is for time = zero, the histogram of dose is shown on the dose axis of time zero (Figure 3.3b). Simulation of the time change of various parameters allows one to calculate the dose histograph at various points in the future. These are shown on Figure 3.3c for four future time points. The frequency histogram is parallel to the dose axis. Each histogram is spread from a minimum dose value to a maximum dose value, with the maximum calculated frequency of the dose occurring near the middle of the histogram. If one forms the dose values over time which are the mean dose rate, one obtains the curve given on Figure 3.3d. Hence, there is a mean dose rate calculated over time, but also a frequency histogram associated with each time point.

In this report, the Monte Carlo simulation results are presented both in the dose-frequency histogram format and mean dose versus time format.

FIGURE 3.3

Three Dimensional Plot Illustrating the Progression of a Hypothetical Set of Dose-Frequency Calculations over Time using Probabilistic Analysis

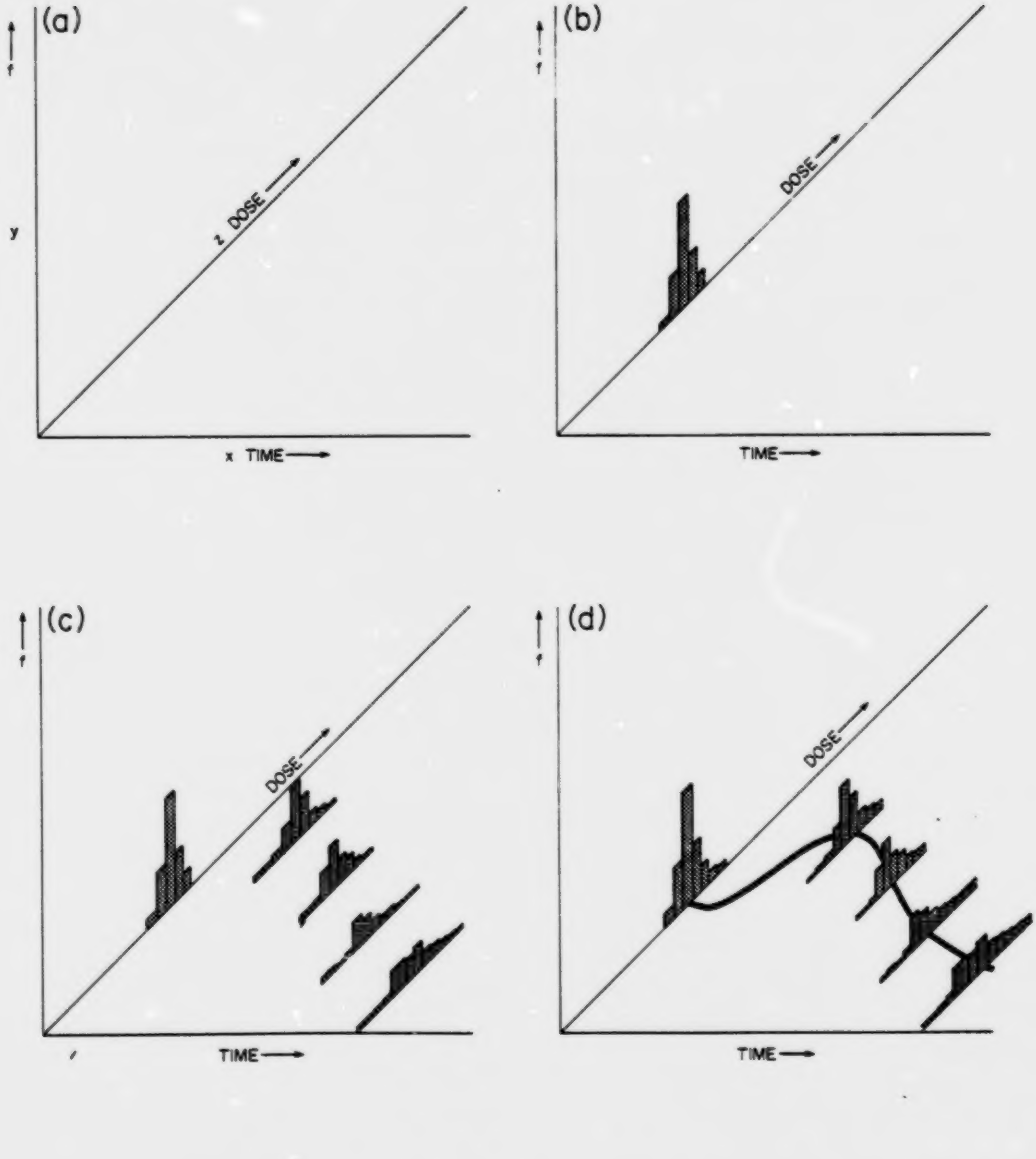
(a)
y
z DOSE
x TIME
(b)
DOSE
TIME
(c)
DOSE
TIME
(d)
DOSE
TIME

4.0 SOURCE TERM MODEL FOR WATERBORNE CONTAMINANTS

This chapter presents the tailings' physical and chemical representation chosen for this project. The assumptions and underlying equations are defined. The relationship of the equations to the code are also presented. The major subroutines used for the source term code are summarized in Table 4.1a. A synopsis of symbols is given in Tables 4.1b and 4.7.

These equations permit calculation of the geochemical evolution of the tailings over time, the flux of contaminants to waterborne pathways and the change in solid phase concentration which interacts with atmospheric pathways. The airborne flux of dust and Rn-222 is described in Chapter 5.

4.1 Physical Representation of Tailings

A 4-box representation has been chosen to describe the tailings: two boxes for the unsaturated zone and two boxes for the saturated zone. The top box (I = 1) is 0.1 m deep and is taken to be the zone from which fines are blown. It is also assumed to be the zone in which particle breakup from coarse to fine material occurs due to freezing and weathering. Similar weathering reactions occur in the rest of the unsaturated zone but are not modelled because it is assumed that loss of solid material by erosion does not occur from the second box.

The third box, the top of the saturated zone, has the largest, horizontal, flow through it. It is assumed that porewater from this zone is transported to surface water seepage streams and to local groundwater pathways. Small amounts of groundwater move from the deep tailings (fourth) box to deep groundwater, but this pathway does not substantially contribute to surface water pathways during the time frame of this evaluation, because of the low contaminant velocity relative to the path length.

The hydrological pathways assumed for the tailings boxes are indicated in Figure 4.1, along with the computer code numbering system. QI(I) is the inflow rate to box I from upstream sources, QD(I) is the downflow rate, QU(I) is the upflow between boxes, and QO(I) is the horizontal outflow rate from box I. The relative values of QI(I), QD(I), QO(I), and QU(I) are user-specified in the input data deck. Their actual value is either specified in the input data deck or calculated as the relative value times the net infiltration rate

TABLE 4.1a: DEFINITION OF MAJOR SUBROUTINES FOR SOURCE TERM

Subroutine Name	Major Operation
1. SOURCE	Controls call statements to other subroutines
2. OPEN	Calculates concentrations of Ca^{2+}, SO_4^{2-}, pH, alkalinity, C_T for unsaturated zone (i.e., zone open to atmosphere)
3. CLOSED	Calculates concentrations of Ca^{2+}, SO_4^{2-}, pH, alkalinity, C_T for saturated zone (i.e., zone closed to atmosphere)
4. OXYGEN	Calculates redox conditions based upon oxygen and sulphate as electron receptors
5. MINOR	Calculates Ni and As concentration in pore water
a) NISOLD	Calculates nickel speciation if $Ni(OH)_2$ exists
b) NISPEC	Calculates nickel speciation and mass balance if $Ni(OH)_2$ has been depleted
c) ARSPEC	Calculates arsenic speciation and mass balance. It assumes that there is no solid precipitate of As
6. FEALPB	Calculates Fe^{3+}, Al^{3+}, Pb^{2+} and Ba^{2+} concentrations in pore water
7. RADIOS	Calculates radionuclide concentrations in solid and solution phase over time

TABLE 4.1b: GLOSSARY OF TERMS FOR SECTION 4

1. **Nomenclature used for the source term components used in equations and figures in text**

Category	Symbol	Units, Examples or Explanation	
Water fluxes	Q	$m^3 \cdot a^{-1}$	• QU(I) = upflow
			• QD(I) = downflow
			• QI(I) = inflow
			• QO(I) = outflow
Concentrations (see Figure 4.1)	C	$mol \cdot m^{-3}$	• CT(I,K) = total aqueous concentration of component K in box I
			• C(I,K) = concentration of uncomplexed component K in box I
			• CIN(K) = inflow concentration (lateral)
			• CTOP(K)= inflow concentration (vertical, downward from top)
			• CBOT(K)= inflow concentration (vertical, upward from bottom)
Equilibrium Constants	K or X	variable	K_{CaSO_4} XCASO4 = solubility constant for $CaSO_4$ (gypsum) solid
	C		C_{CaSO_4} = association constant for the $CaSO_4^0$ ion pair

TABLE 4.1b: GLOSSARY OF TERMS FOR SECTION 4

2. Symbols

Symbol	Description
Activity	
A_{Ca}	Activity of calcium ion (Equation 4.1)
A_{SO_4}	Activity of sulphate ion (Equation 4.1)
A_{CO_3}	Activity of carbonate ion (Equation 4.1)
A_{HCO_3}	Activity of bicarbonate (Equation 4.1)
A_H	Activity of hydrogen (Equation 4.1)
$A_{H_2CO_3*}$	Activity of hydrated carbonic acid (Equation 4.1)
Activity Components	
f_{Ca}	Activity coefficient of calcium
f_{HCO_3-}	Activity coefficient of bicarbonate
f_{SO_4}	Activity coefficient of sulphate
f_{Al}	Activity coefficient of Al^{3+}
f_{CO_3}	Activity coefficient of CO_3^{2-}
f_{AlOH}	Activity coefficient of $AlOH^{2+}$
f_{AlOH2}	Activity coefficient of $Al(OH)_2^+$
f_{AlOH4}	Activity coefficient of $Al(OH)_4^-$
$f_{Fe^{2+}}$	Activity coefficient of Fe^{3+}
f_{FeOH}	Activity coefficient of $FeOH^{2+}$
f_{FeOH2}	Activity coefficient of $Fe(OH)_2^+$
f_{FeOH4}	Activity coefficient of $Fe(OH)_4^-$
$f_{Pb^{2+}}$	Activity coefficient of Pb^{2+}
f_{Ba}	Activity coefficient of Ba^{2+}
$f_{Ni^{2+}}$	Activity coefficient of Ni^{2+}

TABLE 4.1b: GLOSSARY OF TERMS FOR SECTION 4

Symbol	Description
f_{NiOH}	Activity coefficient of NiOH
f_{As}	Activity coefficient of AsO_4^{3-}
f_{H2AsO_4}	Activity coefficient of $H_2AsO_4^-$
f_{HAsO_4}	Activity coefficient of $HAsO_4^{2-}$

Equilibrium and Complexation Constants

Symbol	Description
$K_{CaSO_4^2}$	Gypsum solubility constant (Equation 4.1)
K_{CaCO_3}	Calcite solubility constant (Equation 4.1)
K_1	First dissociation constant of $H_2CO_3^+$ (Equation 4.1)
K_2	Dissociation constant of HCO_3^- (Equation 4.1)
K_H	Henry's Law constant (Equation 4.1)
pCO_2	Partial pressure of CO_2 (atm) (Equation 4.1)
$KAlOH_3$	$Al(OH)_3$ solubility constant (Equation 4.7)
C_{CaSO_4}	Complexation constant for $CaSO_4^o$ (Equation 4.9)
C_{AlOH}	Complexation constant for $Al(OH)^{2+}$ (Equation 4.19)
C_{AlOH_2}	Complexation constant for $Al(OH)_2^+$ (Equation 4.19)
C_{AlOH_3}	Complexation constant for $Al(OH)_3^o$ (Equation 4.19)
C_{AlOH_4}	Complexation constant for $Al(OH)_4^-$ (Equation 4.19)
CFEOH	Complexation constant for $Fe(OH)^{2+}$ (Equation 4.16)
CFEOH2	Complexation constant for $Fe(OH)_2^+$ (Equation 4.16)
CFEOH3	Complexation constant for $Fe(OH)_3^o$ (Equation 4.16)
CFEOH4	Complexation constant for $Fe(OH)_4^-$ (Equation 4.16)
XFEOOH	Goethite solubility constant (Equation 4.17)
XALOH3	Amorphorus aluminum hydroxide solubility constant (Equation 4.20)
CPBOH	Association constant for $Pb(OH)_2$ (Equation 4.21)
CPBCO3	Association constant for $PbCO_3$ (Equation 4.21)
CPBSO4	Association constant for $PbSO_4$ (Equation 4.21)

TABLE 4.1b: GLOSSARY OF TERMS FOR SECTION 4

Symbol	Description
XPBSO4	Solubility constant for $PbSO_4$ (Equation 4.22)
CBASO4	Complexation constant for $BaSO_4$ (Equation 4.23)
XBASO4	Solubility constant for $BaSO_4$ (Equation 4.24)
XMNO2	Solubility constant for MnO_2 (Equation 4.26)
XNIOH2	Solubility constant for nickel hydroxide (Equation 4.28)

Non-Standard Chemical Symbols

C_T	Total inorganic carbon (mol/L) (Equation 4.1)
$H_2CO_3^+$	Dissolved plus hydrated CO_2 (Equation 4.1)
(X)	Concentration of chemical species, X
XIS	Ionic strength (Equation 4.11)
f (with subscript)	Activity coefficient
$f_{\pm 1}$	Activity coefficient of ion of charge +1 or -1
$f_{\pm 2}$	Activity coefficient of ion of charge +2 or -2
$f_{\pm 3}$	Activity coefficient of ion of charge +3 or -3
CS_1	Solid phase concentration at time step t (Equation 4.13)
CS_2	Solid phase concentration at time step t+1 (Equation 4.13)
CS	Solution phase concentration at time step t when no solid phase is present (Equation 4.14)
k_p	Decay rate of parent radioisotope (Figure 4.3)
CS_p	Solid phase concentration of parent radioisotope (Figure 4.3)
DO	Dissolved oxygen concentration (Equation 4.26)
H	Chemical activity of hydrogen ion (Equation 4.28)
NIT	Total aqueous nickel concentration (Equation 4.28)
NIADS	Total adsorbed nickel concentration (Equation 4.28)

TABLE 4.1b: GLOSSARY OF TERMS FOR SECTION 4

Symbol	Description
NITT	Total nickel in dissolved and adsorbed phases (Equation 4.28)
XOH	Number of surface sites for adsorption (mol/L) (Equation 4.28)
ASTT	Total arsenic in adsorbed and dissolved phases (Equation 4.31)
AST	Total aqueous arsenic concentration (Equation 4.33)
ASO_4	Aqueous (AsO_4^{3-}) concentration (Equation 4.33)
ASADS	Total adsorbed arsenic concentration (Equation 4.33)
D	Equilibrium distribution coefficient (Equation 4.38)
lamda	Non-equilibrium distribution coefficient (Equation 4.39)
T	Retardation factor involving adsorption (Equation 4.41)
K	Dissolution rate constant of UO_2 (Equation 4.41)
$CT_{i,k/t}$	Concentration of $CT_{i,k}$ at time t (Equation 4.43)
pK	-log (complexation constant)
N_{ThCa}	Solid phase ratio of thorium in gypsum (Equation 4.46)
D_{ThCa}	Distribution coefficient of thorium in gypsum (Equation 4.46)
(FeOOH)	Solid phase concentration of FeOOH (Equation 4.47)
(MnO_2)	Solid phase concentration of MnO_2 (Equation 4.47)
(Th_s)	Solid phase concentration of thorium (Equation 4.47)
N_{RaBa}	Solid phase ratio of radium in barite (Equation 4.52)
N_{RaPb}	Solid phase ratio of radium in anglesite (Equation 4.52)
N_{RaCa}	Solid phase ratio of radium in gypsum (Equation 4.52)
D_{RaBa}	Distribution coefficient of radium in barite (Equation 4.52)
D_{RaPb}	Distribution coefficient of radium in anglesite (Equation 4.52)
D_{RaCa}	Distribution coefficient of radium in gypsum (Equation 4.52)
Ex_{RaFe}	Exchange rate constant of radium from thorium containing phases (Equation 4.58)
K_{Th}	Thorium decay constant (Equation 4.58)
(RaFe)	Radium concentration on thorium solid phase (Equation 4.59)
(RaTh)	Dimensional constant (Equation 4.58)

TABLE 4.1b: GLOSSARY OF TERMS FOR SECTION 4

Symbol	Description
Pb210 S	Solid phase concentration of Pb-210 (Equation 4.62)
D_{PbPb}	Distribution coefficient of Pb-210 in $PbSO_4$ (Equation 4.62)
D_{PbBa}	Distribution coefficient of Pb-210 in barite (Equation 4.62)
R_{ox}	Zero order consumption rate of oxygen (Equation 4.67)
D_{ox}	Diffusion coefficient of oxygen (Equation 4.67)
C_{ox}	Oxygen concentration at tailings surface (Equation 4.67)

FIGURE 4.1: PHYSICAL REPRESENTATION OF TAILINGS

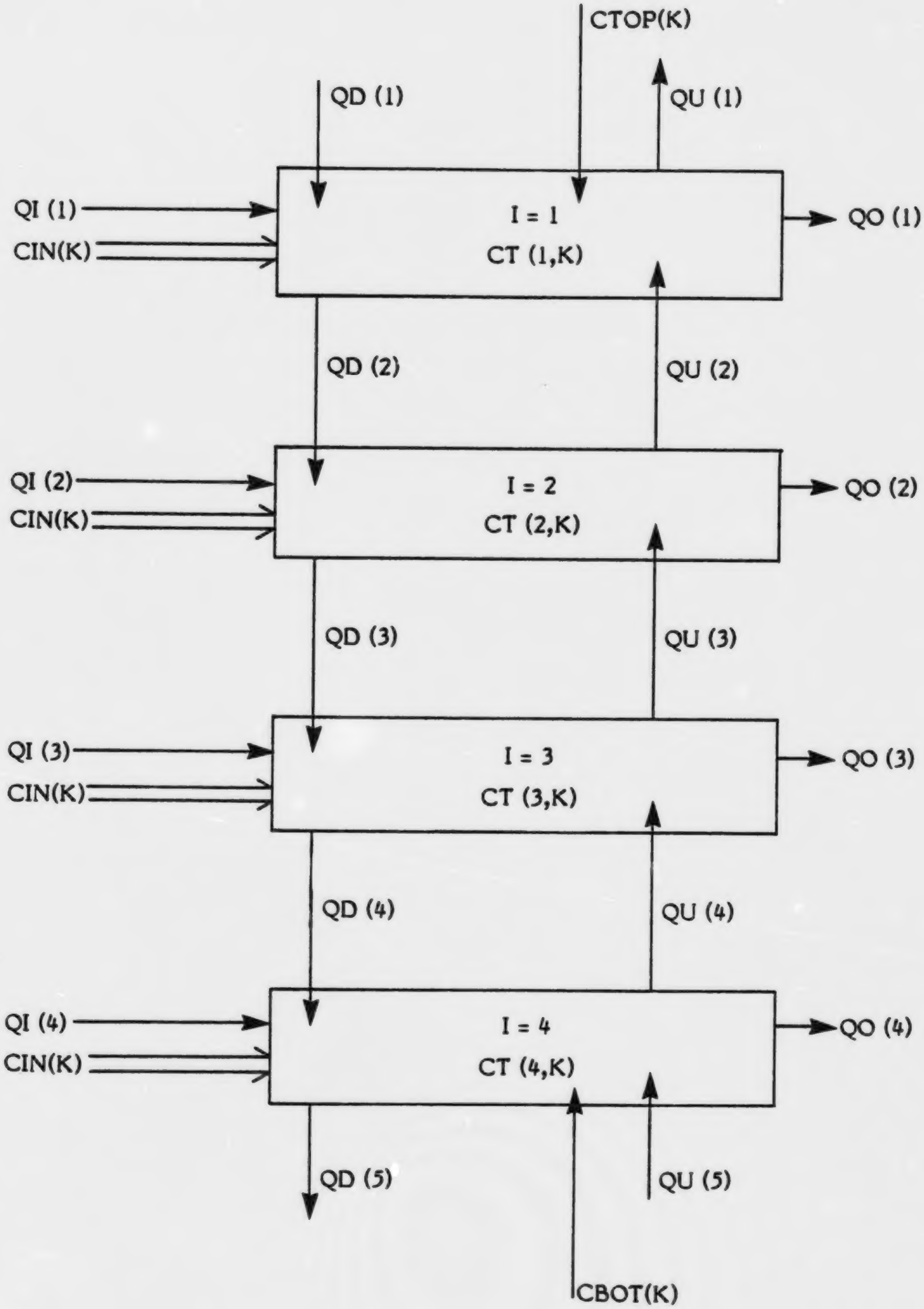
CTOP(K)
QD (1)
QU (1)
QI (1)
CIN(K)
I = 1
CT (1,K)
QO (1)
QD (2)
QU (2)
QI (2)
CIN(K)
I = 2
CT (2,K)
QO (2)
QD (3)
QU (3)
QI (3)
CIN(K)
I = 3
CT (3,K)
QO (3)
QD (4)
QU (4)
QI (4)
CIN(K)
I = 4
CT (4,K)
QO (4)
QD (5)
QU (5)
CBOT(K)

which is a probabilistic variable. If the values are specified, the flow regime is treated as constant for the whole simulation period.

CIN(K) is the concentration of the "K"th contaminant coming from the watershed and groundwater upstream to the tailings pile. If one desired the flexibility for using different values for the concentration of contaminants flowing into the different boxes, the variable CIN would need to be changed from a vector to an array.

CTOP(K) is the concentration of a substance in rainfall. CBOT(K) is the concentration of a substance in deep groundwater. CT(I,K) is the total aqueous concentration of contaminant K in the source term box I, while C(K) is the concentration of the contaminant not including complexes. The boxes are numbered from the surface downward.

For any simulation, the flow rate of each pathway is user specified. The source term code is comprehensive enough to allow for simulation of two extremes: a tailings which is partly saturated or a tailings which is completely underwater. For the underwater case, the downward flow rate is assumed to equal 0. and only vertical upflow is allowed. Alternatively, the effects of advection and dispersion can be considered by assigning appropriate values to QD(I) and to QU(I).

4.2 Chemical Substances Considered in Tailings

The main objective of this report is to consider the transport of radiological and chemical contaminants from the tailings. Radiological contaminants considered are U, Th-230, Ra-226, Pb-210 and Po-210. Chemical contaminants considered are As and Ni.

To evaluate these substances, other chemical elements as well must be considered. A list of the chemical substances considered in this report, and their code nomenclature is given in Table 4.2. The rationale for considering these subtances is given in Table 4.3.

To evaluate the concentration of these various substances in tailings porewater, the solid phases which supply these substances must be determined and assumptions made about the mechanisms controlling solid-solution interactions justified. For most solid phases, equilibrium conditions expressed by the solubility product are used to relate solid-solution conditions. Dissolution of a few solids is assumed to be kinetically controlled. A

TABLE 4.2: NUMBERING SYSTEM FOR SUBSTANCES IN SOURCE TERM CODE

a) Numbering System for Primary Aqueous Substances

Substance	Substance No. (K)	Substance	Substance No. (K)
Calcium (Ca)	1	Aluminum (Al)	10
Sulphate (SO_4)	2	Stable Lead (Pb)	11
Total Inorganic Carbon (C_T)	3	Barium (Ba^{2+})	12
Manganese (Mn)	4	Uranium (U)	13
Alkalinity (ALK)	5	Thorium-230 (Th-230)	14
pH (pH)	6	Radium-226 (Ra-226)	15
Nickel (Ni^{2+})	7	Lead-210 (Pb-210)	16
Arsenic (As)	8	Dissolved Oxygen Carbon (DOC)	17
Iron (Fe^{3+})	9	Dissolved Oxygen (DO)	18

b) Numbering System of Storage Arrays

1. Concentration Arrays:

C(I,K)	Concentration of primary form of substance K in pore water of box I
CT(I,K)	Total aqueous concentration of substance K in pore water of box I
CADS(I,K)	Adsorbed concentration of substance K in box I
CTT(I,K)	Total aqueous plus adsorbed concentration of substance K in box I
CTOT(I,K)	Total concentration of all forms (aqueous, adsorbed, solid precipitate) of substance K in box I

2. Decay Arrays:

a) Radiological Decay (RADIOD(J))

Vector No.	Substance
RADIOD (J=1)	Uranium
RADIOD (J=2)	Th-230
RADIOD (J=3)	Ra-226
RADIOD (J=4)	Pb-210

b) Mineral Dissolution and Organic Carbon Decay (DECAY(I,J))

Array	Substance
DECAY (I,J=1)	NiAsS
DECAY (I,J=2)	UO_2
DECAY (I,J=3)	vegetative POC
DECAY (I,J=4)	DOC
DECAY (I,J=5)	POC (formed by DOC adsorption)

TABLE 4.3: ROLE OF SUBSTANCE IN SOURCE TERM MODEL

Substance	Role of Substance
Calcium	Influences electroneutrality, pH
Sulphate	Influences electroneutrality, pH
C_T	Influences electroneutrality, pH
Manganese	Influences Th-230
Alkalinity	Influences pH
pH	Master chemical variable
Nickel	Chemical toxicity
Arsenic	Chemical toxicity
Iron	Adsorption sites; influences pH
Aluminum	Adsorption sites; influences pH
Lead (Stable)	Influences Pb-210, Ra-226
Barium	Influences Ra-226 chemistry
Uranium	Radiological concern, chemical toxicity
Th-230	Radiological concern
Ra-226	Radiological concern
Pb-210	Radiological concern
DOC	Influences redox
DO	Influences redox

summary of the solid phases, their code names and the code names of the solubility constants (if applicable) are given in Table 4.4. Values for the constants are given in Table 4.7 presented at the end of Section 4.

4.3 Calcium, Sulphate, Carbonate, and pH

The master chemical variables controlling the chemistry of much of the source term are the solution pH and Eh. The following substances influence solution pH:

- Ca^{2+};
- SO_4^{2-} ; $CaSO_4{}^o$;
- $H_2CO_3^*$; HCO_3^-; CO_3^{2-} ;
- Ni^{2+}, $NiOH^+$;
- $H_2AsO_4^-$; $HAsO_4^{2-}$; AsO_4^{3-} ;
- Fe^{3+}, $FeOH^{2+}$, $Fe(OH)_2^+$; $Fe(OH)_3^0$; $Fe(OH)_4^-$; $Fe_2(OH)_2^{4-}$;
- Al^{3+}; $AlOH^{2+}$; $Al(OH)_2^+$; $Al(OH)_3^0$; $Al(OH)_4^-$; $Al_2(OH)_2^{4-}$;
- Pb^{2+}; $PbOH^+$; $PbSO_4{}^o$ and
- UO_2^{2-} ; $UO_2(SO_4)_2^{2-}$.

All substances will influence pH via their contribution to the electroneutrality equation. The substances which hydrolize (C, Ni^{2+}, AsO_4^{3-}, Fe^{3+}, Al^{3+}, Pb^{2+}) particularly influence the solution pH.

An evaluation was made of the major substances which will control solution pH. The basic concepts in the evaluation are:

- what substances make the largest contribution to electroneutrality; and
- what complexing system controls solution pH.

The evaluation indicated that the expected pH range of tailings porewater is 5-8 and that Ca^{2+}, SO_4^{2-} and inorganic carbon species make the largest contribution to electroneutrality. Accordingly, the inorganic carbon buffering system will control solution pH over this pH range.

TABLE 4.4: SOLID FORMS CONSIDERED

Solid Form	Code Nomenclature	Units*	Solubility Constant Code Name
Gypsum	CASO4(I)	mol/m^3	XCASO4
Calcite	CACO3(I)	mol/m^3	XCACO3
Reduced Nickel Arsenide	NIASS(I)	mol/m^3	-**
Residual Uranium Mineral	UO2(I)	mol/m^3	-**
Calcium Arsenate	CAASO4(I)	mol/m^3	XCAASO4
Nickel Hydroxide	NIOH2(I)	mol/m^3	XNIOH2
Iron Hydroxide	FEOOH(I)	mol/m^3	XFEOOH
Aluminum Hydroxide	ALOH3(I)	mol/m^3	XALOH3
Lead Sulphate	PBS04(I)	mol/m^3	XPBSO4
Lead Hydroxide	PBOH2(I)	mol/m^3	XPBOH2
Lead Carbonate	PBCO3(I)	mol/m^3	XPBCO3
Barium Sulphate	BASO4(I)	mol/m^3	XBASO4
Particulate Organic Carbon	POC(I)	mol/m^3	-
Th-230 Coprecipitate***	-		-
Ra-226 Coprecipitate***	-		-
Pb-210 Coprecipitate***	-		-

* Units: mol/m^3 of bulk.

** Kinetic control or dissolution is assumed.

*** Calculated based upon distribution coefficients.

This determination allows one to uncouple the chemical problem for calculating solution pH into component parts rather than simultaneously considering eight major elements and associated complexes. Only calcium, sulphate and carbonate need to be considered simultaneously to give pH. Analytical solutions can be obtained for these three substances. In the case of eight major substances, numerical techniques such as the Newton-Raphson method used in standard computer codes (e.g., MINEQL, REDEQU2, GEOCHEM, EQ3/EQ6) are required to solve the problem.

Two cases are considered depending upon whether the system is chemically open (i.e., the unsaturated soil zone which is exposed to the atmosphere) or closed (i.e., the saturated soil zone which is effectively closed to the atmosphere).

4.3.1 Open System

The open system is considered in subroutine OPEN (see Table 4.1a). It is based on the fact that C_T is a variable entity dependent upon solution pH and pCO_2. The solution pCO_2 is fixed by the partial pressure of CO_2 in the soil gas (assumed to be the same as that of the atmosphere) if dissolved CO_2 in pore water is in equilibrium with the CO_2 gas in the soil pores. Higher values would be used for pCO_2 if development of an organic soil zone is expected at the tailings surface.

(i) Solution Equilibrium with Calcite and Gypsum

The following are the governing equations. Chemical symbols which are standard in chemical textbooks are used to the maximum extent possible. They are defined in the glossary of symbols at the beginning of this chapter (Table 4.1b). The capital 'K' is generally used as a solubility constant, the capital 'A' is used to mean activity of a substance, and lower case 'f' is used to mean an activity coefficient. Round brackets, e.g., '( )', are used to mean concentration of a substance.

Gypsum Solubility: $A_{Ca} \cdot A_{SO4} = K_{CaSO_4}$ (4.1a)

Calcite Solubility: $A_{Ca} \cdot A_{CO3} = K_{CaCO_3}$ (4.1b)

Electroneutrality: $2(Ca^{2+}) + (H^+) = (HCO_3^-) + 2(CO_3^{2-}) + 2(SO_4^{2-}) + Sum$ (4.1c) where sum refers to the sum of other anions minus the sum of other cations which, in this case, are neglible.

Inorganic Carbon
Speciation:

$$\frac{A_{HCO3}\,A_H}{A_{H_2CO_3^*}} = K_1 \qquad (4.1d)$$

$$\frac{A_H \quad A_{CO3}}{A_{HCO_3}} = K_2 \qquad (4.1e)$$

Carbon Mass Balance: $C_T = (H_2CO_3^*) + (HCO_3^-) + (CO_3^{2-})$ (4.1f)

Henry's Law: $(H_2CO_3^*) = K_H\ pCO_2$ (4.1g)

By assuming appropriate simplifications (Stumm and Morgan, 1981), the following equation results:

$$(Ca^{2+})^2 - \frac{f_{Ca}}{2f_{HCO3^-}}\left[\frac{K_1 \cdot K_H \cdot K_{CaCO_3} \cdot pCO_2\,(Ca^{2+})}{K_2 \cdot f_{Ca}}\right]^{1/2} - \frac{K_{CaSO_4}}{f_{SO4}\,f_{Ca}} = 0. \qquad (4.2)$$

This is a fourth order polynomial for which there is not an analytical solution available. However, an analytical solution can be obtained if it can be further simplified. Inspection of the equation shows the second term is due to calcium equilibrium with calcite, while the third term is due to calcium equilibrium with gypsum.

Equation 4.2 is composed of two equations arising from the simplification of Equations 4.1a to 4.1g. They are:

$$(Ca^{2+})^2 = \frac{K_1\,K_H\,pCO_2\,(Ca^{2+})}{2\,f_{HCO_3} \cdot (H^+)} + \frac{K_{CaSO_4}}{f_{SO4}\,f_{Ca}} \qquad (4.3a)$$

$$(Ca^{2+}) = \frac{(H^+)^2 \cdot K_{CaCO_3}}{f_{Ca} \cdot K_1 \cdot K_2 \cdot K_H \cdot pCO_2} \qquad (4.3b)$$

Substitution of H^+ from (4.3b) into (4.3a) gives Equation 4.2. The position on a plot of log Ca^{2+} vs pH where equation (4.3a) intersects equation (4.3b) defines the root of equation 4.2.

These equations are plotted in Figure 4.2 for two values for pCO_2 of $10^{-1.5}$ atm to $10^{-3.5}$ atm. The intersection of equation (4.3b) with (4.3a) indicates that the first term on the right hand side of Equation (4.3a) does not significantly influence the value of the equation in the range of the root of Equation 4.2. The contribution to Ca^{2+} in solution from calcite dissolution is small in comparison to the contribution by gypsum dissolution when the pH is greater than 6 and the pCO_2 is less than about $10^{-1.5}$. Accordingly, the first term on the right hand side of Equation (4.3a) may be ignored. This results in the following equations for the open system:

$$(Ca^{2+}) = \left[\frac{K_{CaSO_4}}{f_{Ca}\, f_{SO4}}\right]^{1/2} \qquad (4.4a)$$

$$(H^+) = \left[K_1 \cdot K_2 \cdot \frac{K_H \cdot pCO_2 \cdot f_{Ca}(Ca)}{K_{CaCO_3}}\right]^{1/2} \qquad (4.4b)$$

$$(SO_4^{2-}) = K_{CaSO_4}/(f_{Ca} \cdot f_{SO_4} \cdot (Ca^{2+})) \qquad (4.4c)$$

$$C_T = pCO_2 \cdot K_H \cdot \left(\frac{(H^+) + K_1}{(H^+)}\right) \qquad (4.4d)$$

$$(HCO_3^-) = \left(\frac{K_1}{(H^+) + K_1}\right) \cdot C_T \qquad (4.4e$$

In addition to solution equilibrium with calcite and gypsum, three other cases may occur which need special consideration:

FIGURE 4.2: ROOTS OF pH DETERMINING EQUATION

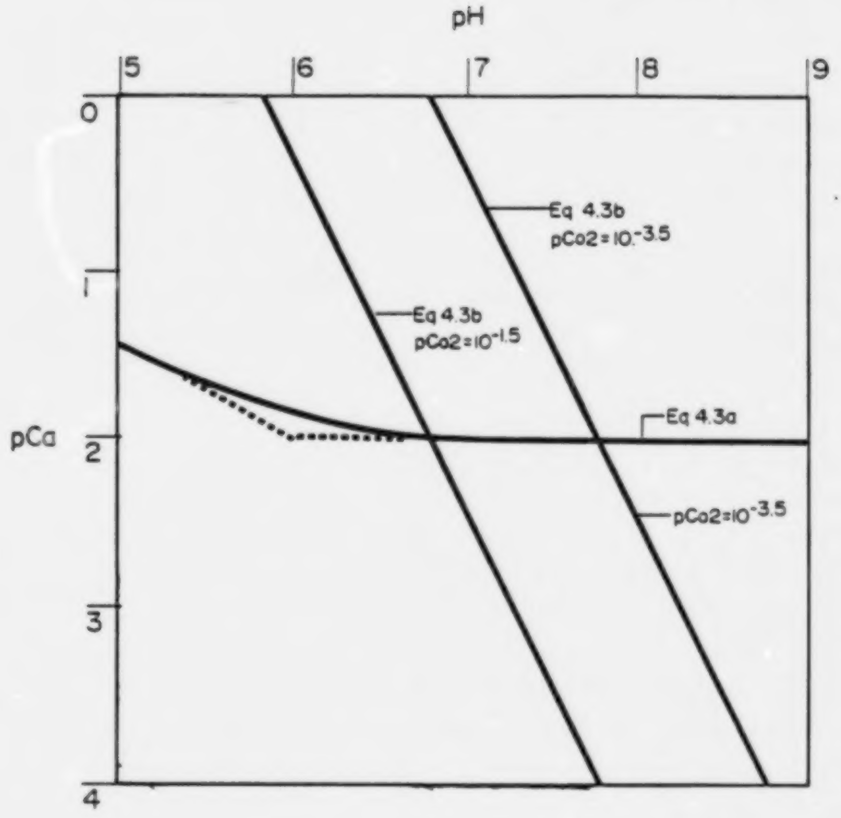

- calcite only may be present;
- gypsum only may be present; and
- neither calcite nor gypsum are present.

(ii) Calcite only is present

Consideration of calcite only results in the following equation:

$$(Ca^{2+})^2 = \frac{1}{(2\, f_{HCO3})^{2/3}} \left[\frac{K_{CaCO_3}}{f_{Ca}} \cdot \frac{K_1}{K_2} \quad K_H \quad pCO_2 \right]^{1/3} \qquad (4.5a)$$

$$(H^+) = \left[\frac{K_1\, K_2\, K_H\, pCO_2\, f_{Ca}\, (Ca)}{K_{CaCO_3}} \right]^{1/2} \qquad (4.5b)$$

$(SO_4{}^{2-})$ is controlled by solution mass balance (4.5c)

$$C_T = pCO_2 \cdot K_H \cdot \left(\frac{(H^+) + K_1}{(H^+)} \right) \qquad (4.5d)$$

$$(HCO_3^-) = \left(\frac{K_1}{(H^+) + K_1} \right) C_T \qquad (4.5e)$$

(iii) Gypsum only is present

Consideration of gypsum only results in the following equations:

$$(Ca^{2+}) = \left[\frac{K_{CaSO_4}}{f_{Ca}\, f_{SO4}} \right]^{1/2} \qquad (4.6a)$$

$$(SO_4{}^{2-}) = (Ca^{2+}) \qquad (4.6b)$$

$$pH = \frac{1}{4} Log \left(\frac{f_{Al}{}^{3+}\, (3 \times 10^{-14})}{KAlOH3} \right) \qquad (4.6c)$$

$$C_T = K_H \, pCO_2 \left(\frac{(H^+) + K_1}{(H^+)} \right) \qquad (4.6d)$$

$$(HCO_3^-) = \left(\frac{K_1}{(H^+) + K_1} \right) C_T \qquad (4.6e)$$

Consideration of gypsum only means that inorganic carbon does not adequately control the pH. If C_T enters the system only from the atmosphere, the pH will be of the order of 5.7 or less. Due to acidic precipitation, the actual pH will be of the order of 4. But $Al(OH)_3$ will buffer the solution at a pH of the order of 6 when the reaction,

$$Al^{3+} + 4H_2O = Al(OH)_4^- + 4H^+$$

is considered. Accordingly, it is assumed that the pH is buffered by $Al(OH)_3(s)$ as long as aluminum hydroxide is present.

(iv) Neither gypsum nor calcite are present

It is assumed that aluminum hydroxide controls the pH if neither gypsum nor calcite are present. If aluminum hydroxide is not present, it is assumed that the dissolution of aluminosilicate to $Al(OH)_4^-$ is a reasonable model reaction for describing the effect of aluminosilicate control on the pH for the time scale of the calculations, and that the solution conditions are similar in both cases.

The resultant equations are:

$$pH = -\frac{1}{4} \mathrm{Log} \left(\frac{f_{Al} \, (3\times10^{-14})}{KAlOH3} \right) \qquad (4.7a)$$

$$C_T = K_H \, pCO_2 \left(\frac{H^+ + K_1}{H^+} \right) \qquad (4.7b)$$

$$(HCO_3^-) = \frac{K_1 \cdot C_T}{(H^+) + K_1} \qquad (4.7c)$$

(Ca^{2+}) = calculated by solution mass balance (4.7d)

(SO_4^{2-}) = calculated by solution mass balance (4.7e)

4.3.2 Closed System

The closed system is considered in subroutine CLOSED (see Table 4.1). It assumes that C_T is a variable entity dependent upon solution pH, CO_3^{2-} in equilibrium with calcite, and mass balance. No exchange of CO_2 is possible between the pore water and the atmosphere. This zone is below the water table. It is assumed that calcite and gypsum are never depleted, and hence that both solid phases set the pH. If either solid phase is depleted, the calculations stop and a warning message is printed. The calculations are programmed to stop because the project team judged it unlikely that all gypsum and calcite would be dissolved for typical management scenarios to be considered. If depletion does occur, either the base data setting up the management problem are in error or else the addition of more code is required.

The basic equations for the closed system are those of Equation 4.1, except that Equation 4.1g does not apply. Simplification of the equations gives the following solution:

C_T = calculation by solution mass balance (4.8a)

$$(Ca^{2+}) = 1/2\,(C_1 + (C_1^{\,2} + 4C_2)^{1/2}) \qquad (4.8b)$$

$$(SO_4^{2-}) = C_2/(Ca^{2+}) \qquad (4.8c)$$

$$(HCO_3^-) = C_T \qquad (4.8d)$$

$$(H^+) = \frac{f_{Ca}\,(Ca^{2+}) \cdot f_{HCO_3^-}\,(HCO_3^-) \cdot K_2}{K_{CaCO_3}} \qquad (4.8e)$$

where:

$$C_1 = C_T/2$$

$$C_2 = \frac{K_{CaSO_4}}{f_{Ca}\,f_{SO4}}$$

4.3.3 Solution Complexes

The relevant solution complexes are calculated based upon the following equations:

$$CaSO_4^o = C_{CaSO4}\, f_{Ca}\, (Ca^{2+})\, f_{SO4}\, (SO_4^{2-}) \tag{4.9a}$$

$$H_2CO_3^* = \frac{(H^+)\, f_{HCO_3^-} \cdot (HCO_3^-)}{K_1} \tag{4.9b}$$

$$(HCO_3^-) = \frac{(H^+)\, f_{CO_3}\, (CO_3^{2-})}{f_{HCO_3^-} \cdot K_2} \tag{4.9c}$$

Note, the equation for ion complexes written as:

$$Ca^{2+} + SO_4^{2-} = CaSO_4^o \tag{4.10a}$$

is written in the opposite direction to that of the protonation reactions such as:

$$H_2CO_3^+ = H^+ + HCO_3^- \tag{4.10b}$$

$$HCO_3^- = H^+ + CO_3^{2-} \tag{4.10c}$$

4.3.4 Ionic Strength Calculations

Ionic strength is calculated using the equation:

$$\text{XIS (Ionic Strength)} = 1/2\,(4 \cdot (Ca^{2+}) + 4(SO_4^{2-}) + \left(\frac{K_1}{(H^+) + K_1}\right) C_T$$

$$+ \left(\frac{9}{f_{Al}} + \frac{4 \cdot C_{AlOH} \cdot H^+}{f_{AlOH}} + \frac{C_{AlOH2}\, (H^+)^2}{f_{AlOH2}}\right.$$

$$\left. + \frac{C_{AlOH4}\, (H^+)^4}{f_{AlOH4}}\right) \cdot f_{Al}\, (Al^{3+}) \tag{4.11}$$

Activity coefficients are calculated using the Davies model (Stumm and Morgan, 1981). It is applicable for the ionic strength range of 0 to 0.5 M. It is:

$$GAM = -0.5 \frac{(XIS)^{1/2}}{1+(XIS)^{1/2}} - 0.3XIS \qquad (4.12a)$$

$$f_{\pm 1} = 10^{GAM} \qquad (4.12b)$$

$$f_{\pm 2} = 10^{4.GAM} \qquad (4.12c)$$

$$f_{\pm 3} = 10^{9.GAM} \qquad (4.12d)$$

In this terminology, $f_{\pm 1}$ refers to ions of charge +1 or -1, $f_{\pm 2}$ refers to ions of charge +2 or -2, and $f_{\pm 3}$ refers to ions of charge +3 or -3.

The constant in Equation 4.12a of 0.3 has been changed from the historical value of 0.2 to reflect the more recent curve fitting and recommendation of Davies (Stumm and Morgan, 1981).

For waters which have an ionic strength greater than 0.5, the Davies model is strictly not applicable. For waters, with ionic strength substantially greater than 0.5, the Pitzer model should be used. Because initial calculations for the gypsum-dominated pore water indicated that the ionic strength should generally be of the order of 0.1 M or less, the Davies model is the only one considered in this report.

If solution conditions occur, which are substantially different from those calculated by this model because of acidic reactions, provision is made in the code to treat the activity coefficient as a probabilistic rather than a deterministic variable.

4.4 Mass Balance Calculations

Common to all substances, including calcium sulphate and inorganic carbon, is the requirement to calculate the change in mass of solid phase and the change in pore water concentration. If the solid phase exists and equilibrium is maintained during a time step, the solution concentration remains the same, but the mass of solid may change when influx and outflux of components is considered because inflowing concentrations may not be equilibrium concentrations. The calculation for this condition is made in Subroutine MASBAL1.

If the solid phase does not exist, or if solid phase dissolution is kinetically controlled, then the solution concentration is set by the mass balance on the solution phase when account is taken of inflow, outflow and mineral dissolution and decay reactions. The calculation for this condition is made in Subroutine MASBAL2. For an element which is on a solid phase but controlled by solution concentrations (i.e., adsorption according to the linear adsorption model, coprecipitation, or ion exchange reactions), the conditions of MASBAL1 are applicable.

A definitional sketch for the mass balance which includes hydraulic pathways, mineral decay and radioisotope decay is given in Figure 4.3. For non-radiological elements, decay terms of the parent and daughter assume zero values. For the condition of the solid phase existing, a mass balance gives the equation for MASBAL1 of:

$$\begin{aligned} CS_2 &= CS_1 + (QI_i \, CIN_{i,k} + QD_i \, CT_{i-1,k} + QU_{i+1} \, B_i \\ &\quad - (QO_i + QU_i + QD_{i+1}) \cdot CT_{i,k}) \cdot DT \end{aligned} \tag{4.13}$$

Here, $CT_{i,k}$ is the total concentration of element k in solution in tailings box i including the primary species (defined by $C_{i,k}$) and solution complexes. CS_2 is the total solid phase composition at time step (t+1) while CS_1 is the total solid phase composition at time step t. A constraint is used that, if CS_2 is less than zero, it is set to 0, but solution conditions are assumed to be defined by equilibrium conditions for the time step.

For conditions where the solid phase does not exist, a mass balance which assumes steady-state conditions for solution gives:

$$CS = \frac{QI_i \cdot CIN_{i,k} + QD_i \, CT_{i,k} + QU_{i+1} \cdot B_i}{QO_i + QU_i + QD_{i+1}} \tag{4.14}$$

This equation is the basic governing equation for MASBAL2.

4.5 Minor Elements (Fe, Al, Pb, Ba, Mn)

The minor elements Fe (K=9), Al (K=10), Pb (K=11), Ba (K=12) and Mn (K=4) are computed in Subroutine FEALPB

FIGURE 4.3: MASTER MASS BALANCE BLOCK DIAGRAM

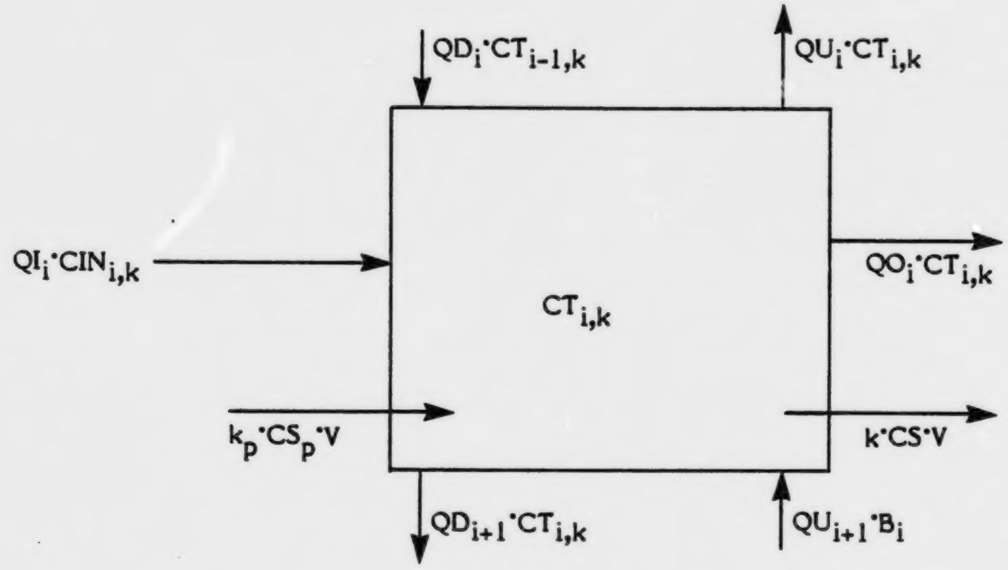
$QD_i \cdot CT_{i-1,k}$
$QU_i \cdot CT_{i,k}$
$QI_i \cdot CIN_{i,k}$
$CT_{i,k}$
$QO_i \cdot CT_{i,k}$
$k_p \cdot CS_p \cdot V$
$k \cdot CS \cdot V$
$QD_{i+1} \cdot CT_{i,k}$
$QU_{i+1} \cdot B_i$

B_i = $CT_{i+1,k}$ for i=1, 2, 3
= CBOT(k) for i=4

Note: $k_p \cdot CS_p \cdot V$ is radioactive decay of parent; $k \cdot CS \cdot V$ is radioactive decay of element considered by mass balance. These two terms are applicable only to radioactive elements (see Sections 4.8 to 4.12).

4.5.1 Iron Chemistry

The following complexation reactions of iron were considered:

$$Fe^{3+} + H_2O = FeOH^{2+} + H^+ \qquad \log K_{11} = -4.97 \qquad (4.15a)$$
$$Fe^{3+} + 2H_2O = Fe(OH)_2^+ + 2H^+ \qquad \log K_{12} = -9.3 \qquad (4.15b)$$
$$Fe^{3+} + 3H_2O = Fe(OH)_3^0 + 3H^+ \qquad \log K_{13} = -15.0 \qquad (4.15c)$$
$$Fe^{3+} + 4H_2O = Fe(OH)_4^- + 4H^+ \qquad \log K_{14} = -23.0 \qquad (4.15d)$$
$$2Fe^{3+} + 2H_2O = Fe_2(OH)_2{}^{4+} + 2H^+ \qquad \log K_{22} = -7.7 \qquad (4.15e)$$
$$3Fe^{3+} + 4H_2O = Fe_3(OH)_4{}^{5+} + 4H^+ \qquad \log K_{34} = -13.94 \qquad (4.15f)$$
$$13Fe^{3+} + 28H_2O = Fe_{13}O_4(OH)_{24}{}^{7+} + 32H^+ \qquad \log K_{13,32} = -98.73 \qquad (4.15g)$$

Other complexes of potential interest include $FeSO_4{}^+$ and $Fe(SO_4)_2{}^-$. Analysis of these complexes indicated that several were not of significance, simplifying the chemical balance for solution iron to:

$$Fe_T = (Fe^{3+}) + (FeOH^{2+}) + (Fe(OH)_2{}^+) + (Fe(OH)_3{}^0) + (Fe(OH)_4{}^-) \qquad (4.16a)$$

which becomes:

$$Fe_T = Fe^{3+} f_{Fe3^+}\left(\frac{1}{f_{Fe^{3+}}} + \frac{CFEOH}{f_{FeOH}\cdot(H^+)} + \frac{CFEOH2}{f_{FeOH2}(H^+)^2} + \frac{CFEOH3}{(H^+)^3} + \frac{CFEOH4}{f_{FeOH4}(H^+)^4}\right) \qquad (4.16b)$$

in which CFEOH, CFEOH2, etc. are the association constants defined in Equation 4.15 (a to d).

If the solid phase FEOOH exists in the box, then Fe^{3+} is calculated from the solubility relationship:

$$(Fe^{3+}) \quad = \quad \frac{XFEOOH}{f_{Fe^{3+}} \cdot (H^+)^3} \qquad (4.17)$$

Fe_T is calculated from 4.16b, and MASBAL1 is used to calculate the change in solid phase composition. If the solid phase does not exist, MASBAL2 is used to calculate Fe_T, and then Fe^{3+} is calculated from Fe_T according to Equation 4.16b.

4.5.2 Aluminum Chemistry

The solution chemistry of aluminum is essentially a replicate of that of iron, except for the solubility and complexation constants involved. The following complexation reactions of aluminum were considered:

$$Al^{3+} + H_2O = AlOH^{2+} + H^+ \qquad \log K_{11} = -4.97 \qquad (4.18a)$$

$$Al^{3+} + 2H_2O = Al(OH)_2^+ + 2H^+ \qquad \log K_{12} = -9.3 \qquad (4.18b)$$

$$Al^{3+} + 3H_2O = Al(OH)_3^0 + 3H^+ \qquad \log K_{13} = -15.0 \qquad (4.18c)$$

$$Al^{3+} + 4H_2O = Al(OH)_4^- + 4H^+ \qquad \log K_{14} = -23.0 \qquad (4.18d)$$

$$2Al^{3+} + 2H_2O = Al_2(OH)_2{}^{4+} + 2H^+ \qquad \log K_{22} = -7.7 \qquad (4.18e)$$

$$3Al^{3+} + 4H_2O = Al_3(OH)_4{}^{5+} + 4H^+ \qquad \log K_{34} = -13.94 \qquad (4.18f)$$

$$13Al^{3+} + 28H_2O = Al_{13}O_4(OH)_{24}{}^{7+} + 32H^+ \qquad \log K_{13,32} = -98.73 \qquad (4.18g)$$

Other complexes of potential interest include $AlSO_4{}^+$ and $Al(SO_4)_2{}^-$. Analysis of these complexes indicated that several were not of significance, simplifying the chemical balance for solution aluminum to:

$$Al_T = (Al^{3+}) + (AlOH^{2+}) + (Al(OH)_2{}^+) + (Al(OH)_3{}^0) + (Al(OH)_4{}^-) \qquad (4.19a)$$

which becomes:

$$Al_T = Al^{3+} \cdot f_{Al^{3+}} \cdot \left(\frac{1}{f_{Al^{3+}}} + \frac{CAlOH}{f_{AlOH} \cdot (H^+)} + \frac{CAlOH2}{f_{AlOH2}(H^+)^2} + \frac{CAlOH3}{(H^+)^3} + \frac{CAlOH4}{f_{AlOH4}(H^+)^4} \right) \qquad (4.19b)$$

in which CAOH, CA1OH2, etc. are the association constants defined in Equation 4.18 (a to d).

If the solid phase $Al(OH)_3$ exists in the box, then Al^{3+} is calculated from the solubility relationship:

$$(Al^{3+}) = \frac{XAlOH3}{f_{Al^{3+}} (H^+)^3} \qquad (4.20)$$

Al_T is calculated from Equation 4.19b, and MASBAL1 is used to calculate the change in solid phase composition. If the solid phase does not exist, MASBAL2 is used to calculate Al_T, and then Al^{3+} is calculated from Al_T according to Equation 4.19b.

4.5.3 Lead Chemistry

Evaluation of Pb chemistry indicated that PbO, $Pb(OH)_2$, $Pb_{10}O(OH)_6(CO_3)_6$ (plumbonacrite), $Pb_3(OH)_2(CO_3)_2$ (hydrocerussite), and $PbCO_3$ (cerussite) are the possible solids that could form in a hydroxide-carbonate matrix. Several possible solution complexes include several monomers: Pb^{2+}, $PbCO_3^{o}$, $Pb(CO_3)_2^{2-}$, $Pb(OH)_3^-$, $Pb(OH)^+$, $Pb(OH)_2^{o}$, and polymers $Pb_4(OH)_4^{4+}$, $Pb_6O(OH)_6^{4+}$, and $Pb_3(OH)_4^{2+}$ (Taylor and Lopata, 1983). Within the hydroxide-carbonate domain of interest, the solids $PbCO_3$ and $Pb(OH)_2$ and the hydroxyl complexes of Pb and the complex $PbCO_3^{o}$ can explain most of the chemical action of significance.

In a sulphate system, the solid $PbSO_4$ and the complex $PbSO_4^{o}$ are additional substances to be considered.

Due to the large sulphate concentration present, it is assumed that $PbSO_{4(s)}$ controls the solubility of Pb over the weakly acidic to weakly basic pH range and that the significant complexes are Pb^{2+}, $PbOH^+$ (dominant in the pH range of 7 to 10 for C_T from 10^{-5} to 10^{-8}), $PbCO_3^{o}$ (dominant in the pH range of 6 to 10 and C_T 10^{-3} to 10^{-5} in the absence of sulphate) and $PbSO_4^{o}$. A composite stability diagram is given in Figure 4.4.

A mass balance for solution complexes gives:

$$Pb_T = (Pb^{2+}) + (PbOH^+) + (PbCO_3^{o}) + (PbSO_4^{o}) \qquad (4.21a)$$

$$= Pb^{2+} f_{Pb^{2+}} \left(\frac{1}{f_{Pb^{2+}}} + \frac{CPBOH*(H^+)}{f_{Pb^{2+}}} + CPBCO3*f_{CO3*}(CO_3^{2-}) + CPBSO4\ f_{SO4} * (SO_4^{2-}) \right) \qquad (4.21b)$$

in which CPBOH, CPBCO3 and CPBSO4 are the association constants of the appropriate complexes.

FIGURE 4.4: THE STABILITY OF LEAD COMPOUNDS IN SOLUTION (FROM GARRELS & CHRIST, 1965)

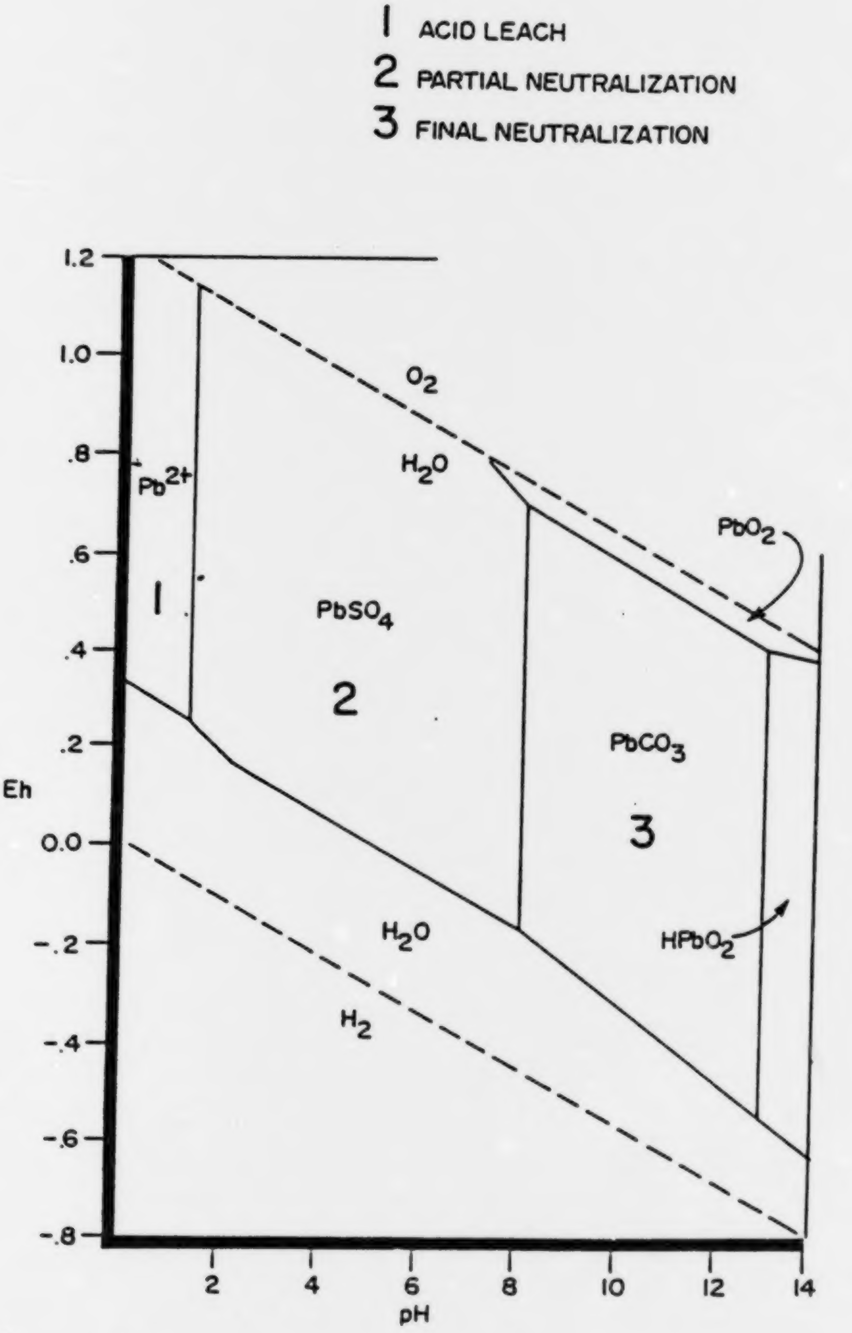

In the presence of the solid phase, Pb^{2+} is calculated from the relationship:

$$(Pb^{2+}) = \frac{XPBSO4}{f_{Pb^{2+}} \cdot f_{SO4}(SO4^{2-})} \qquad (4.22)$$

and the mass balance is calculated using MASBAL1. In the absence of the solid phase, MASBAL2 is used to calculate the solution mass balance for Pb_T, and then, Pb^{2+} is calculated from (Pb_T) and Equation 4.21b.

4.5.4 Barium Chemistry

Barite ($BaSO_4$) is assumed to be the solid which controls barium concentrations at the ambient conditions of this study. $BaCO_3(s)$ is another possible solid phase, but it does not control barium concentrations until elevated pH and C_T values. Of the possible complexes of Ba^{2+} ($BaOH^+$, $Ba(OH)_2^o$, $BaCl_2^o$, $BaSO_4^o$), $BaSO_4^o$ is the main one of significance.

A mass balance for solution complexes of Ba^{2+} gives:

$$Ba_T = (Ba^{2+}) + (BaSO_4^o) \qquad (4.23a)$$

$$= Ba^{2+} (1 + f_{Ba}\, f_{SO4}\, CBASO4\, (SO_4^{2-})) \qquad (4.23b)$$

In the presence of the solid phase, Ba^{2+} is calculated from:

$$(Ba^{2+}) = \frac{XBASO4}{f_{Ba} \cdot f_{SO4}\, (SO_4^{2-})} \qquad (4.24)$$

and the mass balance is calculated using MASBAL1. In the absence of the solid phase, MASBAL2 is used to calculate the solution mass balance for Ba_T, and then, Ba^{2+} is calculated from Ba_T and Equation 4.23b.

4.5.5 Manganese Chemistry

Manganese will exist in the solid phase as MnO_2. It may also be coprecipitated with hydrous iron oxides. Manganese will exist in solution in one of three oxidation states:

Mn^{2+}, Mn^{3+} and Mn^{7+} (Baes and Mesmer, 1976). Mn^{2+} is the most stable aqueous oxidation state. Mn^{2+} is resistant to oxidation by air in both neutral and acidic solutions but, in basic solutions, $Mn(OH)_2(s)$ is more easily oxidized. The solid hydroxide is only slightly amphoteric.

For this work, the following chemistry was considered for manganese:

$$Mn^{2+} + H_2O = MnOH^+ + H^+ \qquad K = 10^{-10.59} \qquad (4.25a)$$

$$Mn^{2+} + H_2O = Mn(OH)_2(s) + 2H^+ \qquad K_{so} = 10^{-15.2} \qquad (4.25b)$$

$$Mn^{2+} + 1/2O_2(g) + H_2O = MnO_2(s) + 2H^+ \qquad K_{so} = 10^{-0.15} \qquad (4.25c)$$

Hydrolysis of Mn^{2+} is not important until the pH is greater than 10. Neither equilibrium reaction satisfactorily predicts the aqueous concentrations of Mn^{2+} expected in oxygenated tailings pore water. The first reaction ($Mn(OH)_2(s)$) predicts an equilibrium concentration in excess of 55,000 mg/L, while the second reaction predicts an equilibrium concentration of $2x10^{-5}$ mg/L for a dissolved oxygen level of 1 mg/L.

Accordingly, natural waters which are oxygenated but which contained "dissolved" Mn must have it present as a colloidal form which passes a 0.45 um filter, or it must be derived from a low redox zone and is undergoing slow oxidation from Mn^{2+} to MnO_2. Furthermore, as noted by Stumm and Morgan (1981), even under relatively clean, well-defined, laboratory conditions, pure MnO_2 does not form; rather, a solid phase forms which has a variable stoichometry from $MnO_{1.3}$ to MnO_2. The variable oxidation number results from incorporation of Mn(II) into the Mn(IV) lattice.

In this study, insufficient time was available to complete the redox model for all substances experiencing redox reactions. Accordingly, Equation 4.25c was assumed to be the governing equation for both oxidized (open system) zones and reduced (closed system) zones with the effective O_2 concentration (DO) assumed to be 1 mg/L for the open system and the effective O_2 concentration assumed to be 10^{-4} mg/L for the closed (non-oxygenated) system.

Thus, the chemical balance for Mn^{2+} is given by:

$$Mn_T = Mn^{2+}$$

and the solution concentration of Mn^{2+} is given by:

$$(Mn^{2+}) = \frac{(H^{+})^{2}}{XMNO2 \cdot (DO)} \tag{4.26}$$

where: XMNO2 $=10^{-1.5}$ and DO = $10^{-4.5}$M for the oxidized zone, and $10^{-9.1}$M for the reduced zone.

As with the above substances (Al, Fe, Pb, Ba), the mass balance is calculated using MASBAL1 in the presence of solid phase. In the absence of the solid phase, MASBAL2 is used to calculate the mass balance for Mn^{2+} and Mn_T (since Mn_T = Mn_2^{2+}). This was installed in the computer code as a hook, or location for optional addition of code if the Mn^{2+} concentrations can be predicted later with a more up-to-date model.

4.6 Toxic Elements (Ni, As)

The toxic elements, nickel and arsenic, are computed in subroutine MINOR. Nickel speciation is calculated in subroutine NISOLD in the case where $Ni(OH)_2(s)$ exists and in NISPEC when $Ni(OH)_2(s)$ does not exist. Adsorption is assumed to occur in both cases. In NISOLD, Ni^{2+} is set by the solid phase concentration while, in NISPEC, Ni is calculated as a function of the relative allocation of Ni among solution, complexation and adsorbed phase. Arsenic speciation is calculated assuming that adsorption is the only significant solid form of arsenic.

4.6.1 Nickel Model

The probable phases controlling nickel speciation have been evaluated in BEAK (1986). The two main solid phases appear to be $Ni(OH)_2(s)$ and $NiFe_2O_4$. A comparison of the equilibrium conditions with observed solution conditions for Key Lake data (see Figure 4.5) show that both solid phases have approximately the same equilibrium nickel concentrations for typical iron concentrations. This indicates that $Ni(OH)_2(s)$ can be used to estimate solid-solution behaviour controlling Ni^{2+}. However, because the field data also indicates that predicted Ni concentrations become too high at low pH values, other goechemical mechanisms may become important. A probable control is the role of adsorption.

FIGURE 4.5: TOTAL NICKEL CONCENTRATIONS AS A FUNCTION OF pH. NICKEL FERRITE AND NI(OH)$_2$ SOLID SOLUBILITY. DATA ARE FROM KEY LAKE (KNIGHT AND PIESOLD, 1985) (AFTER BEAK, 1986)

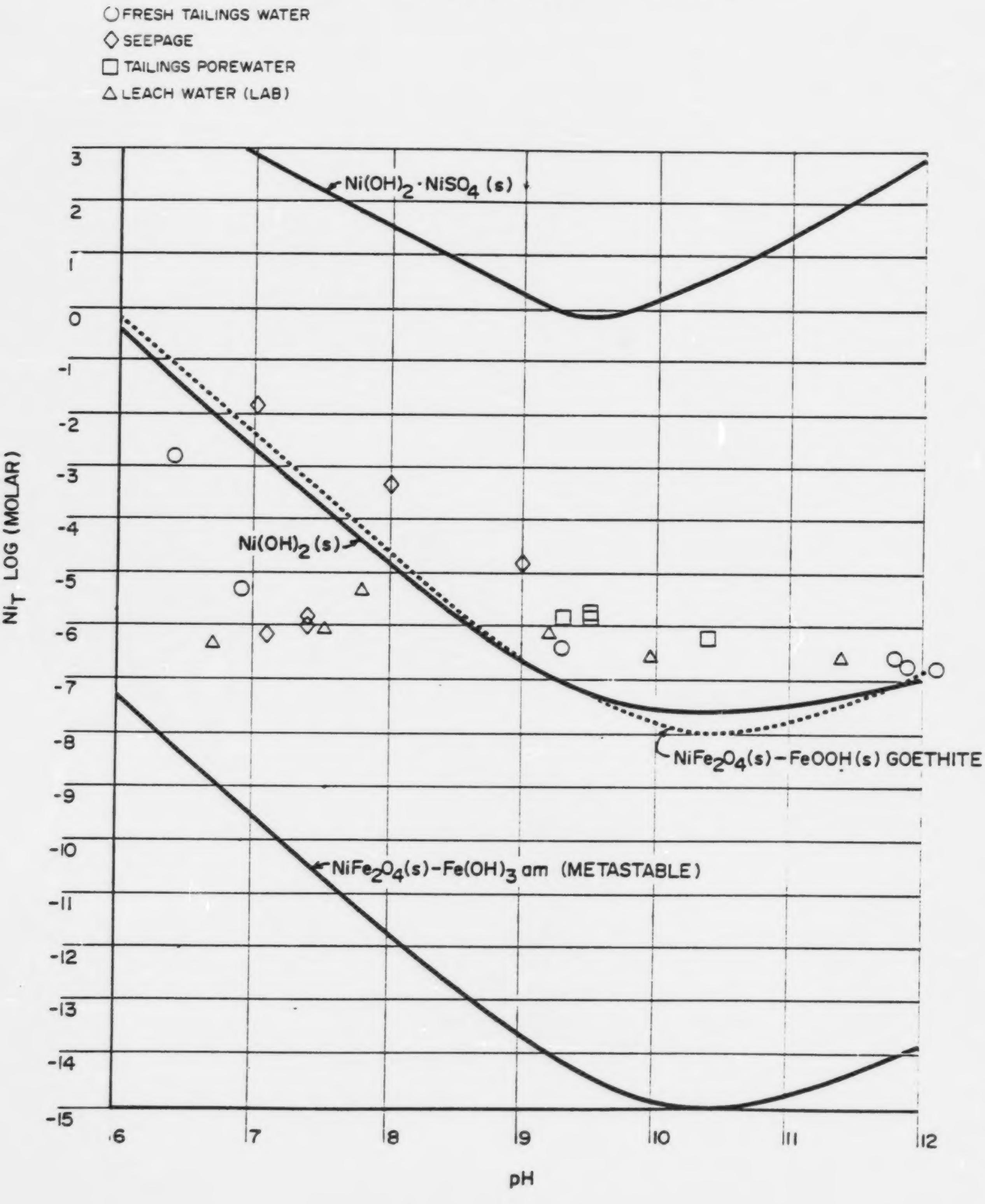

The following reactions are assumed to influence complexation and adsorption reactions for nickel:

$$
\begin{array}{llll}
B11 = 10^{2.32} & Ni^{2+} + SO_4{}^{2-} & = & NiSO_4 \qquad (4.27) \\
B12 = 10^{4.83} & Ni^{2+} + CO_3{}^{2-} & = & NiCO_3 \\
B13 = 10^{12.52} & Ni^{2+} + CO_3{}^{2-} + H^+ & = & NiHCO_3{}^+ \\
B14 = 10^{-9.86} & Ni^{2+} + H_2O & = & NiOH^+ + H^+ \\
B15 = 10^{-18.42} & Ni^{2+} + 2H_2O & = & Ni(OH)_2 + 2H^+ \\
B16 = 10^{-30.0} & Ni^{2+} + 3H_2O & = & Ni(OH)_3{}^- + 3H^+ \\
B17 = 10^{-6.0} & XOH + Ni^{2+} & = & XONi^+ + H^+ \\
B18 = 10^{+7.0} & XOH + H^+ & = & XOH_2^+ \\
B19 = 10^{-9.30} & XOH & = & XO^- + H^+
\end{array}
$$

Here, XO^- refers to the amount of sorbing surface for nickel (mol/L), and the complexation constants are defined by B11, B12.....B19.

If $Ni(OH)_2(s)$ exists, the following equations are used to evaluate nickel speciation:

$$(Ni^{2+}) = \frac{XNIOH2 * (H^+)^2}{f_{Ni^{2+}}} \qquad (4.28)$$

$CO3=1./(f_{CO3})*K1*K2/(H*(K1+H))*CT$

$C1=1+B11*(f_{SO4})^2SO4+(B12*(f_{CO3})^2+B13*(f_{CO3})^2/H)*CO3+$
$\quad B14*(f_{Ni})/(f_{NiOH})*H)+B15*(f_{Ni})/H^2+B16*(f_{Ni})/(f_{NiOH3})*H^3)$

$C2=B17/H$

$C3=B18*H+1.+B19/H$

$XOHO=XT/(C2*NI+C3)$

$NITT=NI*(C1+C2*XT/(C2*NI+C3)$

$NIADS=C2*NI*XOHO$

$NIT=C1*NI$

Here, (Ni^{2+}) or NI is the aqueous nickel concentration, NIT is the total aqueous concentration of nickel, NIADS is the total adsorbed nickel concentration (mol/L), and NITT is the total concentration of nickel in dissolved and adsorbed phases (mol/L).

The mass balance is calculated for $Ni(OH)_2(s)$ by performing a mass balance using MSBAL1 upon total solution complexes.

If $Ni(OH)_2$ does not exist, MSBAL1 is still used initially to calculate the mass balance but, in this case, the mass balance is performed upon the total inventory (NITT), including Ni^{2+}, solution complexes and the adsorbed phase. Thus, the equation is:

$$NITT_{(t+1)} = NITT_t + (\Sigma \text{In} - \Sigma \text{Out}) .dt \qquad (4.29)$$

The total inventory at t+1 is then redistributed among solution and adsorbed phases using the above equations defining CO3, C1, C2 and C3 and the following relationships:

```
D1=C1*C2                                        (4.30)
D2=C1*C3+C2*XT-NITT*C2
D3=NITT*C3
NI=(-D2+(D2**2+4*D1*D3)**0.5)/(2*D1)
XOHO=XT/(C2*NI+C3)
NIADS=C2*NI*XOHO
NIT=C1*NI
```

4.6.2 Arsenic Model

The probable solid phases controlling arsenic speciation have been evaluated in BEAK (1986). The relevant solid phases appear to be an adsorbed phase (probably onto FeOOH) and an equilibrium solid, calcium arsenate, which influences the solution composition only above pH 10. Another possible phase is $FeAsO_4$. Two solid phases for calcium arsenate, previously proposed by others, show a reasonable agreement for predicted solution concentrations with observed porewater concentrations (see Figure 4.6a). However, the thermodynamic data used for the phase controlling a neutral pH ($(CaO)_2 \cdot As_2O_5 \cdot 3H_2O$) appears erroneous; more up-to-date data show that the predicted concentration is over an order of magnitude higher, suggesting that this phase does not control observed pore water concentrations (BEAK, 1986). Adsorption is able to explain observed pore water concentrations in the neutral pH range. A diagram comparing predicted solution equilibrium for adsorption with observed values for Key Lake are given in Figure 4.6b.

FIGURE 4.6a: SOLUBILITY LIMITS OF TWO PROPOSED ARSENATE SOLIDS AS A FUNCTION OF pH. ARSENIC CONCENTRATION DATA ARE FROM KNIGHT AND PIESOLD (1985) (AFTER BEAK, 1986)

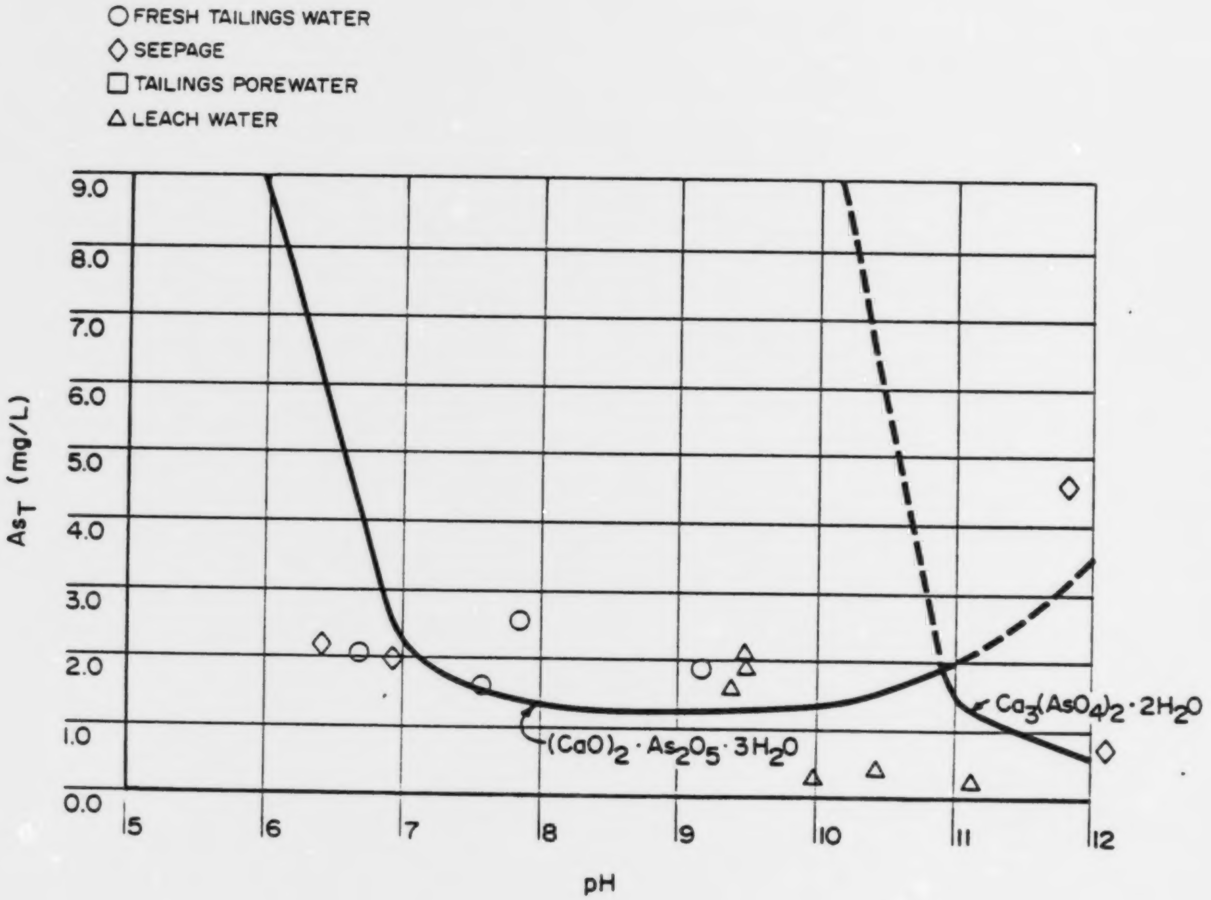

FIGURE 4.6b: ADSORPTION MODEL RESULTS FOR ARSENIC COMPARED TO KEY LAKE ARSENIC DATA. APPROPRIATE SURFACE SITE AND TOTAL AVAILABLE ARSENIC CONCENTRATIONS WERE USED AS INPUT PARAMETERS (AFTER BEAK, 1986)

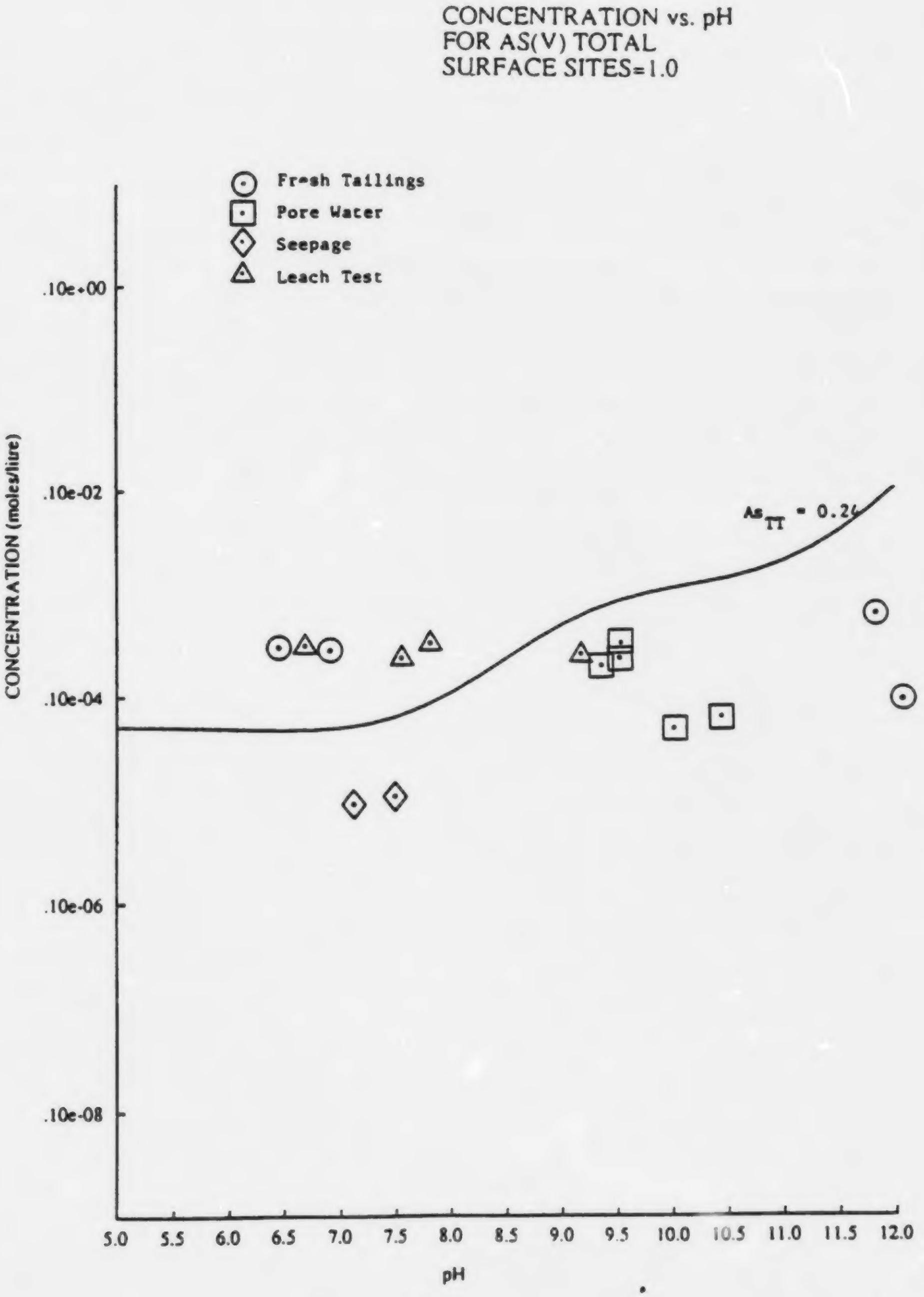

Because the open/closed model calculates that the pH is always in the neutral range for the management sceanrios evaluated in this work, it is assumed that solution complexes and an adsorbed phase are the main controls on arsenic concentration in the neutral pH range. Accordingly, a mass balance on the total inventory (ASTT) is first calculated using MSBAL1 and the equation:

$$\mathrm{ASTT}_{t+1} = \mathrm{ASTT}_t + (\Sigma \mathrm{In} - \Sigma \mathrm{Out})\, dt \tag{4.31}$$

where subscript t refers to time t and (t+1) to the new time step.

Then the inventory ASTT_{t+1} is redistributed assuming the following complexation and adsorption reactions:

$$\begin{aligned}
&3H^+ + As0_4{}^{3-} = H_3As0_4^0 && B1 = 10^{20.68}\\
&2H^+ + As0_4{}^{3-} = H_2As0_4{}^- && B2 = 10^{18.44}\\
&H^+ + As0_4{}^{3-} = HAs0_4{}^{2-} && B3 = 10^{11.5}\\
&XOH + 3H^+ + As0_4{}^{3-} = XH_2As0_4 + H_20 && B4 = 10^{30.7}\\
&XOH + 2H^+ + As0_4{}^{3-} = XHAs0_4{}^- + H_20 && B5 = 10^{24.4}\\
&XOH + H^+ + As0_4{}^{3-} = XAs0_4{}^{2-} + H_20 && B6 = 10^{15.2}\\
&XOH + 2H^+ + S04^{2-} = XHS0_4^0 + H_20 && B7 = 10^{10.6}\\
&XOH + H^+ + S04^{2-} = XS0_4{}^- + H_20 && B8 = 10^{6.2}\\
&XOH + H^+ = XOH_2{}^+ && B9 = 10^{7}\\
&XOH = XO^- + H^+ && B10 = 10^{9.3}
\end{aligned} \tag{4.32}$$

which give the following equations for distributing ASTT:

$$\begin{aligned}
&C1=B9*H+1+B10/H\\
&C2=H*B4+H^2*B5\\
&C3=(H^2*B7+H*B8)*(SO_4{}^{2-})\\
&C4=B1*H^3*f_{As}+B2*H^2*f_{As}/f_{H2ASO4}+B3*H*f_{As}/f_{HAS04}+1\\
&C5=H*B4+H^2*B5\\
&D1=C2*C4\\
&D2=C1*C4+C3*C4+C5*XT-C2*ASTT\\
&D3=AST*(C11*C3)\\
&AS04=(-D2+(D2**2+4*D1*D3))/(2.*D1)
\end{aligned} \tag{4.33}$$

```
XOHO=(AST/AS04-C4)/C5
ASADS=C5*XOHO*AS04
```

4.7 Coprecipitate Control Upon Radioactive Elements

4.7.1 Elements Controlled by Coprecipitation

All the radioactive elements, with the exception of uranium, in the U-238 decay series are considered to be controlled by coprecipitation for this modelling project. The rationale is given in Sections 4.8 to 4.12. Th-230 is assumed to be controlled by MnO_2 and $Fe(OH)_3$. Ra-226 is assumed to be controlled by $BaSO_4$, $PbSO_4$ and gypsum. Pb-210 is assumed to be controlled by $PbSO_4$.

Coprecipitation is modelled analogous to an ion-exchange, adsorption type reaction. It may be viewed as a reversible adsorption reaction with a much higher capacity for taking an element into a solid phase than normal adsorption. Due to the influence by another solid phase, the kinetics of exchange may be quite slow, meaning that the solid-solution relationship may be near to or far from equilibrium.

4.7.2 Relevant Aspects of Coprecipitation Theory

A review of the theory of coprecipitation and other similar mechanisms (codeposition, entrapment) is summarized in Snodgrass and Hileman (1985) in general terms and, in particular, for barium (radium) sulphate. This review is summarized in this section. The work is amplified by more recent work (Riese, 1983; Langmuir and Riese, 1985).

The chemistry of coprecipitation involves formation of the host solid (precipitate) and the entrapment of the "trace" element within the parent solid. A coprecipitate will form when the solution is undersaturated with respect to the trace element but supersaturated with respect to the host mineral and where the host mineral (crystal) has an affinity for the trace element. Hence, the necessary conditions to form a coprecipitate are that the aqueous solution be supersaturated with respect to the host cyrstal, and that the thermodynamics and kinetics of coprecipitation be feasible. This means that an element which is involved in coprecipitation shows a correlation with the cation of the host crystal when the host crystal dissolves.

Some of the first fundamental work on nucleation and crystal growth was conducted on barium sulfate (Nelsen, 1957, 1958, 1961, 1967; Peters et al., 1966, 1968, 1969). Some of the first fundamental work on coprecipitation theory was conducted on barium-radium sulphate (Gordon and Rowley, 1957; Gordon et al., 1959). This has resulted in the crystal growth theory for (Ba, Ra)SO_4 being fairly well developed. More recently, work has centred on extending the theory for coprecipitation to other sparingly soluble salts, and to oxides, hydroxides and sulphides of various cations.

Two principal theories have evolved: The Berthelot-Nernst theory also called the Henderson-Kraczek theory (O'Nions and Powell, 1977), and the Doerner-Hoskins (1925) theory. The Berthelot-Nernst theory is also known as the homogeneous (D) distribution law while the Doerner-Hoskins theory is also called the logarithmic (or lambda: λ) distribution law.

The homogeneous (D) distribution law is applicable to equilibrium reactions. The logarithmic (λ) distribution law is applicable to reactions not at equilibrium.

Under equilibrium conditions, it is assumed that the whole crystal is at equilibrium with the solution composition. This means that the trace element is homogeneously distributed throughout the whole crystal.

Under kinetic conditions, only the surface layer of the crystal is at equilibrium with the solution. Thus, the crystal has a layered distribution with each layer having its own concentration of the trace element. This layer distribution is often described by analogy to an onion with each "onion ring" having a different trace element composition. This ringed structure can form in a batch reactor where precipitation of the host crystal is initially rapid and then becomes progressively slower due to lower degrees of supersaturation over time. A ringed structure may also result in leaching tanks in series in which dissolution of barium from its host mineral and of Ra-226 from the uranium-containing minerals progress at different rates.

The D and "lamda" models are derived mathematically as follows. For the crystal-solution reaction:

$$A^{n+} + MX = M^{n+} + AX \tag{4.34}$$

Here		
	A^{n+}	is the trace element cation undergoing coprecipitation
	M^{n+}	is the parent cation in the crystal (like charge to A)
	X	is the anionic component of the crystal
	MX	is the parent crystal
	AX	is the resultant mixed crystal (containing A in MX)

For coprecipitation of Ra with Ba, the reaction becomes:

$$Ra^{2+} + BaSO_4(s) = RaSO_4(s) + Ba^{2+} \tag{4.35}$$

For coprecipitation of Ra with Pb, the reaction is written as:

$$Ra^{2+} + PbSO_4(s) = RaSO_4(s) + Pb^{2+} \tag{4.36}$$

In both cases, $RaSO_4(s)$ refers to the (Me, Ra) SO_4 mixed crystal solid as opposed to a radium sulfate solid. "Me" in the formula, (Me, Ra) SO_4, refers to Ba or to Pb.

In general form, the reaction of radium with any host crystal of a divalent cation (MX) to form a mixed crystal (RaX) is written as:

$$Ra^{2+} + MX = M^{2+} + RaX \tag{4.37}$$

The value of D is given by

$$D = \frac{\dfrac{N_{RaX}}{N_{MX}}}{\dfrac{(mRa^{2+})}{(mM^{2+})}} \tag{4.38}$$

Here N_{RaX} and N_{MX} are, respectively, the molal fractions of radium and the parent cation in solid solution and (mRa^{2+}) and (mM^{2+}) are the molal aqueous concentrations of radium and the parent metal cation in solution.

The Doerner Hoskins (kinetic) coefficient, λ, is given by:

$$\lambda = \frac{\log \left[\frac{mRa_i^{2+}}{mRa_f^{2+}} \right]}{\log \left[\frac{mM_i^{2+}}{mM_f^{2+}} \right]} \tag{4.39}$$

Here, the subscripts "i" and "f" refer to the initial and final solution concentrations respectively of radium and the metal ion M.

At present, there is no apriori method to predict whether equilibrium or kinetic conditions will be exhibited by the system. One can direct the system towards a given distribution by the method used to force precipitation in the laboratory. Recently, thermodynamic data for predicting D values have been developed for Ra-226. The data provide an estimate of equilibrium conditions for Ra-226 and are used for calculating the coprecipitation model used for Ra-226 in this project. For Th-230, Pb-210 and Po-210, a coprecipitation model is used to explain their solid-solution behaviour, but literature data are not available to adequately define model parameters. This necessitates hypothesizing values for model calibration.

4.8 Uranium Model

Uranium is found in ore as U(IV) in such minerals as uraninite (UO_2), pitchblende (UO_2), brannerite (UTi_2O_6) and as U(V) and U(VI) in other minerals. Brannerite is rare in Saskatchewan except at Beaverlodge. Leaching by acidic or basic solutions dissolves the mineral and brings most of the uranium into solution from which it is later extracted. Residual uranium in the tailings is in the form of the unleached uranium minerals and precipitated or coprecipitated forms taken out of tailings solution by neutralization procedures.

In this study, it is assumed that sulphuric acid is the main leaching agent and that lime and/or limestone are the main neutralization agents. Accordingly, hydroxyl, sulphate and carbonate ions will form the main complexes with uranyl ion (UO_2^{2+}), the main ionic form of uranium under oxidizing conditions. Other possible ions of importance are fluoride and phosphate, depending upon their concentration.

4.8.1 Summary of Uranium Chemistry during Milling

Since the solution, concentration and purification processes (ion exchange, solid liquid separation) are not 100% efficient, some uranium enters the tailings area. The main uranium species formed during the acid leach process include:

UO_2^{2+}, UO_2SO_4, $UO_2(SO_4)_2^{2-}$ and $UO_2(SO_4)_3^{4-}$

Other possible species of importance are hydroxyl and carbonate forms. Speciation diagrams are given in Figure 4.7 for these complexes for specific conditions given in the figure title.

The predominant species in acidic solution is $UO_2\ (SO_4)_3^{4-}$. This species is extracted by ion exchange from the aqueous solution. The concentration of this species in tailings will be dependent upon the efficiency of the column. Assuming 100% efficiency, then $UO_2(SO_4)_3^{4-}$ does not reach the tailings area.

The other sulphate species, UO_2SO_4 and $UO_2(SO_4)_2^{2-}$, will be present in minor amounts in the liquid solution due to the reactions equilibrium (as governed by equilibrium constants) which form:

$$UO_2^{2+} + SO_4^{2-} = UO_2SO_4 \overset{+\,SO_4^{2-}}{=} UO_2(SO_4)_2^{2-} \overset{+\,SO_4^{2-}}{=} UO_2(SO_4)_3^{4-} \qquad (4.40)$$

These species will be minor contributors of uranium to the tailings.

The only uranyl species of major importance reaching the tailings area will probably be UO_2^{2+} in association with gypsum. This association can either be as a result of coprecipitation and/or adsorption.

The formation of other uranium complexes, such as:

$UO_2(CO_3)_3^{4-}$, UO_2CO_3, $UO_2(HPO_4)_2^{2-}$ and $(UO_2)_3(OH)_5^{+}$

FIGURE 4.7a: DISTRIBUTION OF URANYL-HYDROXY AND SULPHATE COMPLEXES VERSUS pH AT 25°C WITH TOTAL U = 10^{-8}M, TOTAL SO_4 = 10^{-3}M (100 PPM).

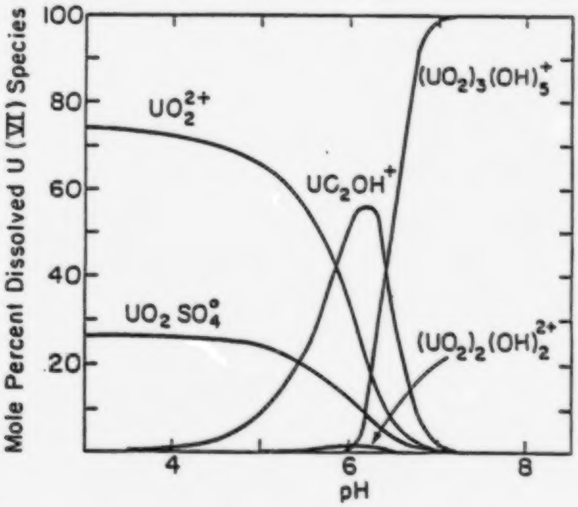

FIGURE 4.7b: DISTRIBUTION OF URANYL-HYDROXY AND CARBONATE COMPLEXES VERSUS pH AT 25°C WITH P_{CO2} = 10^{-2}ATM, TOTAL U = 1^{-8}M.

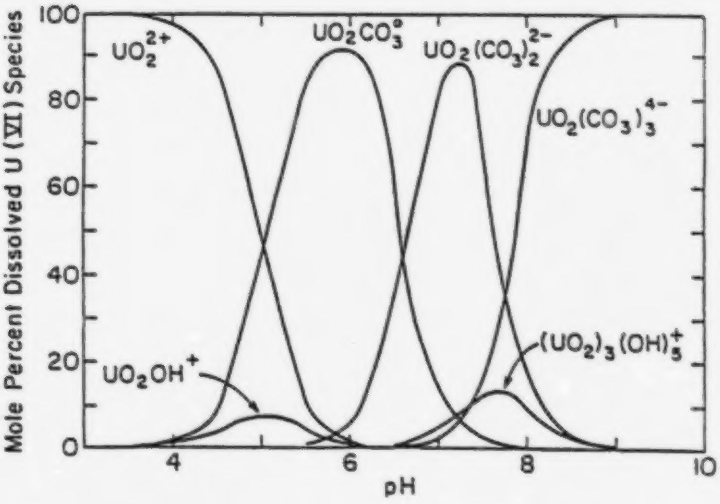

is possible but, because of the low concentrations of ionic species, their formation is likely to be insignificant.

The major uranous species will be contained, as a solid phase, in residual uranium minerals that were not not leached in the mill.

4.8.2 Chemical Model Used for Uranium

It is assumed that the main form of uranium reporting to the tailings after milling is the residual, unleached uranium mineral. This uranium mineral is modelled as UO_2. It is assumed that the amount of uranium coprecipitated in gypsum is small. Because distribution coefficient data for the coprecipitation of uranyl ion in gypsum is not available, this form is neglected for purposes of this project.

A definitional sketch of pathways affecting dissolved uranium concentrations is given in Figure 4.3. Assuming that UO_2 decays according to first order kinetics, and that it adsorbs with a weak distribution coefficient which can be modelled with respect to total dissolved uranium, a mass balance on the solution phase gives:

$$V_w(1+T) \frac{dCT_{i,k}}{dt} = (\Sigma Q_{IN} \cdot C_{IN} - CT \; \Sigma Q_o) + K \cdot UO_2 \cdot V \cdot RHO_T \qquad (4.41)$$

where:

$CT_{i,k}$ is the total aqueous concentration of uranium ($mol \cdot m^{-3}$),

V_w is the pore water volume (m^3),

T is a function of the distribution coefficient,

V is total volume (m^3),

Q_{IN} and Q_o are generic symbols for inflow and outflow pathways ($m^3 \cdot a^{-1}$)

C_{IN} and CT are generic symbols for concentrations associated with all inflow and outflow pathways ($mol \cdot m^{-3}$),

K is the dissolution rate constant (a^{-1}),

UO_2 is the mass of solid phase uranium per unit tailings ($mol \cdot g^{-1}$ tailings), and

RHO_T is the dry bulk density ($g \cdot m^{-3}$).

This has a mathematical solution of:

$$CT_{i,k/t+1} = \frac{B}{ALP}\,(1-\exp(-ALP\cdot delt)) + CT_{i,k/t}\,\exp(-ALP\cdot delt) \qquad (4.42)$$

where: $CT_{i,k/t+1}$ = the aqueous concentration of uranium at time t+1

$a = V_w\,(1+T)$

$T = K_D\dfrac{SURF}{POR}$

$ALP = \dfrac{QD_{i+1} + QO_i + QU_i}{a}$

$B = \dfrac{QI_i\,CIN_{i,k} + QD_i\,CT_{i-1,k} + QU_{i+1}B_i + K\ \ UO_2\ \ V\cdot RHO_T}{a}$

delt = time step (a)

4.8.3 Analysis of Mathematical Solution for Uranium Model

The solution to Equation 4.41 is made, assuming that the fluxes from adjoining boxes are constant for the time period, but that the concentration in a particular box changes with time. This presents a potential numerical discretization error because the concentrations in adjoining boxes and hence the fluxes into box i are changing slowly with time.

A similar numerical discretization error also occurs for the other equations given above for substances such as Ni, As, etc. There, the analogous mathematical solution using MSBAL1 for Equation 4.42 has the form:

$$V_w(1+T)\,CT_{i,k/t+1} = V_w\,(1+T)\,CT_{i,k/t} + (\Sigma Q_{IN}C_{IN} - CT_{i,k/t}\Sigma Q_o + K\,(UO_2)V)(delt) \qquad (4.43)$$

An analysis of whether Equations 4.42 or 4.43 is the more appropriate form of mathematical solution of Equation 4.41 awaits future work. In actuality, either approach should give a valid solution. In this study, the numerical discretization error is minimized by using sufficiently short time steps.

4.9 Thorium-230 Model

4.9.1 Chemistry of Th-230 During Milling

The chemistry of thorium-230 in northern Saskatchewan tailings appears to be controlled by different mechanisms than are typical of Elliot Lake tailings. Characteristics of Elliot Lake tailings (BEAK, 1985; SENES, 1985) suggest that the chemistry of Th-230 is controlled by the chemistry of Th-232, because Th-232 has the largest mass of all thorium isotopes and is present in large quantities. The thorium (Th-232) is present mainly in monazite (Ca, Y, La, Th) (PO_4). Monazite is weakly attacked in the acid leach circuit. Thorium liberated from uranium minerals, such as brannerite, uranothorite and uranothorianite, accounts for the remainder of the thorium-232 in solution during the acid leach. Th-230 is accounted for almost exclusively from the dissolution of uranium-containing minerals.

In the generic Saskatchewan ore, the total thorium content (Th-232) is quite small (about 0.0006%). On a mass basis, the ratio of Th-230 to Th-232 is about 1:17. The amount of thorium-232 which would dissolve in acid leaching tanks is unclear.

During milling, the pH of the acid leach (about pH = 1) ensures that all of the thorium extracted can be considered to be in the Th^{4+} state. Hydrolysis of Th^{4+} is negligible below pH 3. The equilibrium constants for the mononuclear hydrolysis products at 25°C are as follows:

$$\begin{aligned}
Th^{4+} + H_2O &= ThOH^{3+} + H^+ & pK &= 4.12 \\
Th^{4+} + 2H_2O &= Th(OH)_2^{2+} + 2H^+ & pK &= 7.81 \\
Th^{4+} + 3H_2O &= Th(OH)_3^{+} + 3H^+ & pK &= 12.70 \\
Th^{4+} + 4H_2O &= Th(OH)_4^{0} + 4H^+ & pK &= 17.40
\end{aligned} \qquad (4.44)$$

A high H^+ activity (low pH) will drive the reaction to the left. Therefore, any significant formation of a solid phase of $Th(OH)_4$ will only occur upon neutralization. Figures 4.9 and 4.10 show the distribution of thorium in solution.

FIGURE 4.8: THE STABILITY OF SULPHUR SPECIES IN SOLUTION (FROM GARRELS & CHRIST, 1965)

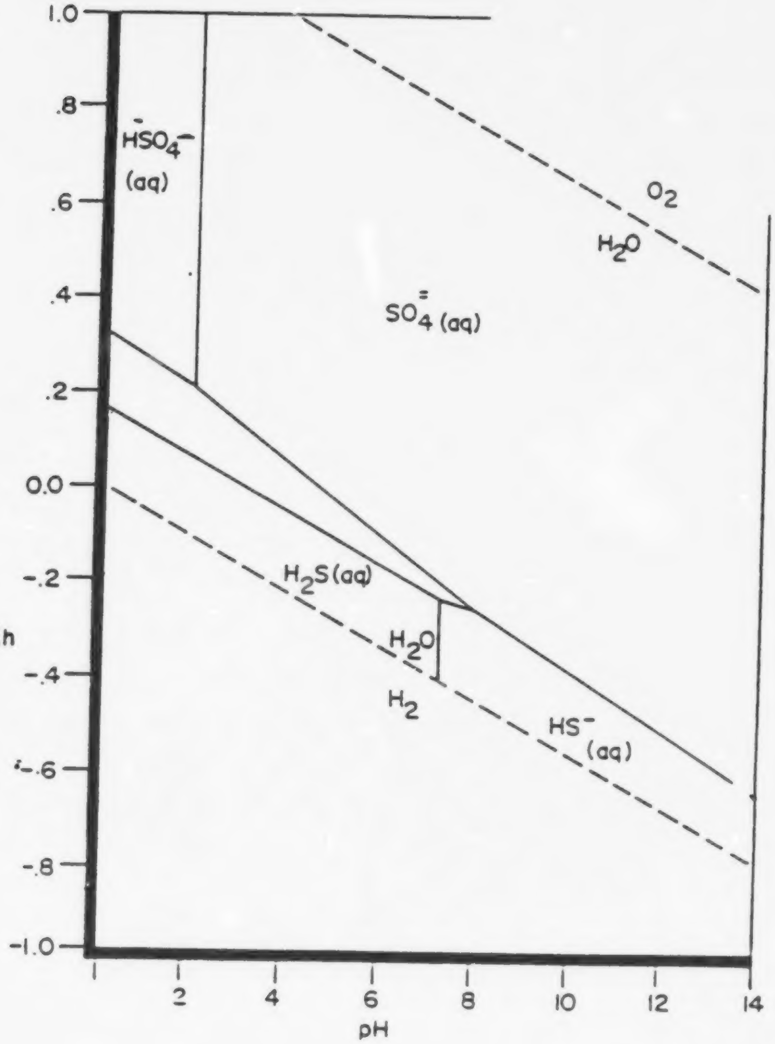

FIGURE 4.9: THE DISTRIBUTION OF THORIUM HYDROXIDE IN THE ABSENCE OF SULPHATE CONCENTRATIONS

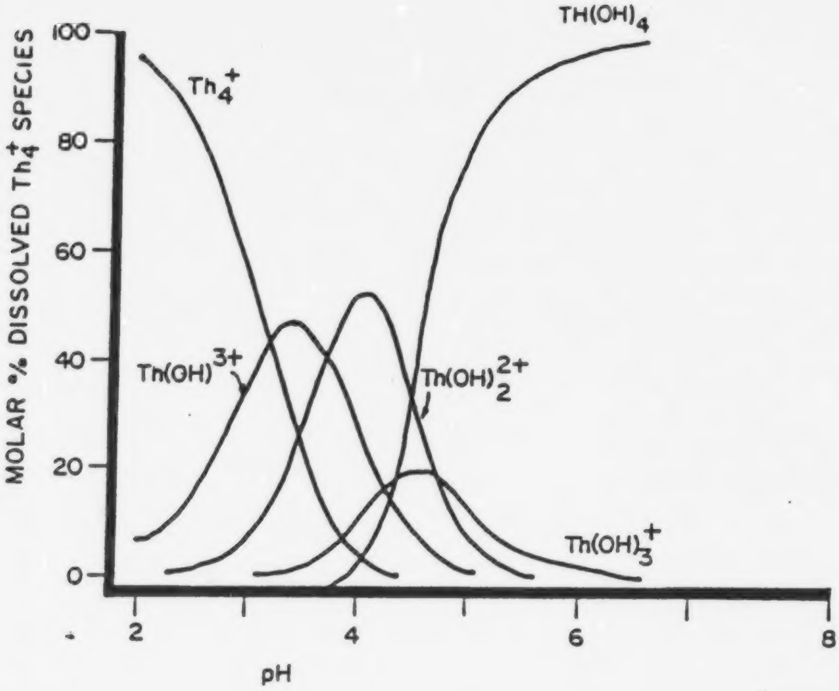

FIGURE 4.10: THE DISTRIBUTION OF THORIUM SULPHATES AND HYDROXIDES AT pH 2-8

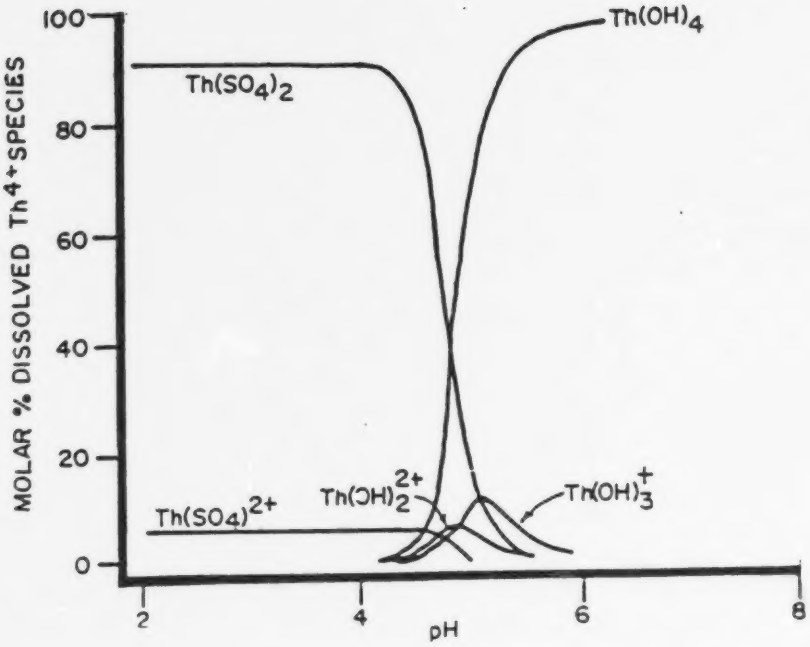

Sulphuric acid, because of its diabasic nature:

$$\begin{array}{lll} H_2SO_4 = H^+ + HSO_4^- & K_1 = 10^3 & (4.45) \\ HSO_4^- = H^+ + SO_4^{2-} & K_2 = 1.26\times10^{-2} & \end{array}$$

will play a role in the chemistry of thorium. At high acid concentrations (acid leach), the bisulphate ion (HSO_4^-) is the main anionic species present (Figure 4.8), and the formation of the $Th(SO_4)_2$ complex is not possible. At low acid concentrations (partial neutralization), the sulphate ion (SO_4^{2-}) becomes more predominant, therefore, the complex $Th(SO_4)_2$ will form. The stability of $Th(SO_4)_2$ decreases with increasing pH (Figure 4.10), leading to the formation of $Th(OH)_4(s)$.

After leaching, the tailings are neutralized and uranium is extracted. Because leaching liquor data for Th-230 on Th-232 Saskatchewan mills are not available to us, it is unclear whether sufficient Th is present in solution to precipitate thorium as thorium hydroxide.

4.9.2 Chemical Model Used for Th-230

Alternate Solid Phases

It is plausible that Th-230 will precipitate as $Th(OH)_4(s)$ or be coprecipitated in the mill. Plausible parent crystals for coprecipitation of Th-230 include gypsum, iron and aluminum hydroxide, manganese dioxide, and thorium hydroxide. Due to observations that Th-230 is removed by coprecipitation reactions with manganese dioxide (containing an iron phase) in Gunnar surface water, it is assumed that Th-230 is coprecipitated with iron hydroxide and manganese in the tailings.

An analysis of tailings pore water data readily available to BEAK has been made using equilibrium chemistry concepts. The two data sets are Gunnar pore water data and Lacnor pore water data. An analysis of available solubility constants for thorium hydroxide phases has also been made. The data are given in Table 4.5.

The aqueous concentration of thorium is plotted in Figure 4.11 as a function of pH for thorianite, the most insoluble phase of thorium (Langmuir and Herman, 1980). The plots indicate that thorium solubility is affected by organic complexes below pH 6.5.

TABLE 4.5: SOLUBILITY CONSTANT FOR THORIUM PHASE

Phase	Phase Name	Reaction Form	Solubility Constant	Reference
am-$Th(OH)_4(s)$	Amorphorus thorium hydroxide	-	?	-
$Th(OH)_4(s)$	not specifically given	Reaction 1 Reaction 2	log K = 9.4 log K = -46.6	Langmuir and Herman (1980) quoting Baes and Mesmer
-	Amorphorus thorium hydroxide	Reaction 1	log K = 6.3	SENES (1985)
ThO_2(act)	Active oxide	Reaction 3 Reaction 1	log K = -6.32 log K = 9.58	Baes and Mesmer (1976)
ThO_2(c)	Name not specifically given	Reaction 1 Reaction 2	log K = 6.3 log K = -49.7	Langmuir and Herman (1980) quoting Baes and Mesmer
ThO_2(c)	Well crystallized oxide	Reaction 3 Equation Rxn 1	log K = -9.6 log K = 6.3	Baes and Mesmer (1976)
ThO_2(th)	Thorianite	Reaction 1 Reaction 2	log K = 1.8 log K = -54.2	Langmuir and Herman (1980)
ThO_2	Completely insoluble (crystalline) thorium	Reaction 1	log K = 1.78	SENES (1985)

Notes:

1. Reaction 1: $ThO_2(s) + 4H^+ = Th^{4+} + 2H_2O$
   Reaction 2: $ThO_2(s) + 2H_2O = Th^{4+} + 4OH^-$
   Reaction 3: $ThO_2(s) + 2H_2O = Th(OH)_4(aq)$
2. Solubility Product Relationships:

   Rxn 1 (logK) = Rxn 2 (logK) - 56
   Rxn 3 (logK) = Rxn 1 (logK) - 15.9

FIGURE 4.11: THORIUM SOLUBILITY AS A FUNCTION OF pH (FROM LANGMUIR AND HERMAN,1980)

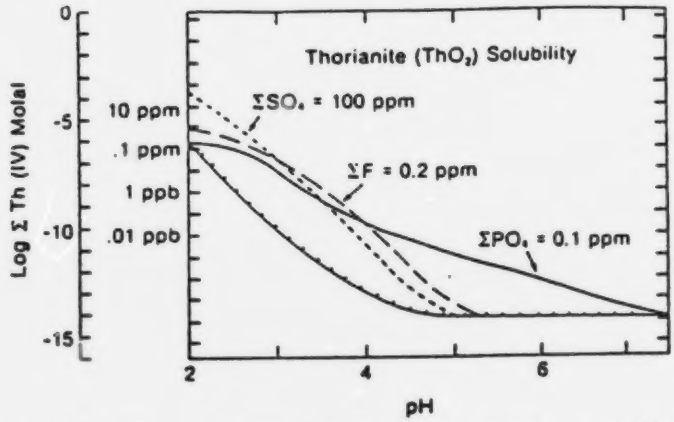

The effect of thorium–sulfate, fluoride and phosphate complexing on the solubility of thorianite, ThO$_2$(c), as a function of pH at 25°C. The cross-hatched curve denotes the solubility of thorianite in pure water. The curves indicating thorianite solubility as affected by complexing have been constructed assuming each ligand present in the absence of the others.

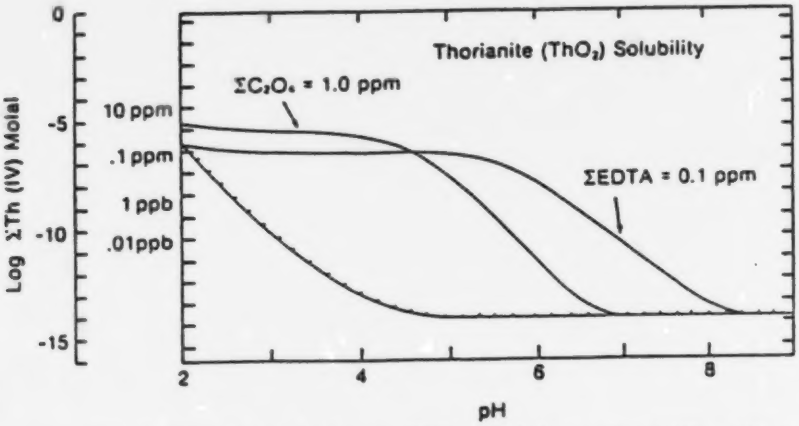

The effect of thorium-oxalate vs thorium–EDTA complexing on the solubility of thorianite, ThO$_2$(c), as a function of pH at 25°C. The cross-hatched curve denotes the solubility of thorianite in pure water. The curves indicating thorianite solubility as affected by complexing have been constructed assuming each ligand present in the absence of the other.

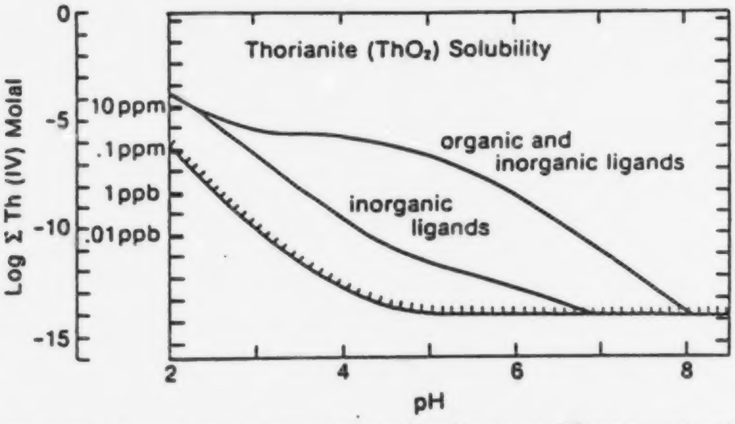

The effect of thorium complexing on the solubility of thorianite. ThO$_2$(c) vs pH at 25°C in a solution of ΣCl = 10 ppm, ΣNO$_3$ = 2.5 ppm, ΣSO$_4$ = 100 ppm, ΣF = 0.3 ppm, ΣPO$_4$ = 0.1 ppm, Σoxalate = 1 ppm, Σcitrate = 0.1 ppm and ΣEDTA = 0.1 ppm.

Assuming that the tailings do not have organics with substantial amounts of EDTA analogues, the solubility-controlled concentration of thorium will be relatively independent of pH above pH = 6.

Figures which give similar solubility curves as Figure 4.11 have not been made for the other thorium phases. However, the conclusion that solubility is relatively independent of pH above pH = 6 is valid for these phases.

The various solid phase data and the terminology used to describe them are summarized in Table 4.5. Combining the terminology of Baes and Mesmer (1976) and that of Langmuir and Herman (1980) results in three possible phases:

- active oxide (terminology by Baes and Mesmer) which is the most soluble phase and presumed to be amorphorus thorium hydroxide (based upon Langmuir and Herman's terminology);
- well-crystallized oxide (terminology by Baes and Mesmer); and
- thorianite phase (terminology by Langmuir and Herman) which is least soluble.

Use of the terminology is somewhat different from that of SENES (1985) who label the "well-crystallized oxide" as "an amorphorus phase".

Langmuir and Herman (1980) note that the full range of log K values (7.6 log units separating the amorphorus and crystalline Th oxides and hydroxides) is "perfectly possible for a quadravalent cation such as Th^{4+}".

Analyses of Gunnar tailings data for thorium solubility is not possible because stable thorium was below the detection limit and measurements of radiological Th-232 was not made because of its low values. Analysis of Lacnor data suggests that pore water concentrations of Th-232 are approximately at equilibrium with a solid phase whose solubility constant is of the order of log K = 6.3 (Reaction 1). The measured concentrations are for acidic solutions (pH ca 3). Hence, it is possible that a different phase may be stable at neutral pH. But, because much of the thorium-232 in Lacnor tailings was originally in a monazite phase, it is plausible that the thorium phase present results from mill-induced (and/or acidic tailings-induced) dissolution of monazite and its precipitation as crystalline $ThO_2(c)$.

An analysis was made of the possibility that Th-230 itself or in combination with Th-232 could form a solid phase which would control thorium-230 activity in the pore water. For 2% UO_2 and complete dissolution of Th-230 into the pore water, the resultant pore water concentration is approximately $4x10^{-6}$M. For the three phases, the solubility limit at neutral pH is approximately $5x10^{-7}$M ($8x10^4$ Bq/L) for the active oxide; $2x10^{-10}$M (40 Bq/L) for the well-crystallized solid and $5x10^{-15}$M (0.001 Bq/L) for the thorianite phase. Hence, it is possible that there is sufficient Th-230 present to form a thorium solid phase.

With respect to stable thorium, the global abundance of thorium in soils is 0.0005%, while the abundance in Cluff Lake ore is of the order of 0.0006%. Assuming that 10% of either source material is dissolved in the leaching pachucas results in approximately $2x10^{-9}$ mol Th-232/g dissolving. This is of a similar magnitude to the Th-230 content of the ore ($1.5x10^{-9}$ mol Th-230/g solids), suggesting that both Th-230 and Th-232 could be involved in solid phase formation.

With respect to coprecipitation, it is plausible that Th-230 might coprecipitate with gypsum or barium sulphate. Barium sulphate is used as a precipitating solid for concentrating and purifying Th-230 for alpha spectrometry (e.g., Burk and Wiles, 1983) and also takes down other ions from solution (Mattioli and Wiles, 1985). In the case of potassium and Fe^{3+}, Mattioli and Wiles (1985) interpret their data to indicate that K coprecipitates with barium sulphate, but that Fe^{3+} either adsorbs or is occluded with the solid phase. With respect to gypsum, a calculation indicates that the distribution of thorium-230 in gypsum (0.25 g gypsum/g tailings) has a distribution coefficient D_{ThCa} of the order of 200 for the relationship:

$$N_{ThCa} = D_{ThCa} \frac{(\text{Th-230})}{(Ca^{2+})} \qquad (4.46)$$

where: N_{ThCa} is the solid phase ratio of thorium in gypsum, and
D_{ThCa} is the distribution coefficient.

This relationship assumes that Th-230 is controlled by coprecipitation with gypsum and that the pore water concentration of Th-230 is 1 Bq/L and calcium is 600 mg/L. The calculation assumes that the distribution law is expressed with respect to $Th(OH)_4^o$ as opposed to with respect to Th^{4+}. However, if the distribution law is expressed with respect to Th^{4+}, the distribution coefficient increases accordingly.

Observations upon Gunnar data indicate that the seepage water from the main tailings area form a precipitate after being allowed to stand for several hours. The precipitate removes most of the Th-230 from solution and is composed mainly of manganese and iron hydroxide. Whether the precipitate is amorphorus or crystalline is unclear.

For this work, the observation upon the Gunnar surface stream is used as a basis for a hypothesis that Th-230 is controlled by coprecipitation with iron hydroxide and manganese oxide. Some further justification for this hypothesis could be sought by considering the ability of thorium (IV) hydroxide to coprecipitate with iron (III) hydroxide and manganese (IV) oxide.

Model for Thorium-230

Solid solution interactions are modelled using a distribution law for Th^{4+} in iron hydroxide and manganese oxide. It is:

$$\frac{(Th_s)}{(Th^{4+})} = D_{ThFe}\frac{(FeOOH)}{(Fe^{3+})} + D_{ThMn}\frac{(MnO_2)}{(Mn^{2+})} \qquad (4.47)$$

Here, (Th^{4+}), (Fe^{3+}) and (Mn^{2+}) are the solution concentrations of thorium-230, Fe^{3+} and Mn^{2+} in solution; (Th_s), $(FeOOH)$ and (MnO_2) are the solid phase concentrations of Th-230, iron in goethite and manganese in MnO_2; and D_{ThFe} and D_{ThMn} are the distribution coefficients of Th-230 in goethite and MnO_2 respectively.

In addition, solution complexes considered include the four hydroxl species of thorium and the two sulphate species of sulphate. Also, Th-230 radiological decay is considered.

The iron chemical module is used to predict the solid solution concentration of iron. However, the manganese chemistry module is incomplete at the time of writing because the redox model has not been completed and the Mn solid phase mass balance has not been completed. For purposes of evaluation, MnO_2 is assumed to have a constant value of 0.01 mol/m^3 and Mn^{2+} is assumed to be redox zone specific with values given above (Section 4.5) being used.

For model calibration, the complexation constants are set. The distribution coefficients, D_{ThFe} and D_{ThMn} are hypothesized to have values of one with a triangular distribution representing the frequency distribution.

4.10 Radium

4.10.1 Chemistry of Radium

Radium has a relatively simple chemistry. Only the divalent state is known. Insoluble inorganic radium compounds include the sulphate and carbonate. Radium is dissolved in the acid leach. It likely reacts with sulphate ions, precipitates as colloidal complexes and/or adsorbs onto the finely powdered tailings gangue. Most of the radium is associated with the fine (less than 200 mesh) fraction.

A potential control for radium in the mill leaching circuit or in tailings is the mineral jarosite. Compounds take the general form $MFe_3(SO_4)_2(OH)_6$, where M is:

$$H_3O^+, Na^+, K^+, Rb^+, Ag^+, NH_4{}^+, Tl^+, Pb^{2+}, Ca^{2+}, Sn^{2+}, Ba^{2+} \text{ or } Hg^{2+}.$$

Jarosite precipitation occurs in strongly acidic media. The mill circuit at pH = 1 provides ideal conditions for the precipitation reaction. Data are not yet available to indicate whether the radium is cationically substituted within the jarosite, or whether ionic radium and colloidal radium sulphate are coprecipitated with, or absorbed onto, this mineral. It is conceivable that cationic radium is substituted within the jarosite. The framework formed by $(Fe(OH)_2)_3\ (SO_4)_2$ in jarosites permits the substitution of an M atom, by elements of different crystallochemical properties. Ionic radii of M ions approaching a difference of 50% have been reported. For example:

$$\text{for } Na^+,\ r = 0.95\ \text{Å and for } Rb^+,\ r = 1.46\ \text{Å}$$

It is probable that in jarosite containing a divalent cation M, every second M position in the crystal lattice is vacant.

The main control for Ra-226 in the leaching circuit appears to be its coprecipitation with barium sulphate, lead sulphate and/or a barium-lead sulphate phase.

During the neutralization raction of the mill effluent with lime, the precipitation of gypsum ($CaSO_4 \cdot 2H_2O$) occurs. The radium could:

- substitute cationically within the gypsum lattice;
- coprecipitate in the ionic and/or colloidal sulphate form; or
- adsorb onto the gypsum.

4.10.2 Derivation of Radium Model

Radium is in solution both as an ion (Ra^{2+}) and as a sulphate complex ($RaSO_4^{\,0}$), and in a solid phase. The solid phase form is as a coprecipitate distributed among gypsum, anglesite ($PbSO_4$) and barite ($BaSO_4$).

For radium as a coprecipitate in a mixed metal sulphate, the overall reaction can be written in a generic fashion as:

$$Ra^{2+} + MX = M^{2+} + RaX \qquad (4.48)$$

Here	Ra^{2+}	is the radium cation undergoing coprecipitation
	M^{2+}	is the parent cation in the crystal (like charge to Ra)
	X	is the parent anion in the crystal
	MX	is the parent crystal
	RaX	is the resultant mixed crystal (containing Ra in MX)

The equilibrium distribution coefficient D for (Ba, Ra) $SO_4(s)$ is given by:

$$D = \frac{\dfrac{N_{RaSO_4(s)}}{N_{BaSO_4(s)}}}{\dfrac{(mRa^{2+})}{(mBa^{2+})}} \qquad (4.49)$$

The Doerner-Hoskins (kinetic) coefficient, λ is given by

$$\lambda = \frac{\log\left(\frac{(mRa_i^{2+})}{(mRa_f^{2+})}\right)}{\log\left(\frac{mBa_i^{2+}}{mBa_f^{2+}}\right)} \qquad (4.50)$$

Here, $N_{RaSO_4(s)}$ and $N_{BaSO_4(s)}$ are the molal fractions of Ra-226 and Ba in solid solution of the $BaSO_4(s)$ crystal, (mRa^{2+}) and (mBa^{2+}) are the molal aqueous concentrations in solution, and the subscripts i and f refer to the initial and final solution concentrations.

For trace Ra in solid solution, one can use the relationship:

$$N_{RaX} = D_{RaX} \frac{(Ra^{2+})}{(M^{2+})} \qquad (4.51)$$

to estimate the equilibrium solid solution composition of radium in MX provided that the solution is saturated or supersaturated with respect to the host precipitate MX.

Values of the distribution coefficient D and of the rational activity coefficients derived by Langmuir and Riese (1985) are given in Table 4.6. D values for anhydrite are higher than those for gypsum ($CaSO_4 \cdot 2H_2O$; Goldschmidt, 1944). Of note are the following points:

- Radium substitution in barium sulphate behaves almost as an ideal solution because the values for γ_{RaSO_4} in barite are near unity at 25°C.
- At ambient radium concentration in natural waters (10^{-11} - 10^{-13} M), values of N_{RaX} are between 10^{-5} and 10^{-11}. These N_{RaX} values are sufficiently low that crystal strain caused by Ra substitution, in the parent lattice, is probably negligible (Langmuir and Riese, 1985). This means that one should be able to use simple thermodynamic principles to explain solid solution behaviour.

TABLE 4.6: DISTRIBUTION COEFFICIENTS (D) AND RATIONAL ACTIVITY (γ) COEFFICIENTS FOR TRACE RADIUM COPRECIPITATED IN VARIOUS METAL SULPHATES

Metal Sulphate	D (25°C)	D (100°C)	γ (25°C)	γ (100°C)
$CaSO_4$ (anhydrite)	(800)*	(40)*	(29.8)*	(5.6)*
$SrSO_4$ (celestite)	280	30	215	69
$PbSO_4$ (angelsite)	11	3	26.8	8.4
$BaSO_4$ (barite)	1.8	0.90	1.11	0.75

* Estimates.

Evaluation of leaching pachuca data, tailings porewater data and experimental data on tailings from sulphuric acid leaching processes (Snodgrass and Hileman, 1985) and experiments on lysimeter solids (Constable and Snodgrass, 1984) from the Elliot Lake area and from Gunnar tailings suggest that Ra^{2+} is present primarily in freshly deposited tailings as a coprecipitate with $BaSO_4(s)$ crystal. Of other plausible crystals involving sulphate, salts of calcium (gypsum), lead (anglesite) strontium (celestite) and iron (FeOOH; jarosite: $KFe_3(SO_4)_2OH_6$), dissolution experiments suggest that lead may be a plausible crystal for coprecipitation. The experimental data cannot be used to prove that Ra-226 is not associated with iron sulphate or calcium sulphate but they do suggest that the role of these two precipitates should be minimal. The experimental data indicate that Ra-226 cannot coprecipitate with strontium sulphate because this solid should not form in the leaching tanks.

The thermodynamic theory of Langmuir and Riese (1985) indicate that of the plausible metal sulphates, Ra-226 is most likely to coprecipitate with metal sulphate crystals in the following order; barium sulphate, lead sulphate, anhydrite and celestite. The thermodynamics of iron sulphate salts were not evaluated.

For purposes of this study, it is assumed that Ra-226 is present in the tailings as a coprecipitate with barite, anglesite, and gypsum. It is assumed that over the long-term, an equilibrium condition exists between soil moisture in the unsaturated zone and the tailings solids in the unsaturated zone and between the porewater and tailings solids in the saturated zone. It is assumed that Ra-226 is primarily associated with barite, lead sulphate, and gypsum formed in the leaching pachucas after the initial placement of the tailings. Because of the large mass of gypsum formed in the final neutralization tanks, it is assumed that Ra-226 is not at equilibrium with this mass upon tailings placement. Rather equilibrium is reached over certain time scales defined by the kinetics of exchange of radium in lead, barium and calcium sulphates formed in the leaching pachucas with the porewater, and the kinetics of exchange between porewater and tailings gypsum.

A mass balance on a unit volume of solids and liquids gives the following relationship for Ra in the solid phase:

$$Ra_T^S = N_{RaBa}\,Ba^S + N_{RaCa}\,Ca^S + N_{RaPb}\,Pb^S \qquad (4.52a)$$

$$= D_{RaBa}\,\frac{(Ra)}{(Ba)}\,Ba^S + D_{RaCa}\,\frac{(Ra)}{(Ca)}\,Ca^S + D_{RaPb}\,\frac{(Ra)}{(Pb)}\,Pb^S$$

$$Ra_T^S = \left[D_{RaBa}\,\frac{Ba^S}{(Ba)} + D_{RaCa}\,\frac{Ca^S}{(Ca)} + D_{RaPb}\,\frac{Pb^S}{(Pb)}\right](Ra) \qquad (4.52b)$$

Here: Ra_T^S is the solid phase radium concentration (mol/m^3)
Ba^S is the solid phase barium concentration (mol/m^3)
Ca^S is the solid phase calcium concentration (mol/m^3)
Pb^S is the solid phase lead concentration (mol/m^3)
N is the mol fraction of RaBa, RaCa, and RaPb respectively
D is the distribution coefficient of RaBa, RaCa, and RaPb respectively

This results in the ratio of radium in the liquid phase to radium in the solid phase being:

$$R = \frac{(Ra)}{Ra_T^S}$$

or:

$$R = \frac{1}{D_{RaBa}\,\frac{Ba^S}{(Ba)} + D_{RaCa}\,\frac{Ca^S}{(Ca)} + D_{RaPb}\,\frac{Pb^S}{(Pb)}} \qquad (4.53)$$

using Equation 4.52b.

Mass Transport

Mass transport for radium is evaluated using the generic transport equation given above, but including the effects of ingrowing from Th-230, the effects of decay of Ra-226 to Rn-222, and the dissolution of residual uranium oxide. This results in the following equations:

$$\text{Invent}_{t+1} = \text{Invent}_t + (\text{XIN} - \text{XOUT})\,dt \qquad (4.54)$$

where Invent is the total inventory of Ra-226 in a unit volume V_i, and XIN is the mass input which increases the inventory and XOUT is the mass outflow which decreases the inventory.

XIN is:

$$\text{XIN} = \underbrace{\text{DECAY}_{UO2} \cdot \text{RaU} \cdot UO_2 \cdot V_i}_{UO_2 \text{ dissolution}} + \underbrace{\text{Ex}_{RaFe}(\text{RaTh})\, V_i}_{\text{Dissolution from Thorium Ingrowing}}$$

$$+ \underbrace{QD_i\, CT_{i-1,k}}_{\text{Downflow}} + \underbrace{QU_{i+1} \cdot B_i}_{\text{Upflow}} + \underbrace{QI_i\, CIN_{i,k}}_{\text{Inflow}} \qquad (4.55)$$

Here, DECAY_{UO2} is the dissolution rate of the UO_2 phase, RaU and RaTh are unit factors, $CT_{i,k}$ is the total aqueous concentration of radium (k = 14) in box i. The derivation of Ex_{RaFe} is given in Equations 4.58 amd 4.59. XOUT is defined by:

$$\text{XOUT} = K_{Ra}\, Ra_T\, V_i - (QD_{i+1} + QO_i + QU_i)\, CT_{i,k} \cdot 1{,}000 \qquad (4.56)$$

The relationship of solid phase concentrations to solution concentrations is governed by the coprecipitation of Ra-226, radium adsorption onto the solid phase and complexation in solution. The total inventory which is dependent upon solution concentrations is:

$$\begin{aligned} \text{Invent} &= Ra^{2+} + \text{Ra Coprecipitate} + RaSO_4{}^{o} + \text{Adsorbed } Ra^{2+} \\ &= Ra^{2+}\left[1 + \frac{1}{R} + C_{RaSO4}\,(SO_4{}^{2-}) + \frac{K_D\, RHO_B}{POR_i}\right] \end{aligned} \qquad (4.57)$$

where C_{RaSO4} is the complexation constant for $RaSO_4{}^{o}$, K_D is the adsorption coefficient (assumed to follow a linear model), RHO_B is the dry bulk density, and POR_i is the tailings porosity.

One term which requires some explanation is the dissolution of Ra-226 from its ingrowth from Th-230 in the hydroxide phase. The formation rate of Ra-226 from ingrowing from Th-230 is easily described by conventional decay kinetics of:

$$\text{Formation Rate of Ra-226 in the Th-230 phase} = \text{RaTh}\, K_{Th}\, (\text{Th-230}) \tag{4.58}$$

where (Th-230) is the activity per m^3, K_{Th} is the radiological decay constant and RaTh is the correction factor relating the activity of Ra-226 formed from the decay of one Bq of Th-230. (Note: the correction factor has a value of 1 if the units of Ra-226 and Th-230 are in mass units rather than in activity units.)

The question of concern is how to describe the dissolution of Ra-226 in the solid phases containing Th-230. One approach is to assume that solid-solution exchange is relatively rapid and hence that coprecipitation theory could be used to describe the Ra-226 distribution among FeOOH and MnO_2, in addition to gypsum, barium sulphate and lead sulphate. This assumption is the one used to describe the distribution of Th-230 between solution and solid phases (FeOOH; MnO_2). Another approach is to assume that exchange between FeOOH and MnO_2 solid phases is kinetically controlled. For this work, the kinetic approach was adopted. The rate of supply of Ra-226 to the solution phase is described by:

$$\text{Rate} = Ex_{RaFe}\, (\text{RaFe}) \tag{4.59}$$

where Ex_{RaFe} is the exchange rate constant (a^{-1}) and (RaFe) is the radium concentration in the Th-230 containing solid phases.

One final question requiring consideration is how to model the time distribution of Ra-226 among the three solid phases of gypsum, barite and anglesite. Due to the sequence of milling processes, Ra-226 will be coprecipitated primarily with barium sulphate and lead sulphate when fresh tailings are first discharged, because these two solids can form in the leaching tanks where Ra-226 is dissolved. Gypsum is formed later where little Ra-226 is available in solution. For some mills, an additional quantity of barium sulphate may form in later tanks due to the direct addition of barium chloride to the tailings slurry. This results in Ra-226 not at equilibrium with gypsum when the tailings are discharged. To model this, one can describe it as a time-based change in distribution coefficients due to solid solution exchange reactions. In the code, the hook was implemented to handle this phenomena, but coding was not completed at the time of writing. For this project, it is assumed that the distribution coefficients of Ra-226 in gypsum, anglesite and barite are independent of time.

4.11 Lead-210

4.11.1 Chemistry of Pb-210

Figure 4.4 shows the stability relation among lead compounds. Under the pH-Eh conditions found in the acid leach, the predominant lead species will be Pb^{2+}. However, as the pH increases from that of acid leach (pH = 1), through that of partial neutralization (pH = 2) to that of tailings neutralization (pH = 8-9), lead precipitates as $PbSO_4$ and $PbCO_3$, respectively. The species distribution will be dependent, both upon pH and upon the anion concentration.

Lead will form $PbSO_4(s)$ at low acid concentrations where the predominant anion is SO_4^{2-} (Figure 4.8). The formation of $PbCO_3(s)$ is not possible in the partial neutralization reaction since the majority of the CO_3^{2-} is released as CO_2. Also, the formation of $PbCO_3$ occurs only at much higher pH's (Figure 4.4).

The lead remaining in solution will reach the tailings area as Pb^{2+}. This portion of the lead (minor) could react with Ca $(OH)_2$ in the neutralization reaction and precipitate as $Pb(OH)_2$. However, low concentrations of CO_3^{2-} can still be present and, due to the stability of $PbCO_3$ versus $Pb(OH)_2$ (Figure 4.4), $PbCO_3$, could precipitate.

The possibility of adsorption of lead by hydrous oxides cannot be eliminated. Indeed, the available evidence from studies of lead adsorption (sediments) suggests that chemical reactions can occur at the oxide surface to form ferro lead or mangano lead oxyhydroxides. Typical reactions include:

$$Pb^{2+} + MnO_2 + H_2O = PbMnO_2(OH)^+ + H^+ \qquad (4.60)$$
$$Pb^{2+} + Fe(OH)_3 = PbFeO(OH)_2^+ + H^+$$

The extent of lead adsorption is influenced by the physical characteristics of the adsorbent and the composition of the aqueous phase (i.e., Eh, pH, lead complexation and competing cations present).

The solubility of lead in the tailings area will be controlled by the solubility of:

$$PbSO_4 \ (-\log K_{sp} = 7.7), \qquad (4.61)$$

to a minor extent by the solubility of:

$$PbCO_3 \ (-\log K_{sp} = 13.1)$$

and by the desorption of lead from the adsorbed surfaces.

4.11.2 Model for Pb-210

Pb-210 is derived primarily from the radioactive decay of Ra-226 in any one tailings box, but also from solution transport from overlying layers. The main sink for Pb-210 is its decay to its daughter Po-210. Solution transport is another sink.

As with the case of Ra-226 derived from ingrowing in the FeOOH and MnO_2 phases, the major question is how to model the exchange of Pb-210 in Ra-226 containing solid phases with solution conditions. For Pb-210, this involves exchange between gypsum, barite and anglesite. Pb-210 will naturally associate with $PbSO_4$ (which is composed primarily of Pb-206 and also Pb-208). If Pb-210 was exclusively in the $PbSO_4$ solid phase, it would have the same solid solution ratio as for stable lead, assuming that isotope separation is not significant. It is expected that Pb-210 would coprecipitate with $BaSO_4$. It might also coprecipitate with $CaSO_4$, but to a lesser extent because of the dissimilarity of ion sizes.

For this work, it is assumed that all the Pb-210 is precipitated with $PbSO_4$ and coprecipitated with $BaSO_4$. The model used is:

$$\frac{(\text{Pb210 S})}{(\text{Pb210})} = D_{PbPb}\frac{(PbSO_4)}{(Pb^{2+})} + D_{PbBa}\frac{(BaSO_4)}{(Ba^{2+})} \qquad (4.62)$$

where (Pb-210 S), ($PbSO_4$) and ($BaSO_4$) are respectively the solid phase activity/concentrations of Pb-210 in the solid phase, anglesite and barite; (Pb-210), (Pb^{2+}) and (Ba^{2+}) are the solution activity/concentration of the named elements, and D_{PbPb} and D_{PbBa} are the distribution coefficients of Pb-210 in $PbSO_4$ and of Pb-210 in $BaSO_4$. In addition to coprecipitation, it is assumed that Pb-210 forms complexes with hydroxyl, carbonate and sulphate ions in solution, similar to the model for stable lead and that it adsorbs onto iron hydroxides and manganese oxides.

For model calibration, D_{PbPb} is assigned a value of 1 to reflect the formation of a precipitate involving Pb-206, Pb-208 and Pb-210 while values for D_{PbBa} centred about 10 are assumed.

The resultant model for the solution phase then is:

$$\mathrm{CFACT} = 1 + \frac{C_{PBSO4}}{f_{PbOH}} 10^{pH} + C_{PBCO3}\, f_{Pb}\, (CO3^{2-}) + C_{PBSO4}\, f_{Pb}\, (SO4^{2-}) \tag{4.63}$$

$$\mathrm{INVENT} = (\mathrm{CFACT} + \frac{K_d{*}\mathrm{SURF})}{\mathrm{POR}} * \mathrm{VW}{*}1{,}000 + \mathrm{Pb210S}{*}V$$

$$\frac{d\,\mathrm{INVENT}}{dt} = \Sigma C_i Q_i - C \Sigma Q_o + (\mathrm{DECAY}{*}\mathrm{Pb210U}{*}(\mathrm{UO2}) + \mathrm{PBRA} * K_{Ra} * (Ra_s) - K_{Pb} * \mathrm{Pb210S})\, V$$

Here: INVENT is the total inventory of Pb-210 (Bq) in a control volume

$\Sigma C_i Q_i$ is the mass flux inflow associated with water flow

ΣQ is the outflow rate (L/year)

C is the aqueous concentration of Pb-210 (Bq/L)

DECAY is the dissolution rate of UO_2 ($year^{-1}$)

Pb210U is the activity of Pb-210 released per gm of UO_2 dissolved

(UO2) is the concentration of UO_2

PBRA is the activity correction for Ra-226 decay

K_{Ra} is the decay rate of Ra-226 (a^{-1})

Ra_s is the total concentration of Ra-226 (Bq/m^3)

K_{Pb} is the decay rate of Pb-210 (a^{-1})

V is the volume of the box

4.12 Polonium

4.12.1 Chemistry of Polonium

Polonium is very stable as Po^{4+} in solution. Polonium is easily adsorbed or coprecipitated with iron and manganese hydroxide. Polonium hydroxide is insoluble and hydroxides of iron and aluminum might carry polonium in the adsorbed state. The chemistry of polonium in the tailings will be controlled by the chemistry of the iron hydroxides and manganese oxides (see discussion of lead).

4.12.2 Model for Po-210

The half-time for Po-210 radioactive decay is 138 days, while the leaching time for Po-210 from the tailings will be of the order of a year or more. Accordingly, the main source of Po-210 is ingrowth from Pb-210, while the main sink is radioactive decay of Po-210. This permits one to assume that Po-210 is approximately at secular equilibrium with Pb-210 in the tailings.

The model for Po-210, then, is that its activity in the liquid phase of the tailings is equal to the activity of Pb-210.

4.13 Redox Model

A redox model is required to estimate the concentration of dissolved oxygen, sulphate and other redox-sensitive elements. These conditions influence whether sulphate is present in solution, and hence the stability of solid phases (e.g., gypsum, etc.) containing radionuclides and the dissolution rates of POC and residual minerals such as UO_2 and nickel arsenide.

A redox model was formulated and partially implemented in the code. Aspects implemented were dissolved oxygen concentrations in the unsaturated zone. Aspects not implemented include sulphate reduction, and the redox chemistry of manganese dioxide and iron oxyhydroxide.

The model is based upon the premise that the decay of dissolved organic and particulate organic carbon and other reduced minerals controls the reduction of the redox potential from fully oxidized conditions. The reduction of potential is mediated by a sequence of reactions. For a perspective of freshwater through salt water systems, at least four aqueous chemical species may be the final electron acceptors for metabolism: oxygen, sulphate, nitrate and organic matter. Other aqueous species of various degrees of importance include iron (Fe III) and manganese (Mn IV).

Equilibrium chemistry provides a reference point for considering the possible sequence of reactions in sediments. In a system containing an excess amount of (i) organic matter, (ii) O_2, (iii) NO^-_3, (iv) $SO_4{}^{2-}$, (v) HCO^-_3, and (vi) oxides of iron (e.g., FeOOH(s)) and manganese (e.g., $MnO_2(s)$), oxidation of organic matter should first occur by reduction of O_2 (Stumm and Morgan, 1981). This would be followed by reduction of nitrate (denitrification or nitrate reduction), $MnO_2(s)$ and FeOOH(s), fermentation of organic matter and reduction of $SO_4{}^{2-}$ and CO_2. The reduction of nitrate and MnO_2 would occur at about the same place in the sequence as would the group of organic matter, $SO_4{}^{2-}$ and CO_2. The sequence of these reactions may occur with depth of tailings as the redox potential becomes increasingly negative or locally in a horizontal fashion into local zones of lower redox potential.

The decay potential (DP, gO_2/year) is estimated from the equation:

$$DP = (k_u R_{O2U} (UO2) + k_{ni} R_{NIAS} (NIASS) + k_p R_{02C} (POC)) V_s + k_d R_{02C} (DOC) V_w \qquad (4.66)$$

Here, k_u, k_{ni}, k_p and k_d are the decay rate constant for the decay (dissolution) of UO_2, NiAsS, POC and DOC, and R_{02U}, R_{NIAS} and R_{02C} are the stoichometric coefficients for $U{:}0_2$, $S{:}O_2$ and $C{:}O_2$.

The actual amount of decay is estimated from the oxygen balance equation given by:

$$\begin{aligned} Flux_i &= (2\ Cox\ Dox\ Rox)^{1/2} \\ O_Z &= Cox - Rox\ (Z) \end{aligned} \qquad (4.67)$$

where: Rox = DP/V

Dox = the diffusion coefficient of oxygen in water or gas,

Cox = the oxygen concentration of the tailings surface,

O_Z = oxygen concentration at depth Z,

V = volume of the tailings box,

q/P = the diffusion path length.

The decay constants (k_u, k_{ni}, k_p, k_d) are multiplied by a decay factor to give the net decay rate of the solids UO_2, NiAsS, POC and DOC. The decay factor is set equal to 1 if dissolved oxygen in the box (DO) is greater than zero, equal to 0 if the DO = 0, and a weighted value between 0 and 1 dependent upon the thickness of the box which has non-zero oxygen concentrations present.

Models for POC formation (in vegetated layer) and DOC were partially formulated. In the simulations, DOC concentrations are calculated from mass balance, while POC is assumed to decay via first order kinetics.

In future work, evaluations should be made of the potential role of sulphate reduction, particularly in its ability to reduce sulphate and hence allow for dissolution of Ra-226 containing phases. For tailings rich in gypsum (e.g., 25% as the present case), the effects of sulphate reduction may be small.

4.14 Parameter Values and Model Simulation

Parameter values for source term variables are given in Table 4.7 and are used to give the probabilistic results described in Section 8.0. Reaction path code calculations are given in Appendix A for various pathways. Particular attention was given to arsenic and nickel concentrations in pore water for thermodynamic equilibrium controls.

Reaction pathway calculations were made to check the calculations of the source term. Thermodynamic data on arsenic and nickel were gathered and reviewed for another study (Beak, 1986). The consistent data base that was developed was then used in a computer code developed previously (Beak, 1985) and called "PATH 1" to study the geochemical controls on arsenic and nickel concentrations in solution when equilibrium is assumed.

The reaction code was used to simulate oxidation by addition of O_2(aq) and acidity by addition of H^+. In addition, because many arsenate solids are sensitive to changes in carbonate content, calculations were conducted to simulate CO_2(g) addition to mixed arsenic and nickel systems. The standard system to which the different "titrants" were added contained a set of minerals that typically occur or are postulated to occur in the tailings. These included gypsum ($CaSO_4 . 2H_2O$) , calcite ($CaCO_3$), nickel hydroxide ($Ni(OH)_2$), calcium arsenate ($Ca_3(AsO_4)_2$), nickel sulphide (NiS) and nickel arsenide (NiAs). The important results and implications of these calculations are summarized below. More detailed results are given in Appendix A.

Oxidation (Titration with O_2(aq))

When oxygen is added to the nickel and arsenic rich solids mixture, the reduced minerals oxidize. Nickel and arsenic are dissolved and arsenite (As(III)) is transformed to arsenate (As(V)). At high pH levels (11 or above), the arsenic and nickel solubilities are controlled by $Ni(OH)_2$ and $Ca_3(AsO_4)_2$ solids at relatively low levels. Oxidation and release of Ni and As does not significantly affect concentrations of these constituents at any particular fixed pH value. However, if pH is allowed to float during the addition of O_2 then the oxidation of reduced arsenide and sulphide minerals causes acidification of the solution with consequent reduction of pH. The presence of calcite maintains the pH level above 6.5. The change in pH from about 12 to 6.5, however, significantly affects the solution concentrations of Ni and As. Increases in arsenic concentration increased by three orders-of-magnitude to about 10^{-2} moles/L. Nickel concentrations increased by the same amount to 10^{-4} moles/L.

Reduction (Titration with H_2 (aq))

These calculations showed that arsenic and nickel concentrations were controlled by the formation of reduced solids. The formation of NiAs solid was particularly significant in limiting concentrations of arsenic. These strongly reducing conditions are not likely to occur in the tailings, however, unless an organic rich environment is created and maintained for some time.

Acid Titration

The results of these calculations show that arsenic solubility generally increases with decreasing pH. Minimum concentrations of arsenic are noted at pH values of about 13 and 11. Arsenic concentrations above 10^{-3} moles/L are predicted at pH values below about 9. Nickel concentrations were predicted to be at a minimum (10^{-8} moles/L) at a pH value of about 10 with concentrations of about 10^{-3} moles/L at pH = 7. These calculations suggest that the solubility control by precipitation and dissolution of a particular solid such as calcium arsenate is not adequate to maintain arsenic concentrations at the lower levels observed in pore waters and seepage at Key Lake for instance (see Figure 4.6b). The predicted behaviour of dissolved nickel was shown to be close to that observed in waters from the Key Lake tailings.

Titration with CO_2 (g)

Carbon dioxide was added to the calcium arsenic system to determine the effect on arsenic concentrations. When CO_2 is added, calcite equilibria is predicted to lower the Ca^{2+} concentrations and thereby increase the solubility of calcium arsenate solids. In addition, the pH is lowered due to the addition of CO_2 and hence the solubility of the calcium arsenate solids is further increased.

Conclusions Regarding Reaction Pathway Calculations

These reaction pathway calculations confirm other work conducted by Beak (1986) which was used as the basis for this source-term for the probabilistic assessment. The predicted concentrations of arsenic based on calcium arsenate solubility are much higher than those observed in the pore water in arsenic-rich tailings at Key Lake. These predictions suggest that solid phases or mechanisms other than solubility control play a dominant role in limiting the concentrations of arsenic to the levels observed in the groundwater environment. The mechanism proposed by Beak (1986) involving adsorption by ferric and aluminum hydroxide solids rather than solubility is the most plausible geochemical controller. Calculations based on independently determined adsorption constants show that the adsorption hypothesis closely reflects data from Key Lake (see discussion of Figure 4.6b). This adsorption mechanism was used in the source term.

Nickel concentrations predicted by $Ni(OH)_2(s)$ solubility are close to those observed at Key Lake. Although there is some deviation at lower pH values, no better mechanism for solubility control has been proposed and this solid is judged to be adequate in controlling nickel concentrations. This solid phase was used for the source term of this work.

TABLE 4.7: SOURCE TERM MODEL VARIABLES

Symbol	Description	Units	Nominal Value	Probabilistic	Source	Computer Symbol
A	Area of Tailings Site	m^2	5E+5	5E+5	INPUT	ATAIL
R	Rainfall Rate	$m \cdot a^{-1}$	0.4	0.4	INPUT	RAIN
I	Infiltration Rate	$m \cdot a^{-1}$	-	N (0.23, 0.09, 0.14, 0.47)	INPUT	INFT
Z_i	Thickness of Box	m	for I = (1,2,3,4), Z = (0.1,1.9,4.0,10.0)		INPUT	ZTAIL(I)
n	Porosity in Box	-	0.5	0.5	INPUT	POR(I)
p	Dry Bulk Density	$g\ cm^{-3}$	1.2	1.2	INPUT	RHOT(I)
g_{po}	Percent of void space which is gas	-	for I = (1,2), g_{pc} = u (0.1,0.5) for I = (3,4), g_{pc} = 0		INPUT	GASPC(I)
Q_d	Downflow rate between boxes	$m^3 \cdot a^{-1}$	for I = (1,2,3,4,5) QD(I) = (1.0,1.0,1.0,0.05,0.001)		INPUT	QDPC(I)
Q_u	Upflow rate between boxes	$m^3 \cdot a^{-1}$	0	0	INPUT	QUT(I)
-	Probabilistic coefficient for varying QUT	-	1.0	1.0	INPUT	QUDIST
Q_i	Inflow rate from upstream	$m^3 \cdot a^{-1}$	1.0	1.0	INPUT	QINT(I)
Q_{udist}	Probabilistic coefficient for varying QINT	-	1.0	1.0	INPUT	QINDIST
Q_o	Outflow rate from boxes	$m^3 \cdot a^{-1}$	-	-	Calculated	QO(I)
Ex	Exchange rate between boxes (diffusional processes)	$m^3 \cdot a^{-1}$	0	0	INPUT	EXCHT(I)
Ex_{dist}	Probabilistic coefficient for varying exchange	-	1.0	1.0	INPUT	EXDIST
$CaSO_4 \cdot 2H_2O$	Concentration of gypsum in tailings solids	$mol \cdot g^{-1}$	1.45×10^{-3} (initial)	-	Calculated (INPUT)	CASO4T
$CaCO_3$	Concentration of calcite in tailings solids	$mol \cdot g^{-1}$	4.99×10^{-4} (initial)	-	Calculated (INPUT)	CACO3T
NiAsS	Concentration of nickel arsenide in tailings solids	$mol \cdot g^{-1}$	2.41×10^{-5} (initial)	-	Calculated (INPUT)	NIASST
UO_2	Concentration of uranium oxide in tailings solids	$mol \cdot g^{-1}$	3.70×10^{-6} (initial)	-	Calculated (INPUT)	UO2T
$Ca_3(AsO_4)_2$	Concentration of calcium arsenate in tailings solids	$mol \cdot g^{-1}$	8.01×10^{-5} (initial)	-	Calculated (INPUT)	CAASO4T
$Ni(OH)_2$	Concentration of nickel hydroxide in tailings solids	$mol \cdot g^{-1}$	1.73×10^{-4} (initial)	-	Calculated (INPUT)	NIOH2T
FeOOH	Concentration of goethite in tailings solids	$mol \cdot g^{-1}$	1.12×10^{-4} (initial)	-	Calculated (INPUT)	FEOOHT
$Al(OH)_3$	Concentration of gibbsite in tailings solids	$mol \cdot g^{-1}$	1.28×10^{-4} (initial)	-	Calculated (INPUT)	ALOH3T
$PbSO_4$	Concentration of lead sulphate in tailings solids	$mol \cdot g^{-1}$	1.65×10^{-6} (initial)	-	Calculated (INPUT)	PBSO4T
$Pb(OH)_2$	Concentration of lead hydroxide in tailings solids	$mol \cdot g^{-1}$	0.0 (initial)	-	Calculated (INPUT)	PBOH2T
$Pb(CO_3)$	Concentration of lead carbonate in tailings solids	$mol \cdot g^{-1}$	0.0 (initial)	-	Calculated (INPUT)	PBCO3T
$BaSO_4$	Concentration of barium sulphate in tailings solids	$mol \cdot g^{-1}$	2.14×10^{-6} (initial)	-	Calculated (INPUT)	BASO4T
$K\text{-}Pb(OH)_2$	Solubility product for lead hydroxide	$Lmol^{-1}$	LN (0.0E0,1.59,-,-)		INPUT	XPBOH2
$K\text{-}PbCO_3$	Solubility product for lead carbonate	$Lmol^{-1}$	LN (7.943E-14, 1.59, 1.995E-14, 3.162E-13)		INPUT	XPBCO3
$K\text{-}BaSO_4$	Solubility product for barium sulphate	Lmol-1	LN (1.00E-10, 1.59, 2.512E-11, 3.918E-10)		INPUT	XBASO4

TABLE 4.7: SOURCE TERM MODEL VARIABLES

Symbol	Description	Units	Nominal Value	Probabilistic	Source	Computer Symbol
I	Ionic strength	$\mathrm{mol{\cdot}L^{-1}}$		Calculated	SOURCE	XIOS
C_{top_j}	Rainfall concentrations	$\mathrm{mol{\cdot}L^{-1}}$	Ca=2.0E-5 SO4=1.0E-5 CT=1.0E-5	-	INPUT	CTOP(J)
C_{in_j}	Inflow concentration to boxes from upstream	$\mathrm{mol{\cdot}L^{-1}}$	all set at zero	-	INPUT	CINT(J)
C_{deep_j}	Concentration going to groundwater	$\mathrm{mol{\cdot}L^{-1}}$	Calculated	-	SOURCE	CDEEP(J)
S_j	Sorbing surface concentration	$\mathrm{m{\cdot}g^{-1}}$ $\mathrm{mol{\cdot}L^{-1}}$ or sites $\mathrm{L^{-1}}$	Dependent on element		INPUT	SURF(J)
Kd_j	Sorption constant	$\mathrm{L{\cdot}kg^{-1}}$	Dependent on element			KDT(J)
$C_{i,j}$	Concentration in pore water of component i in box j	$\mathrm{mol{\cdot}L^{-1}}$	-	-	Calculated	C(I,J)
$C_{T\ i,j}$	Total dissolved concentration of component i in box j	$\mathrm{mol{\cdot}L^{-1}}$	-	-	Calculated	CT(I,J)
$C_{ads\ i,j}$	Concentration of adsorbed component i in box j	$\mathrm{mol{\cdot}L^{-1}}$	-	-	Calculated	CADS(I,J)
$C_{TT\ i,j}$	Total dissolved concentration of component i in box j	$\mathrm{mol{\cdot}L^{-1}}$	-	-	Calculated	CTT(I,J)
$C_{TOT\ i,j}$	Total dissolved, adsorbed and solid concentration of component i in box j	$\mathrm{mol{\cdot}L^{-1}}$	-	-	Calculated	CTOT(I,J)
Th-230	Concentration of Th-230 in tailings solids	$\mathrm{Bq{\cdot}g^{-1}}$	$2.46\times10^{+2}$ (initial)	-	Calculated (INPUT)	TH230T
Ra-226	Concentration of Ra-226 in tailings solids	$\mathrm{Bq{\cdot}g^{-1}}$	$7.46\times10^{+2}$ (initial)	-	Calculated (INPUT)	RA226T
Pb-210	Concentration of Pb-210 in tailings solids	$\mathrm{Bq{\cdot}g^{-1}}$	$2.46\times10^{+2}$ (initial)	-	Calculated (INPUT)	PB210T
$D_{Ra\text{-}Ca}$	Distribution coefficient for Ra in gypsum	-	T (252, 800, 1,200)	-	INPUT	DRACA
$D_{Ra\text{-}Pb}$	Distribution coefficient for Ra in lead sulphate	-	T (6.67, 11.0, 15)	-	INPUT	DRAPB
$D_{Ra\text{-}Ba}$	Distribution coefficient for Ra in barium sulphate	-	T (1.38, 1.8, 2.2)	-	INPUT	DRABA
$D_{Th\text{-}Fe}$	Distribution coefficient for Th in iron hydroxide	-	T (0.5, 1.0, 1.5)	-	INPUT	DTHFE
$D_{Th\text{-}Mn}$	Distribution coefficient for Th in manganese oxide	-	T (0.5, 1.0, 1.5)	-	INPUT	DTHMN
$Ex_{Ra\text{-}Fe}$	Exchange rate constant for Ra from Fe00H	$\mathrm{a^{-1}}$	1×10^{-6}	-	INPUT	EXRAFE
K_s-gypsum	Solubility constant for gypsum	$\mathrm{mol^2{\cdot}L^{-2}}$	LN (2.399E-5, 1.05, 2.138E-5, 2.75E-5)		INPUT	XCASO4
K_s-calcite	Solubility constant for calcite	$\mathrm{mol{\cdot}L^{-1}}$	LN (4.467E-9, 1.05, 3.891E-9, 5.128E-9)		INPUT	XCACO3
K_s-Ni(OH)$_2$	Solubility constant for nickel hydroxide	$\mathrm{L{\cdot}mol^{-1}}$	LN (6.309E+10, 1.59, 1.585E+10, 2.512E+11)		INPUT	XNIOH2
K_s-goethite	Solubility constant for goethite	$\mathrm{L^2{\cdot}mol^{-2}}$	LN (3.98E+1, 3.16, 1.259E0, 1.259E+3)		INPUT	XFEOOH
K_s-gibbsite	Solubility constant for gibbsite	$\mathrm{L^2{\cdot}mol^{-2}}$	LN (2.399E+10, 3.16, 7.587E+8, 7.586E+11)		INPUT	XALOH3
K_s-PbSO$_4$	Solubility constant for lead sulphate	$\mathrm{mol^2{\cdot}L^{-2}}$	LN (1.585E-8, 1.59, 3.98E-9, 6.31E-8)		INPUT	XPBSO4
Decay	Decay rate of particulate material	$\mathrm{a^{-1}}$	10^{-3} for all values		FIXED	DECAY(I,J)

TABLE 4.7: SOURCE TERM MODEL VARIABLES

Symbol	Description	Units	Nominal Value	Probabilistic	Source	Computer Symbol
Radiod	Radionculide decay rate	a^{-1}	(J=2,3,4) = 8.664E-6; 4.273E-3; 3.397E-3		FIXED	RADIOD(J)
f	Activity coefficient	-	-	-	Calculated	F(I,J)
THU	Th-U constant in urananite	$Bq \cdot g^{-1}$	1.656E-5	-	FIXED	THU
RAU	Ra-U constant in urananite	$Bq \cdot g^{-1}$	3.191E-7	-	FIXED	RAU
RATH	Ra-Th mass activity constant	-	49.32	-	FIXED	RATH
PB210U	Pb210-U constant in urananite	$Bq \cdot g^{-1}$	3.618E-9	-	FIXED	PB210U
PBRA	Pb-Ra mass activity constant	-	74.5	-	FIXED	PBRA

5.0 ENVIRONMENTAL PATHWAYS

Radionuclides, arsenic and nickel may be released from the tailings to surface water and groundwater environments, and to the atmosphere. Once in the open environment, environmental transport processes disperse these elements away from the tailings toward the receptor (critical) group, living downstream and downwind. Individuals of the receptor group are exposed directly to these releases through inhalation of airborne materials and through ingestion of contaminated water, and indirectly through consumption of food exposed to these releases. These transport and exposure pathways were depicted earlier (Figure 2.2), and are described in greater detail in the following subsections.

5.1 Atmospheric Pathways

5.1.1 The Dust Source Model

Dust, containing U-238 decay chain radionuclides, arsenic and nickel, is generated by wind erosion of the tailings. These elements are carried downwind with dust to the receptor where they may be inhaled or deposited on soils which produce food for humans or game animals. Dust erosion occurs for the base case simulation where the tailings surface is unsaturated. For the management case, no dust is assumed to be generated since the tailings are flooded.

The dust source model used in this assessment is a revised version of the model used by SENES in their earlier work. The CDOH formula used by SENES was based upon U.S. EPA AP-42 emission factors and generally follows the work of Cowherd et al. (1974). The Cowherd study developed empirical equations based upon the results from experiments involving sand and gravel storage piles. Subsequently, Cowherd proposed a predictive equation to calculate the annual average suspended particulate emission factors for exposed, flat or rolling terrain (Cowherd and Hendricks, 1978). This formulation has several advantages over the previous model, and was thus selected for this study.

The formulation used here is different in the following aspects:

- it was developed for exposed flat or rolling terrain more closely representative of tailings surfaces; and
- it includes a factor relating both precipitation and evaporation in the region (the PE index) rather than a normalized precipitation factor.

The formulation suggested by Cowherd and Hendricks (1978) is:

$$E_{OA} = 0.38 \left(\frac{e}{0.184}\right)\left(\frac{S}{15}\right)\left(\frac{f}{25}\right) \; V \left(\frac{PE^2}{50}\right)^{-1} \qquad (5.1.1)$$

where: E_{OA} = erosion rate in tonnes per square metre per year of exposed land,

e = soil erodibility or potential annual soil loss rate for a wide, unsheltered, isolated field with a bare, smooth surface in tonnes per square kilometre per year,

S = silt content of eroding surface in %,

f = percentage of the time that wind velocity measured 0.3 m above the surface exceeds the nominal wind erosion threshold value of 19 km per hour,

V = fractional value reflecting the reduction of wind erosion due to vegetative cover (bare soil = 1.0), and

PE = Thornthwaite's Precipitation-Evaporation Index.

The 0.38 factor in Equation 5.1.1 is based on empirical fit of the data, and includes a conversion to $t \cdot m^{-2} \cdot a^{-1}$ (E_{OA}) from $t \cdot km^{-2} \cdot a^{-1}$ (e).

Soil erodibility can be estimated from Table B5.1.1. A value representative for silty clay to sandy loam was judged to be appropriate for the generic tailings.

From data given in Jutze and Axetell (1976), the vegetative cover parameter can be estimated from an assumed linear relationship that suggests that up to 28 g/m^2 of air-dried residue are required to initiate a reduction in wind erosion. The erosion decreases linearly until 110 to 220 g/m^2 of air-dried residue totally suppresses wind erosion.

Thornthwaite's Precipitation-Evaporation Index (PE) is a measure of the annual or seasonal surface moisture function and is used to adjust emission rates reflecting normal retained moisture. Using the method outlined in Thornthwaite (1931), NRCC (1982) provides the annual PE index values for Canada.

This formulation is the basis for calculating the emission rate ($Q_i(t)$) of any radionuclide or element from the tailings surface, using the equation:

$$Q_i(t) = \frac{E_{OA}}{31.5} \frac{C_i(t)}{RHO_T} A \tag{5.1.2}$$

where: $Q_i(t)$ = emission rate of the ith radionuclide or stable element at time t ($Bq \cdot s^{-1}$, or $g \cdot s^{-1}$)
E_{OA} = $tonnes \cdot m^{-2} \cdot a^{-1}$,
$C_i(t)$ = surficial concentration of the ith element at time t (Bq/m^3, or g/m^3),
A = the exposed tailings surface area (m^2), and
RHO_T = tailings bulk density ($g \cdot m^{-3}$).

The 31.5 factor is a conversion for time (year to seconds) and mass (tonnes to grams).

The silt content(s) is determined by the proportion of surface material that passes through a 200 mesh screen (minus 76 um), using the ASTM-C-136 method. The silt content decreases over time due to wind erosion. The silt content of the surface layer of tailings is modelled as a function of the initial silt content, assumed here to vary uniformly between 40 and 50%, the rate of formation of silt from the coarse fraction, and the rate of removal due to wind erosion. Using mass balance principles, the silt content at any time is:

$$S' = S_o + S_{weath} - S_{erod} \tag{5.1.3}$$

where: $S_{weath} = f_u (1-S) R_{weath} RHO_T \cdot DT$
$S_{erod} = f'_u \frac{E_{OA}}{ZT_i} DT$
S_o = the initial silt content (as a decimal fraction),
S' = the final silt content (as a decimal fraction),
R_{weath} = the weathering rate constant of coarse material (a^{-1}),
RHO_T = the tailings dry bulk density (g/m^3),

$^{-}ZT_i$ = the depth of the top box (0.1 m),
DT = the time step, and
f_u, f'_u = unit conversion factors.

Appropriate modifications are made to the values of RHO_T and mass inventories of chemical elements in the top box due to silt erosion.

The percentage of the time (f) that the wind speed exceeds 5.4 $m \cdot s^{-1}$ (19 $km \cdot h^{-1}$) at the tailings height can be highly dependent on the time of year. A review of northern Saskatchewan average wind data shows only a minor increase in summer average versus winter average wind speeds. These averages are approximately 20 to 25% lower than the northern Ontario values applied in the SENES Phase II assessment. Winter conditions can reduce wind erosion but, until more definitive data are available, average annual frequencies, as quoted in IEC BEAK (1984), are utilized. The average frequency of 15% represents a composite value for northern Saskatchewan. Without further statistics, a triangular distribution with a minimum of 10, a mode of 15 and a maximum of 20 is used.

The data in NRCC (1982) suggest the annual PE index will be between 40 and 50 in the northern Saskatchewan region (Figure B5.1.1). For this assessment, the PE index is assumed to have a triangular distribution with minimum of 35, mode of 45 and maximum of 55.

The erodibility factor, e, was assumed to follow a uniform distribution and lie between 0.3 and 0.4 $t/km^2/a$ (IEC BEAK, 1984). The initial value of the tailings bulk density, RHO_T, is taken to have the same statistical attributes as applied by SENES (1985 - see Table 5.1). The mass balance on the top box is used to calculate RHO_T over time.

The final variable requiring review is the vegetation factor, V. Data from the Gunnar site would suggest that, after 30 years, a certain proportion of the tailings surface will be revegetated by native species. Complete coverage may not be achieved during the modelling timeframe owing to unfavourable conditions persisting in some areas of the tailings surface. For this assessment, a value of 1.0 (no vegetation) is selected for the initial value. A linear decrease with time to a final value of 0.001 at a time, T_m, when the tailings are almost completely vegetated, is assumed to apply. Thus, $V = 1.0 - T/T_m$ where T is the simulation time (years). This linear decrease is in recognition of a gradual colonization of the tailings by plants over time. T_m is treated as a probabilistic variable ranging from approximately two centuries to three centuries. It is assumed, however, that vegetation cover is essentially complete at some future time, but allows a small erosion rate to continue into the future.

Table 5.1 summarizes the parameter values assumed to apply to atmospheric source terms for the base case assessment. The format used in this table and others like it in subsequent subsections of Section 5 is similar to the format used in the SENES (1985) Phase II user's manual.

5.1.2 The Radon Source Model

Gaseous radon is derived from its emanation from solid and liquid phases where it forms from the decay of Ra-226. In the gas space of the unsaturated zone, radon diffuses according to its concentration gradient. The portion of radon which does not diffuse out of the tailings decays to Pb-210. Once in the atmosphere, radon concentrations are controlled by atmospheric transport processes and decay.

The radon model generates the source term for exhalation of radon from the tailings area. It calculates the radon flux ($Bq/m^2/s$) and also the total discharge (Bq/s). The atmospheric transport model is used to calculate radon concentrations with distance from the tailings area as a function of dispersion, decay and wind direction for the calculated radon discharge to the atmosphere from the tailings.

The radon model is the same as that of SENES (1985), except that the box structure of this work is substituted for the gypsum-depleted and gypsum-enriched zones of the SENES work. The top surface box is equivalent to their "gypsum-depleted layer", and the second box of the unsaturated zone is equivalent to their gypsum-enriched zone. Due to the radium-226 leaching from the first box and then partially from the second box for the 1,000 year timeframe simulated, this representation of the tailings gives a good similarity to the approach of SENES, except that this approach gives somewhat less detail.

Consideration was given to the effects of varying vegetative cover upon radon exhalation. Previous NUTP-funded work has concluded that vegetation has no measured effect upon exhalation compared to the flux from bare tailings, presumably due to moisture content and other factors. Accordingly, vegetation is assumed to have no impact upon radon exhalation.

TABLE 5.1: ATMOSPHERIC SOURCE MODEL VARIABLES

Symbol	Description	Units	Nominal	Probabilistic	Source	Computer Symbol
DUST						
$Q_i(T)$	emission rate of the ith radionuclide at time t	$Bq \cdot s^{-1}$	calculated	calculated	DUST	EMRATE(I)
S	silt content of the tailings (% of particles 75 um)	%	calculated	calculated, initial value U (40, 50)	SILT	SILT
P	annual number of days with more than 0.25 mm of precipitation	days	123	N (123,18,84,156)	INPUT	FPREC
f	percentage of the time that the wind speed exceeds 5.4 m/s at the mean tailings height	-	35	N (35, 6, 23, 46)	INPUT	FWIND1
$C_i(t)$	surficial concentration of ith compound at time t	$Bq \cdot g^{-1}$	calculated	calculated	SOURCE	CTOT(I,J)
A(t)	exposed surface area of the tailings at time t	m^2	calculated	calculated	DUST	AEXPT
RHO_T	tailings bulk density	$g \cdot m^{-3}$	$1.4x10^6$	initialized and then calculated	SILT	RHOT(I)
R_{WEATH}	weathering rate of coarse fraction	yr^{-1}	0.001	T (0.0005, 0.06075, 0.001)	INPUT	RWEATH
Tm	time when tailings are completely vegetated	year	250	U (215, 285)	INPUT	TCUTOFF
e	soil erodibility	-	0.35	U (0.3, 0.4)	INPUT	EI
V	fractional due to vegetation reduction in wind erosion	-	calculated	calculated	DUST	VEGERD
PE	Thornthwaite's Index	-	0.45	T (0.35, 0.45, 0.55)	INPUT	PE
RADON						
a	Reciprocal of radon diffusion length of tailings	m^{-1}	calculated	calculated	RADON	DIFLEN
D	effective bulk radon diffusion coefficient of tailings	$m^2 \cdot s^{-1}$	calculated	calculated	RADON	EBKDFC
E	radon emanation coefficient of tailings	-	0.35	T (0.02, 0.2, 0.9)	INPUT	EMANAT
J(t)	radon flux	$Bq \cdot m^{-2} \cdot s^{-1}$	calculated	calculated	RADON	RNFLUX
M	percent moisture content by weight of tailings	-	calculated	calculated	INPUT	MPCH20
P	porosity of tailings	-	0.4	T (0.35,0.4,0.45)	INPUT	POR(I)
$(Ra)_i(t)$	radium concentration of layer i = 1 or 2	$Bq \cdot m^{-3}$	calculated	initialized then calculated	SOURCE	CTOT(I,15)
$x_1(t)$	thickness of box 1	m	0.1	C (0.1)	INPUT	DEPTH1
$x_2(t)$	thickness of box 2	m	1.9	C (1.9)	INPUT	DEPTH2
	radon decay constant	s^{-1}	$2.1x10^{-6}$	C $(2.1x10^{-6})$	INPUT	RNLAM
A_o	exposed surface area of the tailings at time t	m^2	$5.0x10^5$	C $(5.0x10^5)$	INPUT	ATAIL

The total discharge of radon (J_T) from the tailings (SENES, 1986) is given by:

$$J_T = JA_o \tag{5.2.1}$$

where:

$$J = \frac{-D}{a\cosh(ax_1)}\left(\frac{-(1+\coth(ax_2))\ s_1\exp(ax_1)+s_1-s_2}{\tanh(ax_1)+\coth(ax_2)}\right) \quad \frac{-Ds_1}{a}$$

A_o = tailings surface area (m^2)

D = radon diffusion coefficient ($m^{2}\cdot s^{-1}$)

a = $\sqrt{\frac{lam\ .\ P}{D}}$ = (radon diffusion length)$^{-1}$ (m^{-1})

s_i = $\frac{(Ra)_i\ \ rho_i\ .\ lam\ E_i}{D}$

J = radon flux ($Bq\cdot m^{-2}\cdot s^{-1}$)

$(Ra)_i$ = tailings radium concentration of layer i ($Bq\cdot g^{-1}$)

E_i = emanation coefficient ($0 \leq E_i \leq 1$, dimensionless)

rho_i = tailings density of layer i ($g\cdot m^{-3}$)

lam = radon decay constant (s^{-1})

X_i = thickness of layer i (m)

P = porosity of the unsaturated layer of the tailings

D = effective bulk radon diffusion coefficient

= $0.106 \times 10^{-4} \times P \times \exp(-0.261 \times M)$ ($m^{2}\cdot s^{-1}$)

M = percent moisture content of tailings by weight

= $100 \times \frac{\text{weight of water in tailings}}{\text{weight of wet tailings}}$

and where subscript i = 1 or 2 refers to box 1 or 2, respectively, and the other terms are as previously defined. Note that the product of Ra and rho is sometimes given only by one parameter when Ra is measured in units of $Bq\cdot m^{-3}$. This occurs in the code where Ra is represented by the variable CTOT.

5.1.3 The Air Dispersion Component Model

The air dispersion equation used here in subroutine AIRDIS is the same as the sector-averaged Gaussian plume model applied by SENES in their Phase I and Phase II studies:

$$C_{ai}(t) = (2.032\ f\ Q_i(t)/u\ \sigma_z\ x)\ \exp\ (-H^2/2\ \sigma_z^2) \qquad (5.1.3)$$

where:
$C_{ai}(t)$ = atmospheric concentration of the ith element at the receptor at time t ($Bq \cdot m^{-3}$ or $ug \cdot m^{-3}$),
f = fraction of time that the wind blows from the source to the receptor in one of 16 sectors,
$Q_i(t)$ = emission rate of the ith element at time t ($Bq \cdot s^{-1}$ or $ug \cdot s^{-1}$),
u = mean wind speed from the source to the receptor,
σ_z = the verticle dispersion coefficient (m),
x = downwind distance from the source to the receptor (m), and
H = height of the source (m).

The equation applies strictly to a point source such as a smoke stack. To accommodate an area source, the vertical point source distance is calculated as described in SENES (1984) to be 1,600 m greater than the actual source to receptor distance. That is, the virtual distance is set at 5,600 m (4,000 m + 1,600 m virtual setback).

The fraction of time the wind blows from the source to the receptor is taken as a normally distributed parameter with the same statistical distribution as assumed by SENES in their Phase II assessment.

The tailings height, H, is taken as 12 m, to account for the lower elevation of the receptor at a downstream location. This parameter is allowed to vary uniformly around this value to account for the uneven topography of the tailings surface.

The mean wind speed is allowed to vary with a triangular distribution around a mean annual wind speed of 4.1 $m \cdot s^{-1}$ for Collins Bay, based on 1984 data provided by the Atmospheric Environment Service.

The vertical dispersion coefficient, σ_z, is a function of downwind distance, x, the atmospheric stability category (A to F), and surface roughness (Hosker, 1974). Surface roughness for the zone between the receptor and the tailings includes both very low values over the water of the embayment, and high values for forested terrain. Given the extreme variability in surface roughness in the area of the generic tailings site, the vertical dispersion coefficient is assigned a log uniform distribution with the minimum and maximum set at the values assigned by SENES (1985).

A summary of the air dispersion model variables is given in Table 5.2.

5.2 Soil Deposition

After wind erosion from the tailings, the radionuclides, total U, Th-230, Ra-226, Pb-210 and Po-210, together with arsenic and nickel, are transported in particulate form through the atmosphere and settle onto soil where they may be taken up by plants. The accumulation of these materials in soils can be calculated from the mass balance equation:

$$\frac{dC}{dt} = \frac{W}{V} - \frac{C_{si}}{t_s} - k_i C_{si} + k_i' C_{si}' \qquad (5.2.1)$$

where: C_{si} = the soil concentration of element i ($Bq \cdot m^{-3}$ or $ug \cdot m^{-3}$)
W = the atmospheric loading rate ($Bq \cdot a^{-1}$ or $ug \cdot a^{-1}$)
V = the volume of the soil compartment (= $A_s\ Z_s$) (m^3)
t_s = the leaching time from the soil (a)
k_i = the decay rate constant of the element (a^{-1})
k_i' = the decay rate constant of the parent of the element (a^{-1})
C_{si}' = the soil concentration of the parent (kg/m^3)
A_s = the area of soil considered (m^2)
Z_s = the soil depth in which plant growth actively occurs (m)

W is given by the relationship:

$$W = V_d\ C_{ai}\ (t)\ A_s * 3.1536*10^7$$

TABLE 5.2: AIR DISPERSION MODEL VARIABLES

Symbol	Description	Units	Nominal	Probabilistic	Source	Computer Symbol
$C_{ai}(t)$	Atmospheric concentration of ith radionuclide at time t at the receptor	$Bq \cdot m^{-3}$ ($ug \cdot m^{-3}$ for U, As, Ni)	calculated	calculated	AIRDIS	CAIR
f	Fraction of time wind blows from the source to the receptor	-	0.1	N (0.1, 0.02, 0.06, 0.14)	INPUT	FWIND2
H	Height of the source	m	12	U (11, 13)	INPUT	HSRC
$Q_i(t)$	Emission rate of ith radionuclide at time t	$Bq \cdot s^{-1}$ or $ug \cdot s^{-1}$	calculated	calculated	LDATM	EMRATE
u	Mean annual wind speed	$m \cdot s^{-1}$	4.1	T (3.1, 4.1, 5.1)	INPUT	UWIND
x	Downwind distance to receptor	m	5,600	C (5,600)	INPUT	XDIST
σ_z	Vertical dispersion coefficient	m	60	LU (47.6, 75.7)	INPUT	VDISP

TABLE 5.3: SOIL MODEL VARIABLES

Symbol	Description	Units	Nominal	Probabilistic	Source	Computer Symbol
$C_{ai}(t)$	atmospheric concentration of ith element at time t at receptor	$Bq \cdot m^{-3}$ or $ug \cdot m^{-3}$	calculated	calculated	AIRDIS	CAIR(I)
v_d	depositional velocity	m/s	60	U (47.6, 73.7)	INPUT	VDISP
Z_s	soil depth	m	0.1	U (0.1, 0.2)	INPUT	ZSOIL
t_s	soil detention time	year	200	U (100, 300)	INPUT	TSOIL
C_{si}	soil concentration	$Bq \cdot m^{-3}$ or $ug \cdot m^{-3}$	calculated	calculated	SOIL	CSOIL(I)
A_s	soil area	m^2	1	C (1)	SOIL	-
K	radionuclide decay rate:	$year^{-1}$			INPUT	RADIOS(I)
	- uranium		1.5E-10	C (1.5E-10)		
	- Th-230		8.5E-6	C (8.5E-6)		
	- Ra-226		4.27E-4	C (4.27E-4)		
	- Pb-210		3.397E-2	C (3.397E-2)		
	- Po-210		1.8	C (1.8)		
	- As		0	C (0)		
	- Ni		0	C (0)		

Where V_d is the particulate depositional velocity (m/s) $C_{ai}(t)$ is the atmospheric concentration in air. (Bq . m^{-3} or ug . m^{-3}) and 3.1536E7 is the number of seconds per year.

For purposes of this project, it is assumed that ingrowth is only significant for Pb-210 in the soil and that Po-210 activity can be modelled as equal to the activity of Pb-210. As well, it is assumed that W for Pb-210 does not include deposition from decayed atmospheric Rn-222, but only deposition of Pb-210 originating as eroded particulate matter from the tailings.

A listing of variables and values used in the model are given in Table 5.3.

5.3 Groundwater Dispersion

The radionuclides total uranium, Th-230, Ra-226 and Pb-210, and arsenic and nickel are transported via two groundwater pathways which affect humans: a shallow groundwater pathway which transports elements from the tailings to the first lake, and a deep groundwater pathway which transports elements from the tailings to the well (if present) of the critical group. Elements for the shallow groundwater pathway are assumed to originate from the upper portion of the saturated zone (box 3). Elements for the deep groundwater pathway are assumed to originate from the deep portion of the saturated zone (box 4).

Upon entry into groundwater pathways, elements are transported by advection, diluted by dispersion, and retarded by adsorption onto the solids and radioactive decay. The radioactive elements Th-230, Ra-226 and Pb-210 may also form via ingrowth from their parent. The basic mass balance, equation governing transport, is:

$$\frac{D'C}{D't} = \frac{D'}{R} \frac{D'^{2}C}{D'x^{2}} - \frac{q}{nR} \frac{D'C}{D'x} - \text{lam } C + \text{lam}'C' \; . \quad \frac{R'}{R}$$

Here: $D'/D't$ = the partial derivative with respect to t

$\frac{D'^{2}}{D'x^{2}}$ = the second partial derivative with respect to x

D' = the longitudinal dispersion coefficient (m^2/a)

R = the retardation factor due to adsorption

$$= 1 + \frac{RHO_g}{n} K_D$$

R' = retardation factor for the decay parent

K_D = the linear adsorption coefficient (mL/g)

RHO_g = dry bulk density (g/mL) of geological media

n = porosity

q = Darcy groundwater velocity (m/a)

C = concentration of contaminant in pore water (mass/m^3)

lam = the decay rate constant of the contaminant (a^{-1})

lam' = the decay rate constant of the contaminant's parent (a^{-1})

C' = the concentration of the parent (if any) (mass/m^3)

For this project, the basic groundwater model developed by SENES (personal communication) for Phase III has been incorporated into our code. The model is described in SENES Phase III report (SENES, 1986). For our purposes, the groundwater model was incorporated into our code as separate subroutines to calculate groundwater dispersion for the shallow and deep groundwater pathways. In addition, the model was expanded beyond only considering the four radionuclides to include also arsenic and nickel.

The hydrological concept of SENES were changed for our application. They estimate the volumetric seepage rate (Qs, $m^3 \cdot a^{-1}$) based on the total amount that infiltrates the total depth of the tailings pile and the tailings surface area. For our purposes, we estimate the fraction of outflow from the shallow saturated zone which goes to groundwater (10%) as an input value to the groundwater model. The remainder of this outflow (90%) goes directly to the lake. Similarly, the flow rate to the deep groundwater pathway is treated as an input variable.

To save on calculation time, the time that the chemical front takes to go from the tailings mass to the well is estimated. If this time is longer than the simulation time, then the pathway is neglected.

The assumption of SENES that only Pb-210 ingrowing from Ra-226 is significant over the simulation time (1,000 years) is retained in this work. However, because Ra-226 ingrowth from Th-230 becomes significant over this period, future applications may need to consider this factor. If the groundwater pathway is acidic, the retardation factor for Th-230 may change as a function of pH causing Th-230 to move as fast as Ra-226.

The parameter values used in this study are summarized in Table 5.4.

5.4 Surface Water Component Model

This section develops the equations used to describe elemental concentration and radionuclide activity in the receptor lake.

The drainage basin of the system results in lake characteristics of a chain-lake system. Computationally, this is handled by calculating the concentration in each lake sequentially from the most upstream lake to the most downstream lake. For the reference site, this results in computing concentrations in the upstream lake (**Lake 1**) and then in the embayment, which is connected to the second lake (**Lake 2**).

This project aimed to use the existing SENES component model. It has some limitations which precluded developing the level of detail thought to be appropriate. However, some simplifications give this SENES model some attributes of the greater level of detail.

Including the effects of an embayment, the basic equation for a two-box format (lake water, sediments) is:

$$\frac{dC}{dt} = \frac{W_i}{V_i} + \frac{alpC_L}{t_w} - \left[k_1 + \frac{(1+alp)}{t_w} \right] C + k_2 C_s \qquad (5.4.1)$$

$$\frac{dC_s}{dt} = \frac{W_s}{V_s} + k_1 C - (k_2 + k_3)\ C_s \qquad (5.4.2)$$

which reduces to:

$$\frac{dC}{dt} = a_{11} + a_{12}\ C + a_{13}\ C_s \qquad (5.4.3)$$

TABLE 5.4: GROUNDWATER MODEL VARIABLES

Symbol	Description	Units	Nominal	Probabilistic	Source	Computer Symbol
Shallow Groundwater Variables						
f	fraction of tailings water outflow (Q0(3) which enters surface water	-	0.9	C (0.9)	INPUT	FSURF
X_s	distance along flow path to surface water	m	200	C (200)	INPUT	XRGWAT
A_s	cross-sectional area of groundwater pathway	m^2	1,000	C (1,000)	INPUT	AXGWAT
n_s	porosity of geologic medium along flow path	-	0.33	C (0.33)	INPUT	POGWAT
$alpha_s$	longitudinal dispersivity coefficient	m	25	C (25)	INPUT	LDGWAT
$S.G._s$	specific gravity of geologic medium solids	$kg \cdot m^{-3}$	2,650	C (2,650)	INPUT	SGWAT
k_{di}	distribution of coefficients for the chemical components:	$m^{-3}\ kg^{-1}$			INPUT	DCGWAT(I)
	- uranium		0.01	T (0.02,0.01,0.03)		
	- thorium		0.25	T (0.50,0.25,0.75)		
	- lead		0.50	T (0.67,0.50,0.83)		
	- radium		0.05	T (0.07,0.05,0.09)		
	- nickel		0.10	T (0.11,0.09,0.13)		
	- arsenic		4.0	T (5.06,4.0,6.0)		
Deep Groundwater Variable						
X_w	Distance along flow path to well	m	6,000	C (6,000)	INPUT	XRWELL
A_w	Cross-sectional area of flow to well	m^2	3,000	C (3,000)	INPUT	AXWELL
N_w	porosity of geologic medium	-	0.33	C (0.33)	INPUT	POWELL
$alpha_w$	longitudinal dispersivity coefficient	m	25	C (25)	INPUT	LDWELL
$S.G._w$	specific gravity of geologic medium	$kg \cdot m^{-3}$	2,650	C (2,650)	INPUT	SGWELL
Kd_w	distribution coefficients for chemical components:	$m^3 \cdot kg^{-1}$			INPUT	DCWELL(I)
	- uranium		0.01	T (0.02,0.01,0.03)		
	- thorium		0.25	T (0.5,0.25,0.75)		
	- lead		0.50	T (0.67,0.50,0.83)		
	- radium		0.05	T (0.07,0.05,0.09)		
	- nickel		0.10	T (0.11,0.09,0.13)		
	- arsenic		4.0	T (5.06,4.0,6.0)		

$$\frac{dC_s}{dt} = a_{21} + a_{22}\,C + a_{23}\,C_s \tag{5.4.4}$$

Here:

$a_{11} = \frac{W_i}{V_i} + \frac{alp\,C_L}{t_w}$

$a_{12} = -\left[k_1 + \frac{(1+alp)}{t_w}\right]$

$a_{13} = k_2$

$a_{21} = \frac{W_s}{V_s}$ (element specific; ordinarily having a value of 0)

$a_{22} = k_1$

$a_{23} = -(k_2 + k_3)$

Within this formalism, k_1, k_2 and k_3 are assigned values dependent upon the removal and transfer mechanisms. A more fundamental approach is to describe sediment water transport in terms of particulate setting, diffusion and particulate erosion. This results in:

$$\frac{dC}{dt} = \frac{W_i}{V_i} + \frac{alpC_L}{t_w} - \frac{gfC}{Z} - \frac{k_s}{Z}\left((1-f)C-(1-f_s)C_s\right) - \frac{(1+alp)\,C}{t_w} - kC \tag{5.4.5}$$

$$\frac{dC_s}{dt} = \frac{W_s}{V_s} + \frac{gfC}{Z_s} + \frac{k_s}{Z_s}\left((1-f)\,C-(1-f_s)C_s\right) - \frac{g_sC_s}{Z_s} - \frac{dC_s}{Z_s} - kC \tag{5.4.6}$$

Here:

$f = \frac{K_D(SS)\,10^6}{Epsil}$ and $f_s = K_D\,\frac{RHO_B}{Epsil_s}$

K_D = the adsorption coefficient (g/mL)

(SS) = the suspended solids concentration (mg/L)

Epsil = porosity

RHO_B = dry bulk density (g/cm^3) of the bottom sediments

g = particulate settling velocity (m/a)

d = particulate erosion velocity (m/a)

alp = lake-embayment exchange factor

g_s = sedimentation rate (m/a)

Z = lake mean depth (m)

Z_s = mean sediment depth (m)
k = radioactive decay rate (a^{-1})
C = activity or concentration in lake water (Bq/L or mg/L)
C_L = activity or concentration in lake connected by embayment (Bq/L or mg/L)
C_s = activity or concentration in lake sediments (Bq/L or mg/L)
k_s = sediment-water transfer coefficient (m/a)
t_w = hydraulic residence time (a)
W_i = loading to lake of volume V_i
W_s = loading to sediments of volume V_s

Collection of terms allows one to express k_1, k_2 and k_3 in terms of g, f, k_s, d and g_s and hence to use the mathematical formalism of SENES as a subroutine for calculating concentration of an element in a lake over time.

For certain of the elements considered in this project, namely Po-210, Ni and As, redox reactions are important. This requires use of a three-box model: one for the water column, one for the aerobic sediment layer and one for the shallow anaerobic sediment layer. This level of complexity requires a new mathematical solution.

To model the embayment, two or three additional equations are required to describe the concentration in the main part of the large lake. These are related to Equations 5.4.5 and 5.4.6 through the term, C_L. This results in four to six mixed differential equations; the exact number depends upon the sophistication of the sediment description. The basic equations are given elsewhere (Klapwijk and Snodgrass, 1985; Chapra and Reckhow, 1984; Snodgrass, 1986). For this project, a hook is provided in the code for their later implementation. Redox reactions are considered by changing the model for f_s and the diffusional length for these substances.

The model for f_s for arsenic is based on the data of Cornett (1986). Cornett measured the solid phase and solution phase concentrations of arsenic and nickel in Moira Lake substrates. It is assumed that arsenic speciation is controlled by As (III) in pore water, and that, as suggested by Cornett's data, there is a constant ratio of arsenic (III) concentration in pore water to that on the solid phase. This is analogous to use of a linear distribution coefficient. Analysis of Cornett's data gives $f_s = (1+0.0063*\text{PORSED})^{-1}$ where PORSED is the sediment porosity.

The model for f_s for nickel is based on the hypothesis and data analysis that nickel concentration is controlled by pore water sulphide concentration. For the lakes considered in this project, it is assumed the sulphide concentration is constant and results in a maximum pore water nickel concentration of 0.015 mg/L, and a variable value for f_s. f_s is equal to zero if C_s is less than 15 ug/L on a pore water basis, and equal to the excess sediment concentration above 15 ug/L divided by the total concentration otherwise.

To calculate the thickness of the aerobic zone, a sediment oxygen demand model, based upon oxygen consumption and sulphate reduction, was partially developed. A hook was left in the code for its implementation. From the theory:

$$ZOX = \sqrt{\frac{2COX \cdot DOX}{ROX}}$$

where: COX is the oxygen concentration (g/m^{-3})
DOX is the oxygen diffusion coefficient (m^2/a)
ROX is the oxygen consumption rate ($g/m^3/a$)

For this report, a typically measured value has been used to estimate diffusional distances (ZOX) across the aerobic sediment zone.

To reflect the fact that nickel and arsenic have larger diffusional distances from sediment depths of concentration control to the lake water, typical thickness of the aerobic zone was used to estimate the diffusional length.

For a pH model, the model developed by Kremer (1985) was adapted. It demonstrates that the pH is controlled by alkalinity and total inorganic carbon in typical Shield lakes (low buffering capacity, low nutrient content, low total dissolved solids concentrations) over the pH range of 4 to 7. After performing a mass balance upon total inorganic carbon and alkalinity from the equation:

$$\frac{dC}{dt} = \frac{W_i}{V_i} - \frac{(l+alp)\,C}{t_w} + \frac{alpC_L}{t_w}$$

where C is the concentration of alkalinity (equivalent/L) or total inorganic carbon (M), the pH is calculated from the relationship:

$$(H^+) = \frac{K_1 (C_T - ALK)}{ALK}$$

$$pH = -\log(H^+)$$

Here, (H^+) is the hydrogen ion activity.

The resultant lake parameters and their distribution are given in Table 5.5.

5.5 Uptake by Vegetation

Airborne radionuclides, arsenic and nickel may be transferred to the edible portions of vegetables consumed by members of the critical group, or to plants consumed by game animals hunted by the critical group.

In subroutine VEGDEP described in the SENES (1985) Phase II report, root uptake is not included. Rather, concentrations of radionuclides in plant tissues are calculated based entirely on foliar deposition. Hoffman et al. (1985) demonstrated that for a constant atmospheric radium concentration ($1 pCi/m^3$), steady-state root uptake accounted for 10 to 30% of above-ground tissue concentrations in grass, depending on the uptake model applied. For this project, the root uptake is included, since root uptake may be more significant for other radionuclides, arsenic and nickel, than it is for radium.

Three types of vegetation are modelled; browse (forage for moose), above-ground vegetables, and below-ground vegetables. Lichens and grasses modelled by SENES (1985) for the caribou pathway are replaced herein by browse for a moose pathway (moose do not feed heavily on lichen).

5.5.1 Concentrations in Edible Vegetation from Foliar Deposition (Subroutine VEGDEP)

The equation used here to calculate concentrations of materials in vegetation from foliar deposition is the same as the equation applied by SENES (1985):

TABLE 5.5: LAKE PARAMETERS

Symbol	Description	Units	Nominal	Probabilistic	Source	Computer Symbol
SS	suspended solids concentration	mg·L^{-1}	1	U (0.5, 1)	INPUT	Lake1 SS(1) Lake2 SS(2)
K_D	adsorption coefficient:	mg·L^{-1}			INPUT	
	- U		500	T (250, 500, 750)		KDLAK(1)
	- Th-230		50,000	T (25,000,50,000,75,000)		KDLAK(2)
	- Ra-226		200	T (100, 200, 300)		KDLAK(3)
	- Pb-210		1,000	T (500, 1,000, 1,500)		KDLAK(4)
	- Po-210		1,000	T (500, 1,000, 1,500)		KDLAK(5)
	- As		500	T (250, 500, 750)		KDLAK(6)
	- Ni		500	T (250, 500, 750)		KDLAK(7)
Z	lake mean depth:	m			INPUT	
	- Lake 1		10	C (20)		ZLAK(1)
	- Lake 2		10	C (30)		ZLAK(2)
A	lake area:	m^2			INPUT	
	- Lake 1		1E10^6	C (1E6)		ALAK(1)
	- Lake 2		1E10^6	C (33E6)		ALAK(2)
t_w	detention time:	years			INPUT	
	- Lake 1		1	T (0.1,0.7,1.3)		TW(1)
	- Embayment		3	T (0.2,2.4,3.6)		TW(2)
alp	exchange coefficient:	-			INPUT	
	- Lake 1		0	C (0)		ALPHA(1)
	- Embayment		4	C (4)		ALPHA(2)
por	sediment porosity:	-			INPUT	
	- Lake 1		0.95	C (0.95)		PORSED(1)
	- Lake 2		0.95	C (0.95)		PORSED(2)
g	particulate settling velocity:	m·a^{-1}			INPUT	
	- Lake 1		25	T (15, 25, 35)		G(1)
	- Lake 2		25	T (15, 25, 35)		G(2)
k_s	mass transfer coefficient:	m·a^{-1}			INPUT	
	- U		4	T (2, 4, 6)		FKS(1)
	- Th-230		4	T (2, 4, 6)		FKS(2)
	- Ra-226		4	T (2, 4, 6)		FKS(3)
	- Pb-210		4	T (2, 4, 6)		FKS(4)
	- Po-210		4	T (2, 4, 6)		FKS(5)
	- As		0.4	T (0.2, 0.4, 0.6)		FKS(6)
	- Ni		0.4	T (0.2, 0.4, 0.6)		FKS(7)
g_s	sedimentation rate:	m·a^{-1}			INPUT	
	- Lake 1		0.001	T (0.0002,0.0005,0.0020)		GS(1)
	- Lake 2		0.001	T (0.0002,0.0005,0.0020)		GS(2)
k	radioactive decay rate:	a^{-1}			INPUT	
	- Th-230		8.7E-6	C (8.664E-6)		RADIOD(2)
	- Ra-226		4.27E-4	C (4.273E-4)		RADIOD(3)
	- Pb-210		0.034	C (3.397E-2)		RADIOD(4)
	- Po-210		1.83	C (1.83)		RADIOD(5)
W_o	loading	Bq·a^{-1} or g·a^{-1} or mol·a^{-1}	-	-	calculated	W
C	activity or concentration in lake or embayment	Bq·L^{-1}; g/m^{-3}; mol·L^{-1}	-	-	calculated	CLAK(I,K)
C_s	activity or concentration in lake sediments	Bq·L^{-1}; g·m^{-3}; mol·L^{-1}	-	-	calculated	CSED(I,K)

Lake 1: First receiving lake; also called the upstream lake.

Lake 2: Second receiving lake connected to embayment; also called the 'large lake'. Outflow from Lake 1 goes into the embayment on Lake 2 and then into the main body of Lake 2 (see Figure 2.1).

$$C_{vi}'(t) = C_{ai}(t)\, V_d \quad F_{rv}\, E_v \quad 1 - \exp(-\lambda_{wv} t_v)\, (Y_v\, \lambda_{wv})^{-1} \qquad (5.5.1)$$

where: $C_{vi}'(t)$ = the resulting concentration of radionuclide or stable element i in vegetation v at time t from atmospheric deposition ($Bq \cdot g^{-1}$ or $ug \cdot g^{-1}$ (wet weight))

$C_{ai}(t)$ = the average annual concentration of radionuclide or stable element i in the air at that location at time t ($Bq \cdot m^{-3}$ or $ug \cdot m^{-3}$)

V_d = the deposition velocity ($m.s^{-1}$)

F_{rv} = the fraction of the foliar deposition retained on edible portions of vegetation type v (0 to 1)

E_v = the fraction of the total deposition retained on the plant surface of vegetation type v (0 to 1)

λ_{wv} = a decay constant accounting for weathering losses from vegetation type v (s^{-1})

t_v = the duration of the plant exposure to atmospheric deposition for vegetation type v (s)

Y_v = the yield density for vegetation type v (g (wet weight)$.m^{-2}$)

Table 5.6 lists the variables used in this model. The values for V_d, F_{rv}, E_v, t_v and λ_{wv} for vegetation were allowed to vary uniformly around the nominal values recommended by the U.S. NRC (1982), with the exception of t_v for browse, which was taken from BEAK (1985f). The variables V_d, F_{rv}, E_v and λ_{wv} relate to physical processes affecting the deposition of airborne particulates, and their values are assumed to be common to radionuclides, arsenic and nickel. Values for Y_v were also allowed to vary uniformly around values recommended by BEAK (1985f). Radioactive decay is not incorporated into the model for the short-lived radionuclide, Po-210, as secular equilibrium is assumed to exist between Pb-210 and Po-210 in the atmospheric source term (i.e., the unsaturated zone in the tailings).

5.5.2 Concentrations in Edible Vegetation from Root Uptake (Subroutine VEGDEP)

The equation used here to calculate concentrations of materials in vegetation from root uptake is given by:

TABLE 5.6: VEGETATION UPTAKE MODEL VARIABLES

Symbol	Description	Units	Nominal	Probabilistic	Source	Computer Symbol
$C_{ai}(t)$	air concentration of element i	Bq·m^{-3} (radionuclides) ug·m^{-3} (U, As,Ni)	calculated	calculated	AIRDIS	CAIR(I) (I = 1-7)
$C_{vi}(t)$	vegetation type v concentration of element i	Bq·g^{-1} (radionuclides) ug·g^{-1} (U, As, Ni)	calculated	calculated	VEGDEP	CVEG(I, J) I = elements 1-7 J = vegetation type
	above-ground vegetables					CVEG(I,1)
	below-ground vegetables					CVEG(I,2)
	browse					CVEG(I,3)
F_{rv}	fraction of total deposition retained on surface of vegetation:				INPUT	
	above-ground vegetables		0.2	U (0.1, 0.3)		FDEPSF(1)
	below-ground vegetables		0.2	U (0.1, 0.3)		FDEPSF(2)
	browse		0.2	U (0.1, 0.3)		FDEPSF(3)
E_v	fraction of plant deposition retained on edible portions:				INPUT	FDEPED(J)
	above-ground vegetables		1.0	U (0.8, 1.0)		FDEPED(1)
	below-ground vegetables		0.1	U (0.05, 0.15)		FEDEPED(2)
	browse		1.0	U (0.8, 1.0)		FDEPED(3)
t_v	duration of exposure to deposition	S			INPUT	DUREXP(J)
	above-ground vegetables		5.184E6	U(4.7E6, 5.6E6)		DUREXP(1)
	below-ground vegetables		5.184E6	U(4.7E6, 5.6E6)		DUREXP(2)
	browse		7.8E6	U(6.8E6, 8.8E6)		DUREXP(3)
V_d	deposition velocity	m·s^{-1}	0.02	U(0.003, 0.03)	INPUT	DEPVEL
Y_v	yield density:	g·m^{-2}			INPUT	YDEN(J)
	above-ground vegetables		2000	U(1500, 2500)		YDEN(1)
	below-ground vegetables		2000	U(1500, 2500)		YDEN(2)
	browse		100	U(75, 125)		YDEN(3)
λ_{wv}	decay constant accounting weathering loss:	s^{-1}				VEGLAM(J)
	above-ground vegetables		5.73E-7	U(4E-7, 6E-7)	INPUT	VEGLAM(1)
	below-ground vegetables		5.73E-7	U(4E-7, 6E-7)		VEGLAM(2)
	browse		5.73E-7	U(4E-7, 6E-7)		VEGLAM(3)
B_v	soil-to-plant concentration factor:	(Bq·g^{-1}w.w.)·(Bq·g^{-1}d.w.)$^{-1}$			INPUT	BV(J,I) I = element
	above-ground vegetables	U		LN(1.9E-3,11,1.0E-5,5.5E-1)		BV(1,1)
		Th		LN(3.9E-3,13,5.0E-4,2.5)		BV(1,2)
		Ra		LN(6.0E-3,8.1,8.0E-5,7.0E-1)		BV(1,3)
		Pb		LN(1.3E-2,5.2,7.0E-3,1.3E-1)		BV(1,4)
		Po		LN(2.2E-2,12,2.0E-4,3.5E-1)		BV(1,5)
		As		LN(3.6E-2,16,3.2E-4,1.9E2)		BV(1,6)
		Ni		LN(3.7E-2,4.6,3.8E-3,1.7E0)		BV(1,7)
	below-ground vegetables	U		LN(1.9E-3,11,1.0E-5,5.5E-1)		BV(2,1)
		Th		LN(3.9E-3,13,5.0E-4,2.5)		BV(2,2)
		Ra		LN(6.0E-3,8.1,8.0E-5,7.0E-1)		BV(2,3)
		Pb		LN(1.3E-2,5.2,7.0E-3,1.3E-1)		BV(2,4)
		Po		LN(2.2E-2,12,2.0E-4,3.5E-1)		BV(2,5)
		As		LN(8.7E-2,18,9.0E-4,30)		BV(2,6)
		Ni		LN(1.2E-1,3.7,2.5E-3,5.9)		BV(2,7)
	browse	U		LN(3.8E-3,22,2.0E-5,1.1)		BV(3,1)
		Th		LN(7.8E-3,26,1.0E-3,5.0)		BV(3,2)
		Ra		LN(1.2E-2,16,1.6E-4,1.4)		BV(3,3)
		Pb		LN(2.6E-2,10.4,1.4E-2,2.6E-1)		BV(3,4)
		Po		LN(4.4E-2,24,4.0E-4,7.0E-1)		BV(3,5)
		As		LN(7.2E-2,32,6.2E-4,3.8E2)		BV(3,6)
		Ni		LN(7.4E-2,9.2,7.6E-3,3.4)		BV(3,7)
C_{si}	concentration of element i in soil	Bq·m^{-3} (ug·m^{-3} for U, As, Ni)	calculated	calculated	SOIL	CSOIL(I) (I = 1-7)

$$C_{vi}''(t) = B_v \cdot C_{si}(t)/1.6E6$$

where: $C_{vi}''(t)$ = the resulting concentration of radionuclide or stable element i in vegetation v at time t from root uptake ($Bq \cdot g^{-1}$ or $ug \cdot g^{-1}$ (wet weight))

B_v = plant/soil concentration ratio (unitless)

$C_{si}(t)$ = the concentration of radionuclide or stable element i in the soil root zone at time (t), calculated in subroutine SOIL ($Bq \cdot m^{-3}$ or $ug \cdot m^{-3}$)

1.6E6 = the assumed soil density, in ($g \cdot m^{-3}$) (from U.S. NRC 1977).

Most of the data on soil-to-plant transfer coefficients (B_v's) in the literature are based on measurements of concentrations in fruits, vegetables, leaves and stems that may have a considerable moisture content. The authors of this report measured the water content of three samples of herbaceous plant tissue, and found a typical moisture content of about 75%. We have used this factor to calculate fresh weight B_v values from dry weight concentration data typically reported in the literature (Appendix B). Zach and Mayoh (1982) reported a water content of about 50% in browse forming the diet of moose. This lower water content is likely attributed to a considerable proportion of woody tissues such as twigs in the moose diet. (Woody tissues may be expected to have a lower water content than herbaceous tissues.) Such tissues account for a very large portion of the moose diet, particularly in winter. For this study, we have estimated the distribution of the B_v parameter for browse from the calculated distribution for B_v in above-ground vegetables, with an adjustment to account for the different moisture contents.

Most values for food chain transfer parameters reported in the literature are highly variable. In this and subsequent subroutines, most of these parameters are assumed to be lognormally distributed. This distribution is defined in the model input with a geometric mean, geometric standard deviation, minimum and maximum. All values are expressed arithmetically rather than logarithmically in the input file. Upper and lower limits are assumed to be either the geometric mean ± 3 geometric standard deviations (expressed in $\log_{10}$ units), or the minimum and maximum values defined by data points in the literature. The larger of the two ranges so defined was typically selected.

Soil-to-plant transfer factors (B_{vi}'s) are highly variable and typically lognormally distributed (Cassaday et al., 1985). In the B_v values compiled by Cassaday et al. for Ra-226 and uranium, values for root vegetables and above-ground vegetables did not differ appreciably. When values for grasses, hay and herbage given by Cassaday et al. (1985) are converted to a wet weight basis (75% moisture was assumed), B_v values for this group was similar to B_v values for vegetables. B_v values found at the Gunnar site for semi-aquatic vegetation were close to the geometric mean of values reported by Cassaday et al. (1985) for Ra-226 and uranium (Table B5.5.1). The entire data set given by Cassaday et al. (1985) for these two radionuclides (with an adjustment for the dry weight - wet weight conversion in forage), supplemented by the Gunnar data set, was used to calculate the B_v values for uranium and Ra-226 in Table 5.6. One B_v value is assumed to apply for each radionuclide in all vegetation types, with an adjustment for a lower water content in browse.

B_v values for Th-230, Pb-210 and Po-210 were compiled by Cassaday et al. (1985) and BEAK (1985f). A few values for these radionuclides are also available from the Gunnar site (Table B5.5.1). The B_v values and distributions for these radionuclides were compiled from these databases, with appropriate adjustments to convert value based on plant dry weight to a wet-weight basis. "Less than" values reported for the Gunnar site were assumed to be equal to half of the detection limit.

Uptake of arsenic by plants from soil has been reviewed by NRCC (1981). Arsenic has been widely studied due to its use in pesticides. B_v values calculated from data in NRCC (1981) vary widely, both within plant tissues and among chemical forms of arsenic under study. The data suggest that root tissues accumulate arsenic more readily than other plant parts, although B_v values for potatoes do not appear to differ from those found above-ground parts in other plants. B_v values (and distributions) for arsenic were calculated from the data in NRCC (1981) (Table B5.5.2), with a correction factor applied for data reported on a dry weight tissue basis. Separate B_v values were determined for above-ground and below-ground vegetation.

Data on B_v values for nickel are summarized in Table B5.5.3. These data are based primarily on the work of Whitby (1974) on plants grown in metal-contaminated soils near Sudbury, Ontario. The data suggest that roots accumulate greater concentrations of nickel than do leaves or shoots (Whitby, 1974). The B_v values for nickel in Table B5.5.3 are used to compute the distributions, given in Table 5.6.

Values for vegetation yield, Y_v, for above- and below-ground vegetables were allowed to vary uniformally around the nominal value given by the U.S. NRC (1985) as done by

SENES (1985). Food consumed by moose, termed "browse", consists of a mixture of herbaceous vegetation, leaves, twigs and grasses, as well as aquatic plants in summer (Banfield, 1974). The annual yield of forage grasses, herbs and shrubs ("browse") was allowed to vary uniformly around the value of 300 g/m^2 recommended by IEC BEAK (1984) as appropriate for northern Saskatchewan.

5.6 Uptake by Aquatic Biota

5.6.1 Concentrations of Element i in Edible Portions of Fish (Subroutine AQBIOTA)

5.6.1.1 Concentrations in Fish

A simple aggregate model was used to calculate the concentration of elements in the flesh of fish from lakes downstream from the tailings. It is:

$$C_{fi}(t) = B_{fi}\, C_{swi}(t) \qquad (5.6.1)$$

where:

$C_{fi}(t)$ = the resulting annual average concentration of element i in fish tissue at time t (Bq·g^{-1} or ug·g^{-1} wet weight)

B_{fi} = water to fish transfer coefficient for element i (Bq·g^{-1} or ug·g^{-1} (wet weight) · Bq^{-1}·m^3)

$C_{swi}(t)$ = the calculated average annual concentration of element i in lake water at time t (Bq·m^{-3} or ug·m^{-3}).

The distribution of B_{fi} for radium was determined based on the data given by Halbert et al. (1985) and the supplemental data given in Table B5.6.1. The distribution of B_{fi} values for uranium, lead, arsenic and nickel were taken from the data compiled in Tables B5.6.2, B5.6.3, B5.6.4 and B5.6.5, respectively. B_{fi} values cited as "greater than" or "less than" were excluded from the calculated distributions, since either water or tissue concentrations were below detection limits and adequate quantities of other data were available. Also, only B_{fi} values for muscle or muscle plus skin were used in the calculations, since this is the edible portion.

Data on bioconcentration factors for thorium are sparse. All values are affected by water concentrations below detection limits (Table B5.6.6). B_{fi} values were assumed to be twice the "greater than" values given in Table B5.6.6. The B_{fi} values for thorium were assumed to be log-normally distributed, as typically observed with other bioconcentration factors. The range of the B_{fi} distribution for thorium was defined as the geometric mean plus or minus three geometric standard deviations (expressed on a $\log_{10}$ scale). This range brackets the value of 3.0×10^{-5} $m^3 \cdot g^{-1}$ recommended by Thompson et al. (1972) for thorium in freshwater fish. John and Dalton (1985) found very little thorium in considerable quantities of fish collected from Hidden Bay, which is impacted by uranium tailings discharges, indicating that thorium is accumulated very little by fish. This distribution for B_{fi} reflects this recent evidence, with only the upper extreme of its range encompassing the value cited by Thompson et al. (1972).

Data on bioconcentration factors for polonium were also sparse, and affected by water concentrations below detection limits (Table B5.6.7). The B_{fi} of 50 L/kg recommended by Thompson et al. (1972) for polonium was included in the data points in computing the B_{fi} distribution. B_{fi} values were assumed to be twice the "greater than" values given in Table B5.6.7, and log-normally distributed. The log-normal distribution is truncated at three geometric standard deviations from the geometric mean.

Table 5.7 summarizes the distributions of water to fish model variables.

5.6.1.2 Toxicity Considerations

In the event that arsenic or nickel concentrations resulting in the downstream embayment from tailings leachate are toxic to fish, the fish pathway to man will be eliminated for all elements. The toxicity of arsenic and nickel to fish has been reviewed by NRCC (1978, 1981a). Arsenic is acutely lethal within hours to a few days at concentrations over about 10 $mg \cdot L^{-1}$. Arsenic has a sublethal toxicity at concentrations of 1 $mg \cdot L^{-1}$ and, in a few instances, at even lower concentrations. Nickel is acutely lethal at about 5 to 500 $mg \cdot L^{-1}$, depending on the organism tested and on water hardness. Chronic toxicity occurs at nickel concentrations in the order of 1 $mg \cdot L^{-1}$, again depending on water hardness and the organism tested. For this project, the fish pathway is eliminated from the calculations if the concentration of either arsenic or nickel in the downstream embayment is predicted to be equal to or greater than 1 $mg \cdot L^{-1}$ (i.e., 1×10^6 $ug \cdot m^{-3}$). This is done in the code by designating C_{fi} as zero when C_{swi} for arsenic or nickel is 1 $mg \cdot L^{-1}$ or greater.

TABLE 5.7: WATER TO AQUATIC BIOTA MODEL VARIABLES

Symbol	Description	Units	Statistics	Source	Computer Symbol
B_{fi}	water to fish transfer coefficient for element i:	$(\text{Bq or ug})\cdot g^{-1}$ (wet weight)$\cdot Bq^{-1}\ m^3$		INPUT	BF (I) I = element
	U		LN (1.2E-6, 5.2, 2.6E-8, 1.6E-5)		BF (1)
	Th		LN (6.9E-8, 7.7, 1.5E-10, 3.1E-5)		BF (2)
	Ra		LN (1.5E-5, 4.1, 1.0E-6, 6.0E-4)		BF (3)
	Pb		LN (1.9E-5, 2.9, 2.6E-6, 1.6E-4)		BF (4)
	Po		LN (1.1E-4, 1.6, 2.5E-5, 4.9E-4)		BF (5)
	As		LN (1.1E-5, 8.3, 1.0E-7, 6.4E-4)		BF (6)
	Ni		LN (1.4E-4, 2.4, 5.0E-5, 4.3E-4)		BF (7)
C_{fi} (t)	concentration of element i in fish flesh	$(\text{Bq or ug})\cdot g^{-1}$	calculated	calculated	C FISH (T) I = element 1 to 7
C_{swi} (t)	concentration of element i in embayment water	$(\text{Bq or ug})\cdot m^{-3}$	calculated	LOADLK	CWATER(I) (I = 1-7)
B_{pi}	water to plant transfer coefficient for element i:	$(\text{Bq or ug})\cdot g^{-1}$ (wet weight)$\cdot Bq^{-1} m^3$		INPUT	
	U		LN (1.9E-4, 2.9, 6.2E-5, 1.0E-3)		BP(1)
	Th		LN (3.9E-4, 6.9, 4.3E-5, 1.5E-3)		BP(2)
	Ra		LN (1.1E-3, 3.3, 1.7E-4, 6.9E-3)		BP(3)
	Pb		LN (8.2E-5, 2.0, 1.0E-5, 8.0E-4)		BP(4)
	Po		LU (3.6E-4, 1.1E-2)		BP(5)
	As		LN (3.4E-5, 5.8, 2E-6, 3.3E-4)		BP(6)
	Ni		LN (1.8E-4, 4.1, 4.0E-5, 1.3E-3)		BP(7)
C_{pi}(t)	concentration of element i in plant tissue		calculated		CVEG(4)

The pH of downstream waters is also calculated by the LAKE subroutine. While it is unlikely that extremely acidic drainage would be generated by the non-pyritic tailings, it is worthwhile to incorporate a provision for elimination of the fish pathway in the event of low pH conditions downstream. This provision makes the FISH subroutine more applicable to both pyritic and non-pyritic tailings situations. The NRCC (1981b) reviewed the effects of acidification on fish populations in areas susceptible to acidic precipitation. While the sensitivity of fish to low pH is species-specific and may depend on other environmental and physiological variables, as can be seen from Figure B5.6.1 (Appendix B), most species are stressed or eliminated at a pH less than 5. Presumably, "stressed" populations indicated in Figure B5.6.1. would eventually become extinct over time. For this demonstration, the fish pathway is eliminated from the calculations when the predicted pH of the downstream embayment is less than or equal to 5.0.

5.6.2 Concentrations in Aquatic Plants (Subroutine AQBIOTA)

Aquatic plants account for a considerable portion of the diet of moose in the summer months (Banfield, 1974; Belovsky et al., 1975) and thus may contribute to the body burden of radionuclides, nickel and arsenic in moose feeding in watersheds draining tailings areas. Concentrations of elements in aquatic plants are typically estimated in modelling studies by the ratio of concentrations in plant tissues to the concentrations in water, although it is recognized that bioaccumulation is a dynamic process including uptake from water, uptake from sediments, and elimination by the plant back to the environment. Garner et al. (1985) demonstrated that at steady-state, radium concentrations in fish tissues are predicted equally well by a multi-component, dynamic model and by a simple water-to-fish concentration in factor model because fish transfer kinetics are rapid compared to those of the lake. It is probable that this observation is valid also for plant uptake, due to the comparable kinetics and uncertainties in the parameters involved in bioaccumulation by plants and fishes.

Here, the bioconcentration factor method is used to estimate concentrations of elements in aquatic plant tissues. Concentration factors are computed on a wet weight basis, that is, (concentration in plants (wet weight))/(concentration in water). Many published concentrations in aquatic plants are expressed on a dry weight basis for plant tissues. For this demonstration, dry weight is assumed to be 10% of wet weight. This is based on an average moisture content of 91.3% measured in submergent aquatic plants (primary *Myriophyllum spicatum*) collected in a southern Ontario reservoir by BEAK (unpublished data), and by a typical dry weight/wet weight conversion factor of 10% given by Dietz (1973) for various aquatic species.

The concentration of elements in aquatic plant tissues from lakes downstream of the tailings is:

$$C_{pi}(t) = B_{pi}\, C_{swi}(t) \qquad (5.6.2)$$

where: $C_{pi}(t)$ = the resulting annual average concentration of element i in aquatic plant tissue and time t ($Bq \cdot g^{-1}$ or $ug \cdot g^{-1}$ wet weight)

B_{pi} = water to plant transfer coefficient for element i ($Bq \cdot g^{-1}$ or $ug \cdot g^{-1}$) (wet weight)$\cdot$ $Bq^{-1} \cdot m^3$)

$C_{swi}(t)$ = the calculated annual average concentration of element i in lake water at time t ($Bq \cdot m^{-3}$ or $ug \cdot m^{-3}$)

The bioaccumulation factors for U, Th, Ra, Pb and As were assigned log-normal distributions based on the data given in Tables B5.6.8, B5.6.9, B5.6.10, B5.6.11 and B5.6.12, respectively. Owing to the lack of relevant data, the distribution of the Po bioaccumulation factor was assumed to be log uniform around the value suggested by Thompson _et al._ (1972). An abundance of data was available on the accumulation of nickel by aquatic plants (Table 7.14). In particular, there were considerable Canadian data available on bioaccumulation factors for floating-leaf species (_Nuphar variegatum_, _Nymphaea odorata_ and _Nymphoides cordatum_), the preferred aquatic food of moose (Section 6.0). The distribution of the bioaccumulation factor for nickel in aquatic plants was based on data for these species. Table 5.7 provides a summary of the input parameters for the on the aquatic plant model.

5.7 The Forage-Moose Pathway (Subroutine VEGEAT)

Subroutine VEGEAT calculates the activities (Bq/g wet weight) of Th-230, Ra-226, Pb-210 and Po-210, and the concentrations (ug/g wet weight) of U, As and Ni in moose meat, based on moose feeding habits and levels of contamination in forage plants and drinking water. Forage plant contamination is calculated by the subroutine VEGDEP. Drinking water contamination is calculated by the subroutine LAKE. Other parameters of the subroutine VEGEAT are user-defined.

-Algebraically, the subroutine takes the following form:

$$Cbi_{(t)} = Qb\ Fbi \sum_{v=1} Fv\ Cvi_{(t)} \qquad (5.7.1)$$

where: $Cvi_{(t)}$ = level of contaminant i in vegetation, of type v, at time t ($Bq \cdot g^{-1}$ or $ug \cdot g^{-1}$),

Fv = fraction of total food intake consisting of vegetation type v from the receptor area,

Fbi = feed-to-meat transfer factor for contaminant i to moose tissue b (a/g),

Qb = total food intake of a moose (g/a), including water, and

$Cbi_{(t)}$ = level of contaminant i in moose tissue b at time t ($Bq \cdot g$ or $ug \cdot g$).

Drinking water is treated as a vegetation type (v=5), along with aquatic plants (v=4) and browse (v=3). (Vegetation types 1 and 2 are above and below ground vegetables, which are not in the moose pathway.) Concentrations in drinking water in this case are converted to a mass or activity per gram basis to facilitate computations. The sum of fractions Fv in this pathway may not exceed one (1), but may be less than one if the moose takes some of its food or water from outside the receptor area. The receptor area is the same area for which the Cvi distributions are defined.

Three moose tissue types may be utilized by hunters, including muscle (b=1), liver (b=2) and kidney (b=3). Muscle tissue is consumed in much greater quantities than any of the other types, and is therefore usually the most significant hunter exposure pathway. However, the kidney and liver tend to accumulate higher levels of contamination and are prized by hunters as delicacies. Feed-to-meat transfer factors in the literature usually refer to muscle tissue unless otherwise indicated.

General descriptions of moose feeding habits are given by Peterson (1966), Banfield (1974) and Euler (1979). In winter, moose feed entirely on a diet defined by "browse", whereas, in summer, they supplement their diet with aquatic plants, if available. Waterlilies (Nymphea, Nuphar) and pondweeds (Potamogeton) are favourite aquatic plants. Both leaves and stems are eaten. If aquatic plants are not available, grasses and foliage will be eaten.

A quantitative analysis of winter feeding in Manitoba was completed by Zach et al. (1982). Table B5.7.1 lists preferred browse species according to Euler (1979) and Banfield (1974), along with percentage contribution to dry weight in moose rumens from three Manitoba study areas. In browsing, moose tend to concentrate on a few vegetation species, although these species may vary both from year to year and regionally, in response to the relative availability of local species. Aspen, dogwood, balsam fir and willow seem to be favourite species for browsing in Manitoba.

The Gunnar Mine site in northern Saskatchewan may be considered a typical non-pyritic tailings area. Vegetation surveys list most of the favourite moose forage species, including aspen, dogwood, willow and pondweeds (Harms and Fraser, 1982). Willow is particularly common on the tailings, and pondweeds are found in Langley Bay.

Belovsky (1975) gives daily food intake rates for moose. These were used to estimate annual intake rates in Table B5.7.2 for drinking water, aquatic plants and browsing. Aquatic plant and browsing intake was adjusted from a dry to wet weight basis, assuming a 10% moisture content for aquatic plants (Dietz, 1973) and a 50% moisture content for browse (Zach and Mayoh, 1982). Aquatic plants were assumed to be available for four months of the year. Annual intake rates for each food category can be expressed as a fraction (F) of total food intake (Qb).

A moose occupancy factor was used to derive Fv fractions for drinking water, aquatic plants and browsing. Crichton (1980) estimated that there were 2.3 moose/km^2 in suitable habitat on Hecla Island in Manitoba. However, Prince Albert conservation authorities estimate a density of 0.3 moose/km^2 in the Gunnar area (E. Kowal, pers. comm., 1985). Assuming a moose receptor area of 10.9 km^2, that area would support 3.3 moose, based on the smaller density. The 10.9 km^2 moose receptor area would correspond to a narrow zone 0.5 km wide around the circumference of a roughly circular 33 km^2 receptor embayment. Thus, it is possible for a moose to reside entirely within the receptor area. The occupancy factor was allowed to vary between 0 and 1.

Feed-to-meat transfer factors were derived from feed-to-meat bioaccumulation factors, or taken directly from the published literature. Bioaccumulation factors were divided by the feed intake rate to give a corresponding transfer factor. Belovsky (1975) gives a dry feed intake rate of about 1.8E6 g/a (5 kg/d) for moose (Table B5.7.2). This intake is primarily by browsing and, therefore, equivalent to about 3.6E6 g/a on a wet weight basis (excluding intake of drinking water).

Bioaccumulation factors are listed in Table B5.7.3 for ruminant species, including moose, cattle and sheep. Arsenic and nickel bioaccumulation factors were computed for liver and kidney, as well as muscle tissue, from published concentrations in tissue and dry feed (Peoples, 1964; Calvert, 1975; Lancaster et al., 1971; O'Dell et al., 1971). Radionuclide bioaccumulation factors are given by Letourneau (1984) for moose and other large game animals, on a fresh tissue, dry feed basis. Some lead and polonium bioaccumulation factors for liver and kidney were taken directly from Letourneau's data. Other organ-specific bioaccumulation factors were derived from Letourneau's values for meat, using organ:muscle concentration ratios from other sources (Diem and Lentner, 1970; Persson, 1972; IEC BEAK, 1984).

Peoples (1964), cited by NRCC (1978), gives an arsenic intake rate rather than a dry feed concentration. Thus, the data are suitable for direct calculation of a feed-to-beef transfer factor from As intake and meat concentration. A bioaccumulation factor was also calculated (Table B5.7.3) based on the assumption of 5 kg/d dry feed consumed. This is approximately 1% of fresh body weight per day, and is consistent with domestic livestock feeding standards for adult cattle (NAS/NRC, 1971). A range of As concentrations were given for each tissue; the bioaccumulation factor in Table B5.7.3 is the median value.

Feed-to-mutton bioaccumulation factors, computed from average As concentrations in sheep tissues and feed (Calvert, 1975, as cited by HWC, 1980 and Lancaster et al., 1971), were in agreement with feed-to-beef bioaccumulation factors derived from Peoples' data because kidney and liver accumulations exceeded those in the muscle tissue. This pattern is typical of most heavy metals since the liver and kidney are involved in detoxification and excretion of metals. Hepatic portal circulation in mammals carries absorbed constituents from the gut directly to the liver prior to systemic circulation.

Inorganic arsenic is absorbed more readily than any of the organic arsenicals (NRCC, 1978). Organic complexation may occur in the vegetation on which moose feed. However, because there is little useful data on this feeding process in the literature, the simplest and most conservative approach is to base food chain model parameters on experiments conducted with inorganic arsenic. This approach was followed in selecting data for computation of bioaccumulation factors.

O'Dell et al. (1971) give Ni concentrations in calf tissues on a dry weight rather than wet weight basis. The mean concentrations were adjusted to a wet weight basis, assuming a tissue moisture content of 70%. Lloyd et al. (1978) indicate that this moisture content is typical for muscle, liver and kidney tissues. The only skeletal muscle tissue examined by O'Dell et al. was the tongue; this was considered to be representative of other muscle tissues, although the specialized glandular tissue of the tongue was included in the analysis.

Nickel bioaccumulation factors for cattle derived from the data of O'Dell et al. agree very closely with the arsenic bioaccumulation factors derived from Peoples' (1964) data, for muscle and kidney tissues. However, O'Dell et al. (1971) draw attention to the fact that very little nickel is accumulated in the calf liver, in contrast to the typical internal distribution of other metals, and the significant accumulation of arsenic in the liver during Peoples' (1964) study.

Miller (1973) presents data on nickel concentration in animal bodies and domestic ruminant feeds, which suggest a nickel bioaccumulation factor of less than 0.07. However, this value is based on a rather tenuous juxtaposition of human body burdens (Schroeder, 1962, 1965) and nickel concentration in pasture grass and domestic feeds (Underwood, 1966, 1971). It was not used in defining model parameter distributions for the forage-moose pathway.

Bioaccumulation factors were divided by the dry feed intake rate for moose (1.8E6 g/a, Belovsky, 1975) in order to derive feed-to-meat transfer factors for the forage-moose pathway. These derived values are included in Table B5.7.4, along with radionuclide transfer factors from the published literature (Rayno, 1983; McDowell-Boyer et al., 1980; Garner, 1972; Momeni et al., 1979; NUREG, 1980). Rayno (1983) has reviewed the earlier literature on uranium series radionuclide transfer factors and tabulated transfer factors.

Transfer factors for a number of different ruminant species were pooled in order to define a mean and standard deviation for the feed-to-meat transfer factor of each radionuclide or heavy metal. A log normal distribution of transfer factors was assumed

(Zach, 1980), although the quantity of data available was insufficient to test this assumption.

Parameter distributions for the forage-moose pathway are summarized in Table 5.8. The overall feed intake rate (Qb) is assumed to be a constant (2.22E7 g/a, wet weight), including intake of drinking water, aquatic plants and browse. Limits on the feed-to-meat transfer factor are based on the variability of transfer factors among ruminant species (Table B5.7.4). Limits on the food intake fractions (Fv) are based on average moose feeding habits (Belovsky, 1975) and a variable moose occupancy factor.

Transfer factor distributions for liver and kidney are each assumed to be correlated with the transfer factor distribution for muscle tissue. Thus, a heavily contaminated moose is heavily contaminated in all its tissues. For uranium, thorium, radium and nickel, a constant organ:muscle contamination ratio was assumed for each organ (i.e., correlation coefficient = 1.0). For lead, polonium and arsenic, empirical data contributed to the estimation of correlations between transfer factor distributions.

Distributions of the food intake fractions for different food types (browse, aquatic plants and water) were assumed to be independent. Any correlations between these parameters are likely to be highly site-specific, depending on availability and spatial dispersion of browse, aquatic plants and water sources within and beyond the receptor area.

5.8 Uptake by Man (Subroutine DOSEIN)

5.8.1 Introduction

The impacts of releases of U-238 decay chain radionuclides, arsenic and nickel from non-pyritic tailings on man are measured in terms of ingestion and inhalation. The impact of radionuclide intake by the average member of the critical group is measured by the committed effective dose equivalent. For this project, the incremental intake of arsenic and nickel is expressed on the basis of mass of each element consumed and inhaled per year. Table 5.9 summarizes parameters and distributions for the uptake subroutine.

The annual dose that is calculated in this assessment is the annual effective dose equivalent based on stochastic (zero threshold) effects. Non-stochastic effects for doses

TABLE 5.8: VARIABLES USED IN THE CALCULATION OF MOOSE CONTAMINATION FROM INGESTED FORAGE AND WATER

Symbol	Description		Units	Nominal	Probabilistic	Source	Computer Symbol
FORAGE-MOOSE MODEL (VEGEAT)							
$C_{bi(t)}$	level of element i in moose tissue b:		$Bq \cdot g^{-1}$ ($ug \cdot g^{-1}$ for U, As, Ni)	calculated	calculated	VEGEAT	CMEAT (I, K) I = element, K = tissue type
	o muscle	- U					CMEAT (1,1)
		- Th					CMEAT (2,1)
		- Ra					CMEAT (3,1)
		- Pb					CMEAT (4,1)
		- Po					CMEAT (5,1)
		- As					CMEAT (6,1)
		- Ni					CMEAT (7,1)
	o liver	- U					CMEAT (1,2)
		- Th					CMEAT (2,2)
		- Ra					CMEAT (3,2)
		- Pb					CMEAT (4,2)
		- Po					CMEAT (5,2)
		- As					CMEAT (6,2)
		- Ni					CMEAT (7,2)
	o kidney	- U					CMEAT (1,3)
		- Th					CMEAT (2,3)
		- Ra					CMEAT (3,3)
		- Pb					CMEAT (4,3)
		- Po					CMEAT (5,3)
		- As					CMEAT (6,3)
		- Ni					CMEAT (7,3)
Q_b	Feed intake rate		$g \cdot a^{-1}$	2.22E7	C(2.22E7)	INPUT	FIR
F_{bi}	Feed-to-meat transfer factor for element i to moose tissue b:		$a \cdot g^{-1}$			INPUT	FBI(I, K) I = element, K = tissue type
	o muscle	- U		2.59E-9	LN(2.59E-9,5.04,2.0E-11,3.3E-7)		FBI(1,1)
		- Th		1.06E-9	LN(1.06E-9,2.35,8.2E-11,1.4E-8)		FBI(2,1)
		- Ra		5.55E-9	LN(5.55E-9,2.65,3.0E-10,1.0E-7)		FBI(3,1)
		- Pb		2.36E-9	LN(2.36E-9,3.91,4.0E-11,1.4E-7)		FBI(4,1)
		- Po		6.63E-9	LN(6.63E-9,2.25,5.8E-9,7.6E-7)		FBI(5,1)
		- As		1.75E-9	LN(1.75E-9,2.51,1.1E-10,2.8E-8)		FBI(6,1)
		- Ni		5.56E-10	LN(5.56E-10,10.0,5.6E-13,5.6E-7)		FBI(7,1)
	o liver	- U		7.76E-8	CR(¯7.11,0.70,309,1.00,¯8.59,0.70)		FBI(1,2)
		- Th		3.18E-8	CR(¯7.49,0.37,310,1.00,¯8.98,0.37)		FBI(2,2)
		- Ra		5.55E-9	CR(¯8.26,0.42,311,1.00,¯8.26,0.42)		FBI(3,2)
		- Pb		1.63E-7	CR(¯6.79,0.39,312,0.95,¯8.63,0.59)		FBI(4,2)
		- Po		8.34E-7	CR(¯6.08,0.39,313,0.99,¯7.18,0.35)		FBI(5,2)
		- As		1.34E-8	CR(¯7.87,0.59,314,0.84,¯8.76,0.40)		FBI(6,2)
		- Ni		2.20E-10	CR(¯9.66,1.00,315,1.00,¯9.25,1.00)		FBI(7,2)

TABLE 5.9: VARIABLES USED IN THE CALCULATION OF ANNUAL DOSE AND INTAKES

Symbol	Description	Units	Nominal	Probabilistic	Source	Computer Symbol
VEGETATION MODEL						
$d_{vi}(ing)(t)$	annual whole body dose due to vegetable v ingestion for ith radionuclide; annual ingestion of As and Ni in veg.	$Sv \cdot yr^{-1}$ ($ug \cdot yr^{-1}$ for As and Ni)	calculated	calculated	DOSEIN	VEGDOS(I) (I = 1-7)
$DCF_i(ing)$	whole body DCF for ingestion of element i	$Sv \cdot Bq^{-1}$ ($Sv \cdot ug^{-1}$ for U)			INPUT	DCFING(I) I = element
	- U		2.0E-9	C(2.0E-9)		DCFING(1)
	- Th		1.4E-7	C(1.4E-7)		DCFING(2)
	- Ra		3.2E-7	C(3.2E-7)		DCFING(3)
	- Pb		1.6E-6	C(1.6E-6)		DCFING(4)
	- Po		5.3E-7	C(5.3E-7)		DCFING(5)
	- As		-	C(1)		DCFING(6)
	- Ni		-	C(1)		DCFING (7)
U_v	average annual intake of vegetable type v:	g (wet weight)$\cdot yr^{-1}$			VEGDEP	
	above-ground vegetables		124E3	C(124E3)		VEGINA
	below-ground vegetables		79E3	C(79E3)		VEGINB
$C_{vi}(t)$	concentration of element i in vegetation type v:	$Bq \cdot g^{-1}$ ($ug \cdot g^{-1}$ for U, As, Ni)	calculated	calculated	VEGDEP	CVEG(I,J); I = element, J = veg. type
	o above-ground veg. - U					CVEG(1,1)
	- Th					CVEG(2,1)
	- Ra					CVEG(3,1)
	- Pb					CVEG(4,1)
	- Po					CVEG(5,1)
	- As					CVEG(6,1)
	- Ni					CVEG(7,1)
	o below-ground veg. - U					CVEG(1,2)
	- Th					CVEG(2,2)
	- Ra					CVEG(3,2)
	- Pb					CVEG(4,2)
	- Po					CVEG(5,2)
	- As					CVEG(6,2)
	- Ni					CVEG(7,2)
R_v	fraction on vegetable type v after food preparation:				INPUT	
	o above-ground vegetables		0.5	U (0.25, 0.75)		FACTA
	o below-ground vegetables		0.5	U (0.25, 0.75)		FACTB
L_v	fraction of vegetable type v grown locally:				INPUT	
	o above-ground vegetables		0.5	T (0.1,0.3,0.6)		FLOCA
	o below-ground vegetables		0.5	T (0.1,0.3,0.6)		FLOCB
MOOSE INGESTION MODEL						
$d_{bi}(ing)(t)$	annual whole body dose due to ingestion of ith radionuclide in moose meat; annual ingestion of As and Ni in moose	$Sv \cdot yr^{-1}$ ($ug \cdot yr^{-1}$ for As and Ni)	calculated	calculated	DOSEIN	XMEATD(I) (I = 1-7)
U_b	annual intake of moose meat b:	$g \cdot yr^{-1}$			INPUT	
	o muscle tissue		6.7E4	C(6.7E4)		XMEATM
	o liver		1.8E3	C(1.8E3)		XMEATL
	o kidney		1.8E3	C(1.8E3)		XMEATK
$C_{bi}(t)$	concentration of element i in moose meat:	$Bq \cdot g^{-1}$ ($ug \cdot g^{-1}$ for U, As, Ni)	calculated	calculated	VEGEAT	CMEAT(I,J) I = element, J = meat type
	o muscle meat - U					CMEAT(1,1)
	- Th					CMEAT(2,1)
	- Ra					CMEAT(3,1)
	- Pb					CMEAT(4,1)
	- Po					CMEAT(5,1)
	- As					CMEAT(6,1)
	- Ni					CMEAT(7,1)

TABLE 5.9: VARIABLES USED IN THE CALCULATION OF ANNUAL DOSE AND INTAKES

Symbol	Description	Units	Nominal	Probabilistic	Source	Computer Symbol
	o liver - U					CMEAT(1,2)
	- Th					CMEAT(2,2)
	- Ra					CMEAT(3,2)
	- Pb					CMEAT(4,2)
	- Po					CMEAT(5,2)
	- As					CMEAT(6,2)
	- Ni					CMEAT(7,2)
	o kidney - U					CMEAT(1,3)
	- Th					CMEAT(2,3)
	- Ra					CMEAT(3,3)
	- Pb					CMEAT(4,3)
	- Po					CMEAT(5,3)
	- As					CMEAT(6,3)
	- Ni					CMEAT(7,3)
L_b	fraction of moose meat intake that is from local sources	-	0.5	U (0, 1)	INPUT	FMEAT
DRINKING WATER MODEL						
$d_{wi}(ing)(t)$	whole body dose commitment due to ingestion of radionuclide i in drinking water; annual ingestion of As and Ni in water	$Sv \cdot yr^{-1}$ ($ug \cdot yr^{-1}$ for As and Ni)	calculated	calculated	DOSEIN	WATDOS(I) (I = 1-7)
U_w	average annual water intake	$m^3 \cdot yr^{-1}$	0.6	C (0.6)	INPUT	WATIN
$C_{swi}(t)$	average concentration of element i in drinking water	$Bq \cdot m^{-3}$ or $ug \cdot m^{-3}$	calculated	calculated	LAKE	CDRINK(I)
	- U					CDRINK(1)
	- Th					CDRINK(2)
	- Ra					CDRINK(3)
	- Pb					CDRINK(4)
	- Po					CDRINK(5)
	- As					CDRINK(6)
	- Ni					CDRINK(7)
L_w	fraction of annual water consumption that is local	-	1.0	OF	INPUT	FWAT
K	designates lake water or groundwater source for drinking water					
	- lake	-	1	C(1)		KDRINK(K)
	- well	-	2	C(2)		(K = 1,2)
C_{swi}	average concentration of element i in drinking water from lake	Bq or $ug \cdot m^{-3}$	calculated	calculated	FDCONC	CWATER(I) (I = 1-7)
C_{gwi}	average concentration of element i in drinking water from well	Bq or $ug \cdot m^{-3}$	calculated	calculated	FDCONC	CWELL(I) (I = 1-7)
FISH INGESTION MODEL						
$d_{fi}(ing)(t)$	whole body dose commitment due to ingestion of radionuclide i in fish flesh; annual ingestion of As and Ni in water	$Sv \cdot yr^{-1}$ ($ug \cdot yr^{-1}$ for As and Ni)	calculated	calculated	DOSEIN	FISHDS(I) (I = 1-7)
U_f	average annual intake of fish	$g \cdot yr^{-1}$	8E3	U (4E3, 12E3)	INPUT	FISHIN
C_{fi}	average concentration of element i in fish	$Bq \cdot g^{-1}$ ($ug \cdot g^{-1}$ for U,As,Ni)	calculated	calculated	AQBIOTA	CFISH(I)
	- U					CFISH(1)
	- Th					CFISH(2)
	- Ra					CFISH(3)
	- Pb					CFISH(4)
	- Po					CFISH(5)
	- As					CFISH(6)
	- Ni					CFISH(7)
L_f	fraction of fish intake from local source	-	-	C(1.0)	INPUT	FFISH

TABLE 5.9: VARIABLES USED IN THE CALCULATION OF ANNUAL DOSE AND INTAKES

Symbol	Description	Units	Nominal	Probabilistic	Source	Computer Symbol
INHALATION MODEL (Particulates)						
d_i(inh)(t)	whole body dose commitment due to inhalation of radionuclide i; annual ingestion of As and Ni in	$Sv \cdot yr^{-1}$ ($ug \cdot yr^{-1}$ for As and Ni)	calculated	calculated	DOSEIN	XINDOS(I) (I = 1-5)
DCF_i(inh)	whole body DCF due to inhalation of radionuclide i	$Sv \cdot Bq^{-1}$ ($Sv \cdot ug^{-1}$ for U)			INPUT	DCFINH(I)
	- U		1.0E-6	C (1.0E-6)		DCFINH(1)
	- Th		8.1E-5	C (8.1E-5)		DCFINH(2)
	- Ra		2.6E-6	C (2.6E-6)		DCFINH(3)
	- Pb		3.5E-6	C (3.5E-6)		DCFINH(4)
	- Po		2.5E-6	C (2.5E-6)		DCFINH(5)
	- As		-	C(1)		DCFINH(6)
	- Ni		-	C(1)		DCFINH(7)
U_a	annual inhalation rate	$m^3 \cdot yr^{-1}$	8,400	C (8,400)	INPUT	XINHIN
C_{ai}(t)	average air concentration of element i	$Bq \cdot m^{-3}$ ($ug \cdot m^{-3}$ for U,As,Ni)	calculated	calculated	AIRDIS	CAIR(I)
	- U					CAIR(1)
	- Th					CAIR(2)
	- Ra					CAIR(3)
	- Pb					CAIR(4)
	- Po					CAIR(5)
	- As					CAIR(6)
	- Ni					CAIR(7)
OF	fraction of year at receptor location	-	0.6	T (0.4,0.6,0.9)	INPUT	OF
INHALATION MODEL (Radon)						
d_{Rn}(inh)(t)	whole body dose commitment due to inhalation of radon plus daughters	$Sv \cdot yr^{-1}$	calculated	calculated	DOSEIN	RNDOS
F	equilibrium factor for radon daughters to radon		0.5	T (0.2,0.4,0.7)	INPUT	FRN

received by individual organs are not considered, as it is unlikely that the threshold intake levels for non-stochastic effects would ever be approached by members of the critical group.

The dose conversion factors used to equate annual radionuclide intake to dose are those given by Johnson and Dunford (1983), as summarized in Table B5.8.1. The dose conversion factor for inhalation of radon gas is derived in Subsection 5.8.3.2. Doses from uranium intake are calculated on a Sv/ug rather than a Sv/Bq basis, since uranium data are typically reported in mass concentration units. This permits application of one dose conversion factor for all natural uranium isotopes.

There is some controversy concerning the dose conversion factors given by Johnson and Dunford (1983) for ingestion of thorium isotopes. For Th-230, two dose conversion factors are given, based on gut-to-blood fractional uptake factors (F_1) of 0.03 and 0.0002. The higher F_1 factor was intended to be applicable to thorium in organic form, such as in foods, while the lower factor was for inorganic forms, as expected to occur in drinking water. The higher dose conversion factor is presently under review, since it appears to calculate doses that are too high on the basis of thorium intake and dosimetry data. A downward revision of the higher dose conversion factor is apparently imminent, although it is not yet available for application (J.R. Johnson, Chalk River Nuclear Laboratories, pers. comm., April 1986). For this project, the lower dose conversion factor for Th-230, i.e., 1.4×10^{-7} Sv/Bq, is assumed to apply for all forms of thorium. This factor is nearly the same as the single dose conversion factor of 1.3×10^{-7} Sv/Bq recommended by ICRP (1979) for Th-230.

5.8.2 Ingestion

5.8.2.1 Vegetation

As described in the SENES Phase II assessment (SENES, 1985), the annual average effective whole body dose equivalent commitment, herein labelled "the annual average dose", received by an individual due to the ingestion of above- and below-ground vegetables is:

$$d_{vi}(ing)(t) = DCF_i(ing) \sum_v U_v \, C_{vi}(t) R_v L_v \qquad (5.8.1)$$

where: $d_{vi}(ing)(t)$ = the average annual whole body dose due to the ingestion of radionuclide i in vegetables v (in this case above and below ground vegetables) at time t ($Sv \cdot a^{-1}$); or the average annual intakes of stable element i ($ug \cdot a^{-1}$)

$DCF_i(ing)$ = the whole body dose conversion factor for the ingestion of radionuclide i ($Sv \cdot Bq^{-1}$; $Sv \cdot ug^{-1}$ for U); set at unity for calculating annual intakes of stable elements

U_v = the average annual intake of vegetable type v (in this case above and below ground vegetables) (g (wet wt) $\cdot$ a^{-1})

$C_{vi}(t)$ = the calculated average annual concentration of element i in vegetation type v at time t ($Bq \cdot g^{-1}$ or $ug \cdot g^{-1}$ (wet weight))

R_v = the fraction of activity in vegetable type v remaining after food preparation

L_v = the fraction of the vegetable type v that is grown locally.

R_v is assumed to be uniformly distributed from 0.25 to 0.75 around the nominal value of 0.5 recommended by the U.S. NRC (1982). This differs from SENES (1985) who assumed a uniform distribution between 0.5 and 1.0.

As originally suggested by SENES (1985), L_v was assigned a triangular distribution from 0.1 to 0.6, with a peak at 0.3. The range, although somewhat arbitrary, was chosen in recognition of the fact that it would be very unlikely that someone could or would grow a large percentage of their vegetables in the area being modelled (i.e., northern Saskatchewan).

U_v for above-ground vegetables is assumed to be equal to the average annual consumption of leafy vegetables plus above-ground vegetables given by CSA (1984). The corresponding value for below-ground vegetables given by CSA (1984) is also assumed to apply.

5.8.2.2 Moose

The model used for calculating the average annual dose received by an individual due to consumption of muscle, liver and kidney of moose (U.S. NRC, 1982) is:

$$d_{bi}(ing)(t) \quad = \quad DCF_i(ing) \cdot L_b \sum_b U_{bj} \cdot C_{bi}(t) \qquad (5.8.2)$$

where: $d_{bi}(ing)(t)$ = the average annual whole body dose due to the ingestion of radionuclide i in moose meat at time t ($Sv \cdot a^{-1}$); or the average annual intake of stable element i ($ug \cdot a^{-1}$)

$DCF_i(ing)(t)$ = the whole body dose conversion factor for the ingestion of radionuclide i ($Sv \cdot Bq^{-1}$; $Sv \cdot ug^{-1}$ for U); set at unity for calculating annual intakes of stable elements

U_{bj} = the average annual intake of meat of tissue or organ type b, assumed to be all moose. The annual intake of all three types of meat is assumed to be the average annual meat intake (beef plus pork) given by CSA (1984)

$C_{bi}(t)$ = the calculated average annual concentration of element i in moose meat type b at time t ($Bq \cdot g^{-1}$ or $ug \cdot g^{-1}$)

L_b = the fraction of the annual intake that is local moose meat

Most of the mass of the moose carcass that is consumed is muscle. Liver and kidney account for relatively small fractions of the total mass, but may be consumed by the critical group. Ninety-five percent of the total meat consumption is assumed to be muscle, while liver and kidney are assumed to constitute 2.5% each of the total meat diet.

The fraction of the annual intake, L_b, that is local (i.e., from a moose killed in the immediate area) was allowed to range from 0 to 100% because this factor varies greatly from year to year.

5.8.2.3 Drinking Water

The average annual dose received by an individual as a result of drinking water from the lake was modelled (U.S. NRC, 1982) as:

$$d_{wi}(ing) \quad = \quad U_w \, L_w \, DCF_i(ing) \, C_{swi} \qquad (5.8.3)$$

where: $d_{wi}(ing)(t)$ = the average annual whole body dose due to the ingestion of radionuclide i in drinking water at time t ($Sv \cdot a^{-1}$); or the annual intake of stable element i ($ug \cdot a^{-1}$)

$DCF_i(ing)$ = the whole body dose conversion factor for the ingestion of radionuclide i ($Sv \cdot Bq^{-1}$; $Sv \cdot ug^{-1}$ for U); set at unity for calculating annual intakes of stable elements

U_w = the average annual intake of drinking water ($m^3 \cdot a^{-1}$)

$C_{swi}(t)$ = the calculated average annual concentration of radionuclide i in the drinking water source at time t ($Bq \cdot m^{-3}$ or $ug \cdot m^{-3}$)

L_w = the fraction of the annual intake that is local drinking water.

The fraction of the annual water consumption, that is from the lake, was set equal to the fraction of the year that the critical receptor stays at the site (see Section 5.8.3.1). The annual water consumption is that defined for Reference Man by ICRP (1975).

5.8.2.4 Fish

The average annual dose received by an individual as a result of eating fish from the lake was modelled as follows (U.S. NRC, 1982):

$$d_{fi}(ing)(t) = DCF_i(ing)\, U_f\, C_f(t)\, L_f \qquad (5.8.4)$$

where:

$d_{fi}(ing)(t)$ = the average annual whole body dose due to the ingestion of radionuclide i in fish at time t ($Sv \cdot a^{-1}$); or the annual intake of stable element i ($ug \cdot a^{-1}$)

$DCF_i(ing)$ = the whole body dose conversion factor for the ingestion of radionuclide i ($Sv \cdot Bq^{-1}$ or $Sv \cdot ug^{-1}$ for U); set at unity for calculating annual intakes of stable elements

U_f = the average annual intake of fish ($g \cdot a^{-1}$)

C_{fi} = the calculated average annual concentration of radionuclide i in fish at time t ($Bq \cdot g^{-1}$)

L_f = the fraction of the annual intake that is local fish.

The average intake of fish is based on the average consumption by male residents of Ontario (age 20 to 39) (Nutrition Canada, not dated). Consumption was allowed to vary uniformly between 0.5 and 1.5 times this average consumption. It was assumed that the annual intake of fish is from the downstream embayment, as it would be the easiest source for this individual.

5.8.3 Inhalation

5.8.3.1 Suspended Particulates

The average annual dose received by an individual due to inhalation (excluding radon) was calculated as follows:

$$d_i(inh)(t) = DCF_i(inh)\ U_a\ C_{ai}(t)\ OF \qquad (5.8.5)$$

where: $d_i(inh)(t)$ = the average annual whole body dose due to the inhalation of radionuclide i at time t ($Sv \cdot a^{-1}$); or the annual quantity of stable element i inhaled ($ug \cdot a^{-1}$)

$DCF_i(inh)$ = the whole body dose conversion factor for the inhalation of radionuclide i ($Sv \cdot Bq^{-1}$; $Sv \cdot ug^{-1}$ for U); set at unity for calculating annual inhalation of stable elements

U_a = the average annual inhalation rate of the individual ($m^3 \cdot a^{-1}$)

$C_{ai}(t)$ = the calculated average annual air concentration of radionuclide i at time t ($Bq \cdot m^{-3}$; $ug \cdot m^{-3}$ for U)

OF = the fraction of the year that is spent at that location.

The annual inhalation rate was assumed to be the constant value recommended by ICRP (1975) for reference man. As in the SENES Phase II assessment, the occupancy factor was given a nominal value of 0.6 based on four months away for hunting and trapping, plus a few trips for obtaining supplies, visiting, etc. This was allowed to vary with a triangular distribution from 0.4 to 0.9.

5.8.3.2 Radon and Its Daughters

The radon source and air dispersion models result in an estimation of the atmospheric radon concentration at the receptor. This concentration must be converted to an annual effective equivalent dose so that it can be added to doses from the other exposure pathways.

This conversion requires an estimation of the equilibrium factor, F, between radon and radon daughters. F can range from 0 (no radon daughters) to 1.0 (complete radon daughter ingrowth). The value of F at the receptor depends only on the transit time between the radon source and the receptor, if there are no removal mechanisms for radon daughters other than radioactive decay. But, in reality, the daughters are removed by several mechanisms which are difficult to quantify (e.g., attachment to dust that falls to the ground). Since the major exposure occurs indoors where F is dependent on several additional factors (such as ventilation rate), it has been customary to select (rather than calculate) an F factor that is representative of annual average indoor conditions. Indoor conditions are selected because radon daughter ingrowth outdoors is negligible due to short source-receptor transit times (e.g., a few minutes). In the SENES Phase I study, a constant F value of 0.5 was assumed to be typical. For the SENES Phase II study, the assumed F value was replaced by a triangular input distribution, with a range of 0.2 to 0.7 and a mode of 0.4. This distribution for F is reasonable for this application and is, therefore, applied herein.

Based on an assumed equivalence of 4.8 WLM and 0.05 Sv (ICRP, 1981), a fractional 0.75 of the time spent indoors, as suggested by SENES (1985), and the definitions of working level (WL, the concentration of radon daughters equivalent to 3.7 $\mathrm{Bq \cdot L^{-1}}$ of radon in equilibrium), working level month (WLM, exposure to 1 WL for 170 h), and occupancy factor (OF, the fraction of time at the receptor site), the conversion between exposure to 1 $\mathrm{Bq \cdot m^{-3}}$ of radon and annual dose is given by:

$$\begin{aligned}&0.75 \times \mathrm{OF} \times 1\ \mathrm{Bq \cdot m^{-3}} \times 10^{-3}\ \mathrm{m^{3} \cdot L^{-1}}\\ &\times \mathrm{F\ WL}/(3.7\ \mathrm{Bq \cdot L^{-1}}) \times 8{,}760\ \mathrm{h \cdot a^{-1}} \times \mathrm{WLM}/(\mathrm{WL} \times 170\ \mathrm{h})\\ &\times 0.05\ \mathrm{Sv}/4.8\ \mathrm{WLM}\\ &= \mathrm{OF} \times \mathrm{F} \times 1.09 \times 10^{-4}\ \mathrm{Sv \cdot a^{-1}}\end{aligned} \qquad (5.8.6)$$

The (risk) equivalence of 4.8 WLM and 0.05 Sv is considered debatable by some health physicists, but examination of this equivalence is beyond the scope of this report.)

6.0 SYSTEM CODE

As an aid to developing an appropriate version of the UTAP code for application to a hypothetical northern Saskatchewan site, we obtained the Phase II code from SENES on floppy disk and undertook to run it as a tool for learning its code structure and its transportability. The code and data structure were run directly upon an IBM-XT and IBM-PC. The code structure was modified somewhat to accommodate running it upon our SUN microcomputer and upon a CDC mainframe.

Within approximately one week of obtaining the code, these runs were all made and we were able to ask questions of the code (such as what different results are obtained if a particular parameter has a different probability distribution). For a standard test run involving a 1,000 year simulation period and 500 simulation passes, the SENES code bench-marked at approximately 6.5 hr on the 8088 chip-based IBM-XT (with hard disk memory) and IBM-PC (without a hard disk memory) with each having an 8087 floating-point processor, 45 minutes on the SUN and 25 minutes on the CDC mainframe.

6.1 Structure

6.1.1 Review of SENES Code Structure

As noted by SENES (1985), "the probabilistic analysis process is inherently large and complex, hence a logical, step-by-step approach is required to make it tractable. The process is exceptionally well-suited to the application of a "top-down" computer progamming approach. The top-down approach first involves identification of the overall system requirements, followed by the specification of large, conceptual structures consistent with these requirements, followed in turn by further development of conceptual substructures. The overlying conceptual structures always dictate the nature of lower level structures. The requirements and specifications are subsequently translated into identifiable tasks. Once the conceptual algorithms are developed in this logical, top-down manner, implementation is a fairly mechanical programming exercise".

The system model is composed of "control modules" and "simulation (component) modules". The latter are the mathematical models describing the system of interest. They are, in general, unique to each problem.

The primary control module (RANSIM) is a completely general computer program designed to perform probabilistic analysis of any suitably specified problem. As an interface between the completely general probabilistic "tool" and the many simulation modules required in this analysis, and intermediate control module was developed. The Parameter Allocation and Control (PAC) module fulfills this intermediary role. The conceptual attributes of PAC are generally the same for different component modules however, the details of implementation change.

6.1.2 Code Structure of this Project

The code structure used in this project is similar to that of SENES except that a different data structure was used. In general, there are three elements of the data management structure: management of input/output (I/O), the storage of parameter distribution information, and the storage of the rest of the program variables.

At the start of the project, a thorough review of the whole data management and code structure used by SENES, was undertaken. The attributes of a general program structure were discussed and defined by BEAK. A new structure was proposed by a computer science specialist on our team. The basic ideas concerning this new data structure revolved around a completely dynamic design involving one main data stack accessed by local pointers. The scheme has some advantages and some disadvantages in Fortran, the language used in the code. This dynamic scheme was implemented in this project for the storing of the parameter distribution information due to the manner in which the parameter distribution data structure varies from one data set to another and from one parameter in a given data set to another within the same data set. For example, some distributions require only two defining parameters where others require that the user defines the lower and upper limits. This also allows a flexible input/output structure. New variables to be treated as input can be added to the program input structure without changing other data components.

This dynamic scheme, however, was not used for the main program variables. Rather, a much simpler, static data design was used. In this static design, the data variables are of fixed sizes and most are classified and passed through common blocks. Generally all data variables are of fixed size. A few are of variable size where their size is program determined. Information flow between subroutines is passed via labelled common blocks, or through the subroutine call statements. Labelled common blocks were designed so that variables common to as few subroutines as possible are included in each common block. Common blocks are included in a subroutine only if necessary. This aids in error tracing.

Although the dynamic pointer oriented method would have resulted in a unrestricted data storage setup, it would have done so at the cost of a much more complex (and thus harder to follow) code and a slight increase in memory requirements. Normally, a dynamic design results in lowered memory requirements but its savings in memory is outweighed by the stack pointer system's overhead.

The input distribution data is read into the dynamic structure through a new I/O subroutine, sampled from distributions obtained from SENES and then sent to the various common blocks to be fed into the computational routines, by new subroutines programmed for the project. One new sampling distribution was also added for the project: a correlated log normal distribution.

The random sampling for parameter values, control of the number of simulation passes, and preparation of summary statistics is executed by substructure RANSIM, similar to SENES. The set of execution steps is defined in a subroutine called CONTRLS. The subroutine CONTRLS carries out essentially the same function as PAC in the SENES code, but does not allocate parameter values. Due to the large set of new subroutines written for the project, PAC was essentially rewritten, as this CONTRLS Subroutine. It controls the segregated logic of calculations from the tailings to the human receptor and the time progress of simulation for any one simulation. Information such as the concentration or dose calculated by the different subroutines are either summarized by the summary statistics and written directly to the storage files, or are passed to storage areas by the CONTRL module.

Summary statstics and detailed results of all simulations can be stored on hard disk. These storage files are used as input data which, together with graphic programs, written by team members, are used to produce the output plots given in this report directly by the micro computer system. The plots are visually compared with numerical values in the storage files to ensure their veracity.

6.2 Software Quality Assurance

Software quality assurance attempts to verify that a computer code does what it was designed to do. It involves definition of software objectives, a software development process, application of software standards, verification and testing among other elements. The overall approach and the specific techniques used by SENES (1984,1985) were generally adopted. Additional code tests designed by BEAK were also developed. In this section, the general approach is highlighted. Then specific attributes of the QA procedure are summarized.

The quality assurance program of this project was a particular challenge because of the need to modify the existing data management structure, to modify existing subroutines and retain as many as possible in an intact state, and to develop a new source term. Software development, involved in this undertaking, has two levels of difficulty. The first and easier level comprised development of modules which the existing software and its documentation provided for explicitly. The second level and greater challenge involved modifying the existing subroutines to provide for new computational objectives. These modifications required some resourcefulness in software engineering because, in contrast to the other work, they involved knowledge of interfaces and areas of software interaction points, which were not originally designed to be extended.

6.2.1 Software Development Process and Standards

Computer software embodies an algorithm in a structure. The numerical accuracy that the software can achieve depends, in part, on the algorithm used. Accuracy and most other aspects of quality depend even more strongly on the structure of the software.

The software team's first task was to examine the available documentation for the existing system and to determine where alterations in the algorithms impacted software structure. In particular, opportunities to exploit any software "hooks" that may have been built into the program by its developers were sought. Then any additional information needed was defined and gathered either by reviewing the program codes themselves, and/or through communication with the SENES personnel.

At this point in the process of software development, alteratives with respect to design modifications were defined. The major alternative for data management was summarized above. On the basis of this outline, decisions on preferred alternatives were made by trading off various advantages and disadvantages with respect to hardware and software capabilities. To specialists in the field of computer science, the range of options for the software team were relatively limited: choices of hardware and software, including programming language and operating system, were already made; and software capabilities were defined by the scientific team. To obtain the greatest overall software quality, the selection process used was in line with Boehm's 1978 "software quality characteristics tree". A preferred alternative was selected and a detailed design was generated. This resulted in descriptions of changes to algorithms that are used to represent models in the existing software, and descriptions of new algorithms. These details were reviewed with the appropriate SENES team members, and others and then implemented.

The modified sections of code, and new code was written stubbing new low-level modules for subsequent completion. Writing of code proceeded on two parallel paths. Coding for pathways proceeded in parallel but independent of coding for the source term. Walkthroughs, involving the scientific team, and the software development team, were conducted to expose any inconsistencies with existing codes, linkage problems or remaining misunderstandings about algorithms. Any that were found, were corrected.

Stubbed modules and other components were completed at this stage. Final code walkthroughs were organized and corrections made thus terminating code development. Hooks in the code were provided to handle additional concepts and equations when time in this project did not permit final development of code, its implementation, and quality assurance checks.

Coding was organized along the lines of a Chief Programmer Team. Overall development responsibilities, including design, were in the hands of the Chief Programmer. The actual design of the data structure was determined and developed by the Chief Designer and the Designer Consultant both of whom have a background in computer science. Applications programmers with backgrounds in computer science, geology, and chemical engineering were responsible for developing new code or modifying existing code to achieve the requirements of the source term, pathways equations and of the code design.

- Applications programmers were also responsible for stubbing appropriate modules and conducting walkthroughs of component modules in consultation with personnel knowledgeable about the science behind the equations. The function of Program Librarian/Secretary was carried out by the project manager who was also a member of the scientific team. This structure ensured the availability of a "critical mass" of sound software shells but also kept the project at a manageble size.

Software Standards involve software design, management of code development, and code documentation. Top-down Design, which employs methods and symbolisms similar to those of Yourdon and Constantine (1978) in designing and expressing software structure was used. This is one member of a class of similar methodologies in use by most successful software development organizations. Various techniques were used in code management to ensure the integrity of its software products. This was particularly important, owing to the heavy use of COMMON blocks in the existing codes (Wulf and Shaw, 1973).

Provisions in the existing code to display information about the contents of storage and program states, were extended in the new and/or modified code.

Full use was made of the (albeit) limited possibilities for writing structured code in FORTRAN. The code is portable and readily adaptable to other systems.

The standard for documentation developed by SENES for the existing software was maintained or modified as follows. The procedure for tabularizing variables, etc. was retained and summarized in this report. Full documentation, however, was not made in this report because the objective of this project was not to produce a user's manual.

6.2.2 Verification and Testing

The objective of this phase was to verify the detailed behaviour and correctness of the modified software.

With respect to quality assurance nomenclature, two terms can be defined model verification and model validation. Model verification is defined here as "code verification" - the checking of the computer code to ensure that is performs as specified. "Model validation" is defined here as a comparison of the quantitative calculation by the computer code with field and laboratory data. The quantitative calculations result from the conceptual model and the process of developing its algorithm and computer code. Definitions of the terminology: model construction, model calibration, model validation and model simulation, and model validation tests are given elsewhere (e.g., Thomann, 1983).

Two types of tests were developed. First, "black box" tests were developed on the basis of what the code is supposed to do, without knowledge of how the code works. For example, an external analytical solution was available as a restricted test case. The code results were then compared to the analytical solution results. These were used for the source term subroutines, the river/lake water, the groundwater and air pathways, the food-web and dose-contaminant aspects of the code.

Secondly, "white box" tests were utilized which are dependent on a knowledge of the code itself. In such tests, test cases were developed to ensure that all parts of the code are exercised. For example, transfers of control were tested wherever possible. In addition, for all major subroutines, one technical person not directly involved in flowcharting and coding the subroutines, inspected the equations and the coding and transfer of control statements to ensure that the coding was consistent with objectives of the calculations.

All subroutines were broken down into component parts and the white box tests conducted in conjunction with black box tests. For example for calculation of source term pH, hand calculations were prepared for all major cases involving solids present and not present (gysum and calcite present, gypsum only present, calcite only present, neither solid present) and code calculations compared with the hand calculations and to test the transfer of control. Similar tests were carried out for all subroutines using nominal input values, and the code calculations were checked by hand. The most frequent error encountered related to the order of magnitude for output values on initial trials. Whenever errors were encountered, the code was inspected and revised, and the white box test repeated until valid output was obtained.

The different components were linked and the calculated values at different points along the pathway were inspected. For example predicted radionuclide, arsenic and nickel concentrations in the tailings pore water, receiving water and atmosphere were inspected to assure that they were within the range of typically measured background values. Unreasonably high values were found to be indicators of erroneous conversions of concentration units or of problems in the source term components.

Then similar to SENES, deterministic runs involving nominal values and extreme values and probabilistic runs were made after the logic of the order of all statements was examined via a walkthrough. In these walk-throughs, the input and output generated by the code was carefully examined and checked for numerical accuracy by the modelling scientists and the programming team. Code calculations were hand-checked to ensure that input and output were passed correctly among the various subroutines.

A limited set of probabilistic runs was then carried out using large time steps and a limited number of runs. These runs were carried out to check that the evolution of the source term over time proceeded as intended, and that the system model functioned properly in general. In these tests, some output variables were initially found to "blow up" (approach extremely high or low values). For cases where the equations allow negative values but where physical realty sets a minimum value (e.g., of zero), the values are appropriately constrained.

Code limitations occur, resulting from model assumptions and code design. For example, more substances can be considered but code alterations are required to handle the additional elements and chemical behaviour involved. The desire to handle additional substances was one of the original specifications of the generic data management structure, but was discarded to allow for ease of following code structure and error "debugging". The limitations are documented in this report, particularly by stating assumptions upon which the equations are based.

6.2.3 Quality Assurance Summary

As in the development stages of the systems model, the QA strategy included many activities and was integrated into all phases of software development. Formal and informal reviews were used during the early stages of software development to reach a concensus on component model approach and structure, and to test the functioning of the various modelling components.

The RANSIM component was carefully tested by SENES during its Phases I and II studies. Some testing of RANSIM was carried out to the components added by BEAK for this demonstration.

The component models of the system were subjected to a rigorous QA program. Initially, the modelling specifications, conceptual design and mathematical formulations were subjected to walk-throughs and peer review. Problems in adapting the existing component models and developing new component models were identified and rectified before computer coding or modifications to existing codes were carried out.

After coding was complete, component models were tested individually and in small groups. Initially, models were tested deterministically, using nominal values for input parameters. All substructures were hand-checked to verify computational correctness. As in the Phase II assessment, individual component models were then evaluated probabilistically. The source term components were tested most rigorously, since they are the most complex, and are completely new to this version of the systems model.

7.0 PROBABILISTIC ASSESSMENT RESULTS

7.1 Base Case Simulation

In the base case scenario, the tailings are unflooded, have a 2 m deep unsaturated zone at the surface and an underlying saturated zone 14 m deep. The surficial 10 cm of the unsaturated zone is subject to wind erosion, and becomes gradually vegetated until Year 250 when vegetation is assumed to cover almost all of the tailings surface. Of the total release of aqueous materials from the tailings, 10% is assumed to be transported to shallow groundwater which discharges to a surface water stream 200 m from the tailings, and 90% is assumed to be released directly to the surface water environment.

Results of the probabilistic analysis of this condition, based on 500 simulation passes and using time-steps of 25 years, are summarized in Figures 7.1 to 7.7 which show trends in geometric mean values of predicted results over a 1,000-year modelling period. Figures 7.1 to 7.3 show aspects of predicted committed effective dose equivalents to a member of the critical group receptor. Figures 7.4 and 7.5 show predicted concentrations of nickel and arsenic in various environmental media. Figures 7.6 and 7.7 illustrate predicted geometric mean annual intakes of nickel and arsenic through ingestion and inhalation.

Figure 7.1 illustrates dose versus time by individual environmental pathway. The mean annual total dose is predicted to fall from about 1.2 $mSv \cdot a^{-1}$ at the beginning of the modelling period, to about 0.8 $mSv \cdot a^{-1}$ after 100 to 150 years, and to then gradually decline to about 0.4 $mSv \cdot a^{-1}$ by Year 1000.

Figure 7.1 shows that the relative importance of each pathway to total dose occurs in the sequence: inhalation > vegetation >moose consumption >drinking water >fish. Most of the total inhalation dose is due to radon, with the importance of particulate radionuclides declining over the first 200 years. The decline in the dust pathway's importance can be attributed to the gradual winnowing of the fine silt fraction from the surficial tailings and the gradual coverage of the tailings surface by vegetation which inhibits wind erosion. The radon dose is up to two orders of magnitude greater than the radon dose found for Scenario 1 in the Phase II assessment for a pyritic tailings by SENES (1985). This difference is attributed to an approximately 20-fold greater Ra-226 concentration,

FIGURE 7.1: DOSE vs. TIME
FOR SCENARIO 1, BY PATHWAY
GEOMETRIC MEAN OF 500 TRIALS

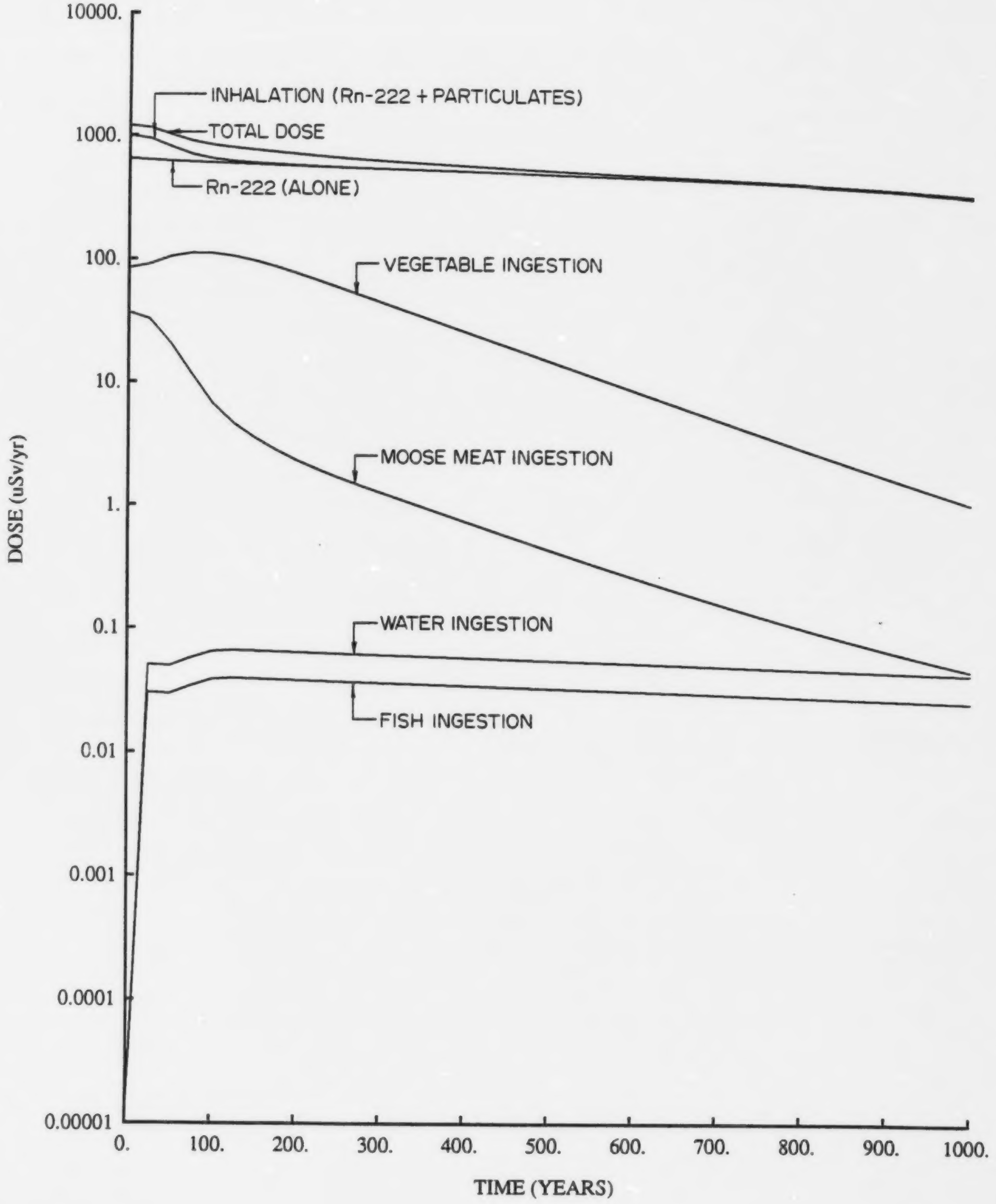

FIGURE 7.2: DOSE vs. TIME
FOR SCENARIO 1, BY RADIONUCLIDE
GEOMETRIC MEAN OF 500 TRIALS

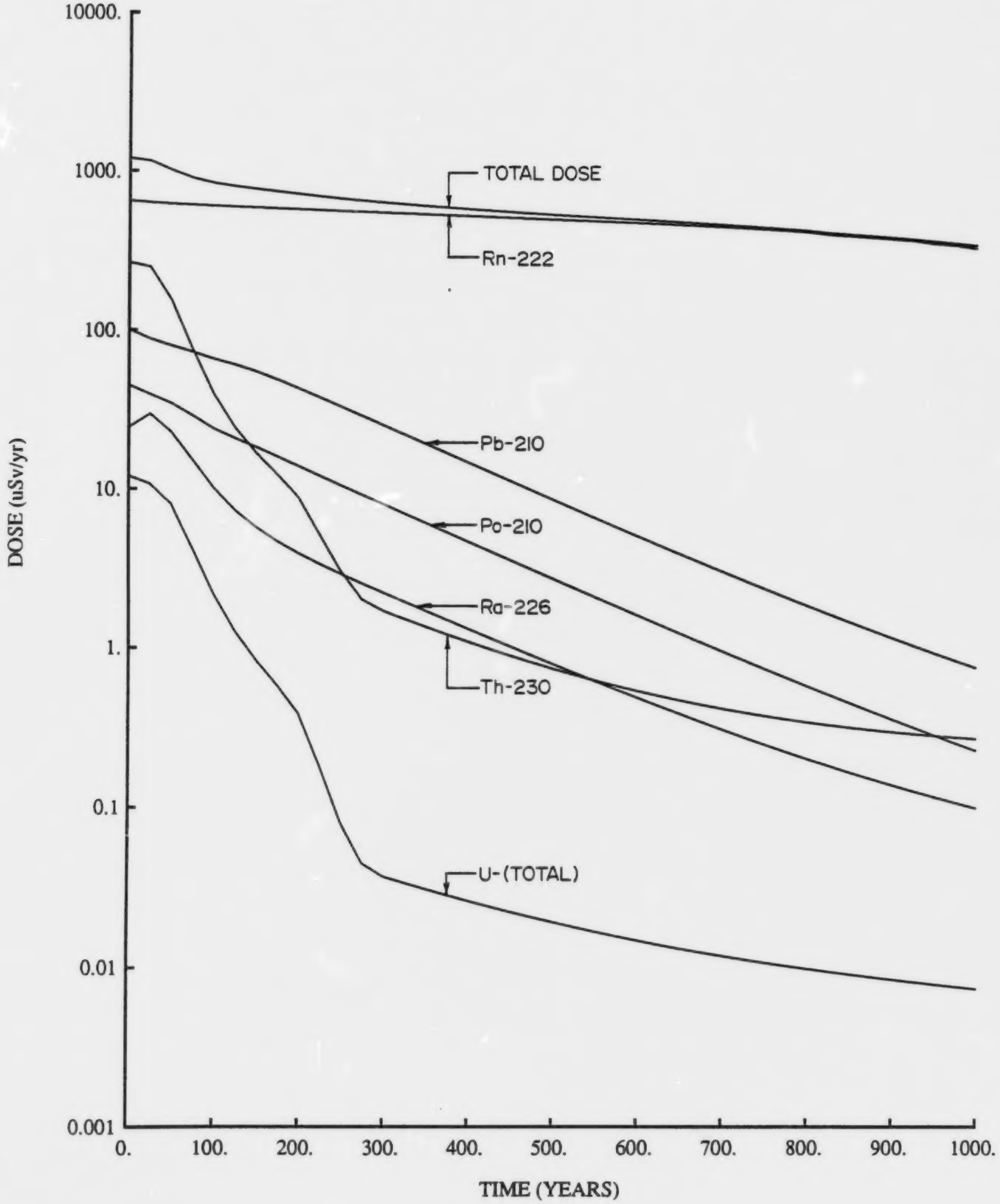

FIGURE 7.3: TOTAL DOSE vs. TIME
FOR SCENARIO 1
GEOMETRIC MEAN OF 500 TRIALS

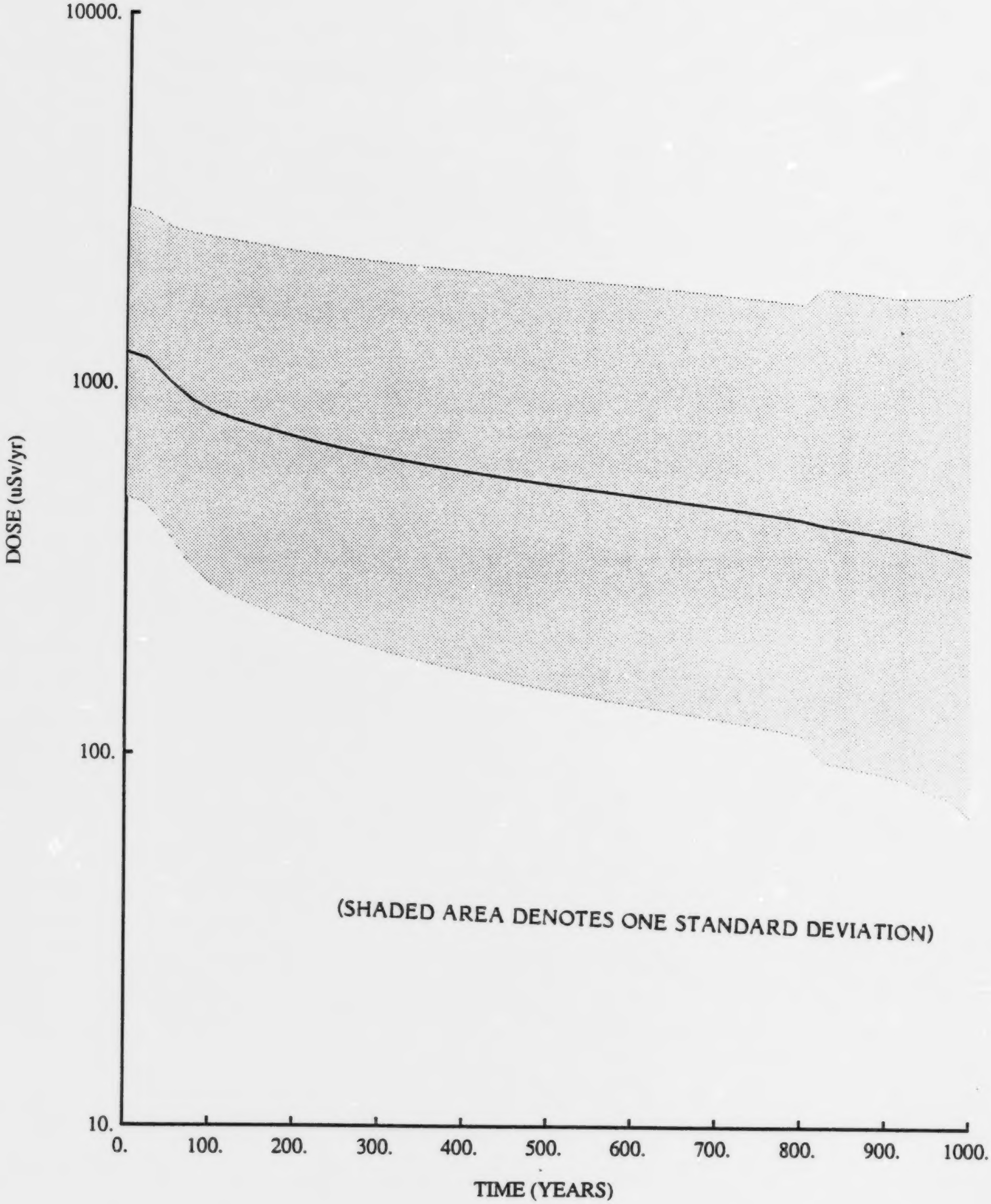

FIGURE 7.4: ARSENIC INTAKE vs. TIME FOR SCENARIO 1, BY PATHWAY GEOMETRIC MEAN OF 500 TRIALS

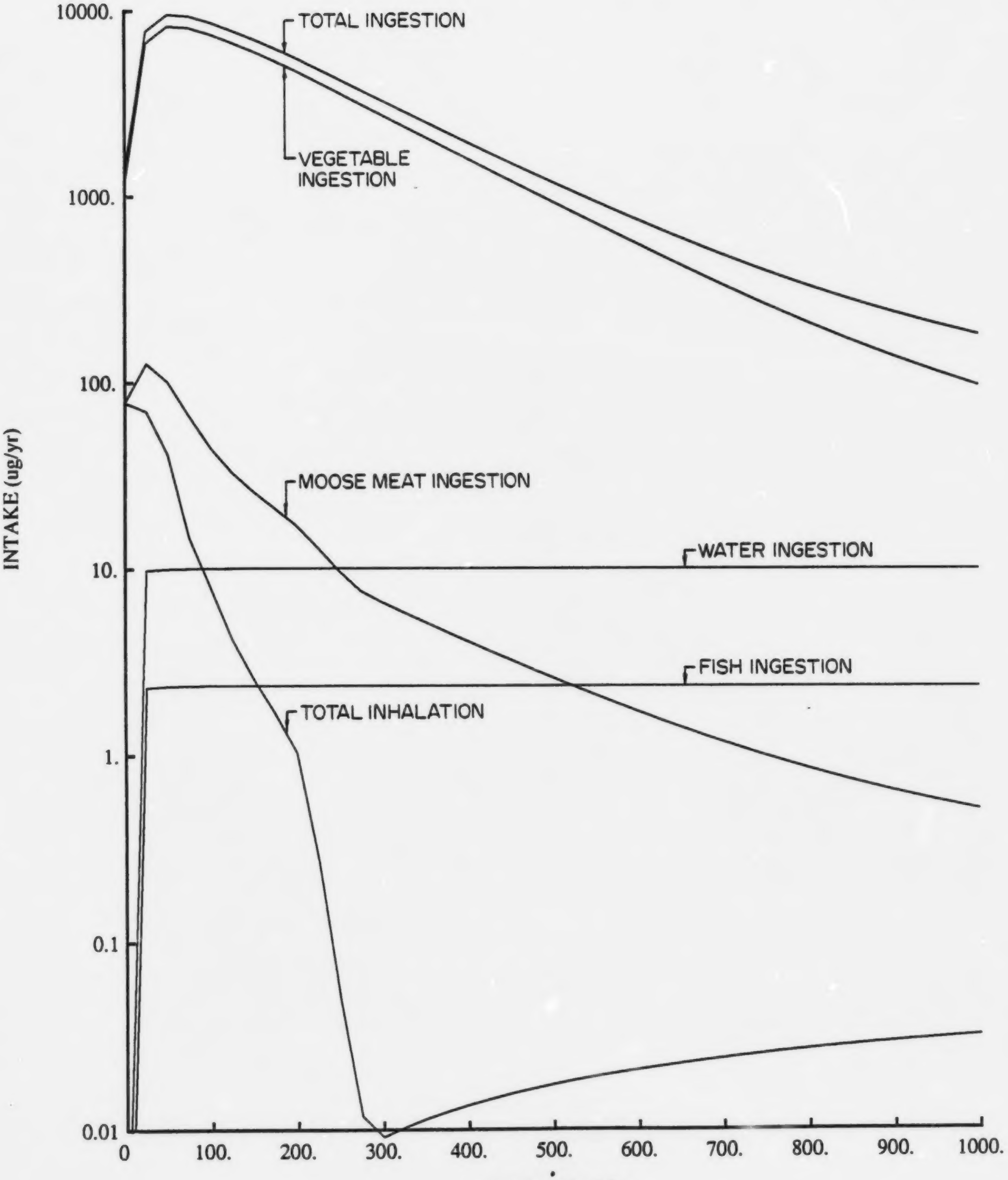

FIGURE 7.5: NICKEL INTAKE vs. TIME
FOR SCENARIO 1, BY PATHWAY
GEOMETRIC MEAN OF 500 TRIALS

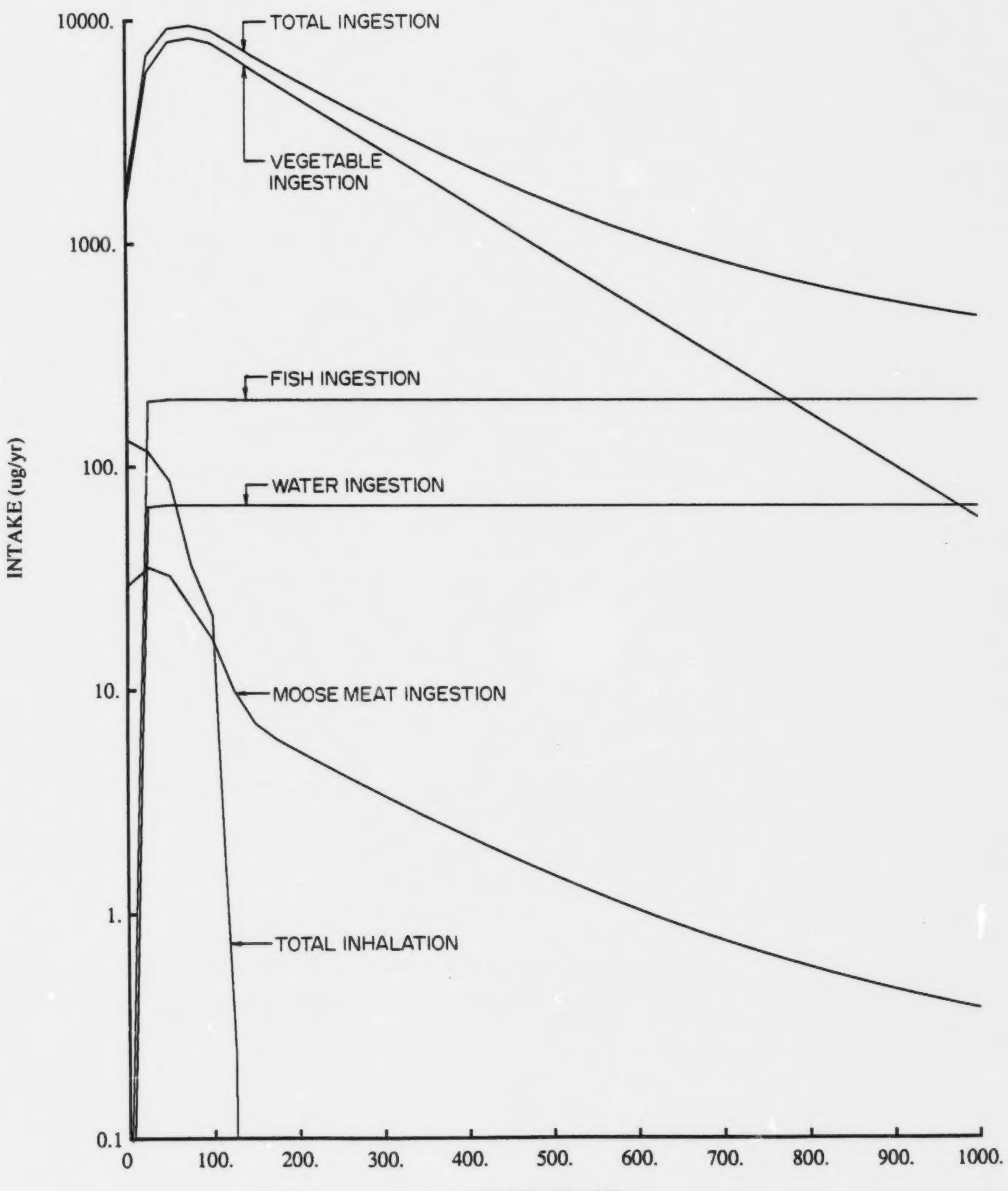

FIGURE 7.6: CONCENTRATIONS OF ARSENIC IN FOOD AND WATER (ppm) AND IN AIR (ug/m^3) FOR SCENARIO 1, BY PATHWAY GEOMETRIC MEAN OF 500 TRIALS

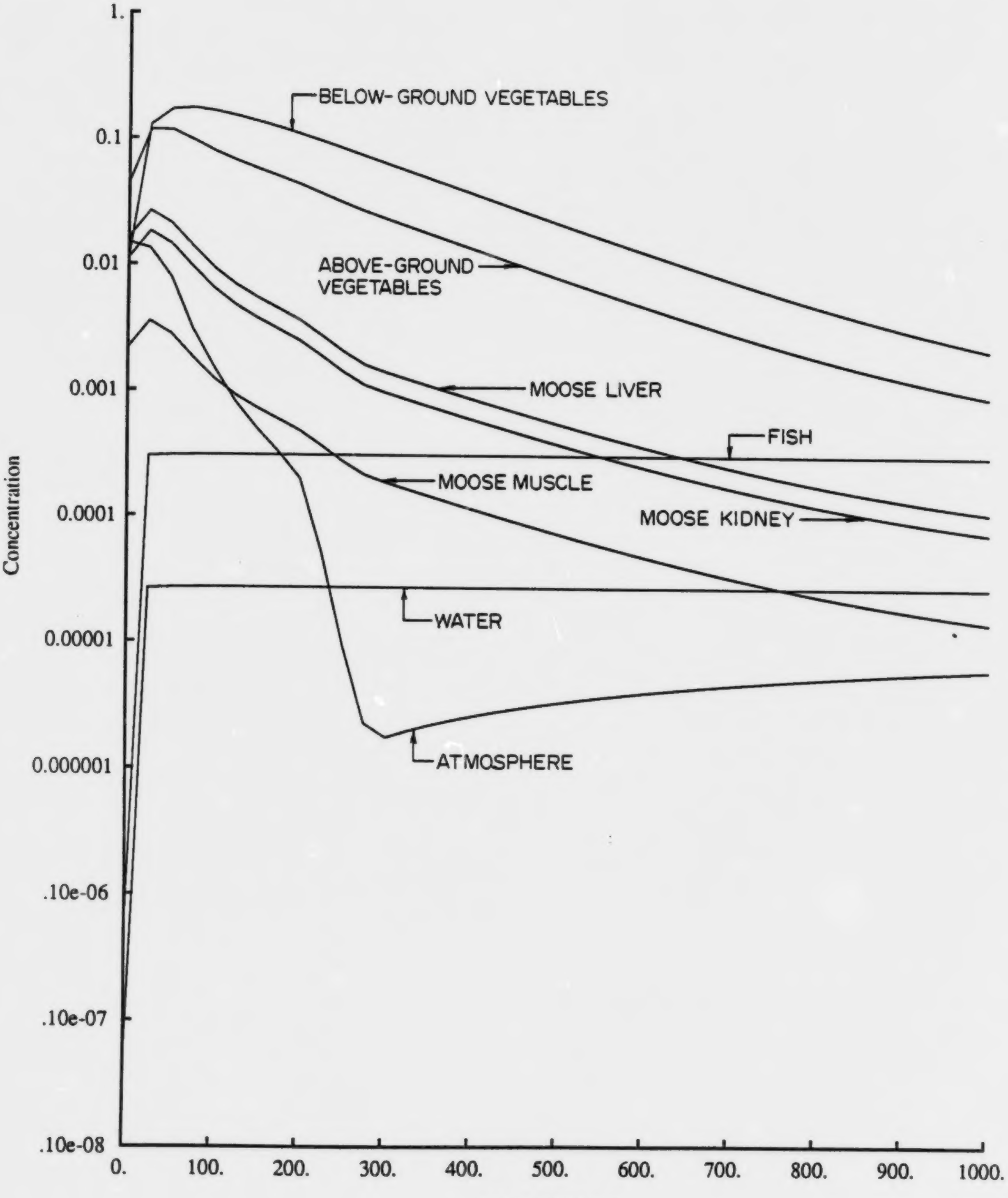

FIGURE 7.7: CONCENTRATIONS OF NICKEL IN FOOD AND WATER (ppm) AND IN AIR (ug/m^3) FOR SCENARIO 1, BY PATHWAY GEOMETRIC MEAN OF 500 TRIALS

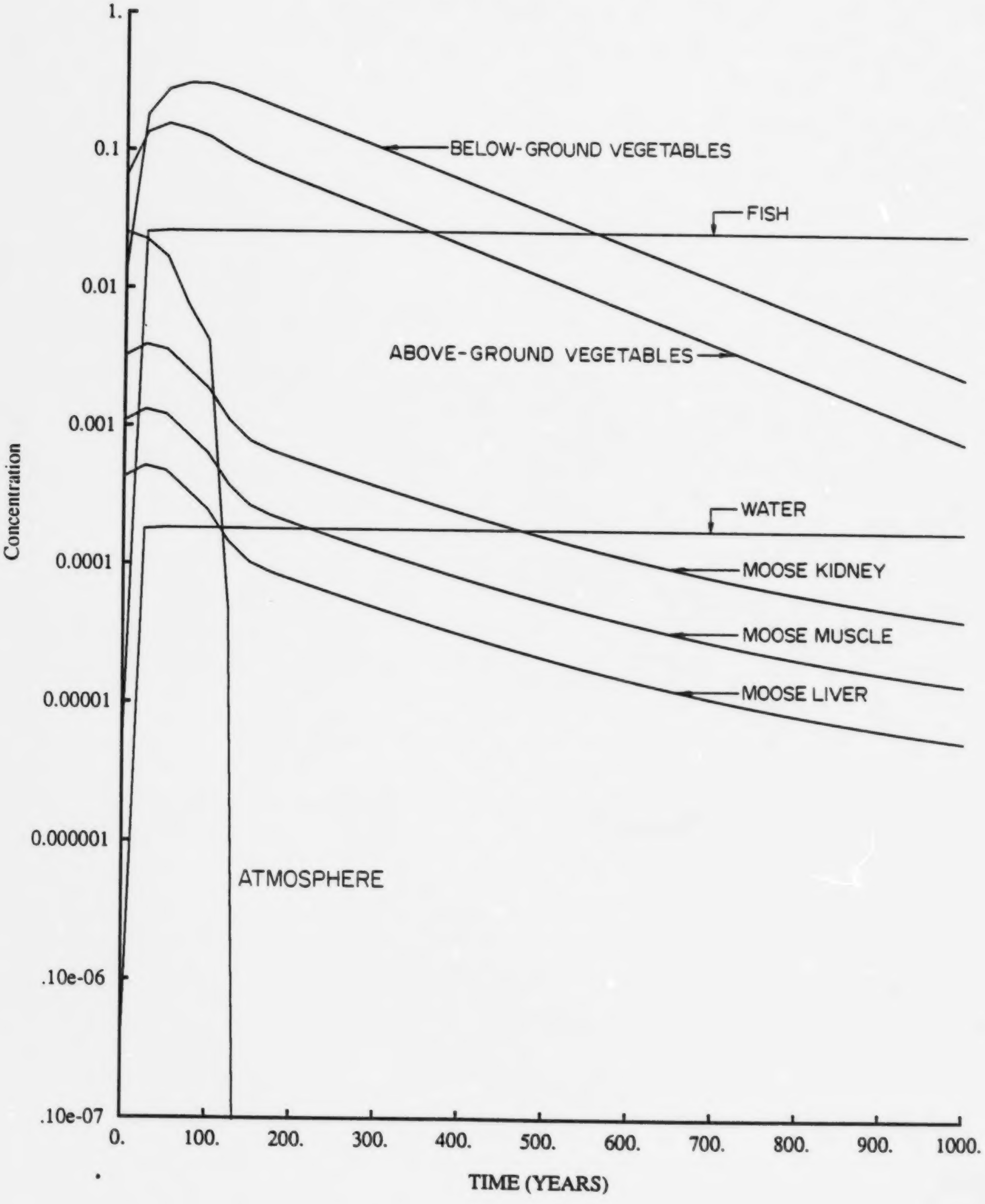

and to a lower moisture content in the tailings considered here. A deterministic check, assuming similar Ra-226 concentrations and source to receptor distance as in the SENES evaluation, produced results similar to those predicted by SENES. The maximum mean doses from radon predicted in the present study are about 800 uSv per year, which is the same as the average annual radon dose from background sources (UNSCEAR, 1982).

Doses from aquatic pathways were found to rise sharply from time zero to about 0.07 $uSv{\cdot}a^{-1}$ for the drinking water pathway and 0.04 $uSv{\cdot}a^{-1}$ for the fish pathway by about Year 20 (Figure 7.1). These dose rates then remain relatively constant for the duration of the modelling period. The initial rapid rise in doses from these aquatic pathways is attributed to the time lag associated with transport to the embayment and gradual accumulation in the water column until an equilibrium condition is reached. The doses from aquatic pathways for all radionuclides in this demonstration are typically two orders of magnitude lower than the corresponding doses from Ra-226 alone in Scenario 1 of the SENES Phase II assessment. This is ascribed primarily to the higher porewater concentrations of Ra-226 in the SENES assessment for pyritic tailings and to the greater dilution assumed for the receptor lake in this study.

In Figure 7.2, doses are plotted by individual major radionuclide for all pathways. Radon was found to be the most important contributor to total dose (typically 90%). Uranium contributes the least of all radionuclides to total dose (1% or less). The small contribution of uranium is reasonable, since 95% of the uranium was assumed to be extracted from the original ore. All of the other U-238 decay chain radionuclides from the ore were assumed to be in the tailings at time zero. The geometric mean dose versus time plots for Ra-226, Pb-210 and Po-210 are approximately parallel, owing to the control of the relatively short-lived Pb-210 and Po-210 decay products by Ra-226. The varying patterns between the dose-time plots for other radionuclides are explained by the varying importance of leaching from the surficial tailings compartment for the various radionuclides. Removal from the surficial tailings by wind erosion and leaching reduces the relative importance of the inhalation and vegetation pathways controlling the doses from particulate radionuclides.

In Figure 7.3, the geometric mean total dose from all pathways and radionuclides is plotted against time for Scenario 1, with ± one geometric standard deviation plotted in log space as the shaded zone about the geometric mean. The geometric standard deviation is associated with the distribution of predicted total doses for 500 iterations in each time-step. The range of doses delineated by the standard deviation is relatively large, and spans a range of about an order of magnitude. This uncertainty associated with the dose predictions is the cumulative result of all non-constant parameters in the model.

Output frequency distributions for total annual dose in Scenario 1 are plotted for selected time-steps in Appendix D, each based on 500 iterations per time-step. These figures also give a summary of the statistical distribution of the data output. Each histogram plot is a "snapshot" at a single point in time of the predicted dose (see discussion of Figure 3.3). In general, the shape of the output distributions for total dose is skewed toward the lower end of the range of predicted values, with a tail of low frequency, high dose predictions. This is largely attributed to the preponderance of log-normal distributions assigned to a large number of the food chain input parameters.

Figures 7.4 and 7.5 show geometric mean annual intakes of arsenic and nickel, respectively, over the 1,000-year time frame. For both elements, mean total intakes rise to a peak of about 10 $mg \cdot a^{-1}$ at about 75 years, and gradually fall to the 0.2 to 0.5 $mg \cdot a^{-1}$ range by the year 1000. Most of this ingested arsenic and nickel is attributed to the vegetable pathway over all of the modelling period for arsenic and over the first 800 years for nickel. The relative importance of other pathways varies over time.

In the aquatic pathways, the relative importance of drinking water exceeds that of fish for arsenic, while the reverse is true for nickel. This is attributed to the greater bioconcentration factor for nickel in fish. The annual quantities of arsenic and nickel inhaled fall rapidly over the first few years, due to the removal of silt by wind action over the early portion of the modelling period. Nickel is leached rapidly from the tailings surface; thus, the dust generated from the tailings contains almost no nickel after 125 years, and the atmospheric source term approaches zero. The slight increase in arsenic inhalation after 300 years results from the combined effects of the gradual coverage of the tailings by vegetation, and the formation of silt in the surface tailings by weathering.

In comparison with the predicted maximum geometric mean dietary intake values of about 10 $mg \cdot a^{-1}$ for arsenic and nickel, Cohen (1985) listed daily intakes that are equivalent to 8 $mg \cdot a^{-1}$ for arsenic and 150 $mg \cdot a^{-1}$ for nickel, based on estimates for the average diet in the U.S. population. Thus, the predicted dietary intakes in this assessment are approximately equal to or less than the average intake from background sources for arsenic, while the predicted nickel intake is much less than background over the entire modelling period. Data on annual intakes of arsenic and nickel through inhalation are not available.

Output frequency distribution plots for total arsenic ingestion for Scenario 1 are given for selected time-steps in Appendix D, each based on 500 iterations per time-step. Many of these histograms are strongly skewed to the left, and include one or two outlier-type of predictions toward the upper extremes of the x-axis. This can be attributed to the low frequency of selection of some of the lognormally distributed food chain parameters from the extreme ends of their specified ranges.

Most environmental guidelines or standards for stable elements such as arsenic and nickel are based on environmental concentrations in various environmental media, particularly air and water. Figures 7.6 and 7.7 show predicted geometric-mean concentrations of arsenic and nickel in air, water and food for the critical group.

The maximum acceptable drinking water guideline for arsenic is 0.05 $mg \cdot L^{-1}$ (Health and Welfare Canada, 1980), or about three orders of magnitude greater than the maximum predicted mean concentration. While there is no federal guideline for nickel in drinking water, the Ontario Ministry of the Environment (1984) lists a surface water objective of 0.025 $mg \cdot L^{-1}$ of nickel for the protection of aquatic life. This is about two orders of magnitude greater than the maximum predicted mean nickel concentration in drinking water.

There are no federal standards available for atmospheric concentrations of nickel or arsenic. As specified under the Ontario Environmental Protection Act, the 24-hour average atmospheric concentration of nickel should not exceed 2 $ug \cdot m^{-3}$. The Ontario Ministry of the Environment 24-hour average tentative air standard for arsenic is 5 $ug \cdot m^{-3}$. Maximum predicted mean concentrations for atmospheric nickel and arsenic are about two orders of magnitude less than these provincial air standards.

Output frequency distribution histograms for arsenic concentrations in embayment water and in the atmosphere at the receptor are given for selected time steps in Appendix D.

7.2 Management Option Simulation

For the second management case considered, the tailings are flooded and assumed to be covered by approximately a metre of water. For modelling purposes, it is assumed that water cover prevents wind erosion of particulate material. Water cover also limits radon exhalation. Radon exhalation was modelled through the water column using data from the Experimental Lakes Area (Snodgrass, 1986) of northern Ontario to calibrate its flux. This calibration results in the relationship:

$$\text{Flux} = 2.1 \times 10^{-8} * \text{EMAN} * C_{Ra}$$

where EMAN is the emanation coefficient and C_{Ra} is the radium concentration in the top box ($Bq \cdot m^{-3}$).

The transport of other substances is modelled as a diffusive type transport process from the pore water to the overlying water. This results in a mass transfer coefficient with a typical value in the order of 10^{-2} $m \cdot a^{-1}$ and distributed uniformly ($\pm$ 0.2×10^{-2} $m \cdot a^{-1}$) for simulation purposes. Net infiltration into the tailings is assumed to be negligible.

Results of the probabilistic simulation are given in Figures 7.8 to 7.14 and are based upon 500 simulation passes, 25 year time-steps and a 1000-year simulation period. These are analogous to the corresponding plots given for the base case simulation in Figures 7.1 to 7.7. Figures 7.8 to 7.10 show aspects of predicted annual effective dose equivalents to a member of the critical group receptor. Figures 7.11 and 7.12 illustrate predicted geometric annual intakes of nickel and arsenic through ingestion. Figures 7.13 and 7.14 show predicted concentrations of nickel and arsenic in various environmental media. In all cases, predicted total doses, elemental intakes and elemental concentrations at the critical group location are two to four orders of magnitude lower than corresponding values predicted for the base case. This is attributed to the elimination of the dust pathway which, in turn, removes the important vegetation pathway from the analysis, and to the diffusion-controlled aqueous transport for radon compared to the hydraulic control operating in the base case.

The most important pathway contributing to the total dose in the management case, as in the base, is radon. However, in this case, the dose from radon is more than three orders of magnitude lower than in the base case due to the covering of the tailings by water. An annual dose of 0.2 $uSv \cdot a^{-1}$ throughout the modelling period is insignificant relative to a typical background dose of 800 $uSv \cdot a^{-1}$ from radon (UNSCEAR, 1982).

In the flooded tailings case, most of the arsenic and nickel ingestion by the critical group is due to the water and fish pathways, respectively. As noted in Section 7.1, the relative importance of the fish and water pathways is dependent upon the bioconcentration factors for these elements. In this scenario, annual intakes through these pathways and concentrations in water and fish tissues are almost two orders of magnitude greater than the corresponding values found in the base case scenario.

Histogram plots of output frequency distribution for this management case are presented in Appendix E.

7.3 Sensitivity and Uncertainty Analysis

Sensitivity analysis refers to the sensitivity of the magnitude of the result to changes in the magnitude of the input parameters. In the historical context, sensitivity analysis of a probabilistic code is run by holding one parameter constant and running all other parameter distributions in the probabilistic framework. It may then be set at a different level and the probabilistic model ran again. One then proceeds parameter by parameter (holding it constant and running the probabilistic code). The results of sensitivity analysis are ranked in order of most sensitive to least sensitive.

Garner and Hoffman (1984) prepared a concise review and discussion of sensitivity analysis methods appropriate for environmental simulation models (SENES, 1984) and compared the relative utilities of classical methods, such as Tomovic, one-at-a-time and factorial sampling, to statistical methods using Spearman correlation coefficients and regression methods. SENES found the sensitivity index, which is based on the relative change in model response relative to change in input parameter, to be very useful in indicating parameter sensitivity. Limitations of this type of sensitivity analysis are partially overcome by application of a combined sensitivity/uncertainty analysis.

As defined by SENES (1984), uncertainty analysis refers to how much of the uncertainty or spread associated with each parameter contributes to the total uncertainty or spread

FIGURE 7.8: DOSE vs. TIME
FOR SCENARIO 2, BY PATHWAY
GEOMETRIC MEAN OF 500 TRIALS

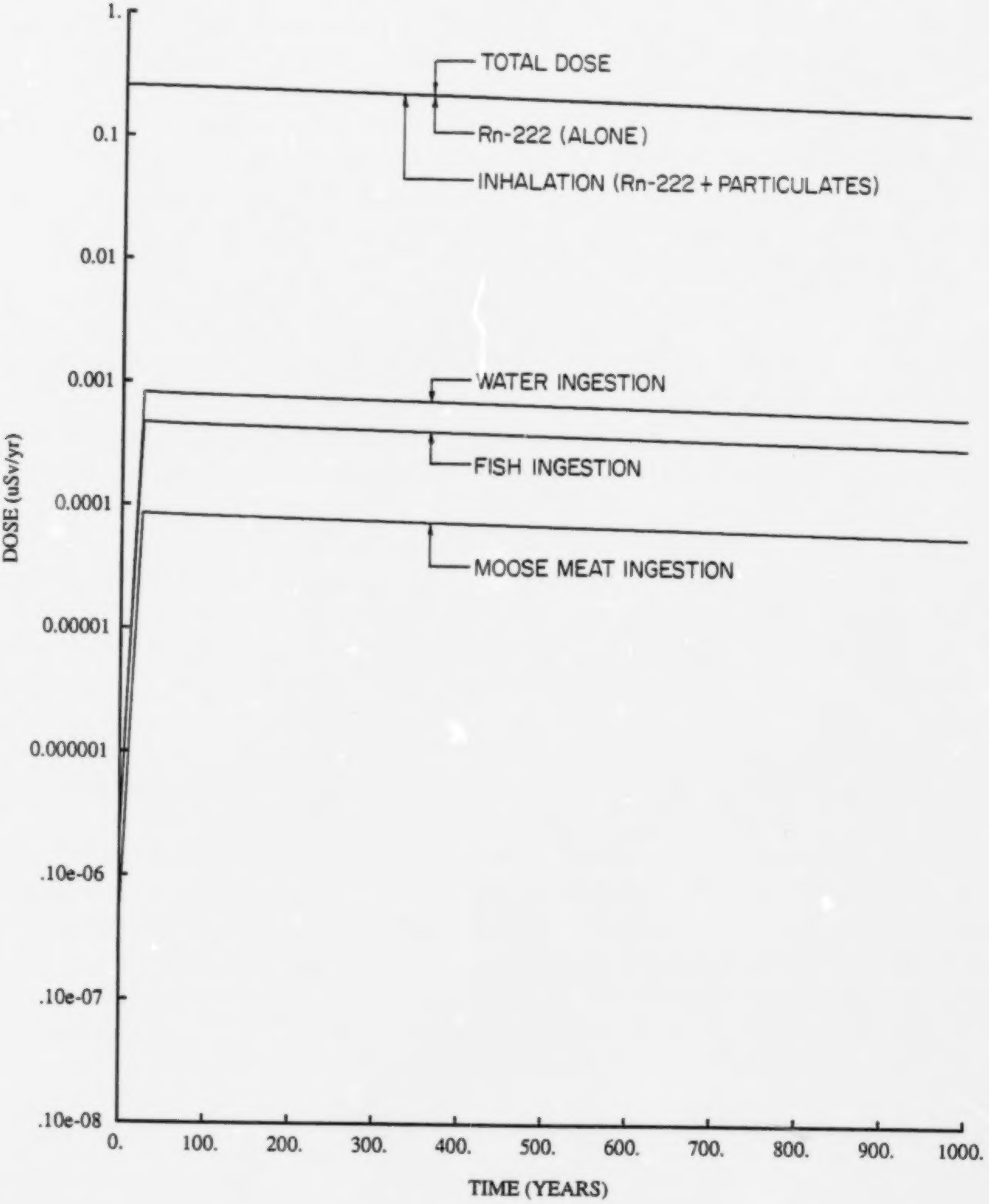

FIGURE 7.9: DOSE vs. TIME
FOR SCENARIO 2, BY RADIONUCLIDE
GEOMETRIC MEAN OF 500 TRIALS

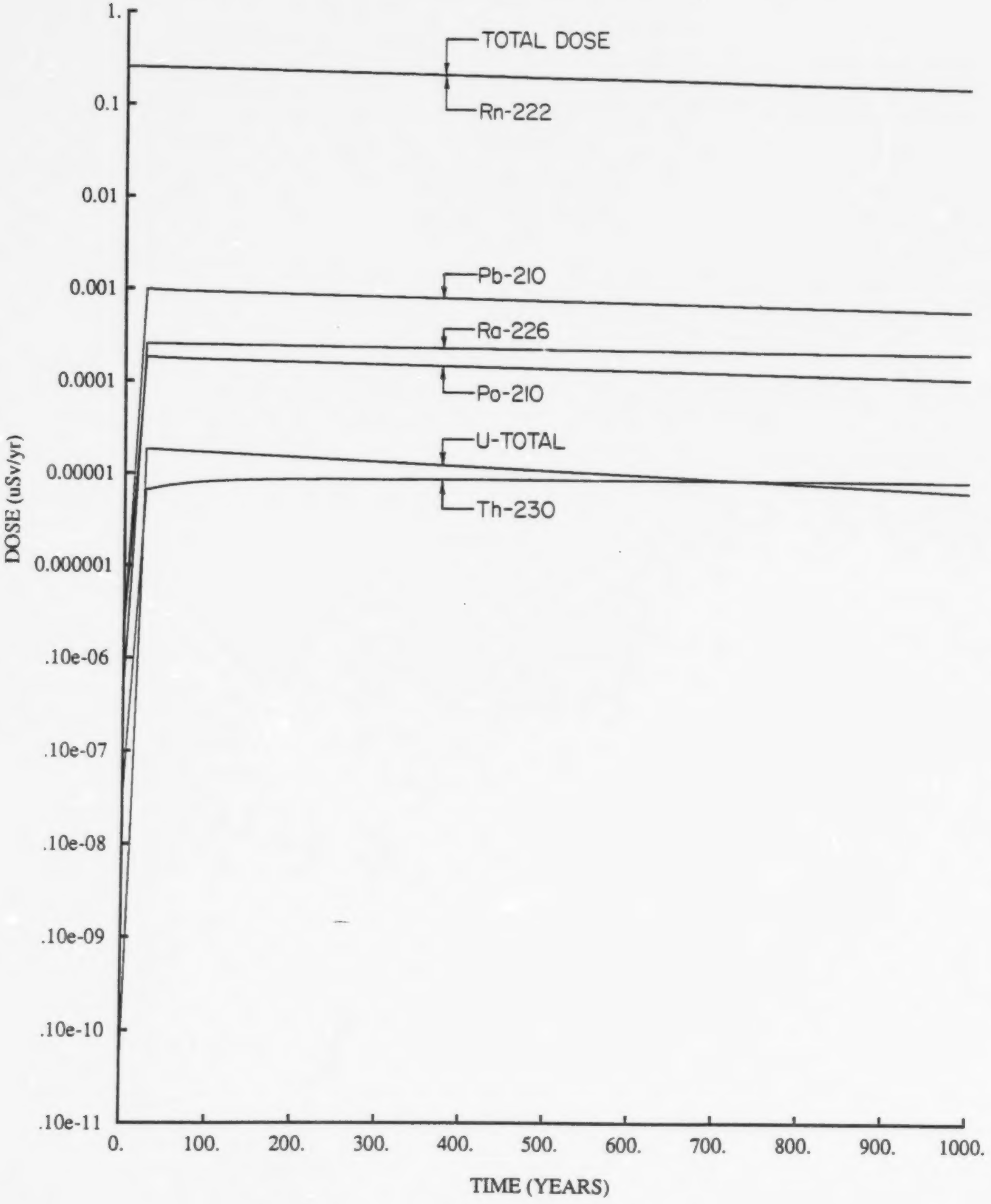

FIGURE 7.10: TOTAL DOSE vs. TIME
FOR SCENARIO 2
GEOMETRIC MEAN OF 500 TRIALS

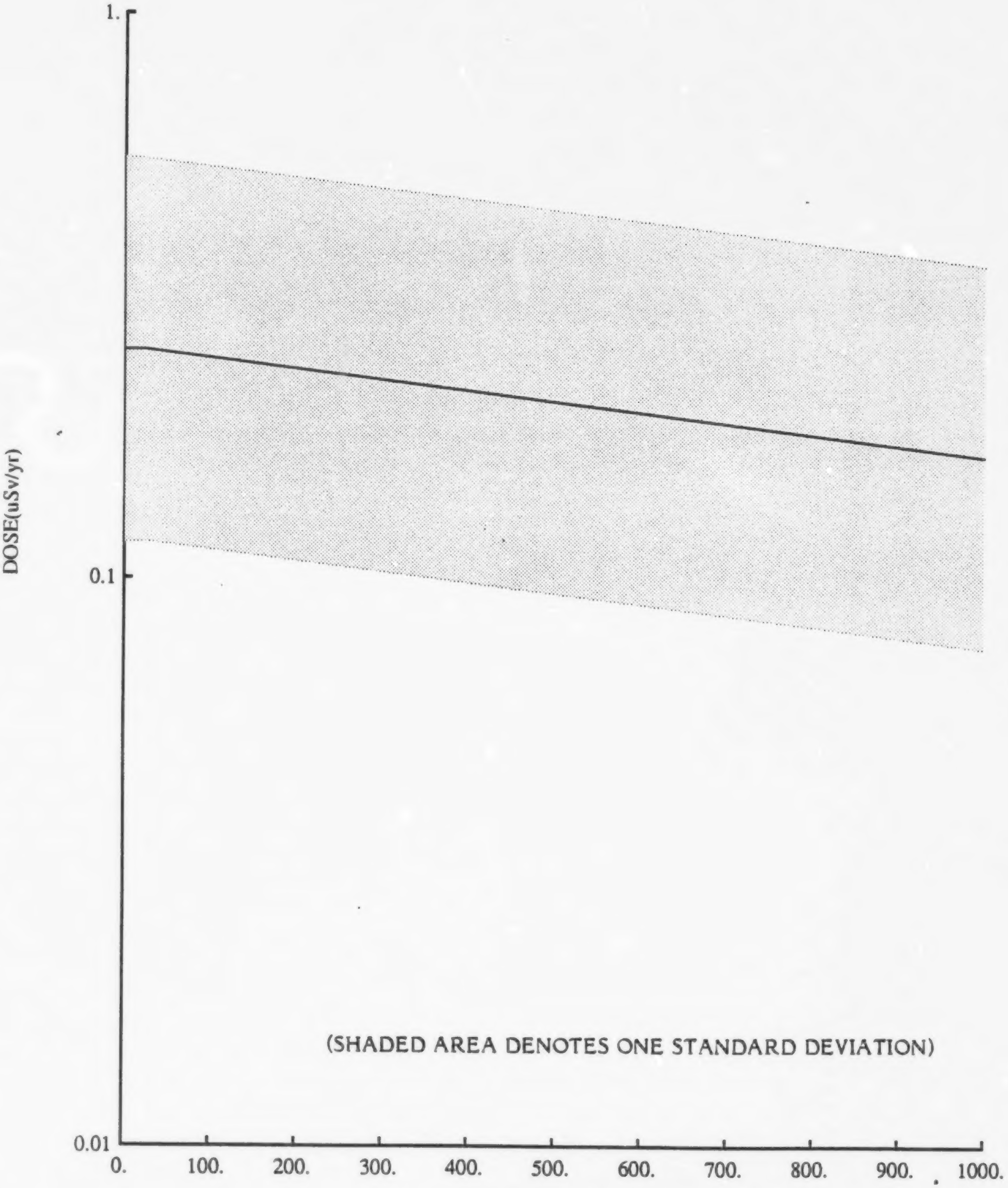

FIGURE 7.11: NICKEL INTAKE vs. TIME FOR SCENARIO 2, BY PATHWAY GEOMETRIC MEAN OF 500 TRIALS

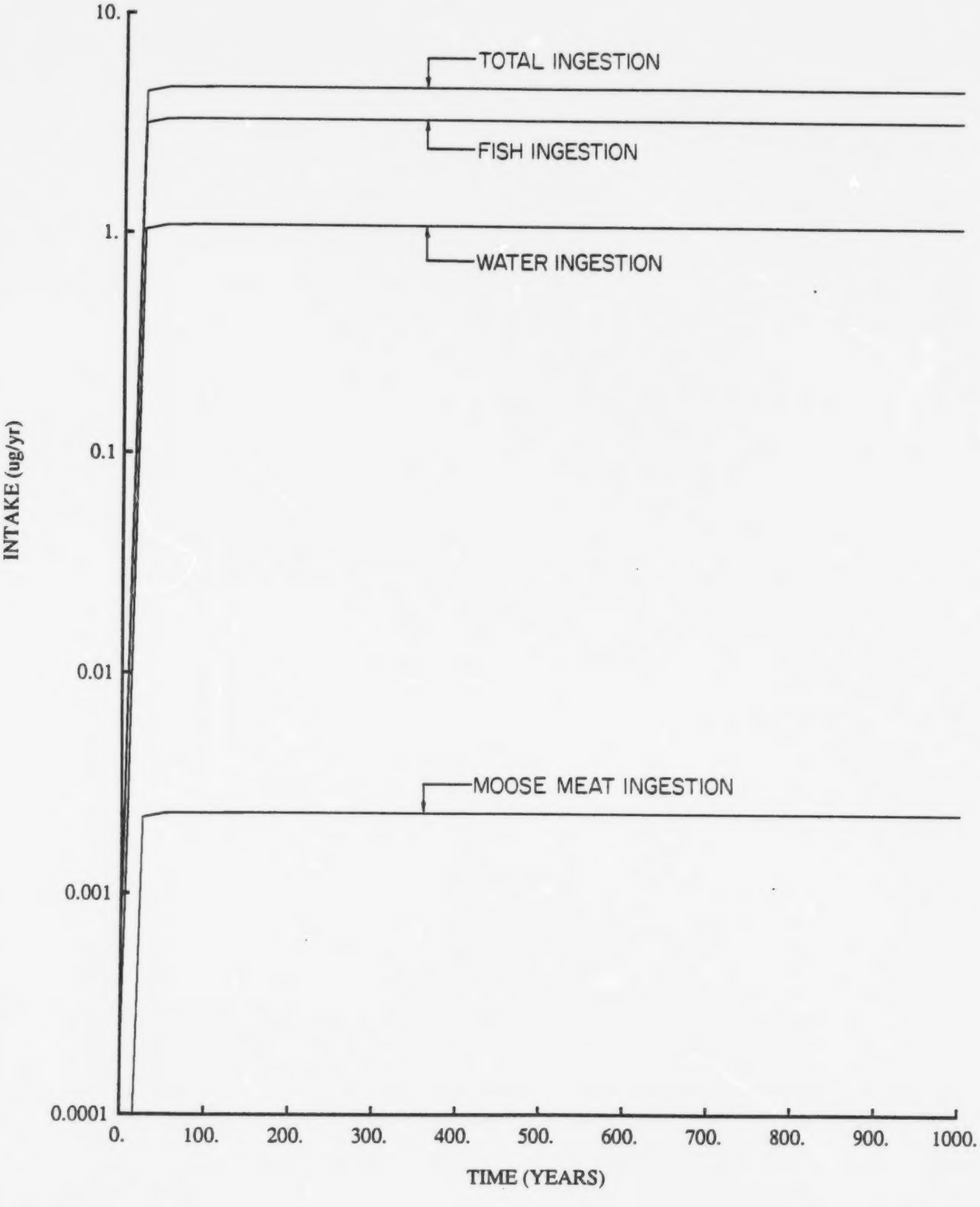

FIGURE 7.12: ARSENIC INTAKE vs. TIME
FOR SCENARIO 2, BY PATHWAY
GEOMETRIC MEAN OF 500 TRIALS

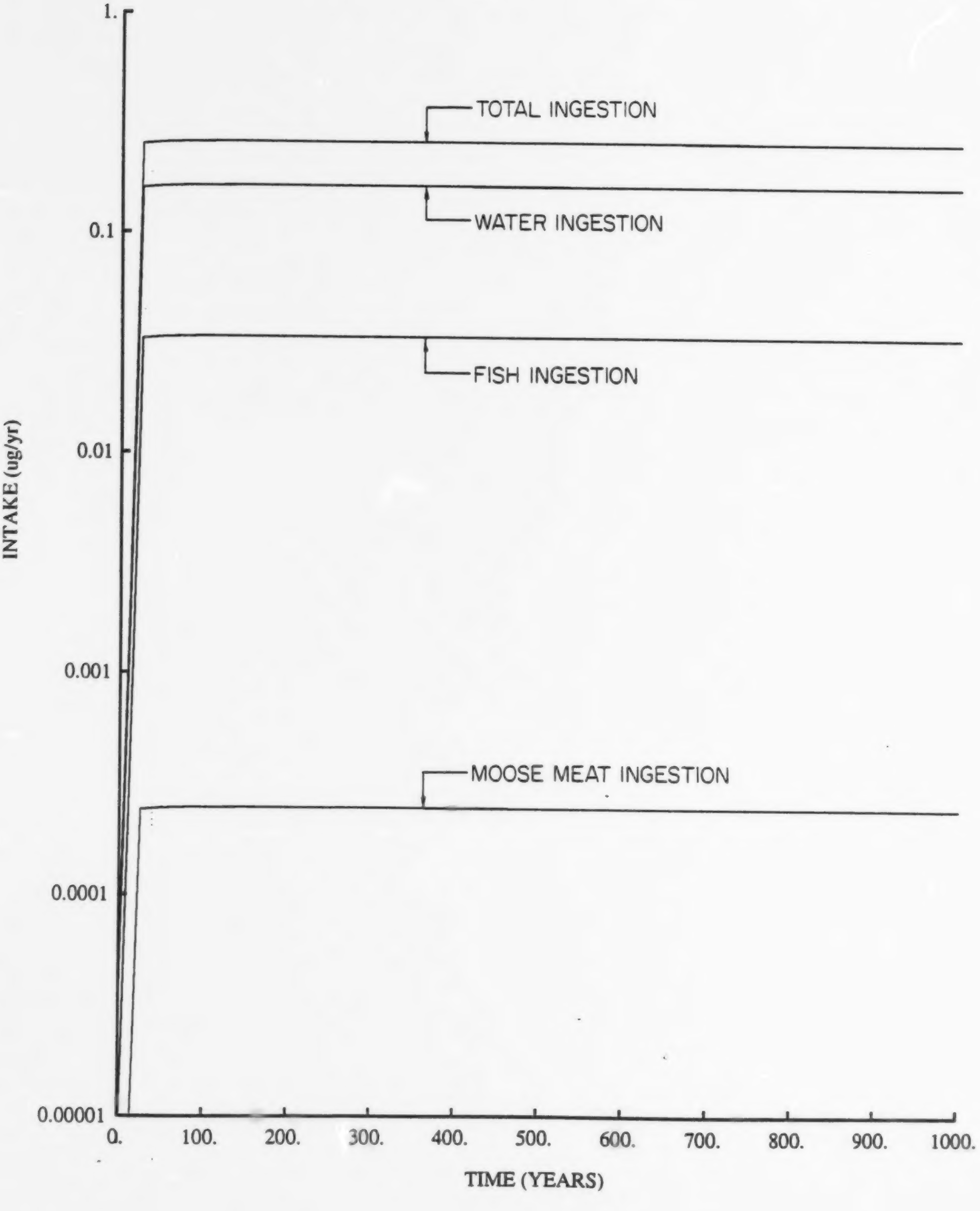

FIGURE 7.13: CONCENTRATIONS OF ARSENIC IN FOOD AND WATER (ppm) AND IN AIR (ug/m^3) FOR SCENARIO 2, BY PATHWAY GEOMETRIC MEAN OF 500 TRIALS

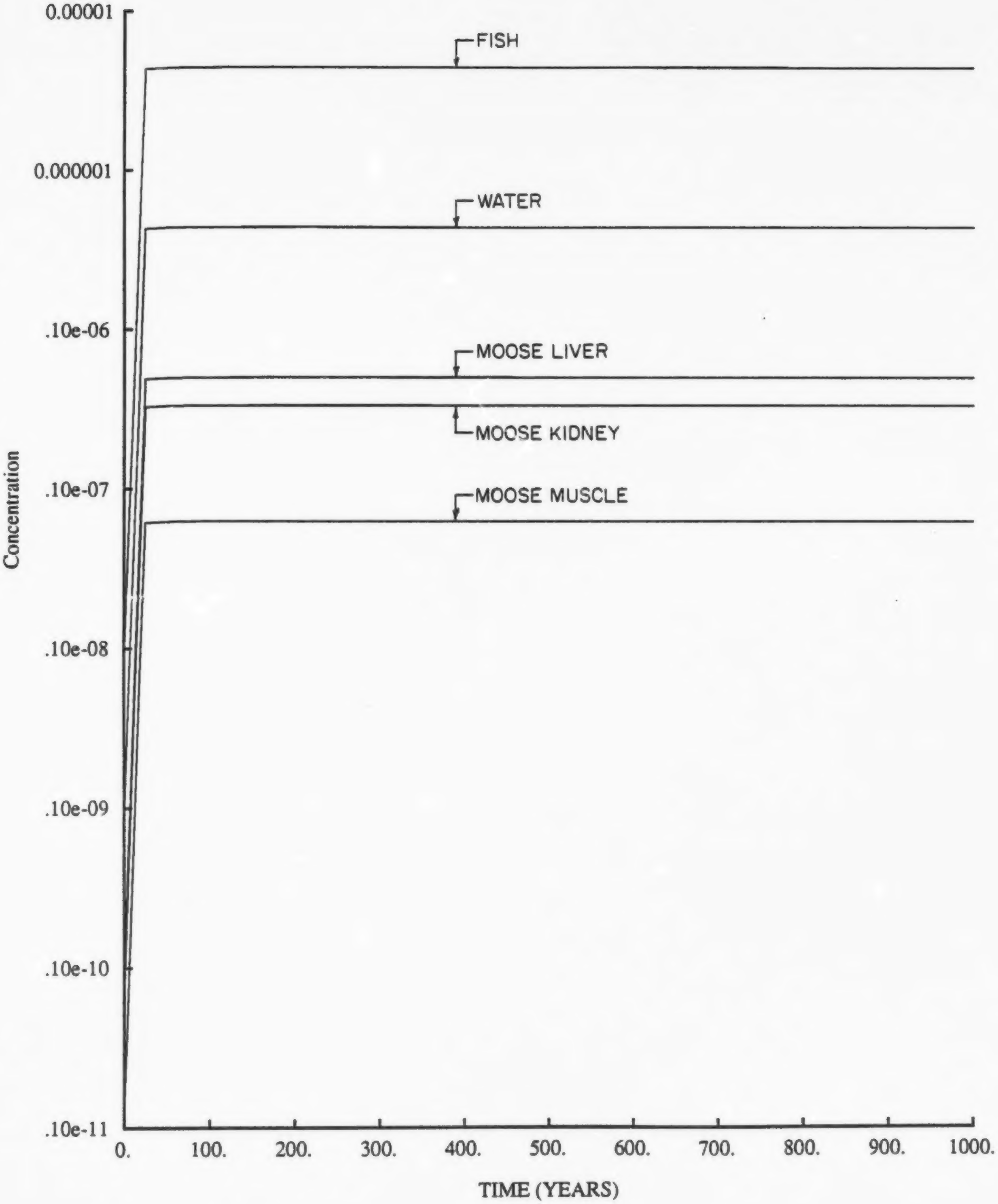

FIGURE 7.14: CONCENTRATIONS OF NICKEL IN FOOD AND WATER (ppm) AND IN AIR (ug/m^3) FOR SCENARIO 2, BY PATHWAY GEOMETRIC MEAN OF 500 TRIALS

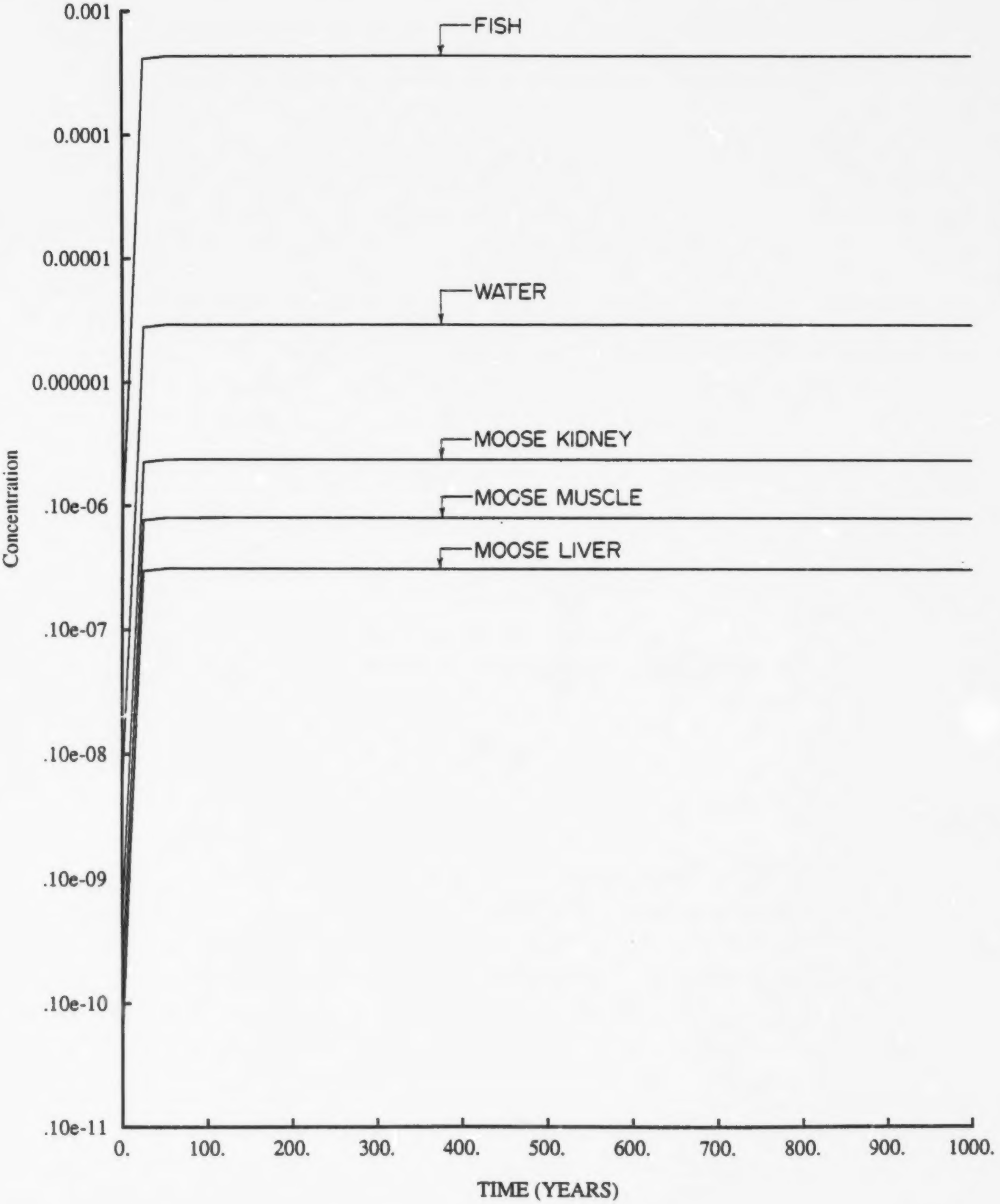

in the result. The "uncertainty index", as applied by SENES (1984), is the ratio of the variance of a particular parameter to the overall variance of the result. This index is only valid for purely additive or multiplicative models, such as the calculation of total dose.

SENES (1984) outlined techniques available to address sensitivity and uncertainty analysis simultaneously. One approach is the SENSYV approach, as applied by AECL at Pinawa. In this approach, a parameter is held constant, typically at a maximum and then at a minimum value within its distribution. All other parameters are allowed to vary within their specified distributions. The results of high and low runs are compared with those of a reference case (where all parameters are varied) by graphically superimposing cumulative plots. This permits comparison between the effects of different levels of variables within the range of variation existing in the remaining variables. SENES found that, while the method consumes a large amount of computer time, it does provide a general clearly interpretable measure of parameter importance.

In this project, calculations for the base case indicate that the airborne pathways (dust and radon transport) make the largest contribution to dose. A sensitivity analysis of these pathways was undertaken using the Phase II SENES code for radon transport and radium-226 transport from direct erosion. Three complementing techniques were used to conduct the sensitivity analysis: a first order error analysis analogue, correlation analysis, and the SENSYV technique. Details of the procedures used and the results are given in Appendix C. These results are summarized here.

The relative order of sensitivity for the parameters on the radon model are given in Table 7.1, while the relative order of sensitivity for the dust model are given in Table 7.2. The calculated ranking of parameters is very similar for each technique.

These results suggest some priorities for designing future model development and in guiding research and monitoring programs. For improving calculations through the radon pathway, factors which affect radon emanation and the source concentrations of Ra-226 are more important than factors which affect radon dispersion in the atmosphere. Similarly, for transport through the dust pathway, factors which affect source concentrations are more important than factors which affect dispersion in the atmosphere. Because radon dose is computed to give a substantial contribution to the

TABLE 7.1: SENSITIVITY ORDER FOR RADON PATHWAY

		Sensitivity Method	
Parameter	First Order Method	Correlation Analysis	SENSYV
EMANAT	1	1	1
MPCH20	2	2	2
F	3	3	3
CONCRA	4	4	4
OF	5	5	5
VDISP	6	6	6
RHOTAL	7	*	7
FWIND2	8	*	*
UWIND	9	*	*
HSRC	10	*	*

* Parameters not statistically significant.

TABLE 7.2: SENSITIVITY ANALYSIS FOR DUST PATHWAY

Parameter	First Order Method	Correlation Analysis	SENSYV
CONCRA	1	1	1
RAINGP	2	2	2 **
OF	3	3	2 **
VDISP	4	4	4
FWIND2	5	5	5
FWIND1	6	*	6
UWIND	7	*	7
FPREC	8	*	*
HSPC	9	*	*

* Parameters not statistically significant.

** Same rank of sensitivity.

total dose over the lifetime of the tailings, future model refinements should be sought related to describing the flux of radon emanating from tailings in addition to considering the sensitivity of dose conversion factors.

8.0 TEMPORAL CHARACTERISTICS OF SOURCE MODEL AND AQUATIC PATHWAYS

The detailed theory of the biogeochemistry and associated behaviour of the tailings mass and of environmental pathways have been given above in section 4 and 5. Probabilistic assessment results describing the dose to humans and other aspects of the model have been given in Section 7.

In this section concentrations calculated for various substances in the tailings mass and to receiving lakes are given using small time steps (7 years) for a 280 year simulation period for the base case. One hundred simulation passes are used to obtain these results, except for a few cases where 400 simulation passes (trials) were used.

8.1 Source Term Characteristics

Calculated concentrations of gypsum, barite and anglesite in the top box are given respectively in Figures 8.1, 8.2 and 8.3. The top box detail is given because these substances influence the concentration of Ra-226 in the top box and hence the atmospheric source term model for Ra-226 and its daughters, including radon gas. The calculated concentrations of the various solids in the top box of the tailings are given in Figures 8.1a, 8.2a and 8.3a assuming a log-normal distribution, and in Figures 8.1b, 8.2b and 8.3b assuming a truncated log-normal distribution. Results are given in Figure 8.1c for one solid assuming a normal distribution. The shaded areas give an estimate of the 95% confidence interval assuming a log-normally distributed parameter.

Initial plots had problems as typified by the log-normal plot for anglesite (Figure 8.3c). The plot suggests that the $PbSO_4$ concentration declines to about year 60, increases to a value of one at year 90 and then decreases. Further analyses showed that there was an error in the existing SENES software for calculating log-normal statistics. It had the property of assigning a value of 1 to the log-value as the value tended towards zero. This limitation was corrected, resulting in the plot given in Figure 8.3a. This error would not affect the statistics for calculation of other parameter statistics except for those whose value is zero - a problem which could occur for certain pathways far into the future.

FIGURE 8.1a: CASO4(1)
FOR SCENARIO 1
GEOMETRIC MEAN OF 100 TRIALS

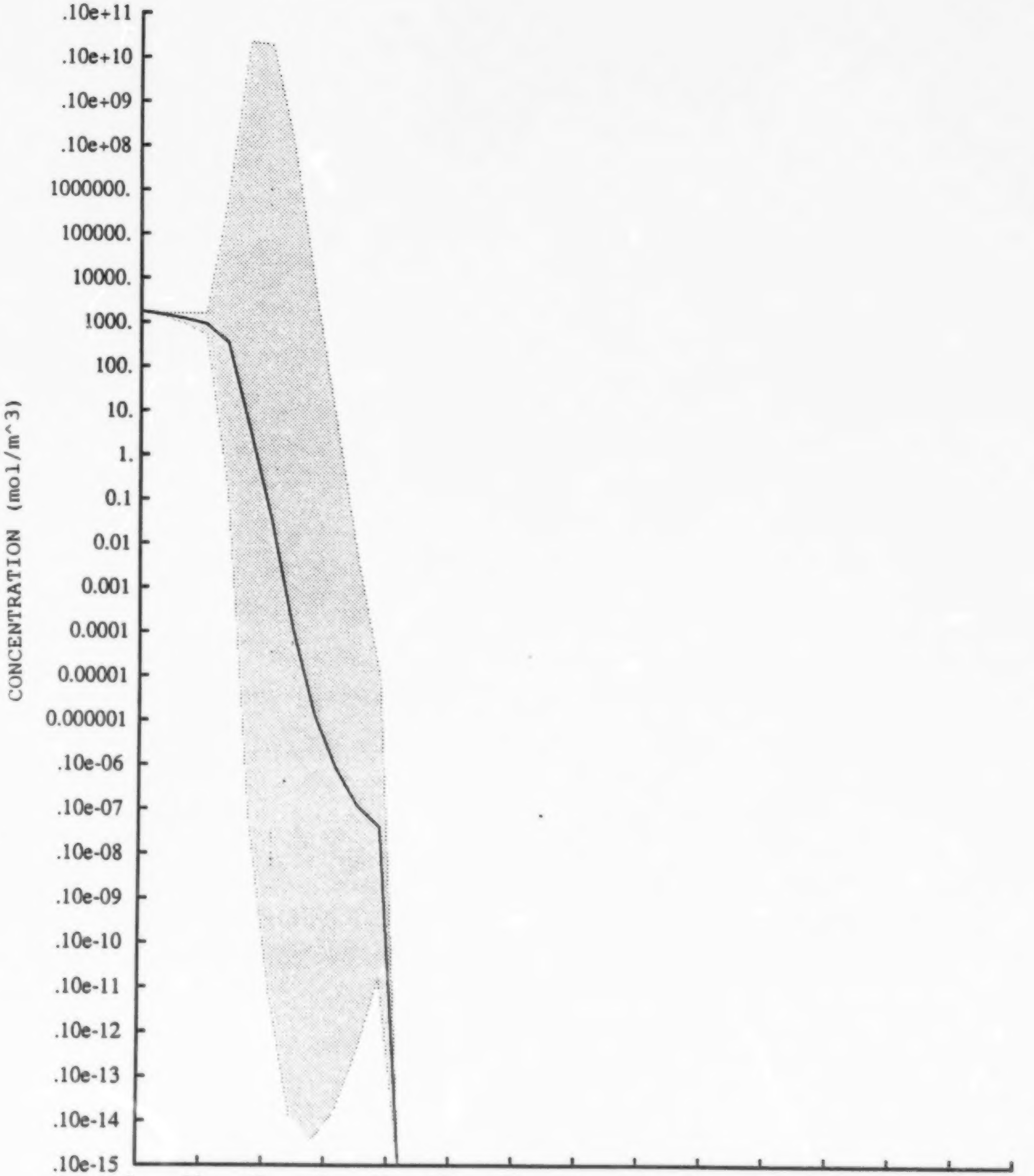

FIGURE 8.1b: CASO4(1)
FOR SCENARIO 1
GEOMETRIC MEAN OF 100 TRIALS

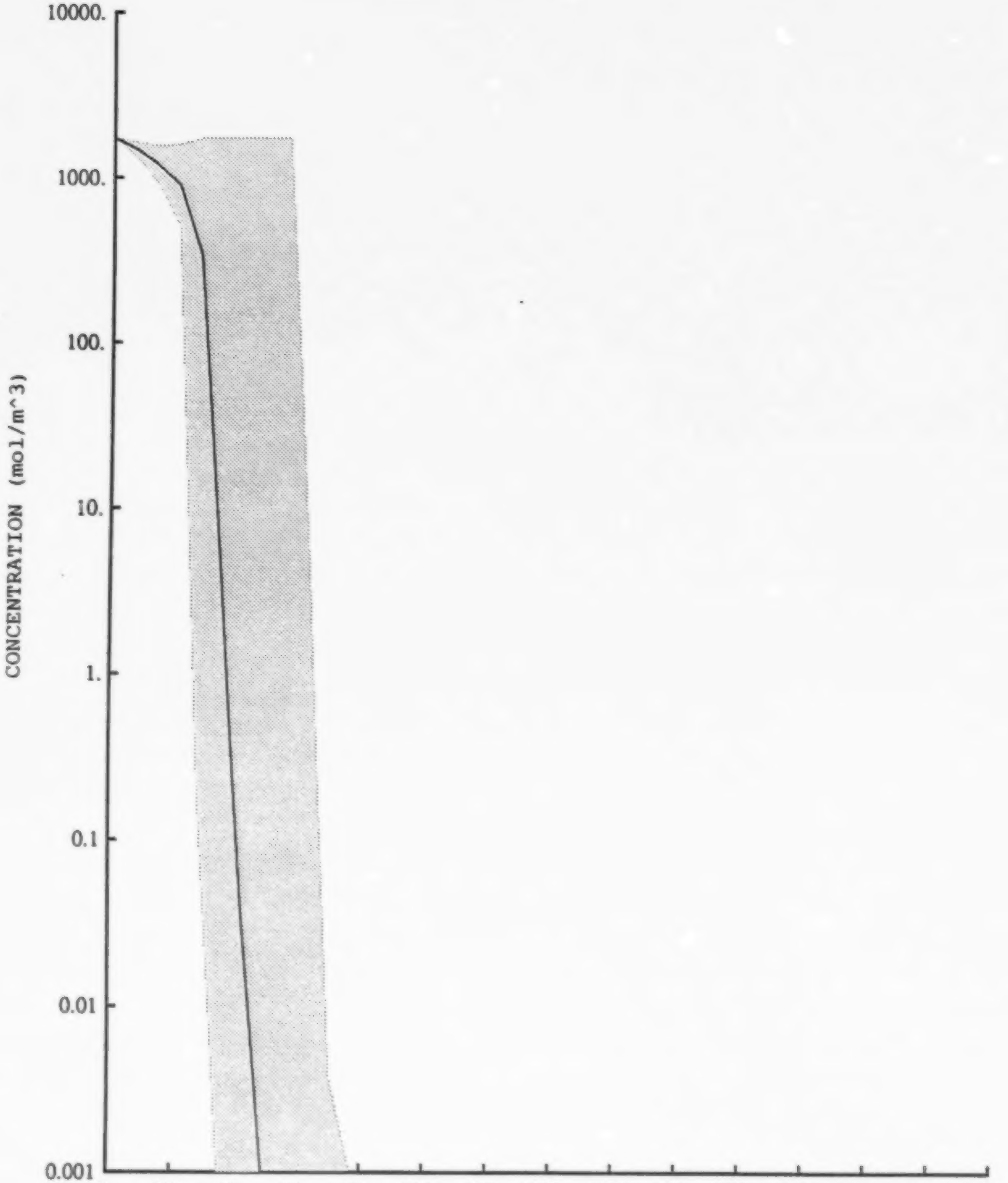

FIGURE 8.1c: GYPSUM (TOP 10 CM)
FOR SCENARIO 1
ARITHMETIC MEAN OF 400 TRIALS

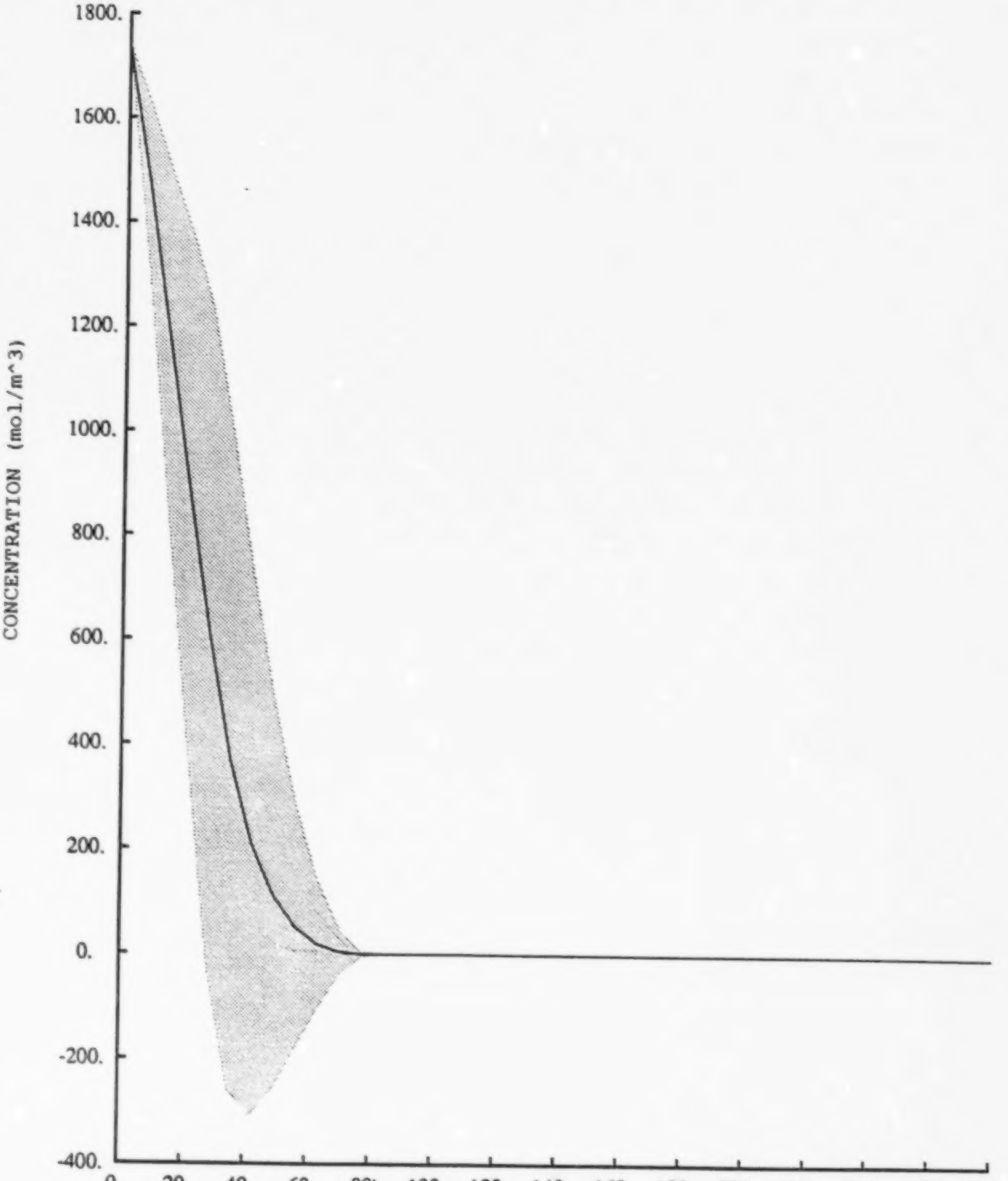

FIGURE 8.2a: BASO4(1)
FOR SCENARIO 1
GEOMETRIC MEAN OF 100 TRIALS

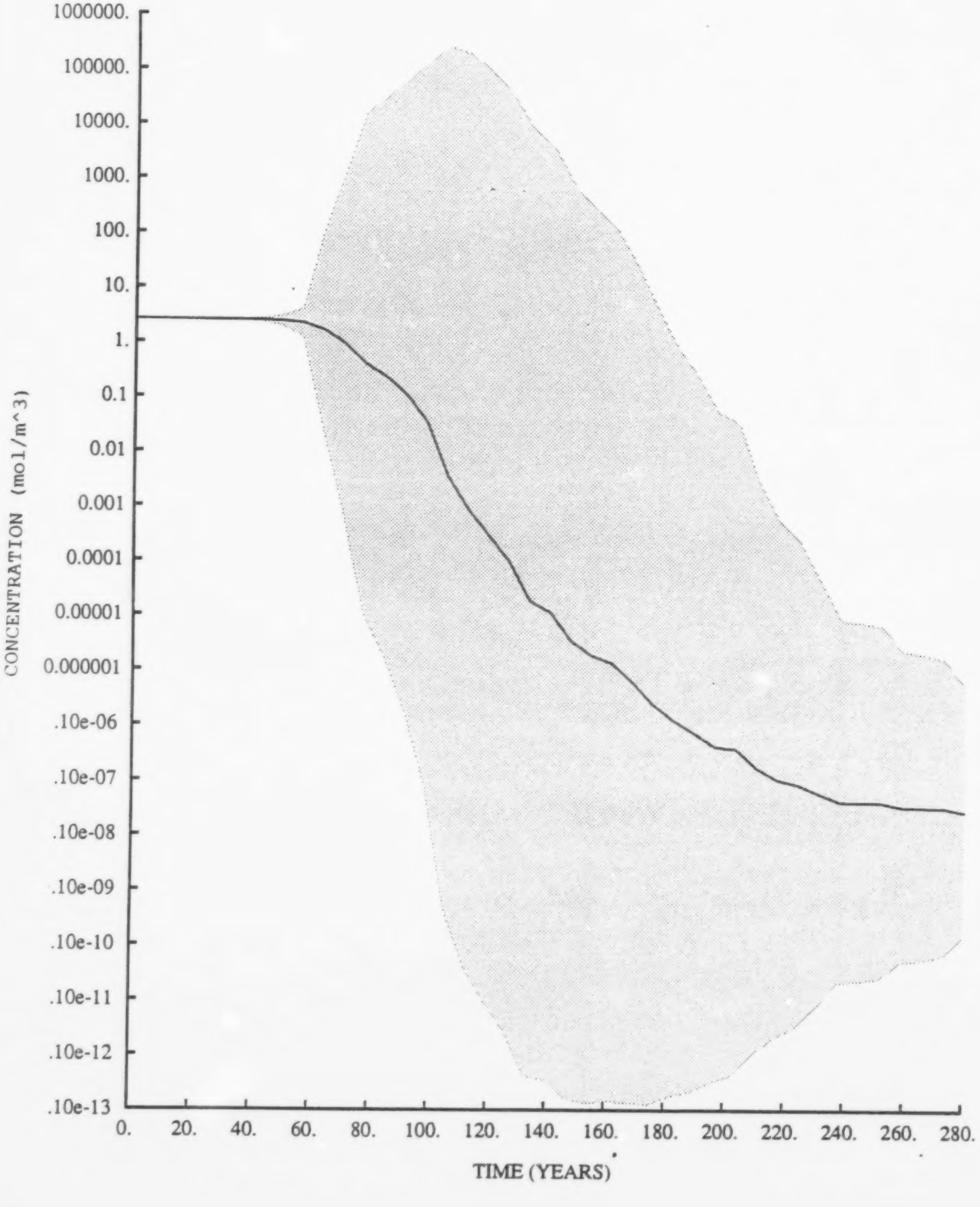

FIGURE 8.2b: BASO4(1)
FOR SCENARIO 1
GEOMETRIC MEAN OF 100 TRIALS

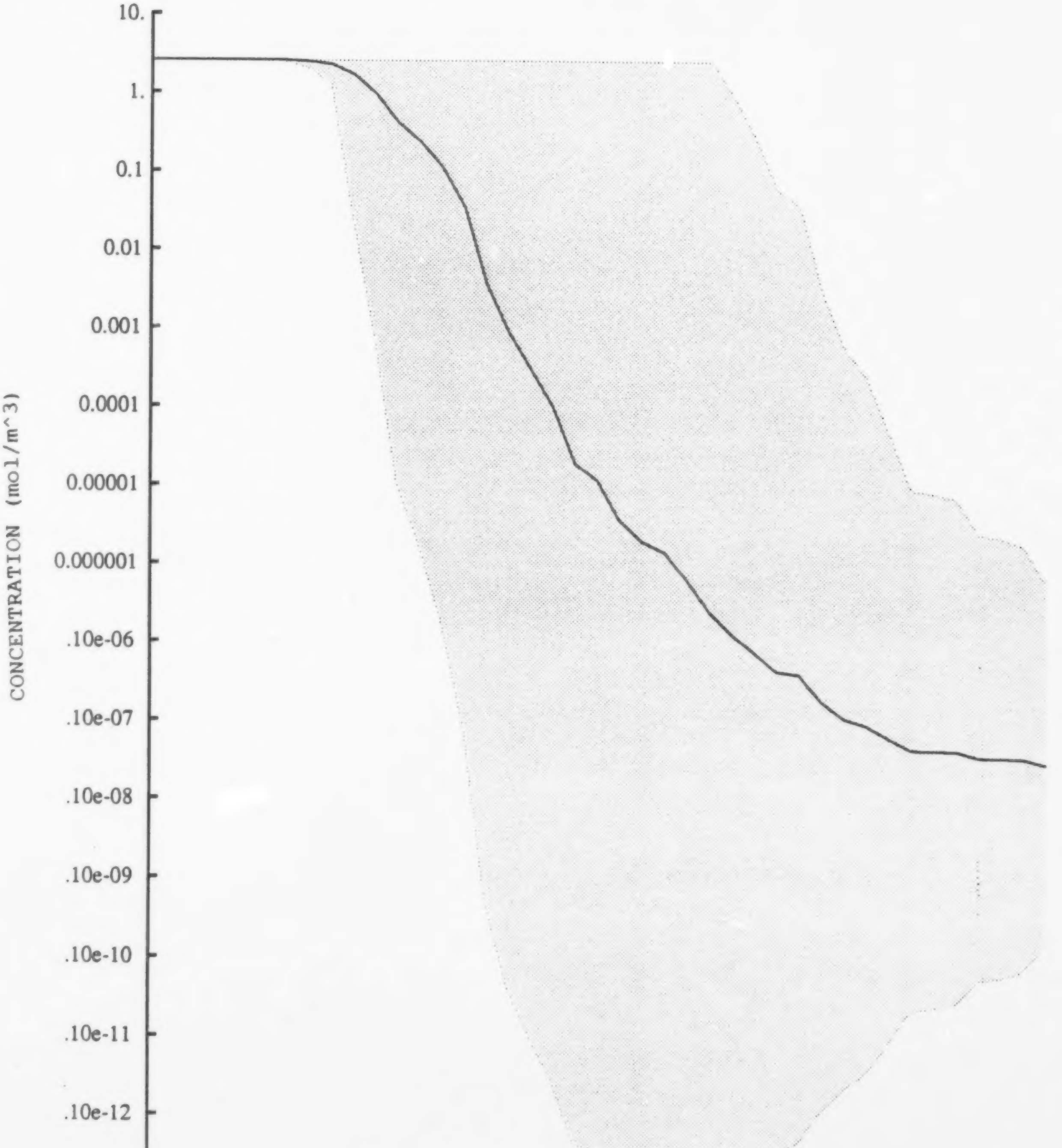

FIGURE 8.3a PBSO4(1)
FOR SCENARIO 1
GEOMETRIC MEAN OF 100 TRIALS

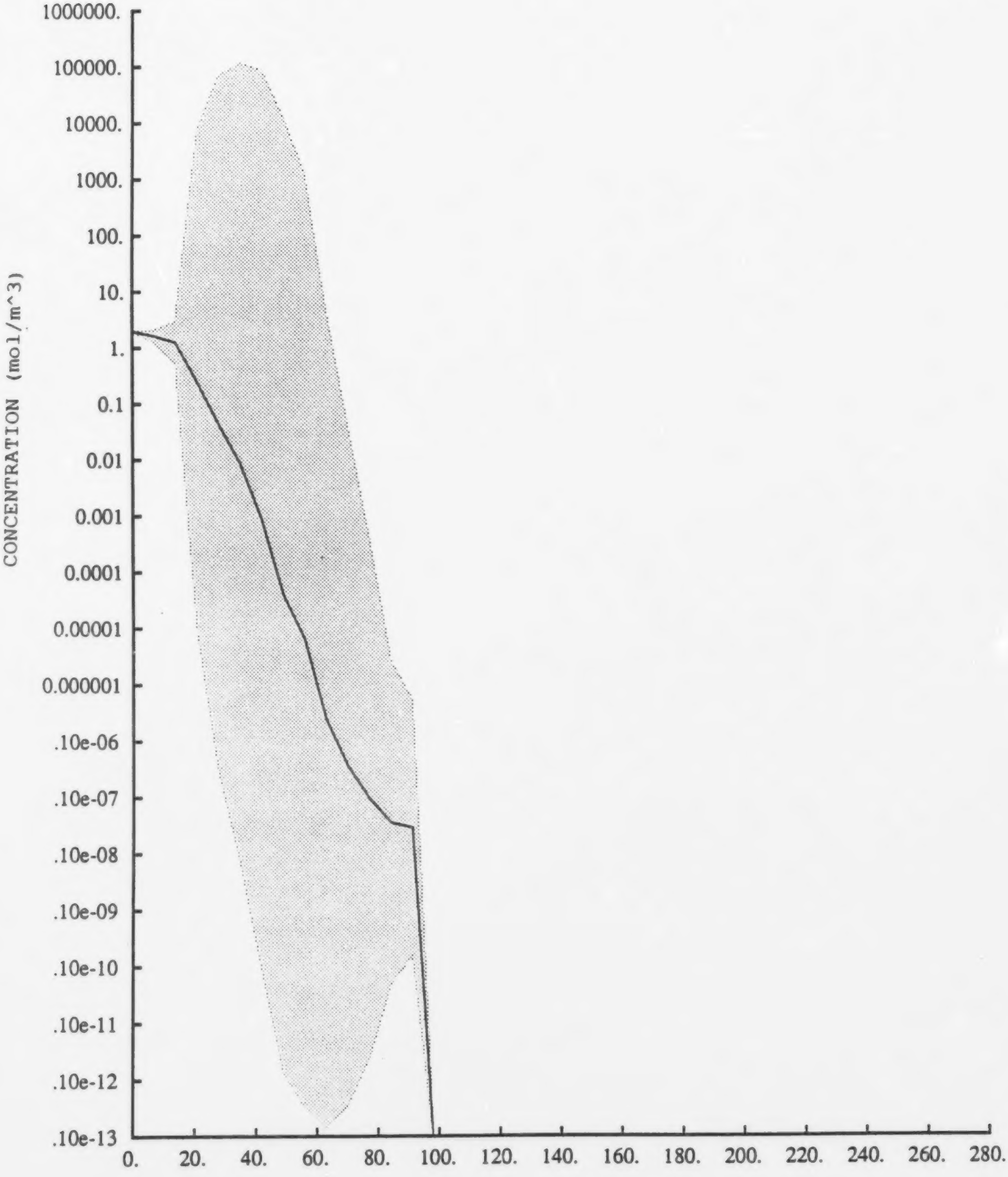

FIGURE 8.3b: PBSO4(1)
FOR SCENARIO 1
GEOMETRIC MEAN OF 100 TRIALS

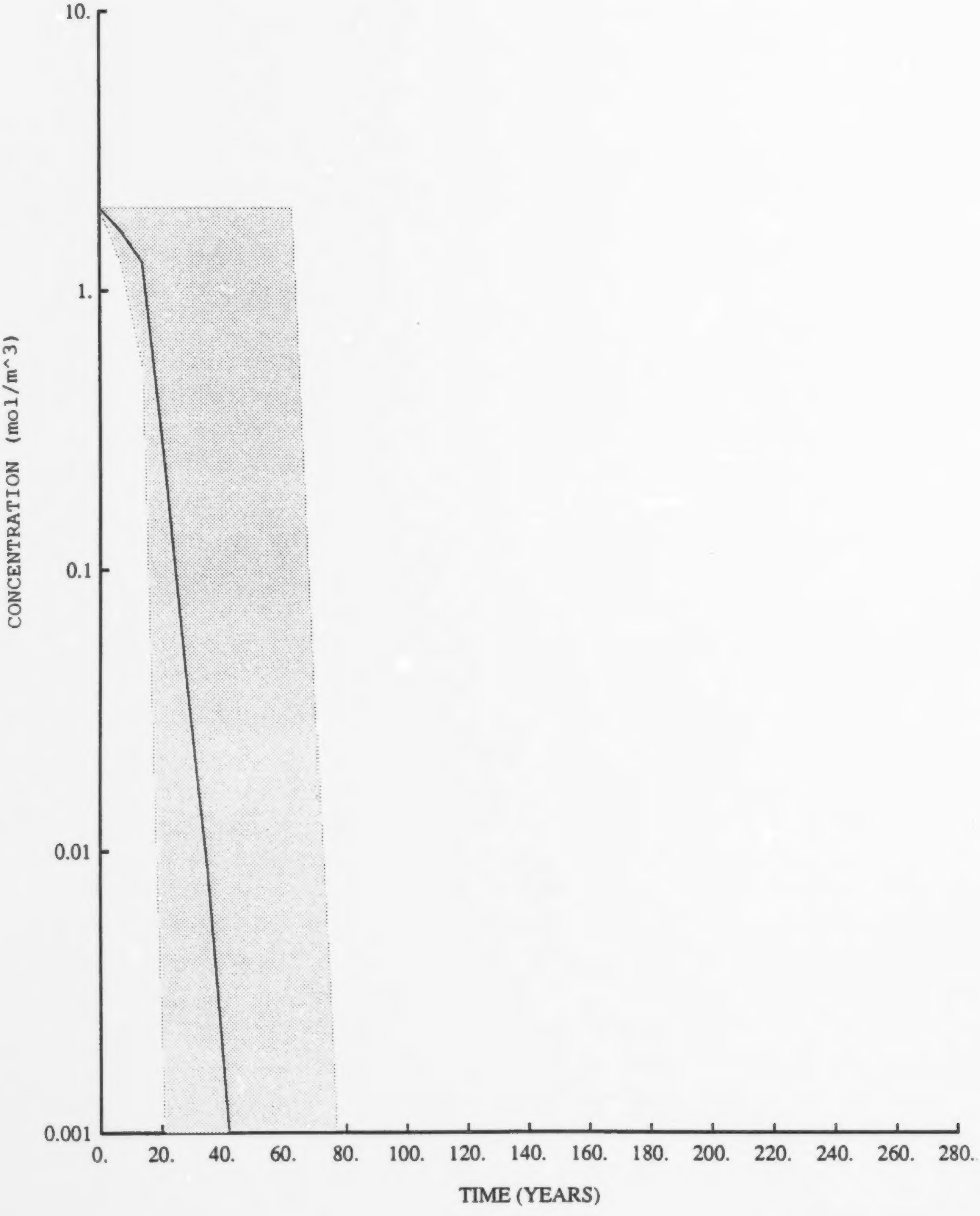

The plots of the 95% confidence interval for the non-truncated log-normal distribution (Figures 8.1a, 8.2a, 8.3a) suggest that the geometric mean concentration in the surface box decreases after a period of time but that the upper limit of the confidence interval increases above the initial value. This is impossible because the concentration in the surface box never increases above its initial value for these three solid phases. Extreme-event theory provides a method for plotting a 95% confidence interval for the calculated histogram. Evaluation of the predicted probability distribution function indicated that it is a skewed log-normal distribution constrained at the upper limit by the initial mass present. Parameters for this distribution were summarized, but the statistics calculated by the existing software are inappropriate and would require revision. This was not done for this report. Hence, the truncated (Figures 8.1b, 8.2b, 8.3b) log-normal distribution best represents the behaviour of the three solid phases in the top box.

Evaluation of the time behaviour of the solid phases indicate that gypsum essentially disappears at approximately 50 years, lead sulphate at approximately the same time and barium sulphate at 100 to 120 years.

The corresponding aqueous activity of Th-230 and Ra-226 in the top box (respectively Figures 8.4a, 8.4b) shows a wide variance. The trend in the activity of Th-230 is influenced mainly by variation in solid phase concentrations of iron hydroxide and manganese oxide. The increase in Ra-226 is caused initially by the disappearance of most of the gypsum, lead sulphate, and barium sulphate from the top box in 50-100 years allowing Ra-226 to enter solution. The decrease after 80 years results from completion of dissolution of BaS04 and washout. High solution concentrations of Ra-226 are required to remove all Ra-226 from the surface box.

The concentration of uranium ($mol \cdot L^{-1}$) and the activity of Th-230, Ra-226 and Pb-210 in the pore water in the top of the saturated zone (box3) are given respectively in Figures 8.5a-d. The shaded areas represent the 95% confidence interval for the predicted log-normal distribution. The results indicate that the predicted distribution function for uranium is relatively more narrow than that of the other radionuclides.

The activity of Th-230 is approximately 0.5 $Bq \cdot L^{-1}$, while those of Ra-226 and Pb-210 are approximately 1 to 2 $Bq \cdot L^{-1}$. The level of Th-230 is relatively constant while that of Pb-210 essentially follows that of Ra-226. The Pb-210 activity in the porewater is

FIGURE 8.3c: ANGELSITE (TOP 10 CM)
FOR SCENARIO 1
GEOMETRIC MEAN OF 400 TRIALS

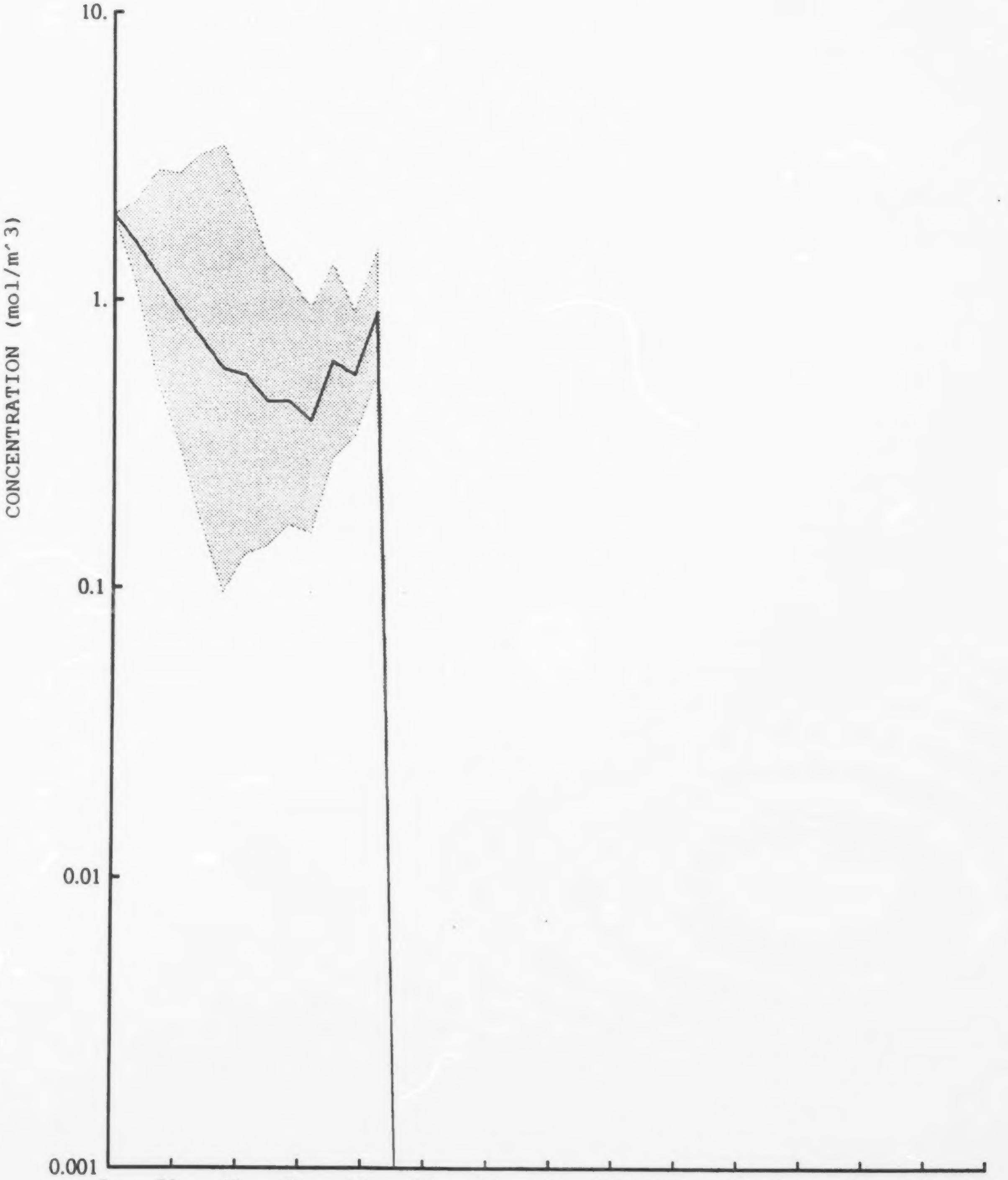

FIGURE 8.4a: AQUEOUS Th-230 (TOP 10 CM)
FOR SCENARIO 1,
GEOMETRIC MEAN OF 400 TRIALS

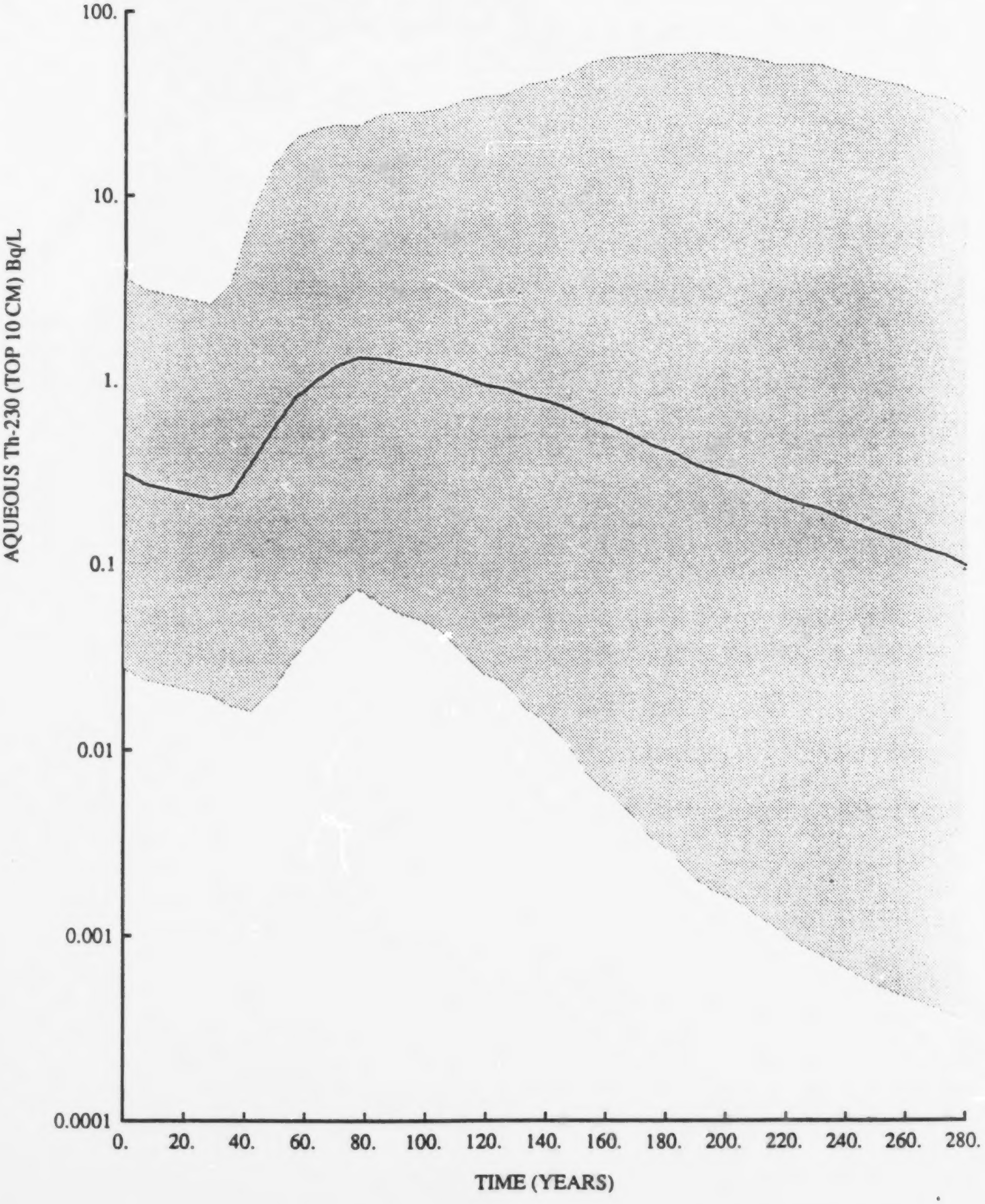

FIGURE 8.4b: AQUEOUS Ra-226 (TOP 10 CM)
FOR SCENARIO 1,
GEOMETRIC MEAN OF 400 TRIALS

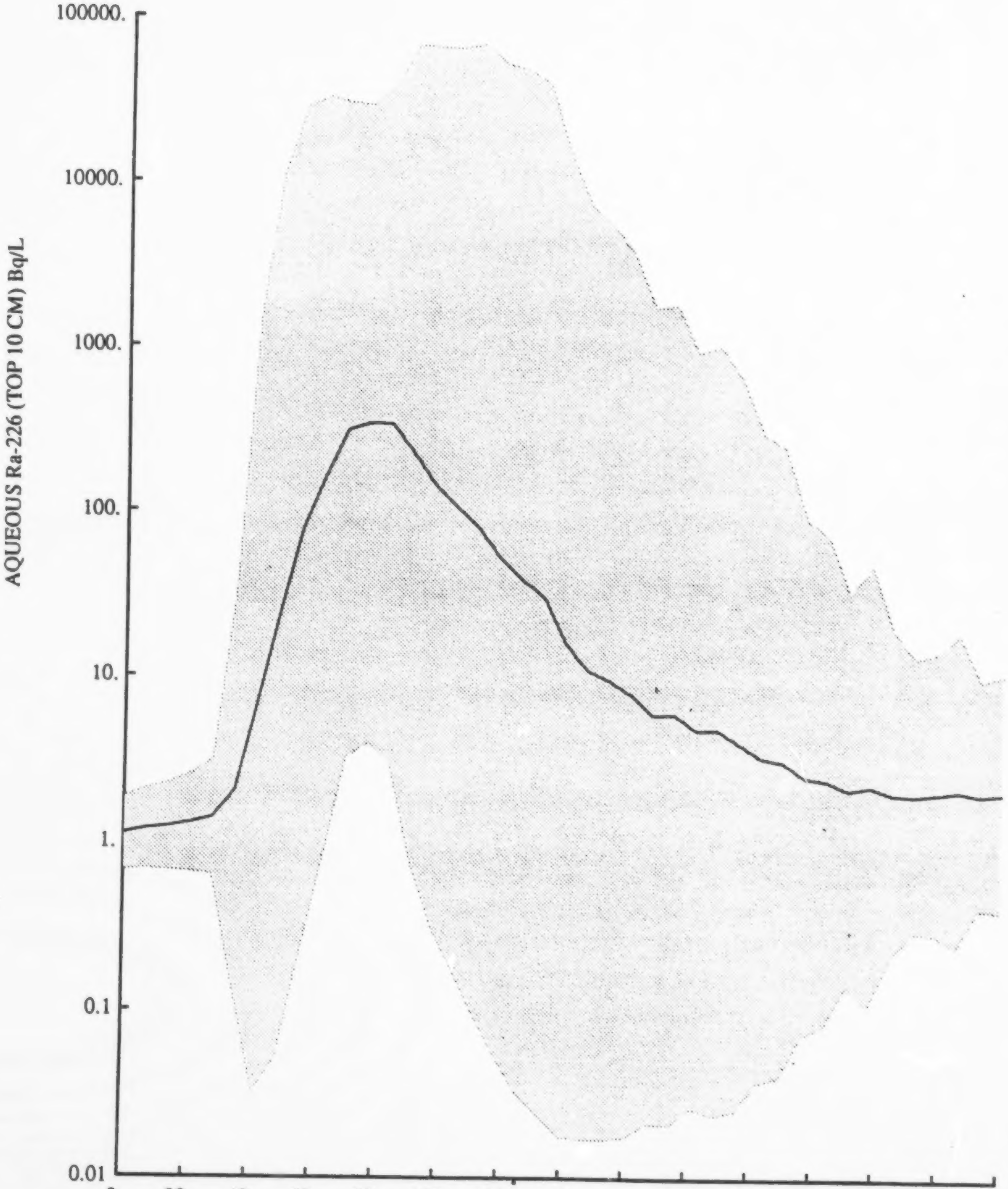

FIGURE 8.5a: URANIUM CONC. IN PORE WATER FOR SCENARIO 1, GEOMETRIC MEAN OF 100 TRIALS

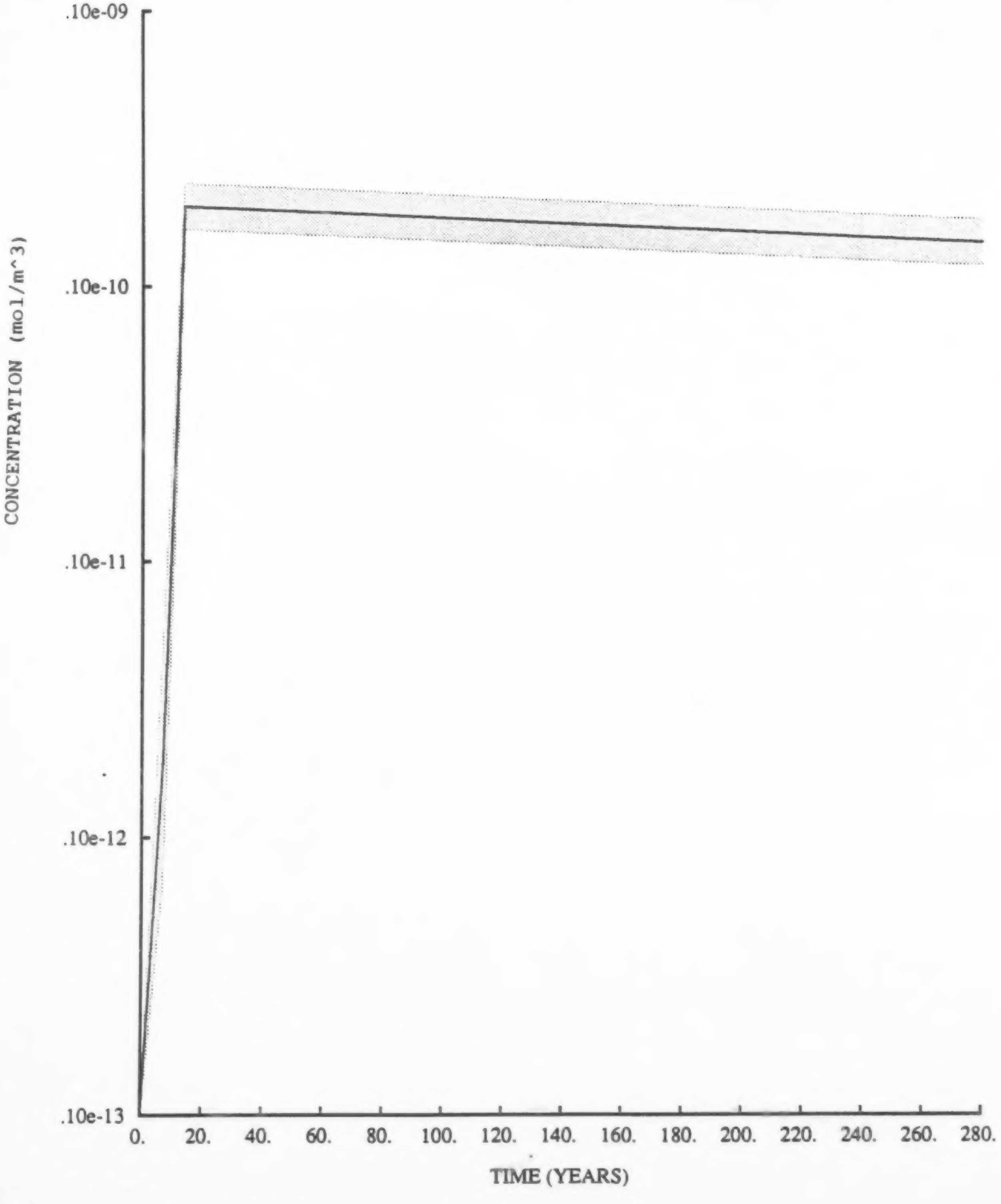

FIGURE 8.5b: Th-230 ACTIVITY IN PORE WATER FOR SCENARIO 1, GEOMETRIC MEAN OF 100 TRIALS

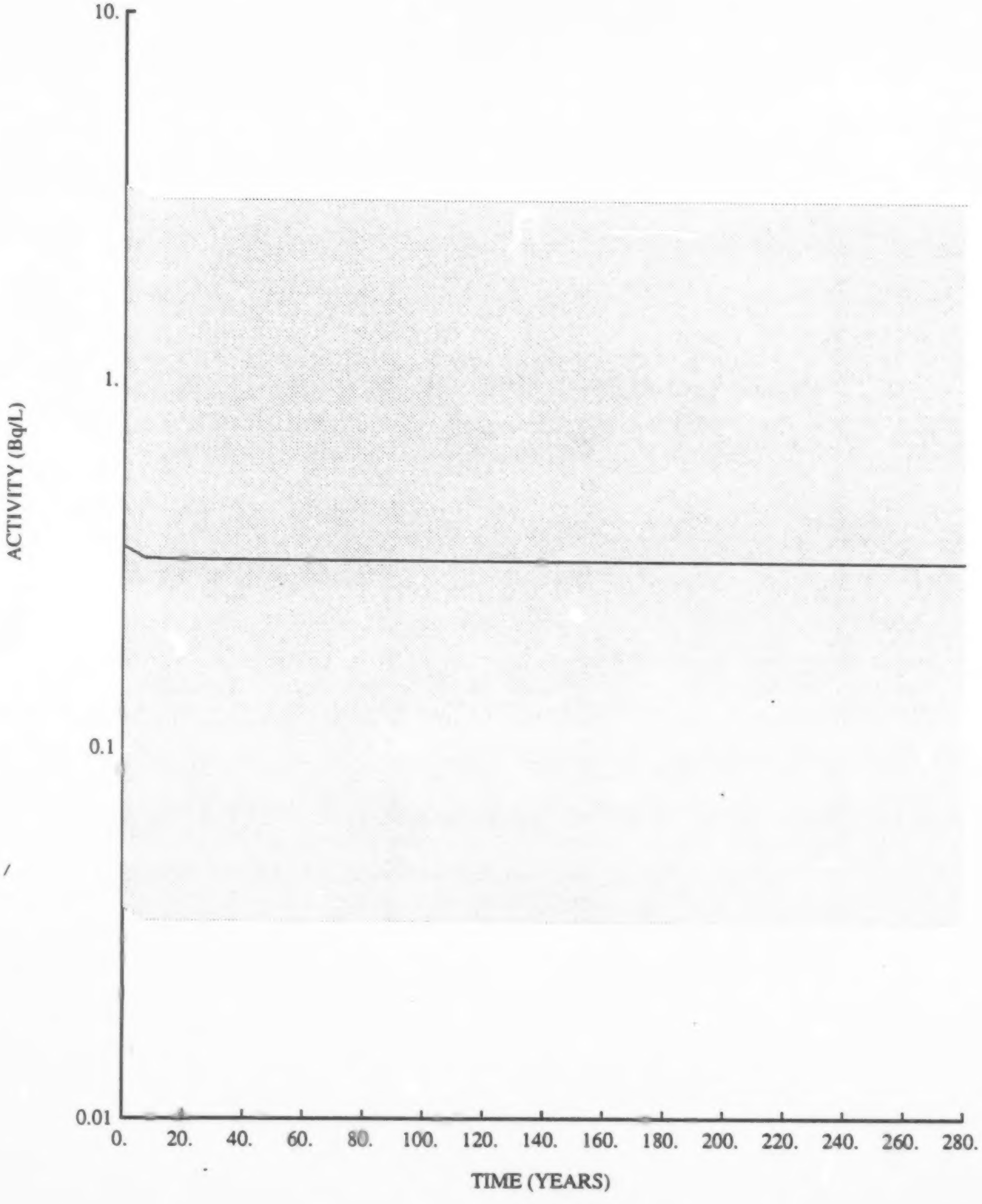

FIGURE 8.5c: Ra-226 ACTIVITY IN PORE WATER FOR SCENARIO 1, GEOMETRIC MEAN OF 100 TRIALS

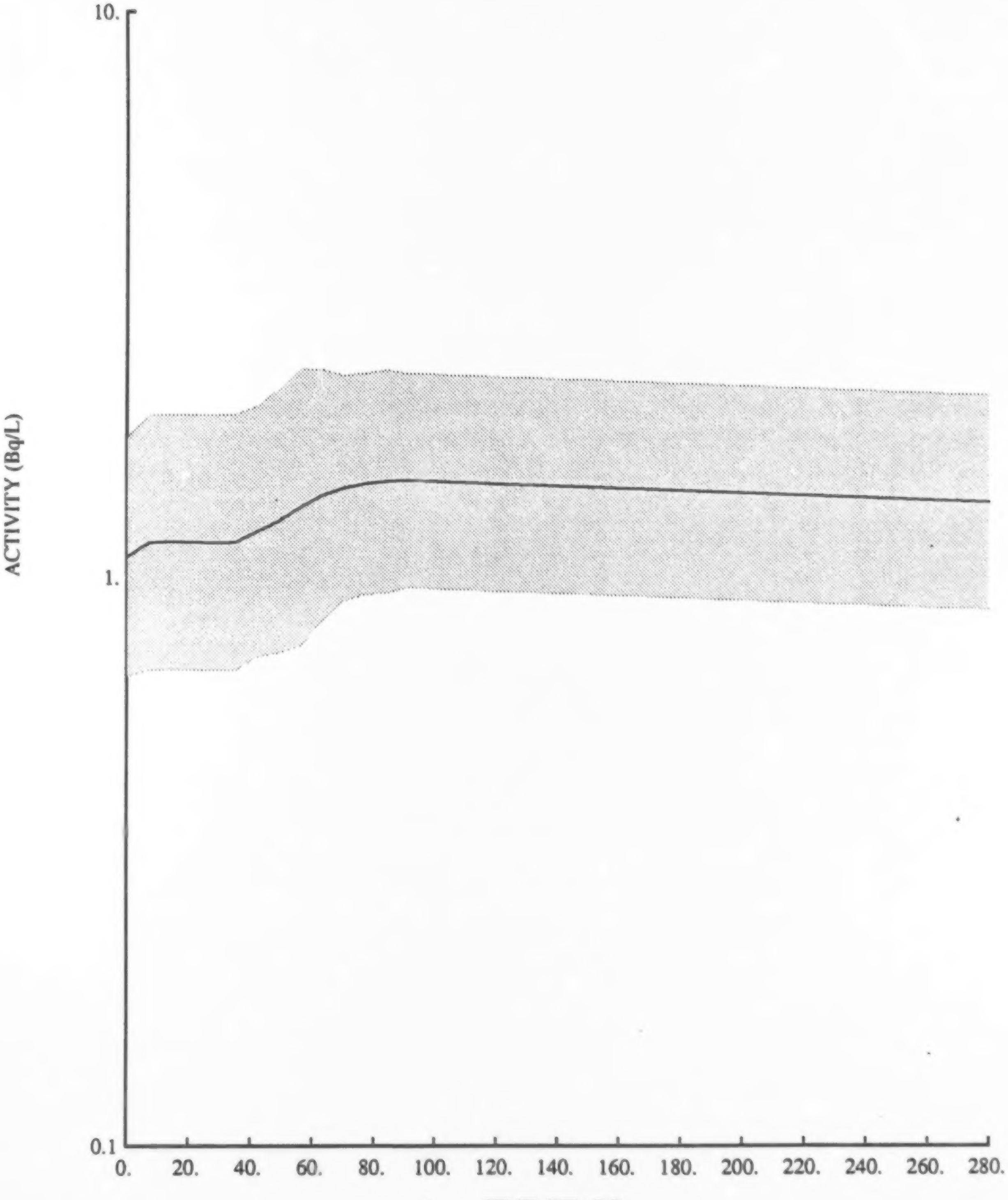

FIGURE 8.5d: Pb-210 ACTIVITY IN PORE WATER FOR SCENARIO 1, GEOMETRIC MEAN OF 100 TRIALS

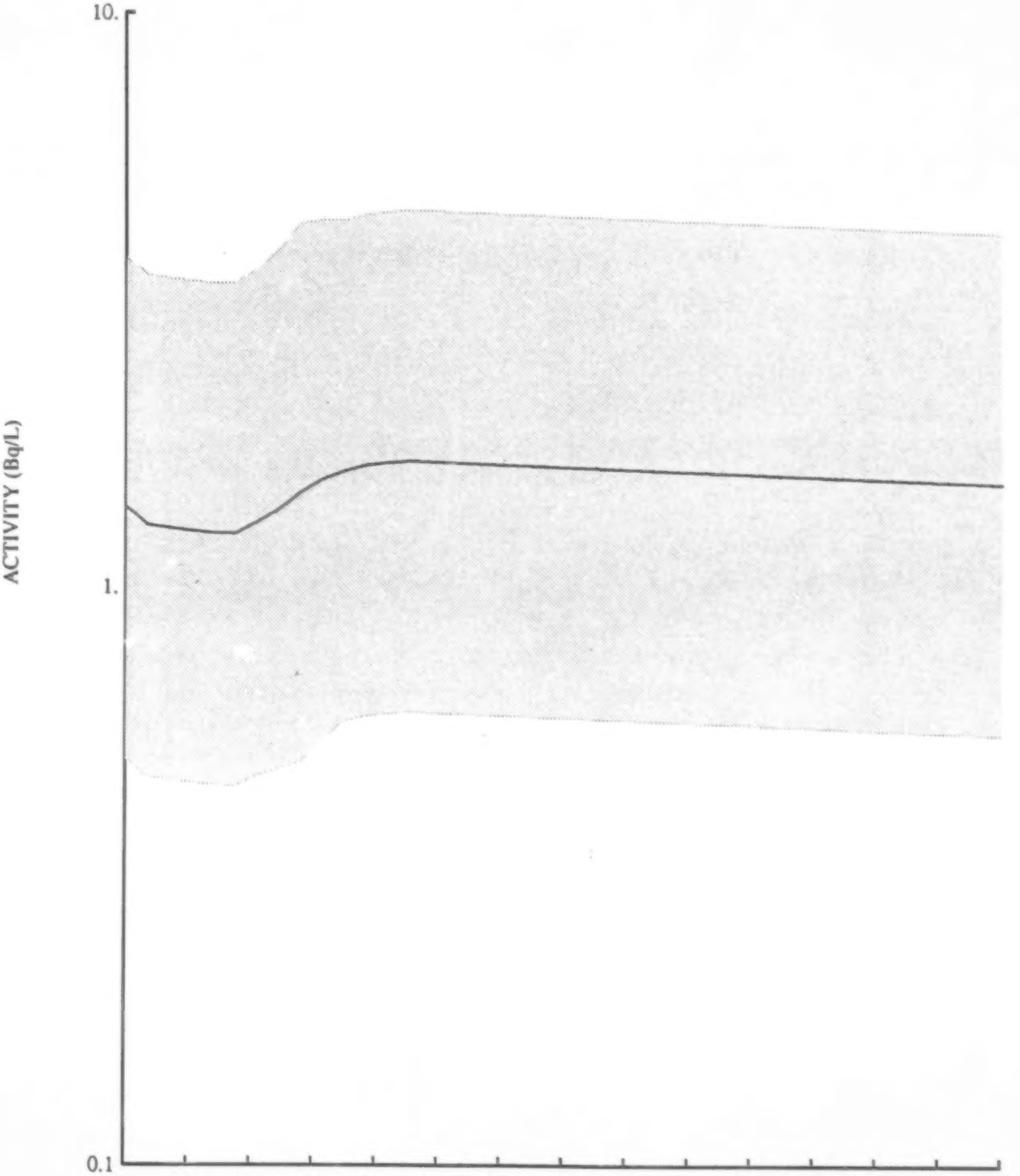

marginally higher than that of Ra-226 because the solid-solution calibration (i.e., the selection of values for distribution coefficients) results in slightly more Pb-210 in solution than for Ra-226.

With respect to comparing the model's predictions with field observations, the present calibration may not result in enough Th-230, Ra-226 and Pb-210 in solution if field observations consistently prove to be closer to 10 Bq/L over the long term. The present calibration for Ra-226 (i.e., the values of the distribution coefficients derived by Langmuir and Riese, 1985) is judged to be reasonable in a relative sense because it is based upon thermodynamic data. But these data require further laboratory testing. The calibration of coefficient values for Pb-210 incorporation into $BaSO_4$ also require further evaluation. The calibration for Th-230 and the model for its control requires substantially more evaluation.

8.2 Reviewing Lake Characteritics

The concentration of uranium and activity of Th-230, Ra-226 and Pb-210 are given respectively in Figures 8.6a-d for the first receiving lake, and in Figures 8.7a-d for the second receiving lake (i.e., the embayment). The trend of concentration calculated in all cases follows that of the source term. The differences in concentration between the first lake and the embayment are caused mainly by exchange between the large lake and the embayment. The concentration calculated for the embayment is low because the simplified model does not consider that material builds up in the lake. The significance of this error is dependent upon the size of the lake. It results from simplifying the lake model to the two-equation format. It can readily be modelled in future work by using four differential equations (see Section 5.4).

For both lakes, some loss occurs to the sediments but the main differences are caused by dilution of the pore water concentration. Further work should centre upon refining the calibration used to describe sediment water transfer parameters.

FIGURE 3.6a: URANIUM CONC. IN FIRST LAKE FOR SCENARIO 1, GEOMETRIC MEAN OF 100 TRIALS

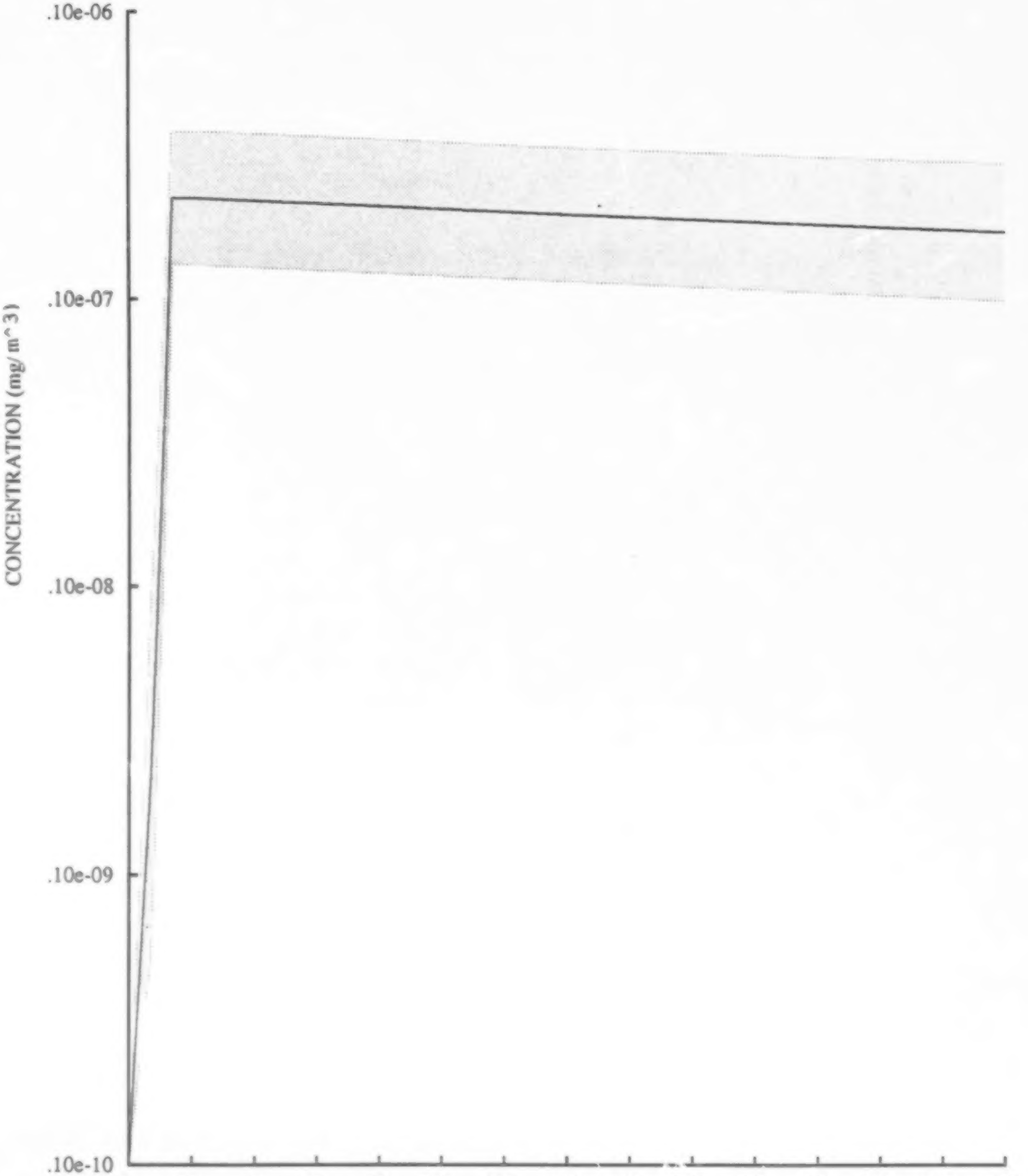

FIGURE 8.6b: Th-230 ACTIVITY IN FIRST LAKE
FOR SCENARIO 1,
GEOMETRIC MEAN OF 100 TRIALS

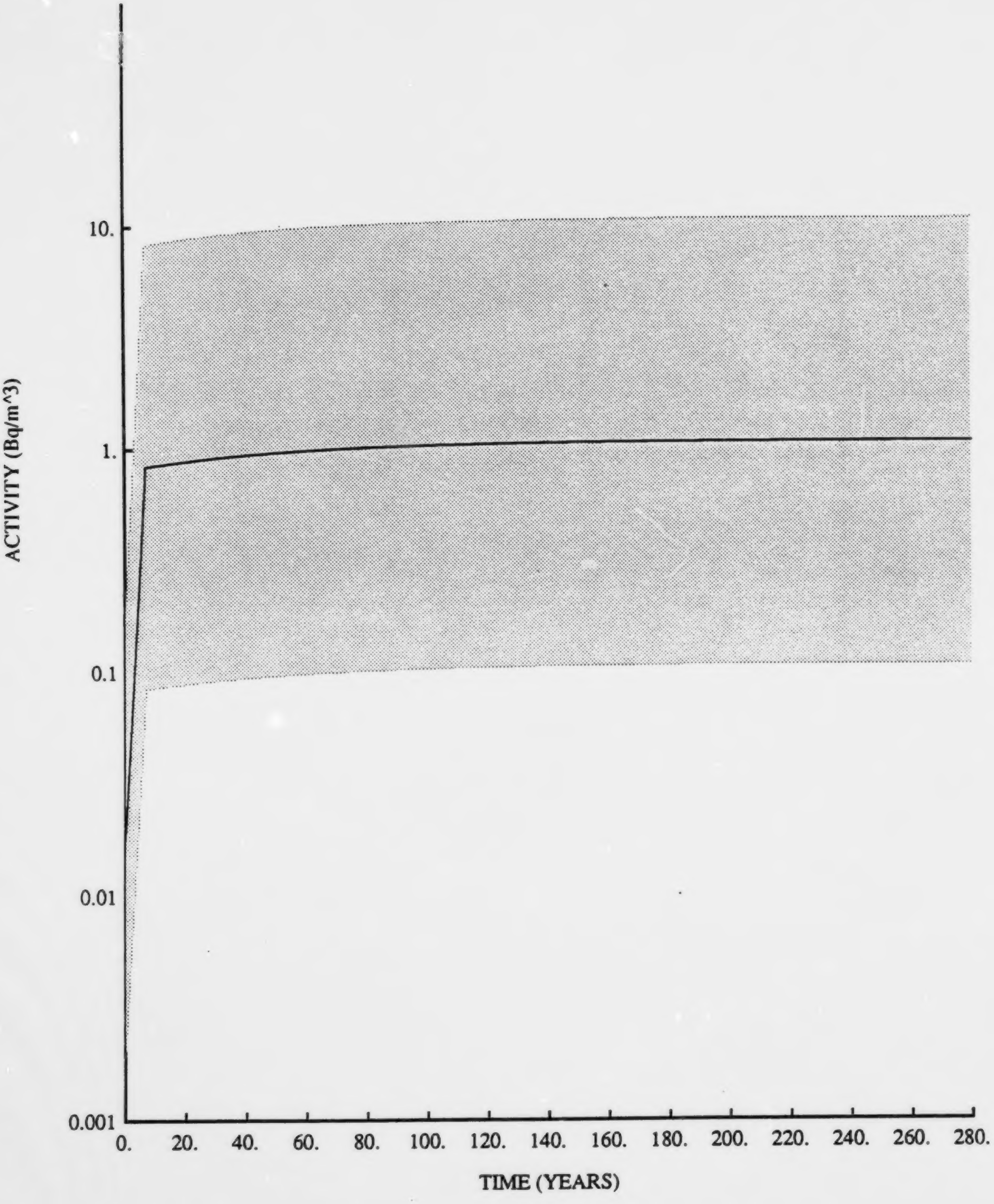

FIGURE 8.6c: Ra-226 ACTIVITY (Bq/m^3) in FIRST LAKE
FOR SCENARIO 1,
GEOMETRIC MEAN OF 100 TRIALS

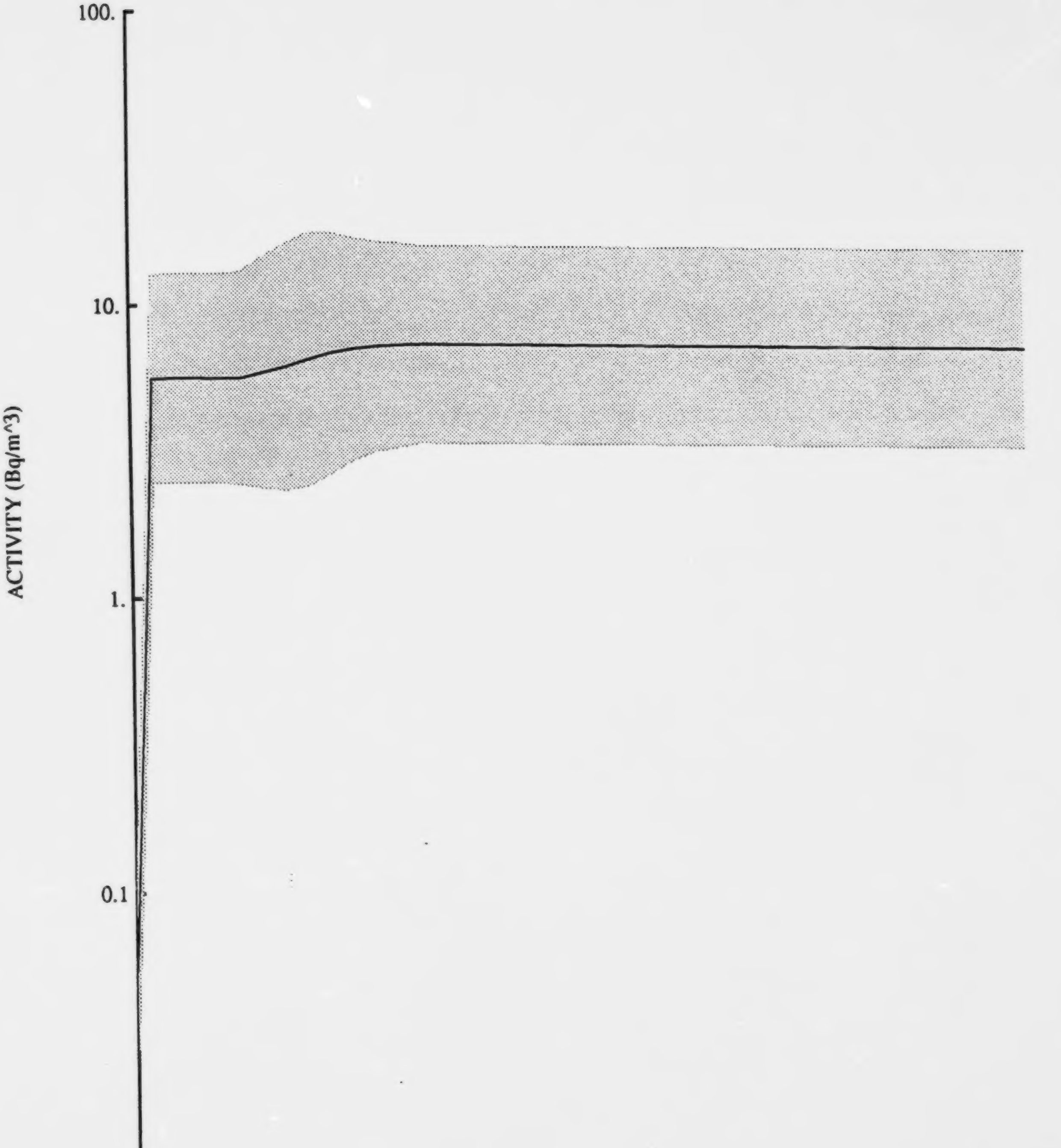

FIGURE 8.6d: Pb-210 ACTIVITY IN FIRST LAKE FOR SCENARIO 1, GEOMETRIC MEAN OF 100 TRIALS

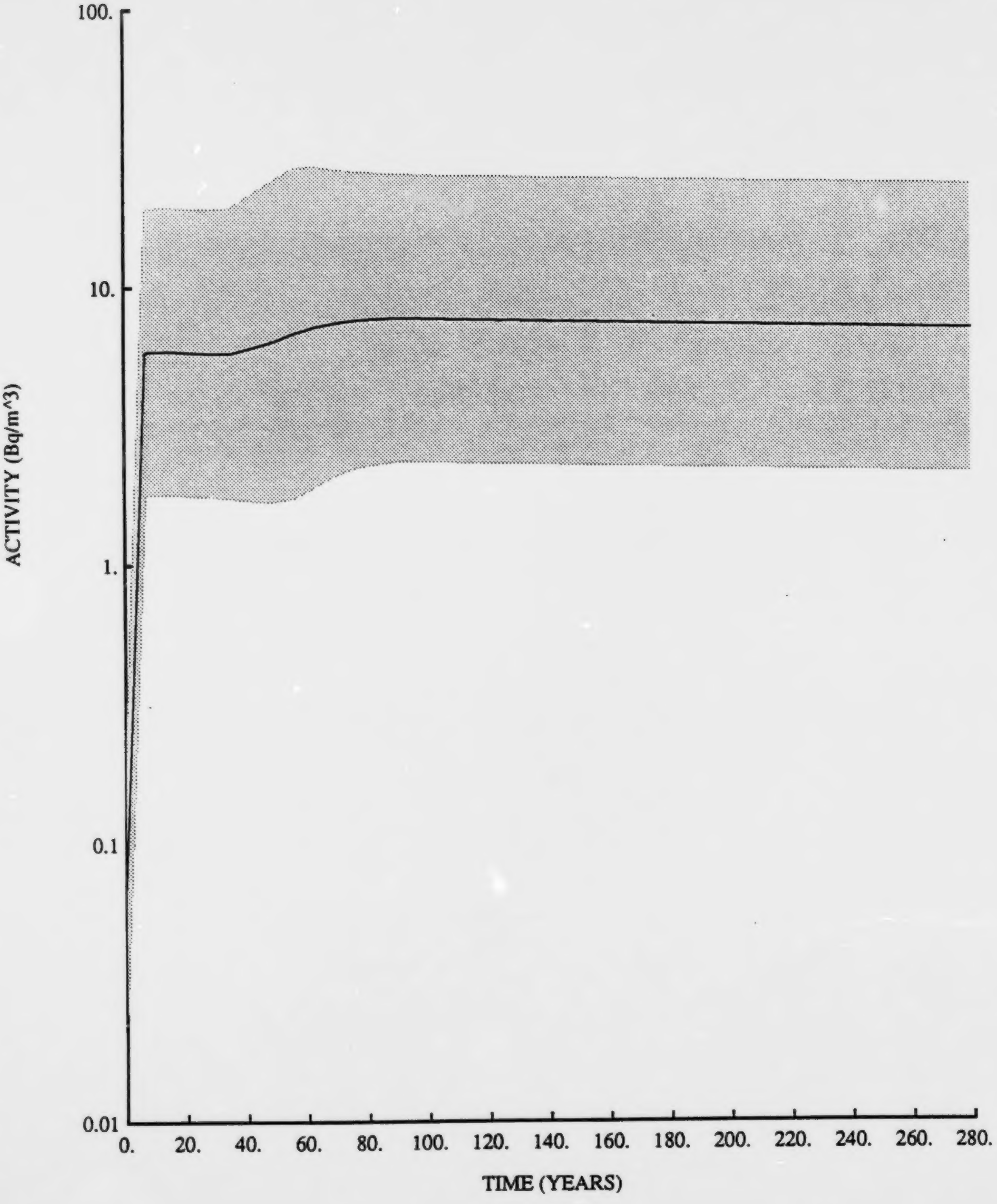

FIGURE 8.7a: URANIUM CONC. IN SECOND LAKE FOR SCENARIO 1, GEOMETRIC MEAN OF 100 TRIALS

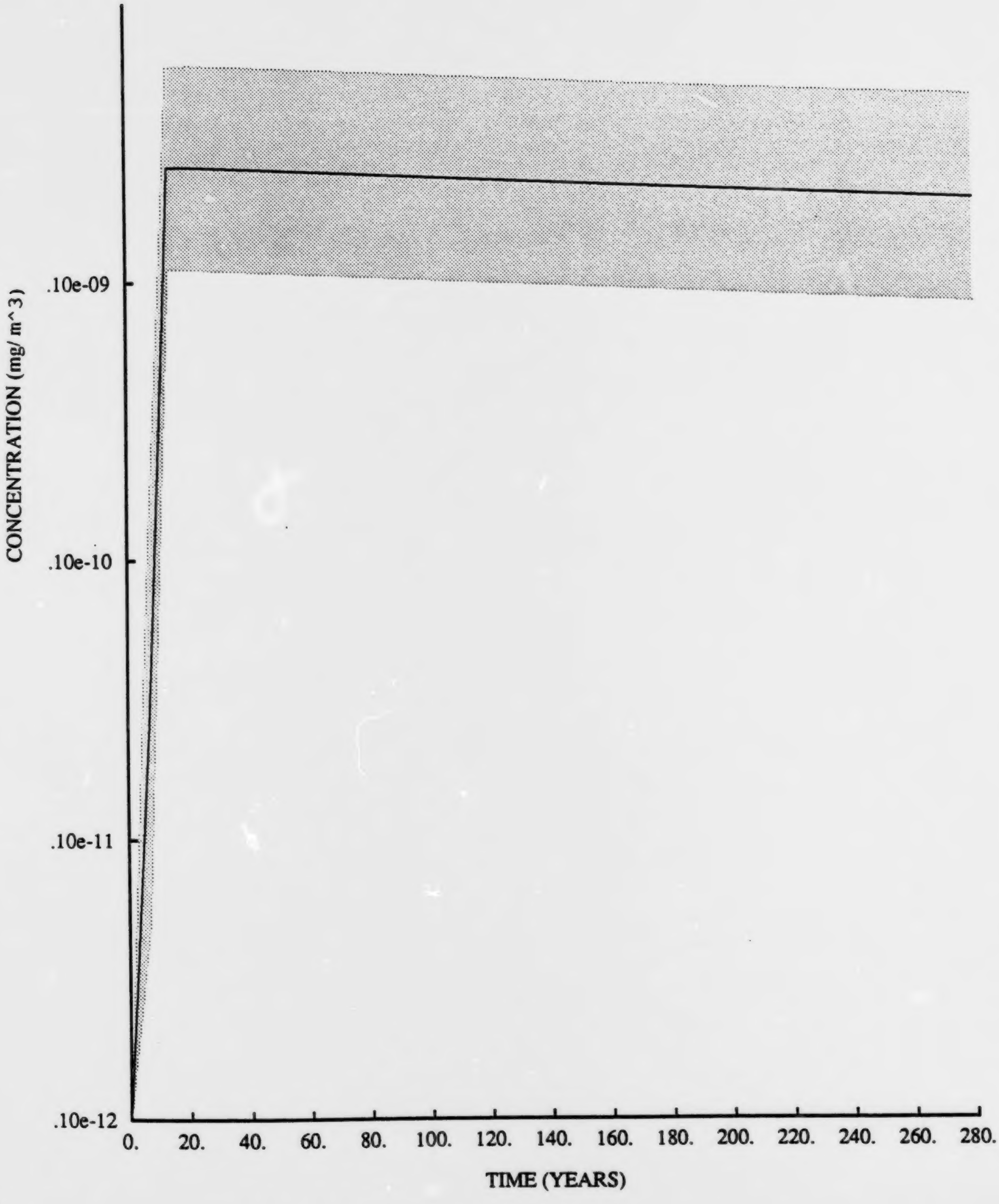

FIGURE 8.7b: Th-230 ACTIVITY IN SECOND LAKE FOR SCENARIO 1, GEOMETRIC MEAN OF 100 TRIALS

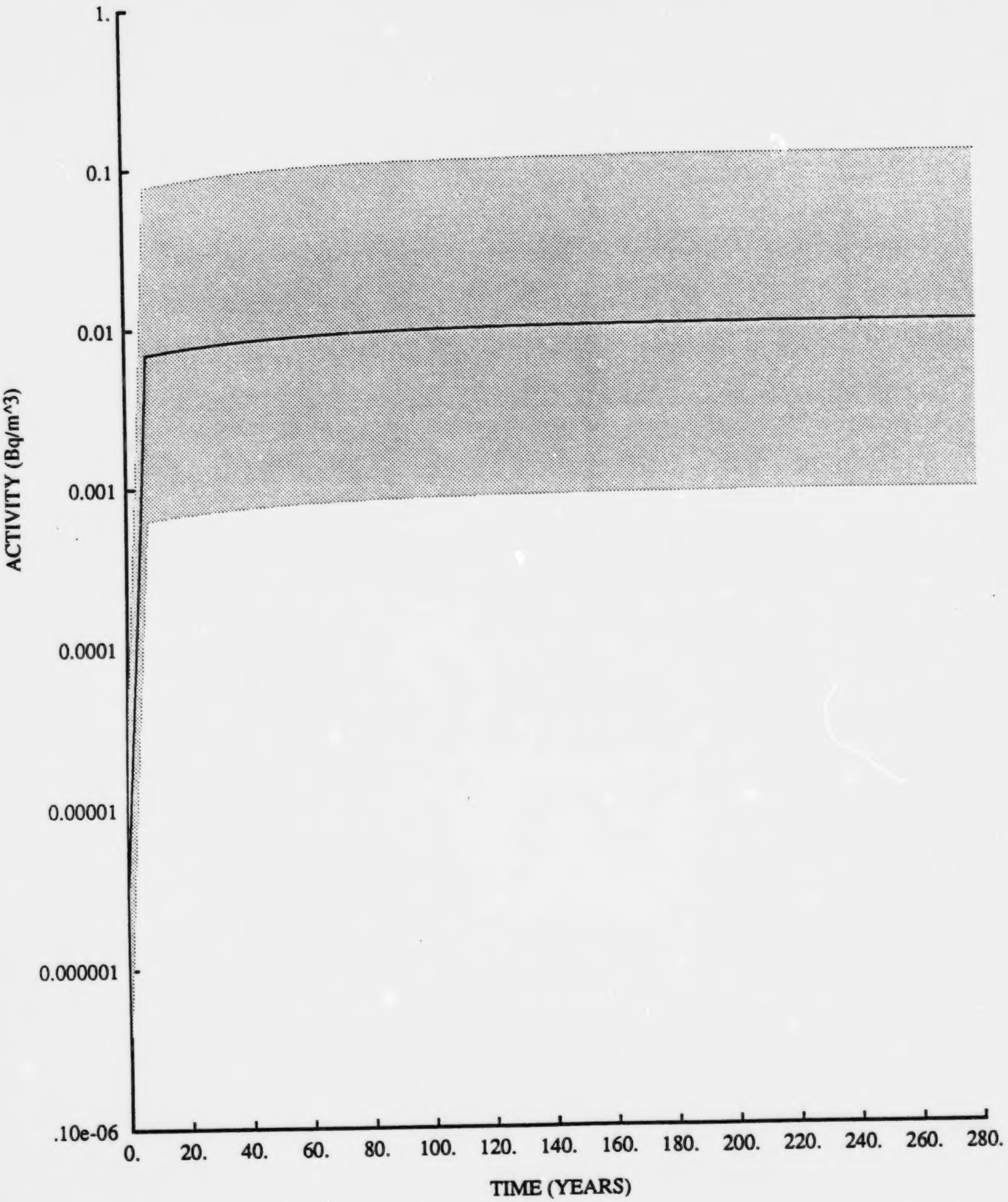

FIGURE 8.7c: Ra-226 ACTIVITY IN SECOND LAKE FOR SCENARIO 1, GEOMETRIC MEAN OF 100 TRIALS

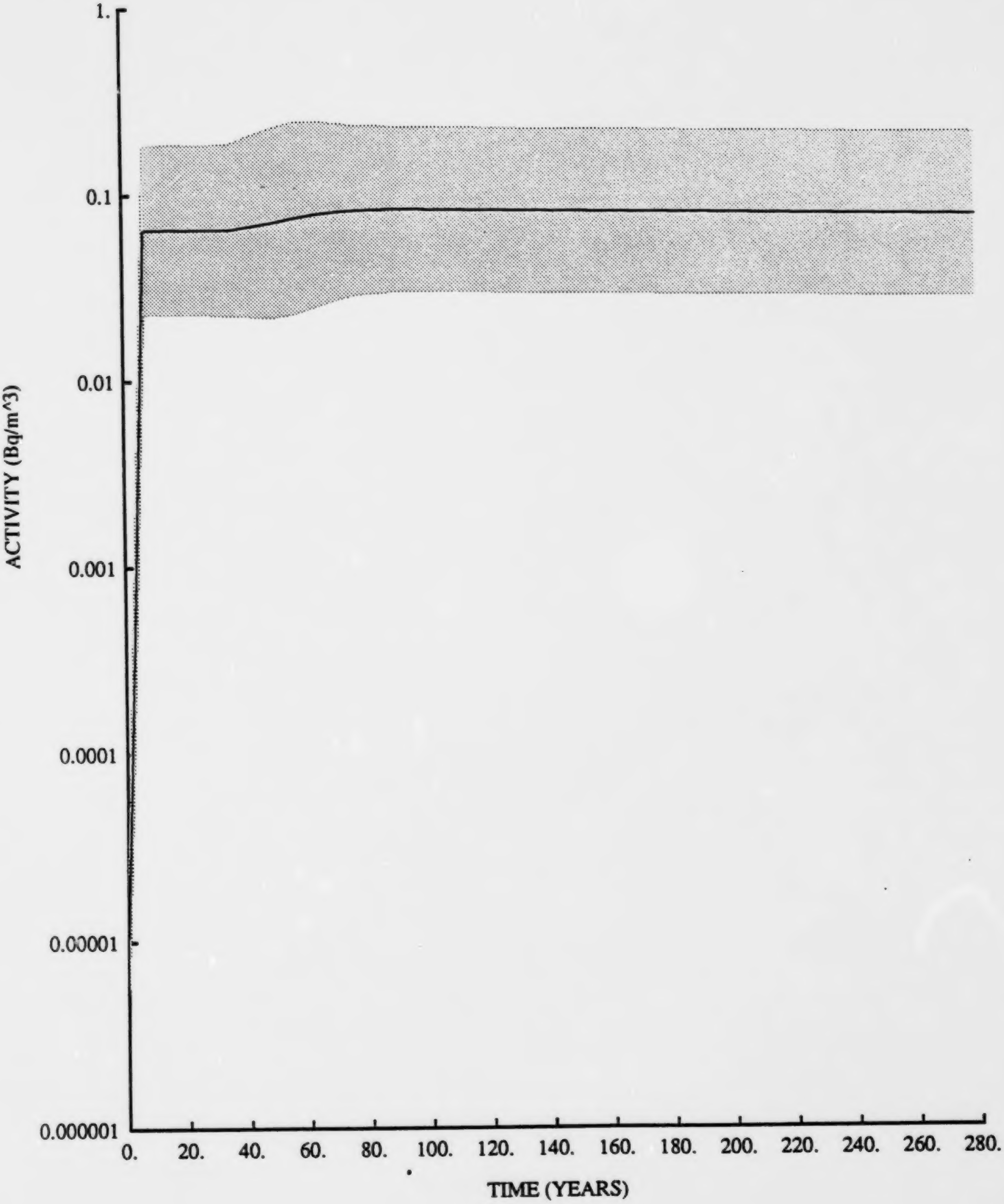

FIGURE 8.7d: Pb-210 ACTIVITY IN SECOND LAKE FOR SCENARIO 1, GEOMETRIC MEAN OF 100 TRIALS

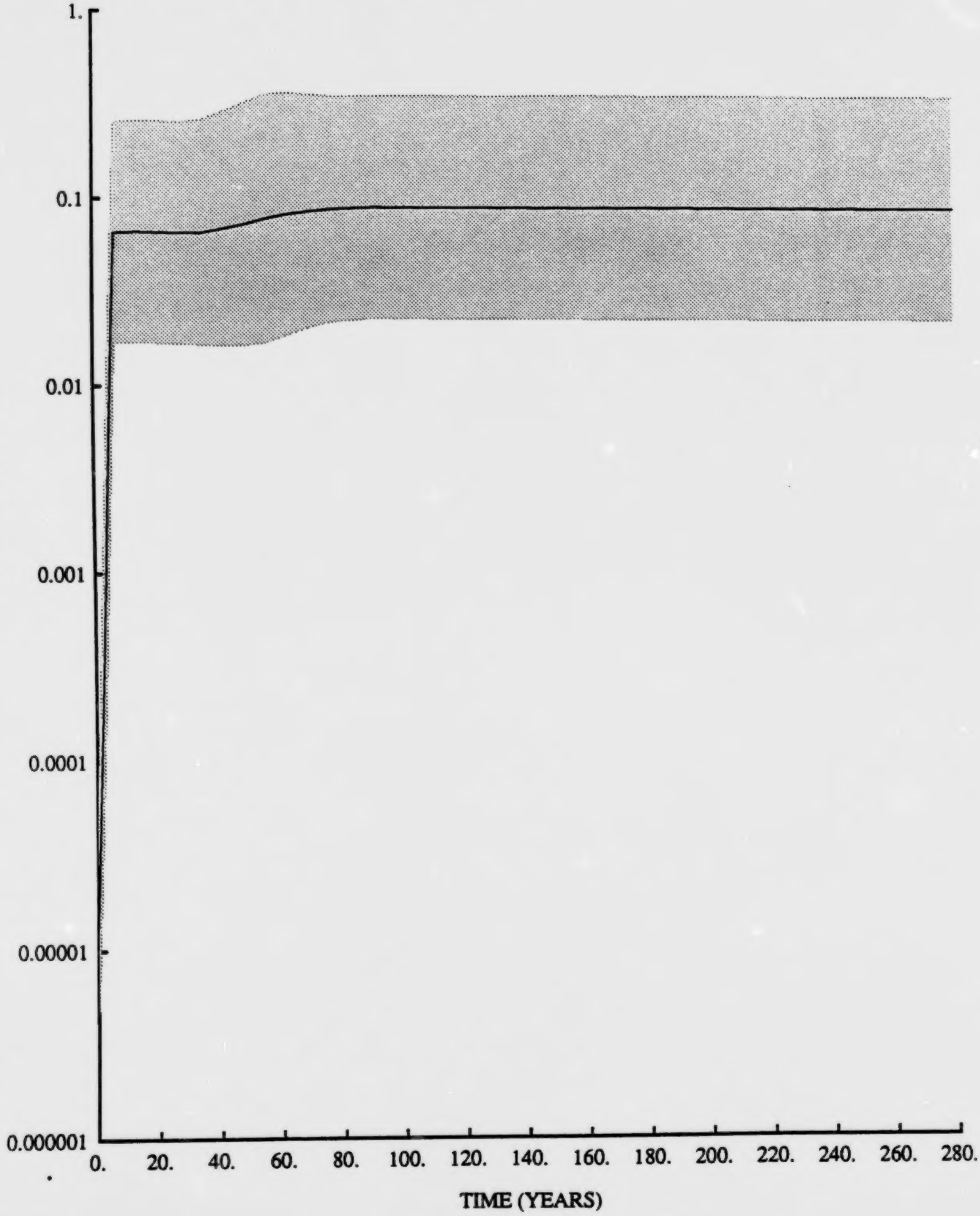

9.0 SUMMARY AND RECOMMENDATIONS

A model and computer code (UTAP) were developed previously to carry out a probabilistic assessment of uranium mill tailings (SENES, 1985). The hypothetical, reference site selected for their tailings was pyrite-rich, characteristic of the Elliot Lake mining district, and had substantial acid generation potential.

Using this model as a base, the objectives of this present study were:

- to develop reference site conditions, of a non-pyritic uranium mill tailings rich in arsenic and nickel, including the source-term (tailings) description, the pathways and receptor components;
- to modify the system model according to the conditions developed above;
- to apply the modified model; and
- to document the model and results.

This present study has emphasized the following:

- model demonstration;
- adaption of UTAP to the non-pyritic ore type;
- sufficient detail on pathways to allow calculation of fluxes of contaminants from the tailings;
- a new source term model;
- coding of these aspects into the UTAP systems code;
- the incorporation of quality assurance of code testing;
- the coding of flexibility in the source-term to accommodate such requirements as wide ranging management options and future code modifications;
- the documentation of all aspects of the study.

The results give time trends of dose rate to a critical group and concentration of radionuclides and arsenic and nickel in various environmental media.

The results suggest priorities for future studies and model development including:

- theoretical evaluation of a model for Th-230 in the source term requires information upon the role of Th-232 in the tailings and data for calibrating the distribution coefficient for Th-230 during its coprecipitation with goethite, manganese dioxide, barium sulphate and gypsum. This work modelled Th-230 dissolution using the coprecipitation model, but it is possible that Th-230 dissolution may be controlled by the solubility product of Th-232 if sufficient Th-232 dissolves in the mill;
- further evaluation of modelling Rn-222 emanation from the tailings. This evaluation is suggested because Rn-222 emanation is one of the most important pathways, but the model was not significantly evaluated in this project;
- evaluation of the Th-230 transfer coefficient from water and air via various pathways to man; and
- testing the calibration used in this work to determine the relative importance of atmosphere and aquatic pathways to the dose impact upon members of the critical group.

10.0 REFERENCES

Abo-Rady, M.D.K. 1980. Aquatic macrophytes as indicator for heavy metal pollution in the River Leine (West Germany). Arch. Hydrobiol. 89: 387-404.

Anastasi, F.B. and W.J. Kender. 1973. The influence of soil arsenic on the growth of lowbush blueberry. J. Environ. Qual. 2(3): 335-337.

Baes, C.F., and R.E. Mesmer. 1976. The Hydrolysis of Cations. Wiley. 489pp.

Baker, R.S., W.L. Barrentine, D.H. Bowman, W.L. Hawthorne and J.V. Pettiet. 1976. Crop response and arsenic uptake following soil incorporation of MSMA. Weed Sci. 24(3): 322-326.

Banfield, A.F.W. 1974. The Mammals of Canada. University of Toronto Press, Toronto.

Beak Consultants Limited. 1985a. Benthological, chemical, radiological and chronological evaluation of sediments in Port Hope Harbour, Ontario. A report to the Environmental Protection Service, Ontario Region.

Beak Consultants Limited. 1985b. An environmental evaluation of the effects of the Eldor Mines Rabbit Lake operations on Wollaston Lake. A report to the Saskatchewan Department of Environment.

Beak Consultants Limited. 1985c. A survey of the benthos and sediments of Quirke Lake, Ontario. A report to the Ontario Ministry of the Environment, Northeastern Region.

Beak Consultants Limited. 1985d. Benthological, chemical, radiological and chronological evaluation of sediments in Port Hope Harbour, Ontario. A report to the Environmental Protection Service, Ontario Region.

Beak Consultants Limited. 1985e. Study to assess the distribution of radionuclides in the aquatic ecosystem in the vicinity of the Serpent River mouth. A report to the Environmental Protection Service, Ontario Region.

Beak Consultants Limited. 1985f. Derivation of release limits for a typical uranium mining and milling facility. AECB Research Report No. INFO-0165.

Beak Consultants Limited. 1986. Gunnar field study. Research Report prepared for the National Uranium Tailings Program, CANMET, EMR, under Supply and Services Canada Contract No. 55SQ.2341-4-1674X.

Belovsky, G.E., P.A. Jordan and D.V. Botkin. 1975. Proceedings of an International Symposium on Moose Ecology, Quebec City, March 1973. Laval University Press, Quebec City.

Blaylock, B.G. 1982. Radionuclide data bases available for bioaccumulation factors for freshwater biota. Nucl. Safety 23: 427-438.

Blaylock, B.G. and M.L. Frank. 1979. A comparison of the toxicity of nickel to the developing eggs and larvae of carp (Cyprinus carpio). Bull. Environ. Contam. Toxicol. 21: 604-611.

Burk, R.C. and P.R. Wiles. 1983. Coprecipitation of Th-234 with $BaSO_4$. J. Radioanal. Chem, 79(2), 185-196.

Calvert, C.C. 1975. Arsenicals in animal feeds and wastes. In: Arsenical Pesticides. E.A. Woolston (Ed.). American Chemical Society Symposium Series 7, Washington, D.C., pp. 70-79.

Canadian Standards Association (CSA). 1984. CSA Standard N288.1. Guidelines for calculating derived release limits for radioactive material in airborne and liquid effluents for normal operation of nuclear facilities (draft).

Cassaday, V.J. 1985. The data base available to develop parameter distributions for use in modelling the transfer of airborne radioactivity to terrestrial vegetation. App. I. In: SENES Consultants Ltd. Probabilistic model development for the assessment of long-term effects of uranium mill tailings in Canada - Phase II. A report for the National Uranium Tailings Program. DSS Contract No. 0SQ84-00207.

Chapman, W.H., H.L. Fisher and M.W. Pratt. 1968. Concentration factors of chemical elements in edible aquatic organisms. Lawrence Radiation Laboratory, Livermore, California. UCRL-50564.

Chapra, S.C. and K. Recknow. 1983. Engineering Approaches for Lake Management. Ann Arbor Science.

Chepil, W.S. 1958. Soil conditions that influence wind erosion. U.S. Department of Agriculture, Agricultural Research Service and Kansas Agricultural Experiment Station, Washington, D.C. Technical Bulletin No. 1185.

Cohen, B.L. 1985. Transport of element from soil to human diet: and alternative approach to pathway analysis. Health Phys. 49: 239-245.

Copeland, R.A., R.H. Beethe and W.W. Prater. 1973. Trace element distributions in Lake Michigan fish: a baseline study with calculations of concentration factors and equilibrium radioisotope distributions. ERG Special Report No. 2, 139 p.

Cornett, J. 1986. Speciation of nickel-arsenic in Moiya Lake Sediments. NUTP Report.

Cowgill, U.M. 1974. The hydrogeochemistry of Linsley Pond, North Branford, Connecticut. I. The chemical composition of the aquatic macrophytes. Arch. Hydrobiol./Suppl. 45: 1-119.

Cowherd, C., Jr., K. Axetell, Jr., C.M. Guentner and G.A. Jutze. 1974. Development of emission factors for fugitive dust sources. Office of Air Quality, Planning and Standards, Research Triangle Park, U.S. Environmental Protection Agency. Available from NTIS, Report No. PB-238 262/OSL.

Cowherd, C. and R.V. Hendricks. 1978. Development of fugitive dust emission factors for industrial sources. Paper 78-55.4 presented at the 71st Annual Meeting of the Air Pollution Control Association, Houston, Texas.

Craig, D.G. and J.W. Turelle. 1964. Guide for wind erosion control on cropland in the great plains states. U.S. Department of Agriculture, Soil Conservation Service.

Crichton, V.F.J. 1980. Manitoba's second experimental moose hunt on Hella Island. Manitoba Department of Natural Resources, 37 pp.

Diem, K. and C. Lentner. 1970. Scientific Tables. 7th Ed. J.R. Geigy, Basle, Switzerland.

Dietz, F. 1973. The enrichment of heavy metals in submerged plants. Adv. Water Pollut. Res., Proc. Int., Conf., 6th, pp. 53-62.

DiToro, D.M. and L.M. Horzempa. 1982. Reversible and Resistant Components of PCB Adsorption-Desorption: Isotherms. Envir. Sci. Technol., 16, pp. 594-602.

Dixon, D.G. and J.B. Sprague. 1981. Acclimation-induced changes in toxicity of arsenic and cyanide to rainbow trout, Salmo gairdneri Richardson. J. Fish. Biol. 18: 579-589.

Dreesen, D.R., J.M. Williams, M.L. Marple, E.S. Gladney and D.R. Perrin. 1982. Mobility and bioavailability of uranium mill tailings contaminants. Environ. Sci. Technol. 16: 702-709.

Dvorak, A.J. and B.G. Lewis. 1978. Impacts of coal-fired power plants on fish, wildlife and their habitats. Fish and Wildlife Service, U.S. Department of the Interior. FWS/OBS-78/29.

EPS. 1978. A study of water pollution in the vicinity of the Eldorado Nuclear Limited Beaverlodge operation 1976 and 1977. Surveillance Report EPS 5-NW-78-10. Northwest Region, Environmental Protection Service, Fisheries and Environment Canada (Ruggles and Rawley, 1978).

EPS. 1981. A study of water pollution in the vicinity of two abandoned uranium mills in northern Saskatchewan, 1978. Report EPS-WNR-5-81-2. Western and Northern Region, Environmental Protection Service, Environment Canada.

Euler, D. 1979. Vegetation management for wildlife in Ontario. Ontario Ministry of Natural Resources, Toronto.

Falk, M.R., M.D. Miller and S.J.M. Kostiuk. 1973. Data supplement to: Biological effects of mining wastes in the Northwest Territories. Environment Canada, Fish. Mar. Serv. Data Report Series No. CEN/D-73-1, 54 p.

Fitchko, J. 1978. The distribution, mobility and accumulation of nickel, copper and zinc in a river system draining the eastern part of the metal-polluted Sudbury smelting area. Ph.D. Thesis, University of Toronto, 209 p.

Fitchko, J. 1986. Definition of mercury and heavy metals in sediments in unnamed drain, former Magnetic Materials Plant, Edmore Michigan. Beak Consultants Limited Report for General Electric, Fairfield, Connecticut.

Garner, R.J. 1972. Transfer of Radioactive Materials from the Terrestrial Environment to Animals and Man. CRC Press, The Chemical Rubber Company.

Garner, R.H., B.G. Blaylock and F.O. Hoffman. 1985. A dynamic model of radium-226 in an oligotrophic lake. App. G. In: SENES Consultants Ltd. Probabilistic model development for the assessment of long-term effects of uranium mill tailings in Canada - Phase II. A report for the National Uranium Tailings Program. DSS Contract No. 0SQ84-00207.

Garrels, R.M. and C.L. Christ. 1965. Solutions, Minerals and Equilibria. Freeman, Cooper and Company, San Francisco.

Gilderhus, P.A. 1966. Some effects of sublethal concentrations of sodium arsenite on bluegills and the aquatic environment. Trans. Amer. Fish. Soc. 95: 289-296.

Gordon, L. and K. Rowley. 1957. Analyt. Chemist., pp. 34-37.

Gordon, L., M.L. Satutsky and H.H. Willard. 1959. Precipitation from Homogeneous Solution, Wiley.

Halbert, B.E., D. Stone and V.J. Cassaday. 1985. The data base available for estimating radium-226 bioaccumulation in fish flesh. App. H. In: SENES Consultants Ltd. Probabilistic model development for the assessment of long-term effects of uranium mill tailings in Canada - Phase II. A report for the National Uranium Tailings Program. DSS Contract No. 0SQ84-00207.

Halstead, R.L., B.J. Finn and A.J. MacLean. 1969. Extractability of nickel added to soils and its concentration in plants. Can. J. Soil Sci. 49: 335-342.

Harms, V.L. and W.P. Fraser Herbarium. 1982. A plant taxonomic survey of the Uranium City region, Lake Athabasca north shore. Emphasizing the naturally colonizing plants of uranium mine and mill wastes and other human-disturbed sites. TWPFH Report 82-1 to the Saskatchewan Department of Environment.

Harvey, H.H. 1979. The acid deposition problem and emerging research needs in the toxicology of fishes. Proc. 5th Annual Aquatic Toxicity Workshop, Hamilton, Ontario, 7-9 November 1978. Fish. Mar. Serv. Tech. Rep. 862: 115-128.

Health and Welfare Canada (HWC). 1980. Guidelines for Canadian drinking water quality 1978. Supporting Documentation. Minister of Supply and Services, Ottawa.

Hoffman, F.O., R.H. Garner and B.G. Blaylock. 1985. The transfer of radium from the atmosphere to terrestrial vegetation. App. J. In: SENES Consultants Ltd. Probabilistic model development for the assessment of long-term effects of uranium mill tailings in Canada - Phase II. A report for the National Uranium Tailings Program. DSS Contract No. 0SQ84-00207.

Hosker, R.P., Jr. 1974. Estimates of dry deposition and plume depletion over forests and grassland. In: Proceedings of IAEA Symposium, Physical Behaviour of RadioacW.P. Fraser Herbarium. 1982. A plant taxonomic survey of the Uranium City region, Lake Athabasca north shore. Emphasizing the naturally colonizing plants of uranium mine and mill wastes and other human-disturbed sites. TWPFH Report 82-1 to the Saskatchewan Department of Environment.

Harvey, H.H. 1979. The acid deposition problem and emerging research needs in the toxicology of fishes. Proc. 5th Annual Aquatic Toxicity Workshop, Hamilton, Ontario, 7-9 November 1978. Fish. Mar. Serv. Tech. Rep. 862: 115-128.

Health and Welfare Canada (HWC). 1980. Guidelines for Canadian drinking water quality 1978. Supporting Documentation. Minister of Supply and Services, Ottawa.

Hoffman, F.O., R.H. Garner and B.G. Blaylock. 1985. The transfer of radium from the atmosphere to terrestrial vegetation. App. J. In: SENES Consultants Ltd. Probabilistic model development for the assessment of long-term effects of uranium mill tailings in Canada - Phase II. A report for the National Uranium Tailings Program. DSS Contract No. 0SQ84-00207.

Hosker, R.P., Jr. 1974. Estimates of dry deposition and plume depletion over forests and grassland. In: Proceedings of IAEA Symposium, Physical Behaviour of Radioactive Contaminants in the Atmosphere. Vienna, November 1973. Internat. At. Energy Ag., Vienna.

Hutchinson, G.E. 1975. A Treatise on Limnology. Volume III. Limnological Botany. John Wiley & Sons, 660 p.

Hutchinson, T.C. and H. Czyrska. 1975. Heavy metal toxicity and synergism to floating aquatic weeds. Verh. Internat. Verein. Limnol. 19: 2102-2111.

Hutchinson, T.C., A. Fedorenko, J. Fitchko, A. Kuja, J. Van Loon and J. Lichwa. 1976. Movement and compartmentation of nickel and copper in an aquatic ecosystem. In: Environmental Biogeochemistry Volume 2. Metals Transfer and Ecological Mass Balances. Ed. J.O. Nriagu, Ann Arbor Science Publ. Inc., pp. 565-585.

IEC Beak Consultants Ltd. 1984. An assessment of the radiological impacts of uranium mining in northern Saskatchewan. A report for the Environmental Protection Service, Industrial Programs Branch, Environment Canada, Ottawa, Ontario.

International Commission on Radiological Protection (ICRP). 1975. Report of the Task Group on Reference Man. ICRP Publication 23, Pergamon Press.

International Commission on Radiological Protection (ICRP). 1979. Limits for Intakes of Radionuclide by Workers. ICRP Publication 30, Pergamon Press.

International Commission on Radiological Protection (ICRP). 1981. Limits for inhalation of radon daughters by workers. ICRP Publication 32, Annals of the ICRP, Vol. 6, No. 1.

John, R.D. and J.L. Dalton. 1985. Fish study for the National Uranium Tailings Program (NUTP). NUTP Report NUTP-IR-4.

Johnson, J.R. and D.W. Dunford. 1983. Dose conversion factors for intakes of selected radionuclides by infants and adults. Atomic Energy of Canada Limited Report AECL-7919. Chalk River Nuclear Laboratories, Chalk River, Ontario.

Jutze, G.A. and K. Axetell. 1976. Factors influencing emissions from fugitive dust sources. Presented at the Symposium on Fugitive Emissions, Measurement and Control, 17-19 May, Hartford, Conn. pp. 159-179.

Klapwijk, A. and W.J. Snodgrass. 1985. Model for lake-bay exchange. J. Great Lakes Res. 11: 43-52.

Knight and Piesold. 1985. "Monitoring of Layered Uranium Tailings - Phase 1". Report for NUTP. Energy, Mines and Resources, Ottawa, Canada.

Kowal, E. 1985. Saskatchewan Department of Parks and Renewable Resources, Wildlife Ecologist, personal communication.

Kremer, R. 1985. Analysis of mechanisms controlling pH in neutralized and fertilized lakes. Poster Session presented at the Conference on Acidification, Muskoka, Ontario.

Kulikov, N.V. 1973. Radioecology of freshwater plants and animals. In: Radioecology. M. Klechkovskii, G.G. Polikarpov and R.M. Aleksakhin (Eds.). John Wiley & Sons.

Lancaster, R.J., M.R. Coup and J.W. Hughes. 1971. Toxicity of arsenic present in lakeweed. N.Z. Vet. J. 19: 141-145.

Langmuir, D. 1978. Uranium solution - mineral equilibria at low temperatures with applications to sedimentary ore deposits. In: Uranium Deposits and their Minerology and Origin. Minerological Association of Canada. pp 17-55.

Langmuir, D. and J.S. Herman. 1980. "The Mobility of Thorium in Natural Waters at Low Temperatures". Geochem. Cosmochem. Acta., v. 44, p. 1753-1766.

Langmuir, D. and R.A. Riese. The Thermodynamic Properties of Radium. Geochem. et Cosmochem. Acta. 49(7), 1593-1601.

Letourneau, C. 1984. Migration des radionucleides des chaines de desintegration de l'uranium et du thorium dans les milieux aquatique et terrestre (draft report). Atomic Energy Control Board, Ottawa.

Liebig, G.F., Jr., G.R. Bradford and A.P. Vanselow. 1959. Effects of arsenic compounds on citrus plants in solution culture. Soil Sci. 80: 342-348.

Lloyd, L.E., B.E. McDonald and E.W. Crompton. 1978. Fundamentals of Nutrition. 2nd Edition. W.H. Freeman and Co., San Francisco.

Lush, D. and S. Swanson. 1981. Pathway analysis and transfer coefficients. pp. 108-144. In: Proceedings of Seminar on Comparative Ecotoxicity of Uranium Mining and Milling Emissions. Saskatchewan Research Council Report, A-751-10-D-81.

Mathis, B.J. and T.F. Cummings. 1973. Selected metals in sediments, water and biota in the Illinois River. J. Water Pollut. Control Fed. 45: 1573-1583.

Mattioli, T.A. and P.R. Wiles. 1985. The Comprecipitation of K^+ and Fe^{3+} with barium sulphate. Inorganic Chimica Acta, 103: 37-40.

McBee, G.G., P.R. Johnson and E.C. Holt. 1967. Arsenic residue studies on coastal bermudagrass. Weeds 15: 77-79.

McDowell-Boyer, L.M., A.P. Watson and C.C. Travis. 1980. A review of parameters describing terrestrial food chain transport of lead-210 and radium-226. Nuc. Safety 21: 486-495.

Miller, W.J. 1973. Dynamics of absorption rates, endogenous excretion, tissue turnover, and homeostatic control mechanisms of zinc, cadmium, manganese and nickel in ruminants. Federation Proceedings 32: 1915-1920.

Momeni, M.H., Y. Yuan and A.J. Zielan. 1979. The uranium dispersion and dosimetry (UDAD) code. NUREG/CR-0553, ANL/ES-72, Argonne National Laboratories. Report for the U.S. Nuclear Regulatory Commission, Washington, D.C.

NAS/NRC. 1971. Nutrient requirements of domestic animals - beef cattle. National Academy of Sciencies, Washington, D.C.

NRCC. 1978. Effects of arsenic in the Canadian environment. National Research Council of Canada, Associate Committee on Scientific Criteria for Environmental Quality. NRCC No. 15391.

NRCC. 1981a. Effects of nickel in the Canadian environment. National Research Council of Canada, Associate Committee on Scientific Criteria for Environmental Quality. NRCC No. 18568.

NRCC. 1981b. Acidification in the Canadian aquatic environment. Scientific criteria for assessing the effects of acidic deposition on aquatic ecosystems. National Research Council of Canada, Associate Committee on Scientific Criteria for Environmental Quality. NRCC No. 18475.

National Research Council of Canada. 1982. Effects of aerosols on atmospheric processes. Panel on Atmospheric Aerosols, Subcommittee on Air, NRCC Associate Committee on Scientific Criteria for Environmental Quality. Environmental Secretariat Report No. NRCC 18473.

Nielson, A.E. 1961. Homogeneous Nucleation in Barium Sulphate Precipitation. Acta Chem. Scand. 15, (2), 441-442.

Nielson, A.E. 1967. Nucleation in Aqueous Solution in Crystal Growth (H.S. Peiser Ed.). Pergamon Press, pp. 419-426.

Nielson, A.E. 1958. The Kinetics of Crystal Growth in Barium Sulphate Precipitation. Acta Chem. Scand. 12, 951-958.

Nielson, A.E. 1957. Nucleation in Barium Sulphate Precipitation. Acta Chem. Scand. II, 1512-1515.

NUREG. 1980. Final generic impact on uranium milling. NUREG-0706, Vol. 2, Appendix G-3. U.S. Nuclear Regulatory Commission, Washington, D.C.

Nutrition Canada. not dated. Food consumption patterns report. Prepared by the Department of National Health and Welfare.

O'Dell, G.D., W.J. Miller, S.L. Moore, W.A. King, J.C. Ellers and H. Jurecek. 1971. Effect of dietary nickel level on excretion and nickel content of tissues in male calves. Journal of Animal Science 32: 769-773.

O'Nions, R.K. and R. Powell. 1977. The thermodynamics of trace element distribution. In Thermodynamics in Geology (ed., D.G. Fraser). D. Reidel Pub. Co. Dordrecht-Holland, pp 349-636.

Ontario Ministry of the Environment. 1984. Water Management - Goals, Policies, Objectives and Implementation Procedures of the Ministry of the Environment. Ontario MOE publication.

Parkhurst, B.R., R.G. Elder, J.S. Meyer, D.A. Sanchez, R.W. Pennak and W.T. Waller. 1984. An environmental hazard evaluation of uranium in a Rocky Mouontain stream. Environ. Toxicol. Chem. 3: 113-124.

Peoples, S.A. 1964. Arsenic toxicity in cattle. Ann. New York Acad. Sci. 111: 644-649.

Persson, B.R. 1972. Lead-210, polonium-210 and stable lead in the food chain lichen, reindeer and man. In: Comparative Studies of Food and Environmental Contamination. IAEA Publication STI/PUB/348, International Atomic Energy Agency, Vienna.

Peterson, R.L. 1966. The Mammals of Eastern Canada. Oxford University Press, Toronto.

Petres, J., G. Dezelic and B. Tezak. 1966. "Monodisperse Sols. of Barium Sulphate 1. Preparation of Stable Sols." Croat. Chem. Acta 38, 277-282.

Petres, J. 1968. Monodisperse Sols. of Barium Sulphate II Morphological Characteristics, Aging and Dissolution of Particles. Croat. Chem. Acta 40, 213-225.

Petres, J. 1969. Monodisperse Sols. of Barium Sulphate III. Electron-Microscopic Study of Internal Structure of Particles. Croat. Chem. Acta 41, 183-186.

Porter, E.K. and P.J. Peterson. 1975. Arsenic accumulation by plants on mine waste (U.K.). Sci. Total Environ. 4: 365-371.

Ragaini, R.C., H.R. Ralston and N. Roberts. 1977. Environmental trace metal contamination in Kellogg, Idaho, near a lead smelting complex. Environ. Sci. Technol. 11: 773-781.

Ray, S.N. and W.J. White. 1979. Equisetum arvense - an aquatic vascular plant as a biological monitor for heavy metal pollution. Chemosphere 3: 125-128.

Rayno, D.R. 1983. Estimated dose to man from uranium milling via the beef/milk food chain pathway. The Science of the Total Environment 31: 219-241.

Reay, P.F. 1972. The accumulation of arsenic from arsenic-rich natural waters by aquatic plants. J. Appl. Ecol. 9: 557-565.

Riese, A.C. 1983. "Adsorption of Radium and Thorium onto Quartz and Kaolinite: A Comparison of Solution/Surface Equilibria Models." Ph.D. Thesis, Colorado School of Mines.

Rogers, J.H., Jr., D.S. Cherry and R.K. Guthrie. 1978. Cycling of elements in duckweed (Lemna perpusilla) in an ash settling basin and swamp drainage system. Water Res. 12: 765-770.

Rosehart, R.G. and J.Y. Lee. 1973. The effect of As_2O_3 on the growth of white spruce seedlings. Water Air Soil Pollut. 2(4): 439-443.

Schiefer, K. and D. Lush. 1984. Resource management study of toxic elements and sport fishes Pukaskwa National Park. Report on analytical results. Beak Consultants Limited Report for Parks Canada, Cornwall, Ontario.

Schroeder, H.A. 1965. J. Chronic Diseases 18: 217.

Schroeder, H.A., J.J. Balassa and I.H. Tipton. 1962. Abnormal trace elements in man - nickel. J. Chronic Diseases 15: 51-65.

SENES Consultants Ltd. 1984. A study to develop and demonstrate techniques for the probabilistic assessment of the long-term effects of uranium mill tailings in Canada - Phase 1. Research Report prepared for the National Uranium Tailings Program, CANMET, EMR, under Supply and Services Canada contract No. 0SQ83-00236.

SENES Consultants Ltd. 1985a. Probabilistic Model Development for the Assessment of the Long-term Effects of Uranium Mill Tailings in Canada - Phase II. Vol 1. Main Report. Research Report prepared for the National Uranium Tailings Program, CANMET, EMR, under Supply and Services Canada Contract No. 05Q84.00207.

SENES Consultants Ltd. 1985b. Probabilistic Model Development for the Assessment of the Long-term Effects of Uranium Mill Tailings in Canada. Phase II. Vol. 2. Topical Discussion Papers.

SENES Consulants Ltd. 1985c. Probabilistic Model Development for the Assessment of the Long-term Effects of Uranium Mill Tailings in Canada. Phase II. Vol. 3. Probabilistic Analyses User's Manual and Documentation.

SENES Consultants Ltd. 1986. Probabilistic Model Development for the Assessment of the Long-term Effcts of Uranium Mill Tailings in Canada. Phase III. (In press)

Sorenson, E.M.B. 1976. Toxicity and accumulation of arsenic in green sunfish, Lepomis cyanellus, exposed to arsenate in water. Bull. Environ. Contam. Toxicol. 15: 756-761.

Snodgrass, W.J. 1986. Modelling Radionuclide Transport Between Lake Water and Seidments in "Sediment-Water Interactions" (P.J. Sly edit). pp. 209-227.

Snodgrass, W.J. and E.O. Hileman. 1985. On the Geochemical Mechanism Controlling Ra-226 Dissolution in Uranium Mill Tailings. NUTP Report 23241-4-1678.

Steevens, D.R., L.M. Walsh and D.R. Keeney. 1972. Arsenic residues in soil and potatoes from Wisconsin potato fields - 1970. Pestic. Monit. J. 6(2): 89-90.

Stumm, W., and J.J. Morgan. 1981. Aquatic Chemistry. Wiley.

Swanson, S. 1982. Levels and effects of radionuclides in aquatic fauna of the Beaverlodge area (Saskatchewan). SRC Publ. No. C-806-5-E-82. Saskatchewan Research Council, Atomic Energy Control Board, Environment Canada, Saskatchewan Environment.

Swanson, S.M. 1983. Levels of ^{226}Ra, ^{210}Pb and ^{total}U in fish near a Saskatchewan uranium mine and mill. Health Physics 45: 67-80.

Taylor, P and V.J. Lopata. 1983. Stability and solubility relationships between some solids in the system $PbO-CO_2-H_2O$. Can J. Chem. 62: 396-401

Thomann, R.V. 1983.

Thomann, R.V. 1982. Verification of Water Quality Models. J. Envir. Eng. Div., ASCE, 108 (EES), p 923-940.

Thompson, S.E., C.A. Burton, D.J. Quinn and Y.C. Ng. 1972. Concentration factors of chemical elements in edible aquatic organisms. Rev. 1, Lawrence Radiat. Lab., U.S. AEC Rep. UCRL-50564.

Thornthwaite, C.W. 1931. The climates of North America according to a new classification. Geographical Review 21: 633-655.

Tones, P.I. 1982. Limnological and fisheries investigation of the flooded open pit at the Gunnar uranium mine. SRC Publ. No. C-805-10-E-82. Saskatchewan Research Council. 64 p.

Underwood, E.J. 1966. The Mineral Nutrition of Livestock. Central Press, Aberdeen.

Underwood, E.J. 1971. Trace Elements in Human and Animal Nutrition. 3rd Edition. Academic Press, New York.

UNSCEAR. 1982. United Nations Scientific Committee on the Effects of Atomic Radiation. Ionizing radiation: Sources and biological effects. United Nations.

U.S. Environmental Protection Agency. 1985. Ambient water quality criteria for arsenic - 1984. EPA 440/5-84-033.

U.S. Environmental Protection Agency. 1985. Ambient water quality criteria for lead - 1984. EPA 440/5-84-027.

United States Nuclear Regulatory Commission (U.S. NRC). 1977. Calculation of annual doses to man from routine releases of reactor effluents for the purpose of evaluating compliance with 10CFR Part 50, Appendix I. (Revision 1), Regulatory Guide 1-109.

United States Nuclear Regulatory Commission (U.S. NRC). 1982. Calculational models for estimating radiation doses to man from airborne radioactive materials resulting from uranium milling operations. Regulatory Guide No. 3.51. March 1982.

Van Hassel, J.H., J.J. Ney and D.L. Garling, Jr. 1980. Heavy metals in a stream ecosystem at sites near highways. Trans. Amer. Fish. Soc. 109: 636-643.

Ward, N.I., R.R. Brooks, E. Roberts and C.R. Boswell. 1977. Heavy metal pollution from automotive emissions and its effect on roadside soils and pasture species in New Zealand. Environ. Sci. Technol. 11: 917-920.

Whitby, L. 1974. The ecological consequences of airborne metallic contaminants from the Sudbury smelters. Ph.D. Thesis, University of Toronto, 262 p.

Wilkinson, R.E. and W.S. Handcastle. 1969. Plant and soil arsenic analyses. Weed Sci. 17(1): 536-537.

Williams, K.T. 1940. As distribution in soils and its presence in certain plants. U.S. Dept. Agric. Technol. Bull. 732: 1-20.

Wulf, W. and M. Shaw. 1973. Global variables considered harmful. ACM SIGPLAN Notes.

Yourdon, E. and L.L. Constantine. 1978. Structured Design: Fundamentals of a Discipline of Computer Program and Systems Design. Yourdon Press.

Zach, R. 1980. Transfer coefficients to terrestrial food products in equilibrium assessment models for nuclear installations. AECL-6449. Atomic Energy of Canada Ltd.

Zach, R., V.F.J. Crichton, J.M. Stewart and K.R. Mayoh. 1982. Early winter food habits of Manitoba moose as determined by three rumen analysis methods. Can. J. Zoology 60: 1300-1304.

Zach, R. and K.R. Mayoh. 1982. The transfer of fallout cesium-137 from browse to moose. Part I: Moose Food Habits. AECL-6832. Atomic Energy of Canada Ltd.

APPENDIX A

Source Term: Reaction Path Code Calculations

C-8206.195.10

REACTION PATH SIMULATIONS OF CONTAMINANT RELEASE FROM As/Ni RICH URANIUM TAILINGS

Frank Garisto*, Robert J. Lemire* and Nava C. Garisto**

* Research Chemistry Branch
** Fuel Waste Technology Branch

Whiteshell Nuclear Research Establishment
Pinawa, Manitoba ROE 1L0

1986 March

CONTENTS

Page

1. INTRODUCTION 1

2. REACTION PATH SIMULATIONS 2

2.1 TITRATION WITH O_2(AQ) 5
2.2 TITRATION WITH H_2(AQ) 19
2.3 TITRATION WITH CO_2(GAS) 29
2.4 TITRATION WITH H^+ 33
2.5 THE EFFECT OF IRON (III) 41
2.6 RADIUM RELEASE 42

3. DISCUSSION 44

4. CONCLUSIONS 47

APPENDIX: THE THERMODYNAMIC DATABASE 49

REFERENCES 51

1. INTRODUCTION

This report describes the results of a modelling study required for estimating the release of radionuclides and toxic contaminants from As/Ni rich uranium tailings. The work has been carried out for BEAK CONSULTANTS LIMITED during the period February to March, 1986. This study focuses on the geochemical controls of arsenic and nickel concentrations in the tailings. Radium concentrations are also discussed.

Section 2 describes the results of reaction path calculations of the system with the titrants $O_2(aq)$, $H_2(aq)$, $CO_2(g)$ and H^+. These calculations simulate the behaviour of the system in both the unsaturated and saturated zones. The concentrations of arsenic, nickel and radium in equilibrium with the mineral assemblage of the tailings are presented and interpreted. The effect of iron (III) is also described. The results (presented in Section 2) are discussed in Section 3 in terms of the thermodynamic data on which they are based. Section 4 summarizes the overall conclusions from the present study.

2. REACTION PATH SIMULATIONS

In this section we describe the thermodynamic reaction path calculations [1] that are used to model a chemical system containing both arsenic and nickel. In reaction path calculations, the chemical system of interest is titrated with a particular compound, e.g., $O_2(aq)$, $H_2(aq)$. That is, the equilibrium composition of the chemical system is studied as a function of the number of moles of titrant added to the system. The reaction coordinate, ξ, is used to specify the number of moles of titrant added to the system.

In thermodynamic reaction path calculations, equilibrium calculations determine the composition of the chemical system along the reaction coordinate. Therefore, the chemical system follows the path of minimum Gibbs energy and not the path determined by kinetics.

Various "titrants" were used (see Table 1) in our reaction path calculations: $O_2(aq)$, $H_2(aq)$, $CO_2(g)$ and $H^+(g)$.

However, in all cases, the titrant was added to the chemical system consisting of the compounds listed below:

Compound	Number of Moles
H_2O	55.0
$CaSO_4 \cdot 2H_2O$	1.5
$CaCO_3$	5.5×10^{-1}
$Ni(OH)_2(\beta)$	3.17×10^{-1}
$Ca_3(AsO_4)_2$	6.3×10^{-2}
NiS	1.7×10^{-2}
$NiAs$	6.65×10^{-3}
$BaSO_4$	2.1×10^{-3}
$RaSO_4$	1.2×10^{-8}

The solid mixture compsition provided by Beak Consultants Ltd. contained $Ca_{0.4}Mg_{0.6}CO_3$. Early in the calculations it was found that

TABLE 1

REACTION PATH CALCULATIONS FOR THE ARSENIC-NICKEL SYSTEM

Case Number	Figure Numbers	pH	Gas Phase	Titrant
1	1	12	---	$O_2(aq)$
2	2	10	---	$O_2(aq)$
3	3	10	CO_2/Inert Gas	$O_2(aq)$
4	4-6	8	---	$O_2(aq)$
5	7	6	---	$O_2(aq)$
6	8-11	floating	---	$O_2(aq)$
7	13	12	---	$H_2(aq)$
8	14-16	8	---	$H_2(aq)$
9	17-19	floating	CO_2/Inert Gas	$H_2(aq)$
10	20-22	floating	Inert Gas	$CO_2(g)$
11	23-25	---	Inert Gas	$H^+(g)$
12	26-29	---	O_2/Inert Gas	$H^+(g)$

inclusion of Mg^{2+}, magnesium arsenates and dolomite provided little information beyond that obtained if all $Ca_{0.4}Mg_{0.6}CO_3$ in the original standard solid waste was considered as $CaCO_3$ (on a mole for mole basis). This simpler procedure was followed for most of the calculations described below.

The sources of most of the chemical thermodynamic data have been noted in an earlier report [2]. Additional values were taken from the NBS compilation [3]. The Gibbs energy for NiAs was calculated from the $\Delta_f H^\circ$(NiAs) and S°(NiAs) as assessed by Kubaschewski and Alcock [4]. The thermodynamic data used in the present calculations are tabulated, for completeness, in an Appendix.

2.1 Titration with $O_2(aq)$

Case 1 (Figure 1)

At pH = 12, $Ca_3(AsO_4)_2 \cdot Ca(OH)_2$ is the stable arsenic solid. The arsenic concentration in solution is about 4×10^{-5} mol•kg^{-1} for all values of ξ.

$Ni(OH)_2(\beta)$ is the predominant nickel solid. Ni_3S_2 is also formed but it dissolves as ξ increases and disappears for $\xi \geq 0.05$ moles.

$[Ra^{2+}]$ varies from 4.9×10^{-10} to 3.8×10^{-10} mol•kg^{-1} as ξ increases.

Case 2 (Figure 2)

At pH = 10, $Ca_3(AsO_4)_2$ is the predominant arsenic solid. NiAs is also formed for $\xi < 0.05$ moles. NiAs is oxidized and disappears as ξ increases. The oxidation of NiAs results in formation of additional calcium arsenate and in an increase in arsenic concentration. The arsenic concentration in solution is greater at pH = 10 than at pH = 12.

At pH = 10, the sulphate concentration in solution is less than at pH = 12. This explains the increased solubility of $RaSO_4(s)$. $[Ra^{2+}]$ varies from 1.2×10^{-8} to 1.3×10^{-9} mol•kg^{-1} as ξ increases. The decrease in $[Ra^{2+}]$, as ξ increases, is indirectly linked to the increase in arsenic concentration: (i) the increase in arsenic concentration causes a decrease in $[Ca^{2+}]$ since equilibrium must be maintained with $Ca_3(AsO_4)_2$, (ii) gypsum is also present, therefore the decrease in $[Ca^{2+}]$ must result in an increase in sulphate concentration, and (iii) the increase in sulphate concentration leads to a decrease in $[Ra^{2+}]$.

Case 3 (Figure 3)

In the presence of $CO_2(g)$, $p(CO_2) = 4.16 \times 10^{-3}$ atm, the arsenic and nickel concentrations in solution are enhanced significantly. The presence of $CO_2(g)$ produces a large increase in carbonate concentration. Thus, most of the calcium in the system is tied up as $CaCO_3(s)$. Even gypsum is not present. Since calcium is not available to form calcium arsenate the arsenic remains in solution. The increase in nickel concentration is due to formation of the aqueous nickel species $NiCO_3(aq)$ and $NiSO_4(aq)$.

$[Ra^{2+}]$ is low, 2.4×10^{-11} mol·kg^{-1}, since the dissolution of gypsum leads to large sulphate concentrations.

Case 4 (Figures 4-6)

The total concentration of arsenic in solution is large, i.e., greater than 10^{-2} mol·kg^{-1}. At the start of the calculation (low ξ values) the arsenic solids $Cs_3(AsO_4)_2$, NiAs and $Ca(AsO_2)_2$ are in equilibrium. As oxygen is added to the system NiAs and $Ca(AsO_2)_2$ are eventually oxidized to form $Ca_3(AsO_4)_2$.

The solubility of $Ni(OH)_2(\beta)$ increases as the pH is lowered from pH = 10 to pH = 8.

$[Ra^{2+}]$ decreases from 1.2×10^{-8} to 3×10^{-9} mol·kg^{-1} as ξ increases along the reaction path.

Case 5 (Figure 7)

At pH = 6, $Ni_3(AsO_4)_2$ is the stable arsenic solid along the reaction path. The arsenic and nickel concentrations are high at low ξ values. $H_3AsO_3(aq)$ is the predominant arsenic species in solution for low ξ. As oxygen is added to the system the arsenite species are oxidized to arsenates which, in turn, become tied up as $Ni_3(AsO_4)_2$ because of the high nickel concentrations. Thus, as ξ increases the arsenic concentration decreases and the amount of nickel arsenate increases.

At pH = 6, all the radium in the system is in solution so $[Ra^{2+}] = 1.2 \times 10^{-8}$ mol•kg^{-1}.

Case 6 (Figures 8-11)

In this case the pH is not fixed along the reaction path. The pH varies from 11 to 7.6 (Figure 8) as ξ increases. The nickel and arsenic concentrations are low at high pH, and increase as the pH decreases. The arsenic and nickel solids formed along the reaction path are shown in Figures 10 and 11, respectively.

The pH would tend to decrease as ξ increases because the oxidation of NiAs produces H^+ ions as illustrated by the reaction

$$2NiAs + \frac{7}{2}O_2 + 5H_2O \rightarrow 2Ni(OH)_2 + 2AsO_4^{3-} + 6H^+ \quad .$$

However, $Ca_3(AsO_4)_2 \cdot Ca(OH)_2$ buffers the pH

$$Ca_3(AsO_4)_2 \cdot Ca(OH)_2 + 2H^+ \rightarrow Ca_3(AsO_4)_2 + Ca^{2+} + 2H_2O$$

Once all the $Ca_3(AsO_4)_2 \cdot Ca(OH)_2$ disappears the pH is able to decrease rapidly leading to an increase in arsenic and nickel concentrations. At low pH $Ni_3(AsO_4)_2$ is formed.

$[Ra^{2+}]$ increases from 5.7×10^{-9} to 8.7×10^{-9} as ξ increases.

Figure 1: Total Arsenic and Nickel Concentrations
Titrant = $O_2(aq)$
pH = 12

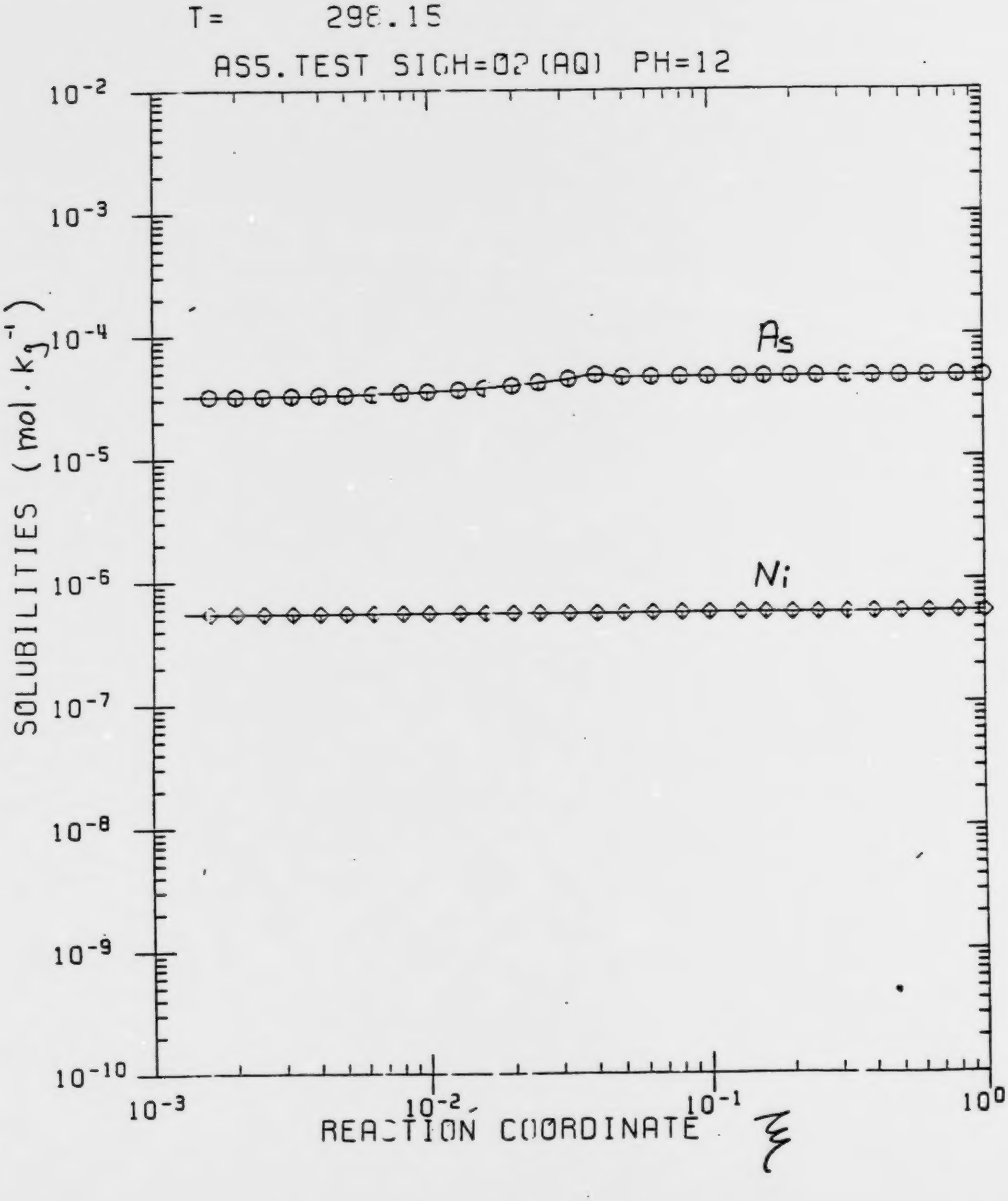

Figure 2. Total Arsenic[4] and Nickel Concentrations

Titrant = $O_2(aq)$
pH = 10

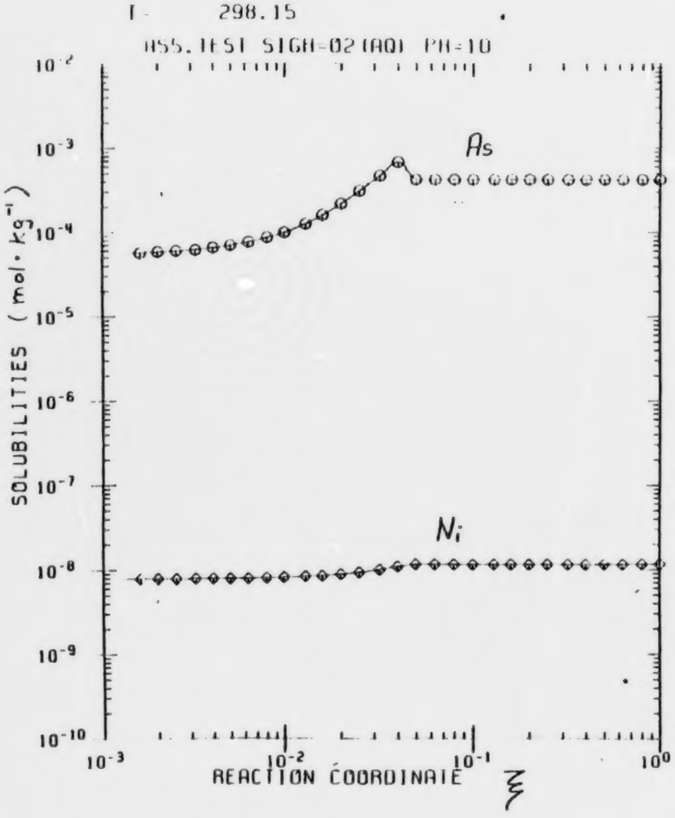

Figure 3. Total Arsenic and Nickel Concentrations

Titrant = $O_2(aq)$
pH = 10
CO_2 in gas phase above solution $p(CO_2) = 4.16 \times 10^{-5}$

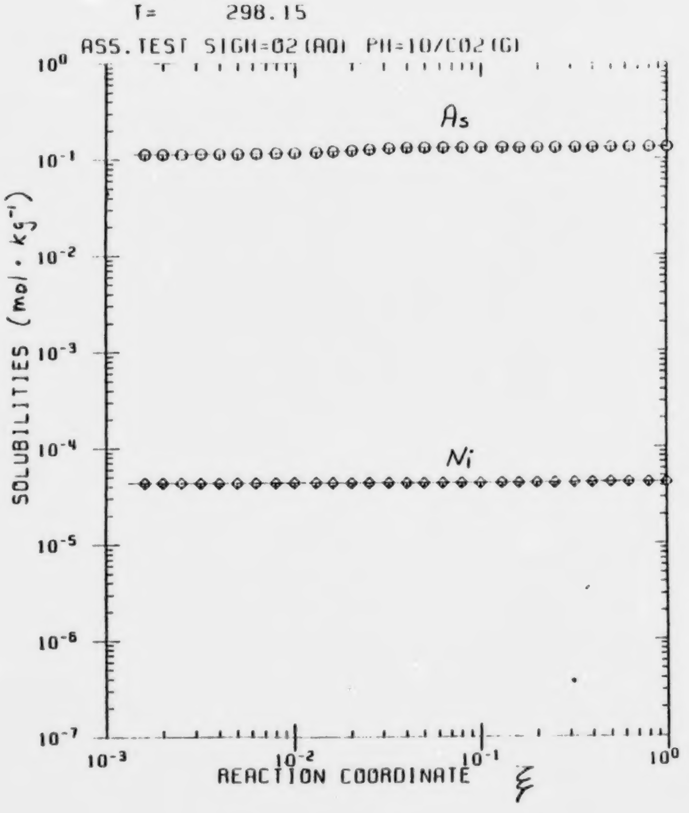

Figure 4 · Total Arsenic and Nickel Concentrations

Titrant = $O_2(aq)$
pH = 8

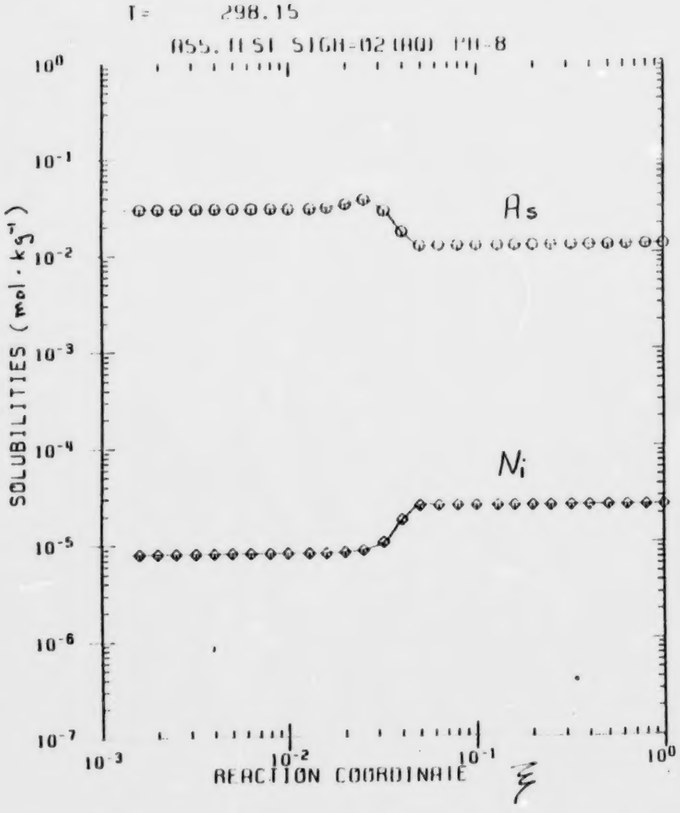

Figure 5:

Titrant = $O_2(aq)$
pH = 8

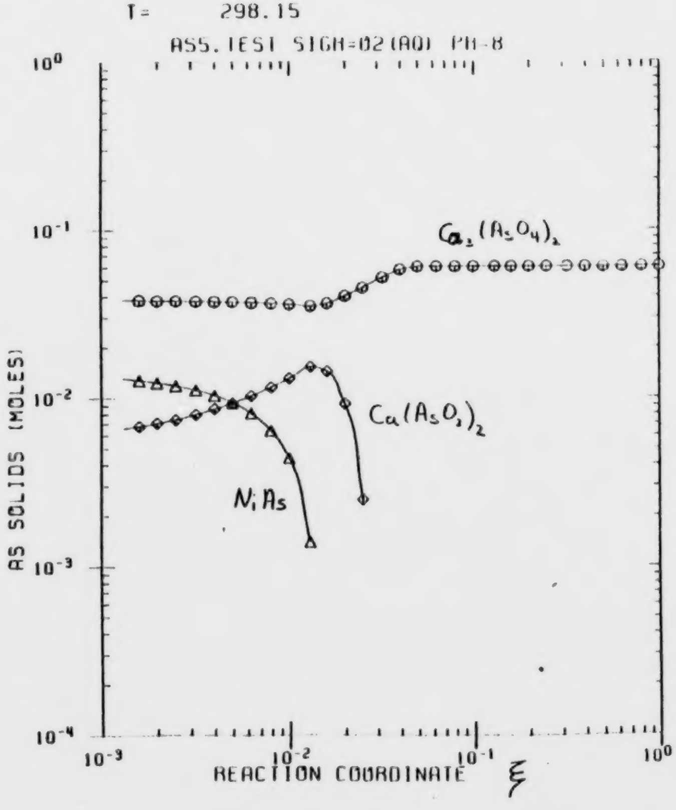

Figure 6.

Titrant = $O_2(aq)$
pH = 8

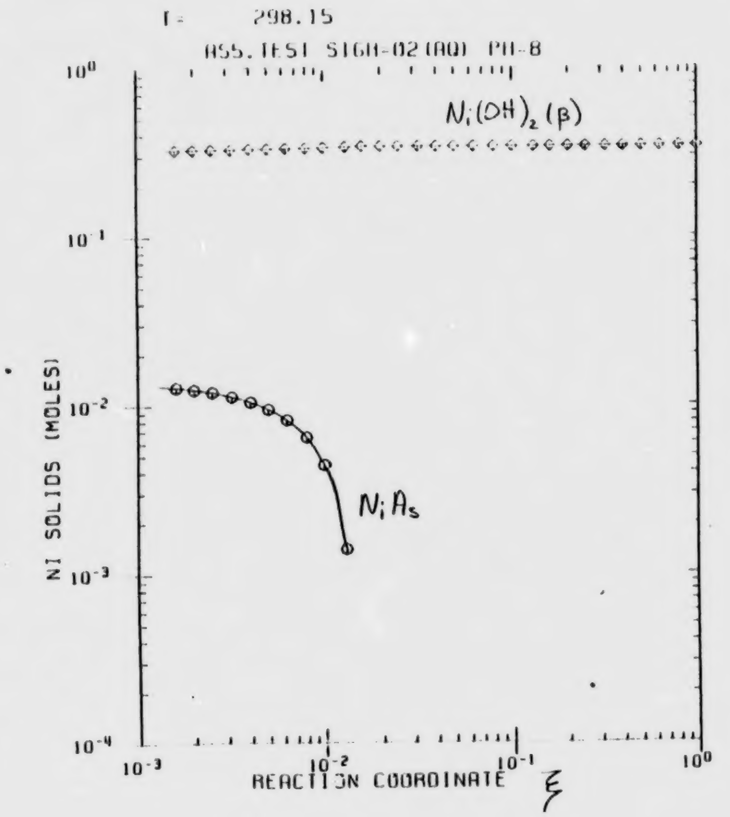

Figure 7: Total Arsenic and Nickel Concentrations

Titrant = $O_2(aq)$
pH = 6

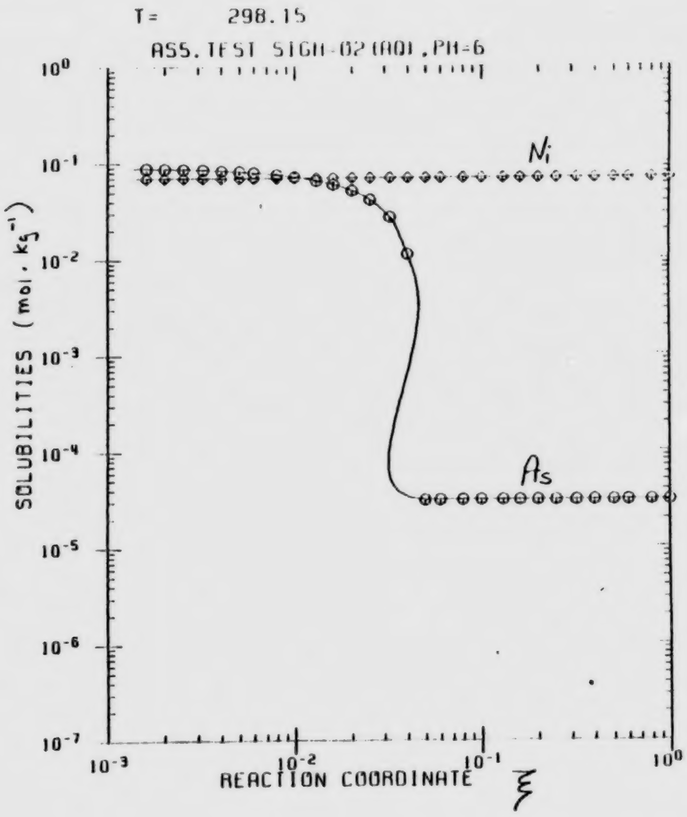

Figure 8 :

Titrant = O_2 (aq)
pH = floating

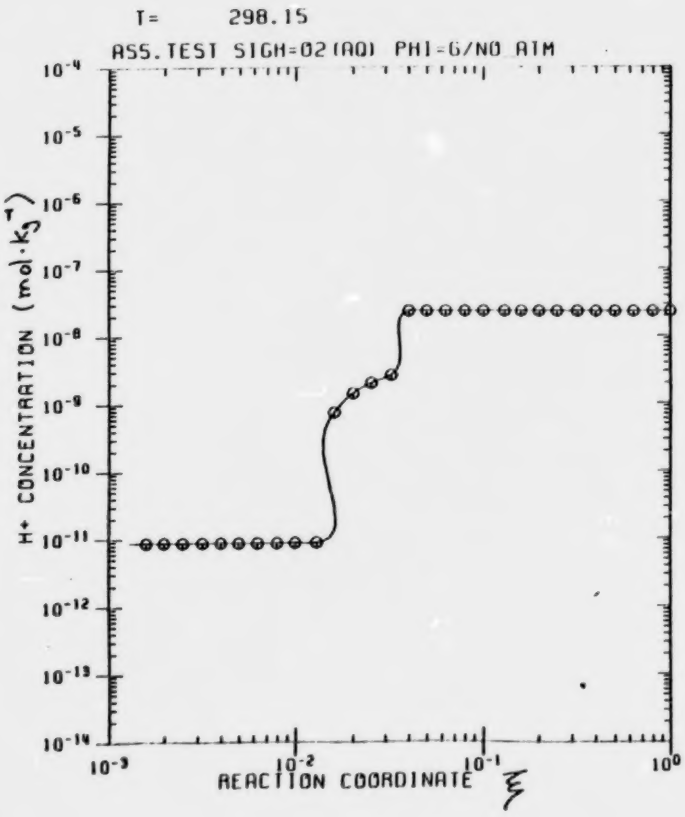

Figure 9: Total Arsenic and Nickel Concentrations

Titrant = O_2 (aq)
pH = floating

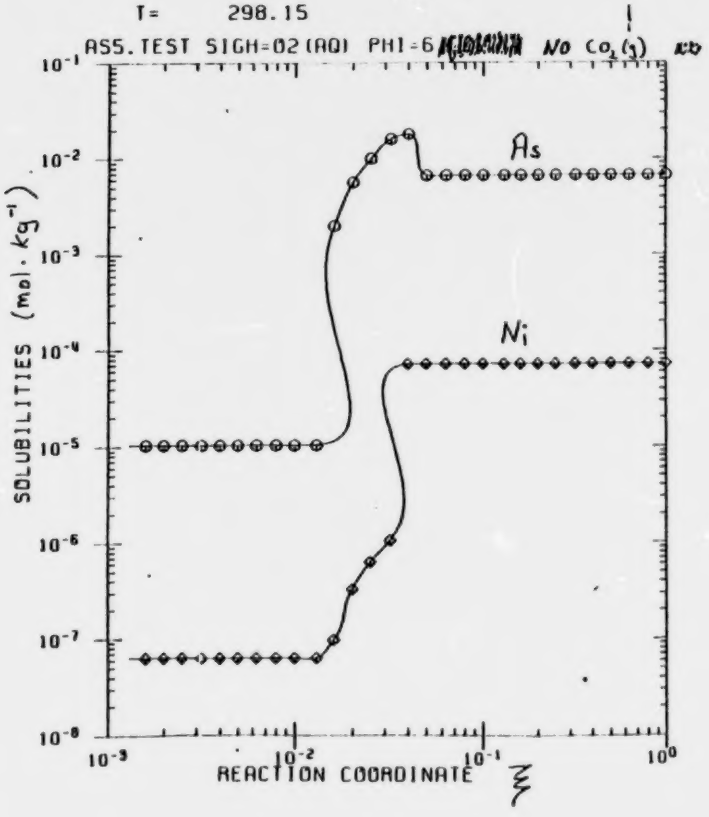

Figure 10:

Titrant = O_2 (aq)

pH = floating

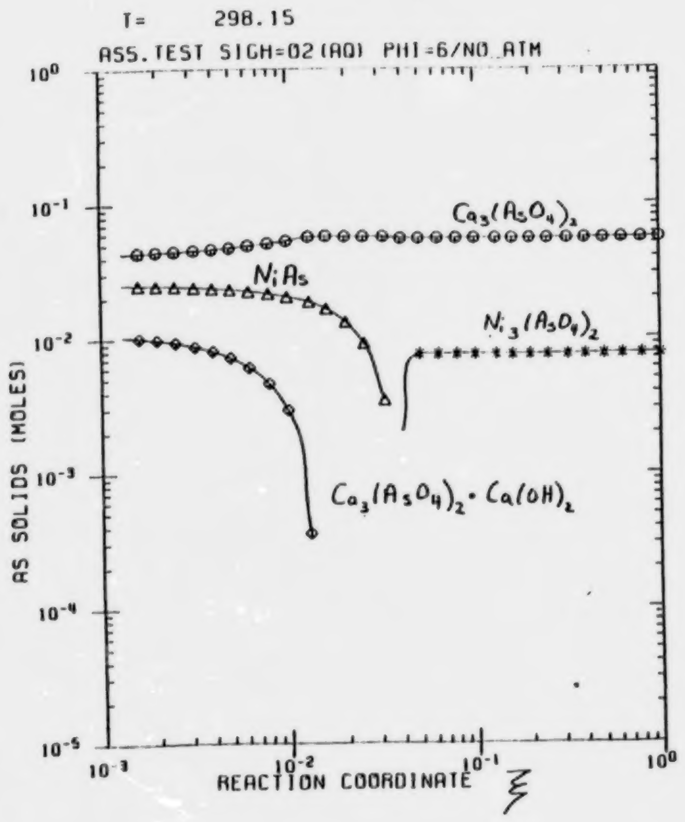

Figure 11:

Titrant = O_2 (aq)

pH = floating

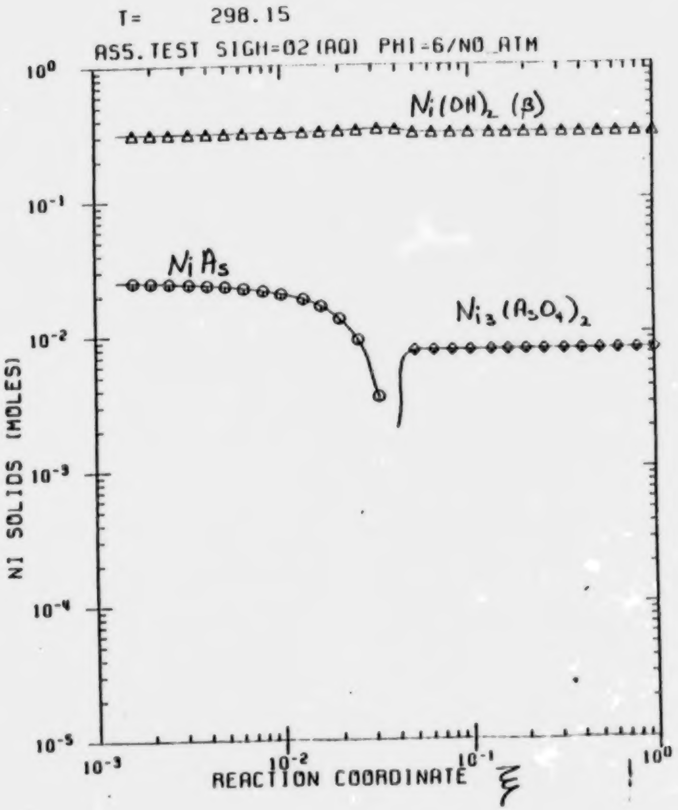

2.2 Titration with $H_2(aq)$

Case 7 (Figures 12-13)

At pH = 12, the arsenic concentration is low and decreases significantly at large values of ξ, i.e., very reducing conditions. Virtually all of the arsenic is tied up as the solid $Ca_3(AsO_4)_2 \cdot Ca(OH)_2$ (0.0663 moles). $Ni(OH)_2(\beta)$ and Ni_3S_2 are at equilibrium but $Ni(OH)_2(\beta)$ is reduced to Ni_3S_2 as H_2 is added to the system:

$$3Ni(OH)_2 + 2CaSO_4 + 9H_2 \rightarrow Ni_3S_2 + 2Ca(OH)_2 + 10H_2O \ .$$

The reduction of gypsum increases the calcium concentration in solution. This reduces the arsenic concentration in solution. Since the gypsum is present at equilibrium the increase in $[Ca^{2+}]$ causes a decrease in sulphate concentration. Thus $[Ra^{2+}]$ increases from 4.9×10^{-10} to 1.2×10^{-8} as ξ increases. All the radium is in solution for $\xi \geq 0.4$ moles.

Case 8 (Figures 14-16)

At pH = 8, the arsenic concentrations are much higher than at pH = 12 (Case 7). The arsenic and nickel solids are shown in Figures 15 and 16, respectively. As H_2 is added to the system the arsenic solids $Ca(AsO_2)_2$ and $Ca_3(AsO_4)_2$, in that order, are reduced and more NiAs is formed. Once $Ca_3(AsO_4)_2$ disappears, the solubility of NiAs controls the arsenic concentration. As in Case 7, $Ni(OH)_2(\beta)$ is reduced at high ξ values. However, at pH = 8, NiS is the stable nickel sulphide rather than Ni_3S_2.

At pH = 8, all the radium is in solution ($[Ra^{2+}] = 1.2 \times 10^{-8}$ $mol \cdot kg^{-1}$). The existence of the solids $CaCO_3(s)$ and gypsum makes the sulphate concentration in solution pH dependent. As the pH decreases, $[CO_3^{=}]$ also decreases. Since $CaCO_3(s)$ is present at equilibrium $[Ca^{2+}]$ must increase and, therefore, since gypsum is present, $[SO_4^{2-}]$ decreases. Low sulphate concentrations lead to high radium concentrations.

Case 9 (Figures 17-19)

For this case, the arsenic-nickel system is titrated with $H_2(aq)$ in the presence of $CO_2(g)$ ($p(CO_2) = 3.3 \times 10^{-4}$ atm). Although the pH is allowed to change it remains essentially constant, i.e., pH = 7.7 ± 0.07. The presence of CO_2 increases the arsenic concentration (cf. Figures 14 and 17). Only $Ca_3(AsO_4)_2$ is present at low ξ values (cf. Figures 15 and 18). Initially, as H_2 is added to the system, only the calcium arsenate is reduced and the arsenic concentration in solution increases. Once $Ca_3(AsO_4)_2$ disappears, $Ni(OH)_2(\beta)$ begins to be reduced and NiAs is formed. The formation of NiAs

$$Ni(OH)_2 + H_3AsO_3 + \frac{5}{2}H_2 \rightarrow NiAs + 5H_2O$$

tends to decrease in arsenic concentration because, H_3AsO_3, the predominant arsenic solution species is also reduced.

$[Ra^{2+}]$ decreases from 8.9×10^{-9} to 5.7×10^{-9} $mol \cdot kg^{-1}$ as ξ increases.

Figure 12 Total Arsenic and Nickel concentrations

Titrant = $H_2(aq)$
pH = 12

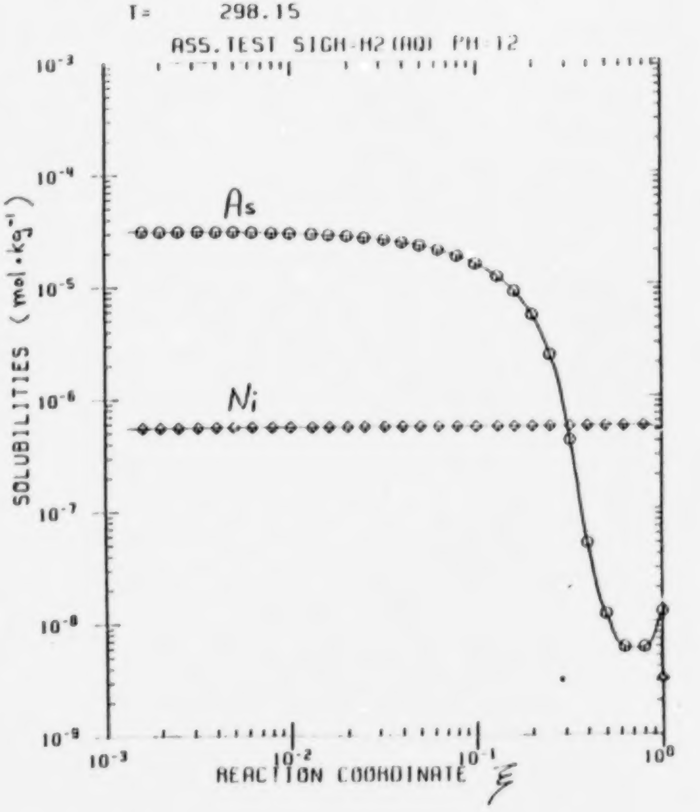

Figure 13

Titrant = $H_2(aq)$
pH = 12

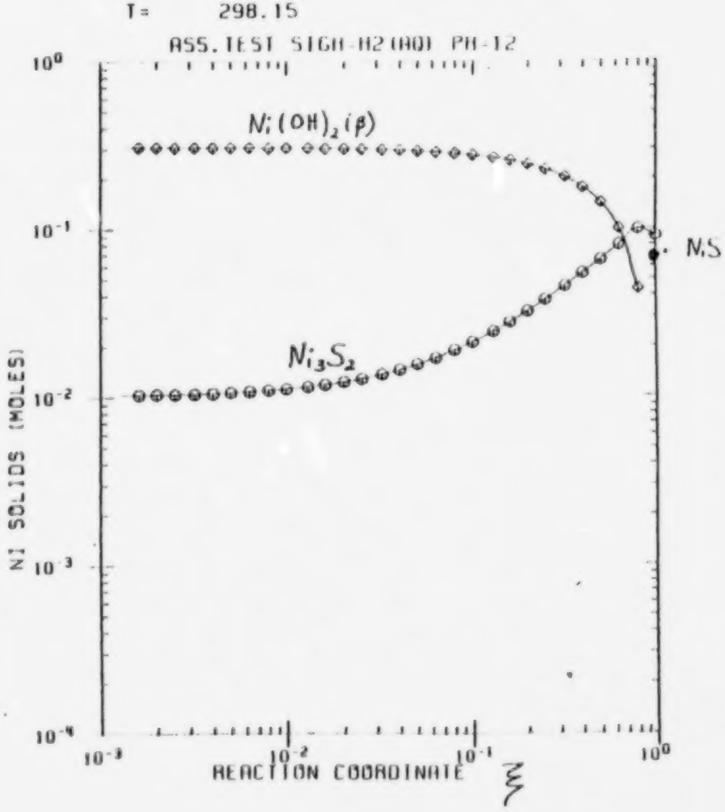

Figure 14: Total Arsenic and Nickel Concentrations

Titrant = $H_2(aq)$
pH = 8

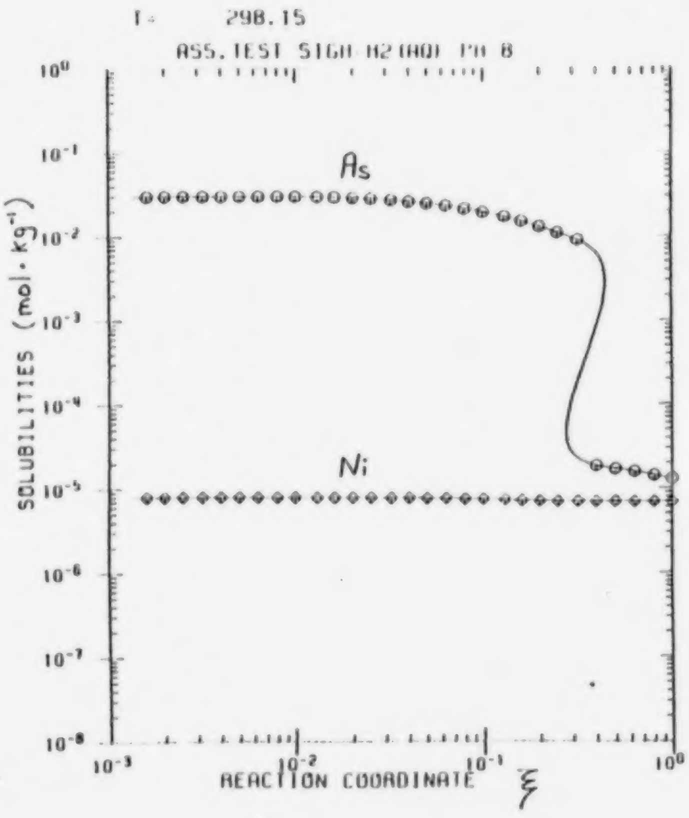

Figure 15:

Titrant = $H_2(aq)$
pH = 8

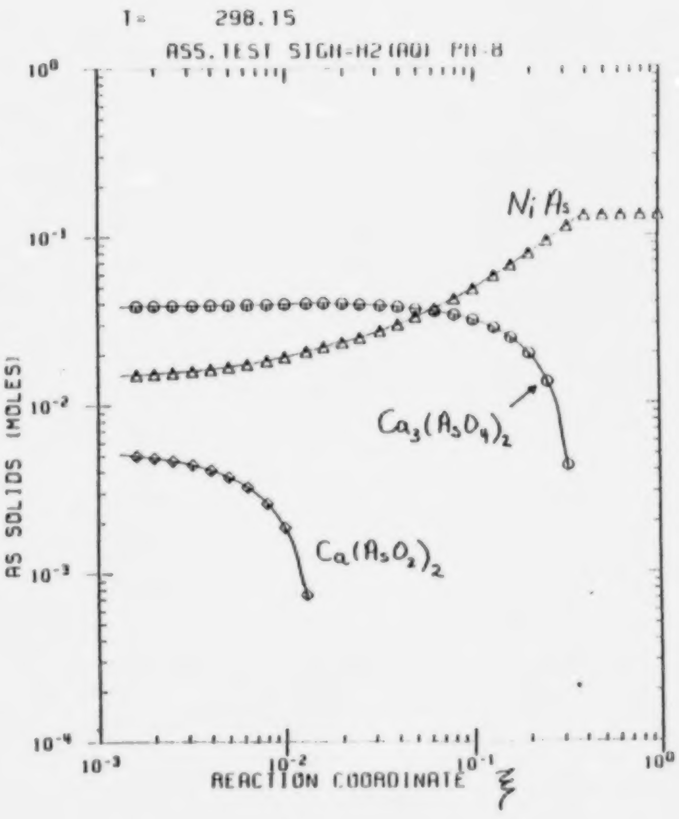

Figure 16:

Titrant = $H_2(aq)$

pH = 8

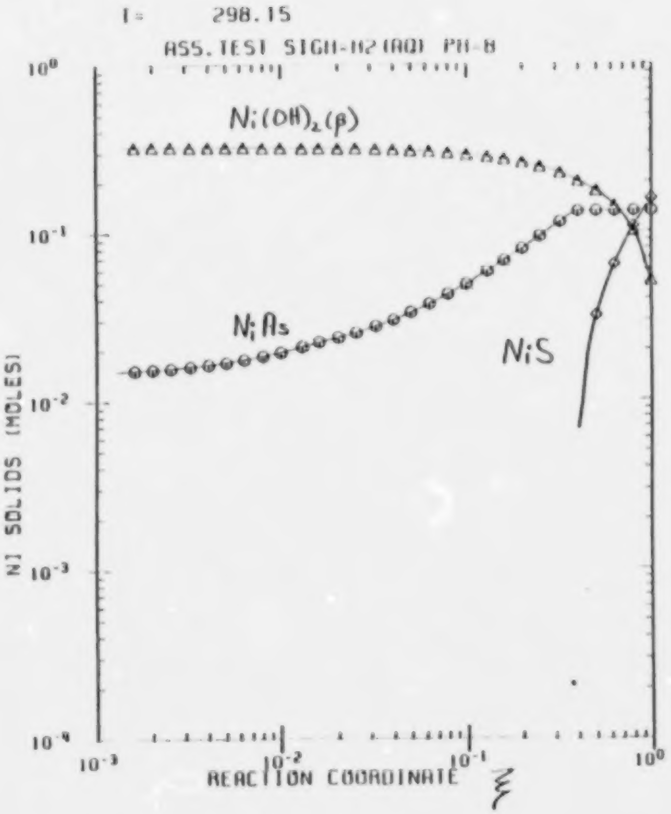

Figure 17. Total Arsenic and Nickel Concentrations

Titrant = $H_2(aq)$

pH = floating

CO_2 in gas phase above solution : $p(CO_2) = 3.3\times10^{-4}$ atm

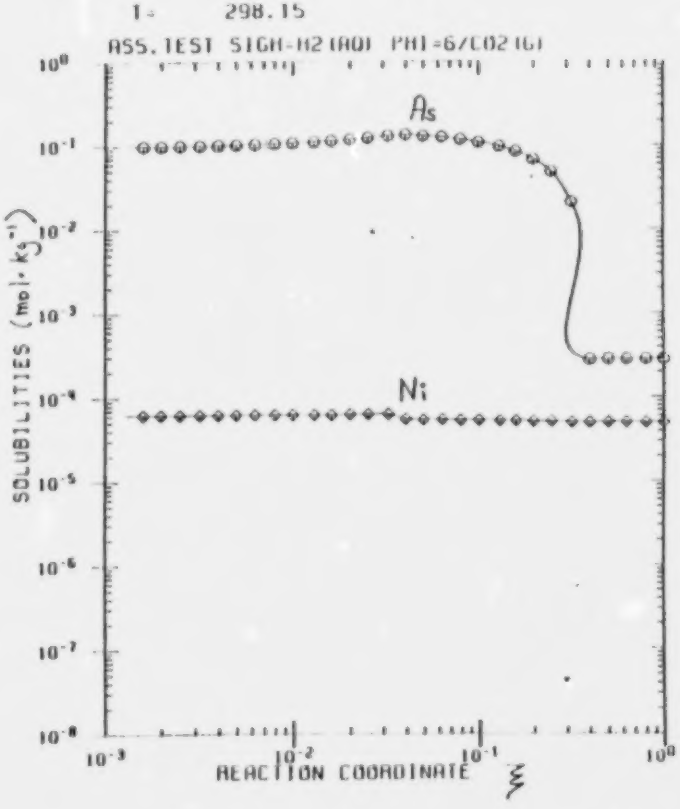

Figure 18:

Titrant = $H_2(aq)$
pH = floating
CO_2 in gas phase above solution

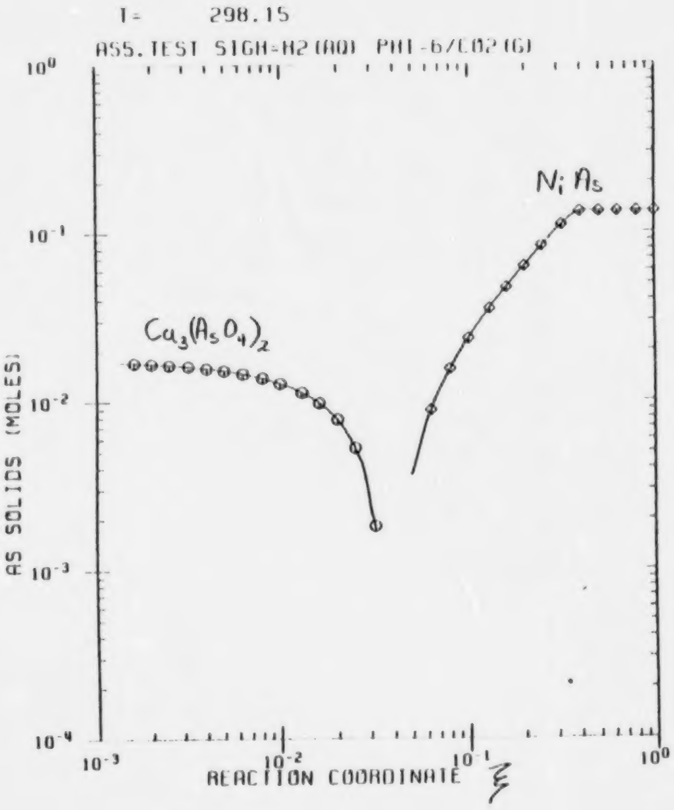

Figure 19:

Titrant = $H_2(aq)$
pH = floating
CO_2 in gas phase above solution

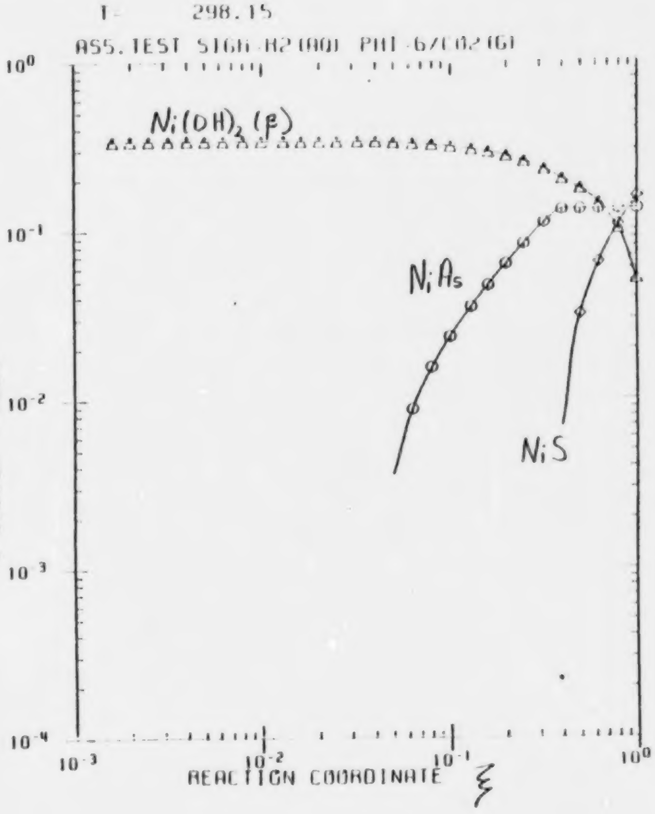

2.3 Titration with $CO_2(g)$

Case 10 (Figures 20-22)

In Case 10 we study the arsenic-nickel system as a function of the CO_2 partial pressure. ξ in this calculation gives the number of moles of CO_2 in the gas phase. Since the gas phase also contains 10^{27} moles of inert gas, the partial pressure of CO_2 is given by

$$p(CO_2) = 10^{-27}\xi \text{ atm.}$$

in terms of the reaction coordinate ξ.

At low CO_2 partial pressures the arsenic and nickel concentrations are low since for small ξ the pH is quite high. In fact, pH = 12.3 for $\xi = 10^{12}$, 10^{13} and 10^{14}. At $\xi = 10^{15}$, pH = 12.0 and the pH decreases by 0.5 pH units as ξ increases by one order of magnitude so that at $\xi = 10^{22}$ the pH is equal to 8.5. pH decreases as ξ increases due to the reactions

$$H_2O + CO_2 \rightarrow H_2CO_3 \rightarrow 2H^+ + CO_3^= \ .$$

Therefore, since $[CO_3^{2-}]$ increases, the presence of $CaCO_3$ forces the $[Ca^{2+}]$ to decrease. This decrease in $[Ca^{2+}]$ and pH cause an increase in the arsenic and sulphate concentrations. Thus, $[Ra^{2+}]$ decreases from 9.5×10^{-9} to 6.8×10^{-9} mol$\cdot$kg^{-1} as ξ increases.

The arsenic and nickel solids are shown in Figures 21 and 22, respectively.

Figure 20: Total Arsenic and Nickel Concentrations

Titrant = $CO_2(g)$
pH = floating

Partial Pressure $CO_2(g)$ = $10^{-27}\ \xi$

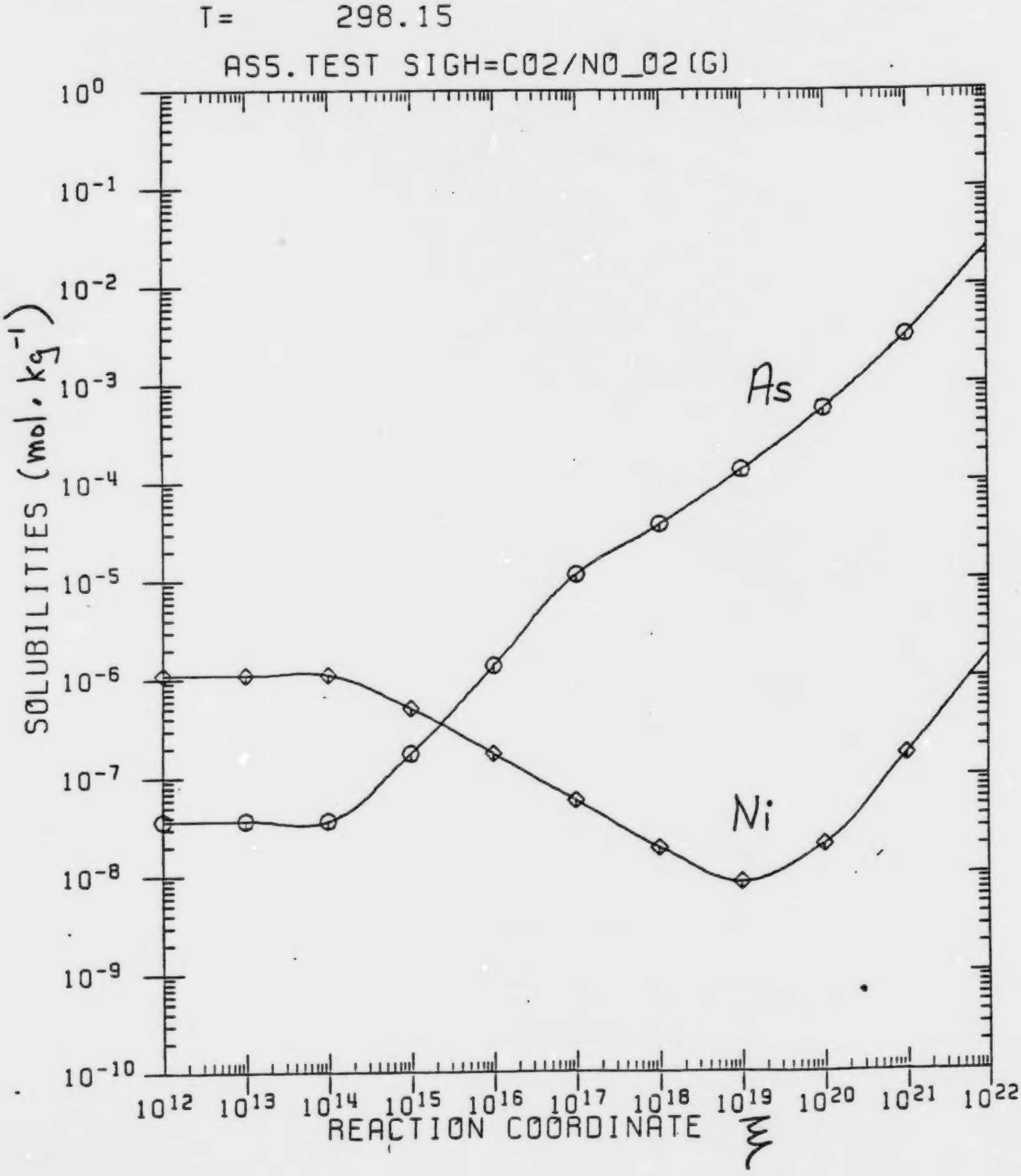

Figure 21.

Titrant = $CO_2(g)$

pH = floating

Partial Pressure $CO_2(g)$ = $10^{-27}\xi$

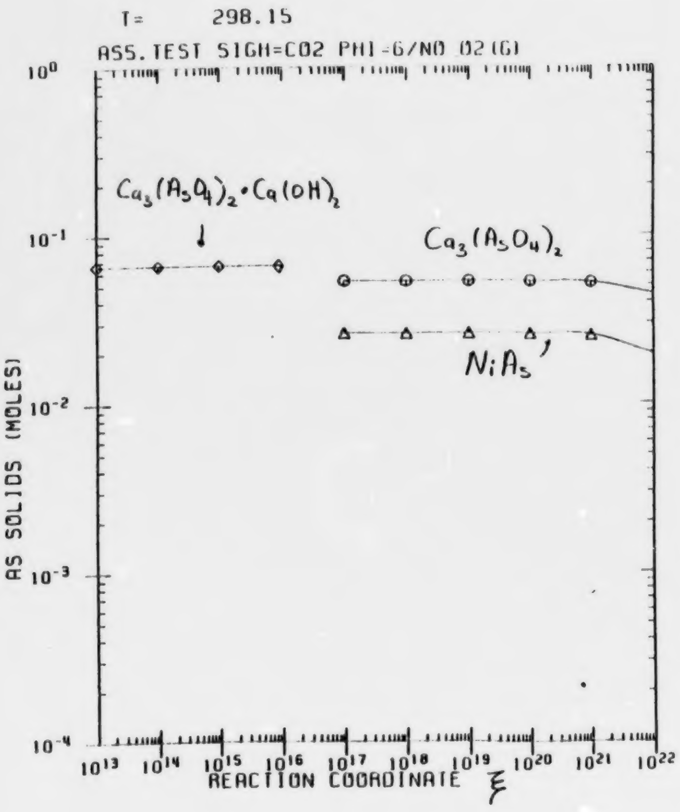

Figure 22:

Titrant = $CO_2(g)$

pH = floating

Partial Pressure $CO_2(g)$ = $10^{-27}\xi$

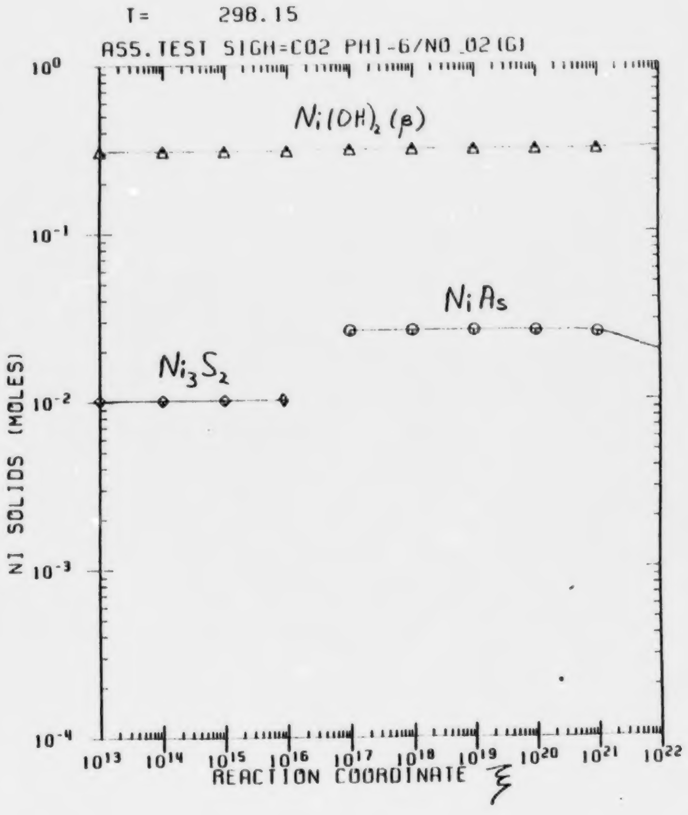

2.4 Titrations with H^+

Case 11 (Figures 23-25)

In Cases 11 and 12 we study the arsenic-nickel system as a function of pH. ξ in these calculations gives the number of moles of $H^+(g)$ in the gas phase. Since the gas phase also contains 10^{27} moles of other gases, the pH is given by the formula

$$pH = -\log(10^{-27}\xi)$$

since $\Delta_f G^o(H^+(g))$ is taken to be equal to zero. In general, these sets of runs summarize many of the previous results.

The pH has a profound effect on the concentration of arsenic and nickel in solution (see Figures 23 and 26). The amphoteric nature of $Ni(OH)_2(\beta)$ is also evident in these figures. The arsenic and nickel solids present at equilibrium change with pH as seen in Figures 24 and 25. This has previously been observed in Cases 1 - 5.

$[Ra^{2+}]$ decreases from 1.2×10^{-8} at $pH = 4$ ($\xi = 10^{23}$) to 4.8×10^{-10} at $pH = 13$ ($\xi = 10^{14}$).

Case 12 (Figures 26-28)

This run is similar to Case 11 except that $O_2(g)$ is also present at a partial pressure of 0.21 atm. Comparison of Figures 24 - 28 shows that, as expected, solids such as NiAs and Ni_3S_2 are not formed at equilibrium under oxidizing conditions.

$Ni_3(AsO_4)_2$ is the stable arsenic solid below pH = 6. However, more $Ni_3(AsO_4)_2$ is formed in the presence of oxygen (cf. Figures 24 and 27). Moreover, we see in Figure 26 that, in the presence of O_2, the arsenic concentration has a (local) minimum at pH = 6 ($\xi = 10^{21}$). In Case 11, i.e., no $O_2(g)$, H_3AsO_3 (or equivalently $HAsO_2$) is the most important arsenic species in solution. Its concentration remains constant as the pH increases from 4 to 7. However, under oxidizing conditions (Case 12) at pH = 4, $H_2AsO_4^-$ is the predominant arsenic solution species. Its concentration decreases as pH increases. This explains the decrease in the total arsenic concentration from pH = 4 to pH = 6 (see Figure 26). At pH = 7, the enhanced stability of $Ni(OH)_2(\beta)$ produces a sharp drop in nickel concentration (see Figure 26). This, in turn, increases the concentration of arsenic in solution since $Ni_3(AsO_4)_2$ is in equilibrium with the solution.

As pH increases nickel arsenate becomes unstable with respect to formation of calcium arsenate and $Ni(OH)_2(\beta)$. The solubility of calcium arsenate decreases as pH increases since the concentration of the aqueous arsenic species $H_2AsO_4^-$ and $HAsO_4^{2-}$ decrease as pH increases. Finally, for very basic conditions $Ca_3(AsO_4)_2 \cdot Ca(OH)_2$ is formed.

$[Ra^{2+}]$ decreases from 1.2×10^{-8} to 3.8×10^{-10} as the pH increases from 4 to 13.

Figure 23: Total Arsenic and Nickel Concentrations

Titrant = $H^+(g)$

$pH = -\log(10^{-27}\xi)$

Inert Gas Atmosphere

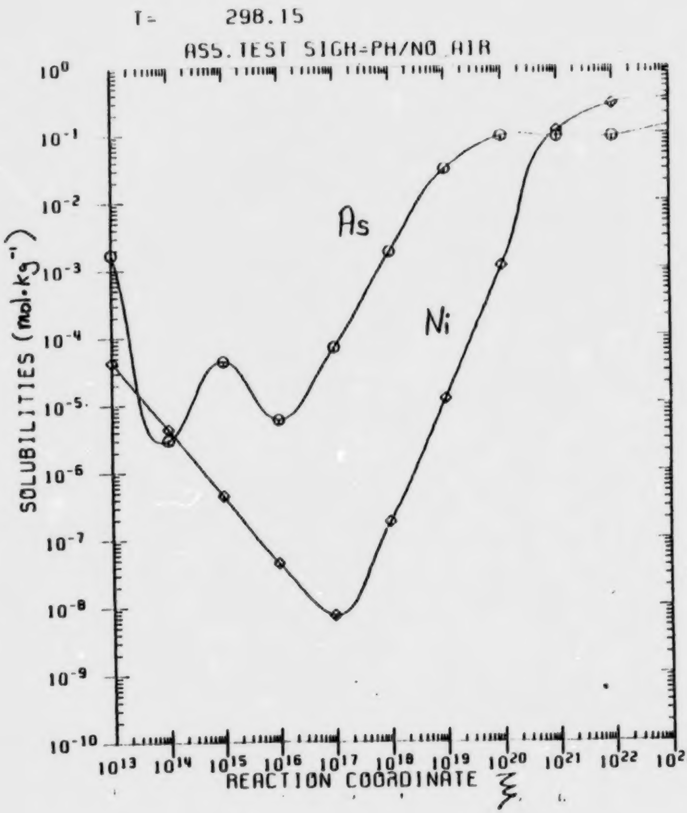

Figure 24

Titrant = $H^+(g)$

$pH = -\log(10^{-27}\xi)$

Inert Gas Atmosphere

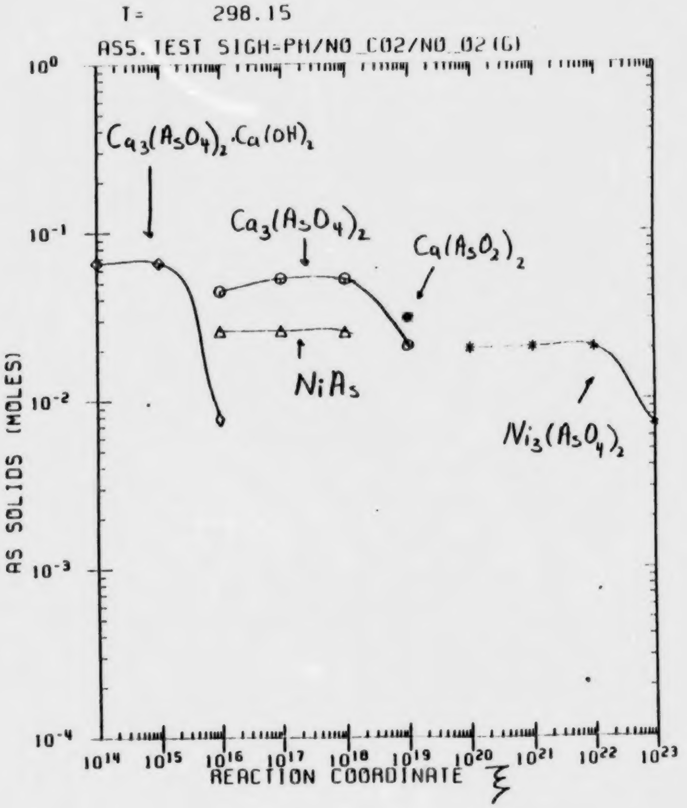

Figure 25:

Titrant = $H^+(g)$

$pH = -\log(10^{-27}\xi)$

Inert Gas Atmosphere

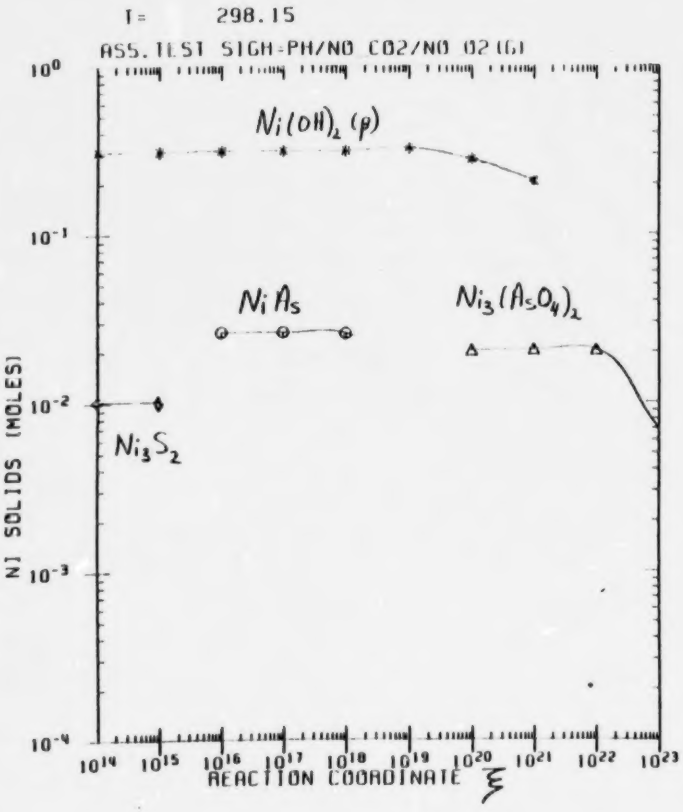

Figure 26: Total Arsenic and Nickel Concentrations

Titrant = $H^+(g)$

$pH = -\log(10^{-27}\xi)$

Oxygen Atmosphere : $p(O_2) = 0.21$ atm

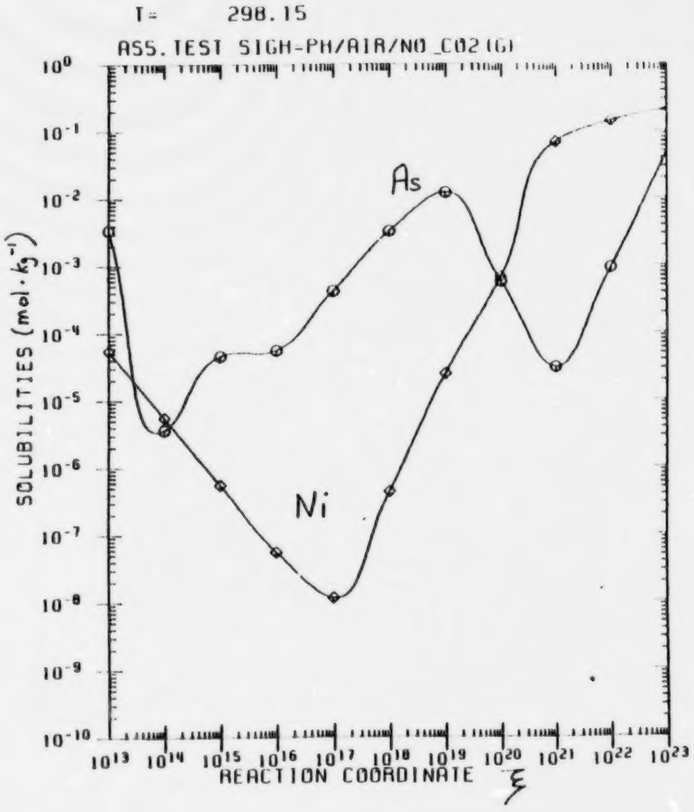

Figure 27:

Titrant = $H^+(g)$

$pH = -\log(10^{-27}\xi)$

Oxygen Atmosphere : $p(O_2) = 0.21$ atm

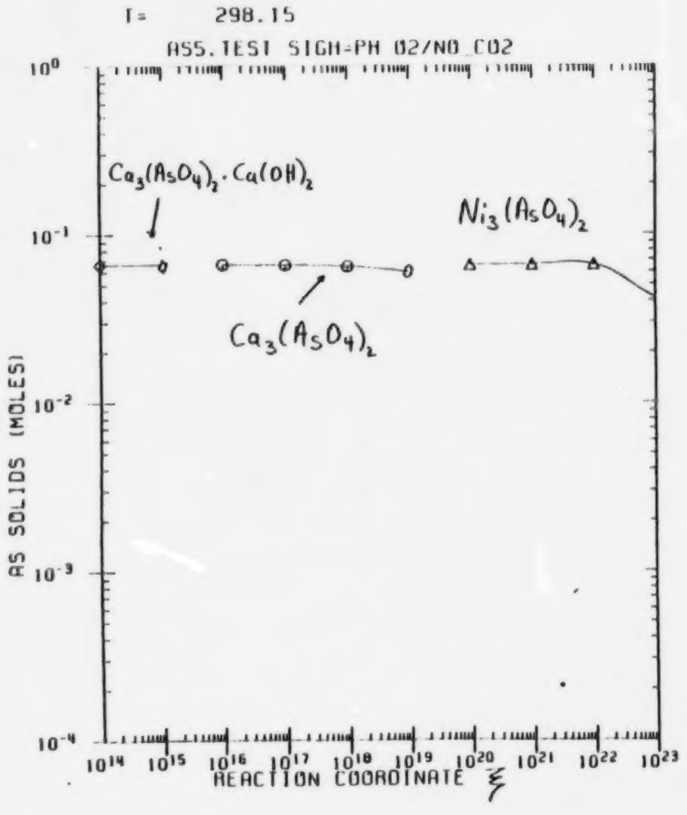

Figure 28

Titrant = $H^+(g)$

$pH = -\log(10^{-27}\xi)$

Oxygen Atmosphere : $p(O_2) = 0.21$ atm

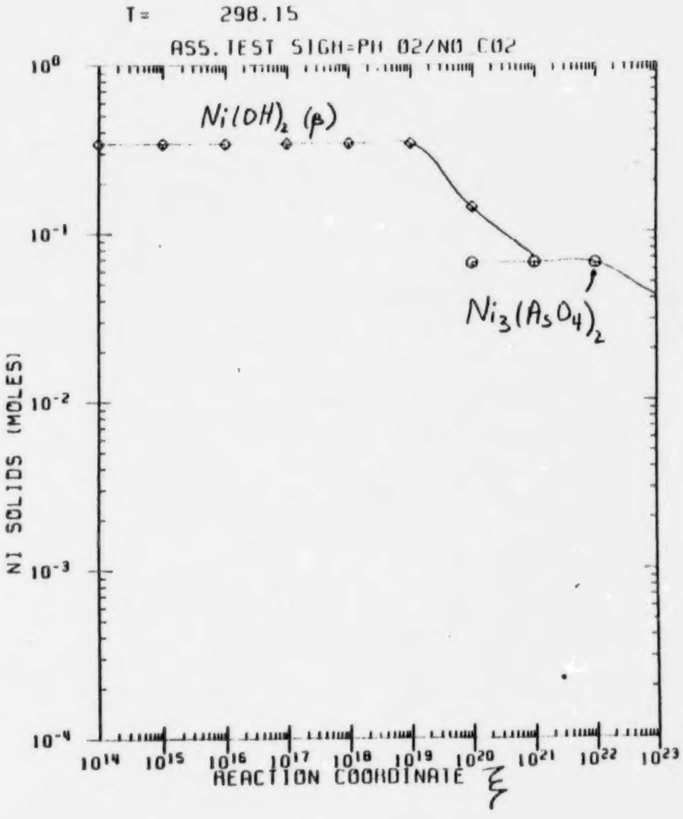

2.5 The Effect of Iron (III)

Addition of iron (III) to the system does not reduce arsenic concentrations through formation of iron (III) arsenates, at least for neutral and basic solutions. Even $Fe(OH)_3$ will form in preference to the iron (III) arsenates near pH = 7 (although Fe_2O_3 is actually the stable iron oxide solid). In neutral and basic solutions the iron does, however, form a stable nickel ferrate ($NiFe_2O_4$). This will form in preference to nickel arsenate, and, hence, increase the arsenic concentrations.

2.6 Radium Concentrations

The arsenic-nickel system studied in this report also includes barium and radium. The radium and barium concentrations in solution are separately controlled by the solubility of $RaSO_4(s)$ and $BaSO_4(s)$, respectively. However, the radium sulphate, which coprecipitates with barium sulphate, may, in fact, be "locked up" in the barium sulphate crystal. The small amount of radium in the $BaSO_4(s)$ lattice will not significantly affect the thermodynamic properties of $BaSO_4(s)$. Thus, if we assume that radium is only released into solution when $BaSO_4(s)$ dissolves, we would expect that the fraction of radium in solution is equal to the fraction of barium that has dissolved (i.e., congruent dissolution).

The arsenic-nickel system includes 2.1×10^{-3} moles of $BaSO_4$ and 1.2×10^{-8} moles of $RaSO_4$. In the reaction path calculations described in Sections 2.1 - 2.4, the total barium concentration varies from 1.8×10^{-9} $mol{\cdot}kg^{-1}$ (at high pH) to 1.8×10^{-6} $mol{\cdot}kg^{-1}$ (at low pH). Thus, in our model, one expects the radium concentration in solution to vary from 10^{-14} $mol{\cdot}kg^{-1}$ (at high pH) to 10^{-11} $mol{\cdot}kg^{-1}$ (at low pH) since the Ra:Ba ratio is equal to 5.7×10^{-6}. These radium concentrations are approximately 3 orders of magnitude less than the radium concentrations determined from the $RaSO_4(s)$ solubility! A similar calculation can, of course, be carried out if radium is incorporated in a $CaSO_4$ matrix.

It is also possible to treat the $RaSO_4$ mixture as a solid solution. However, one would require the equivalent of a Henry's law constant for a dilute solution of $RaSO_4(s)$ in $BaSO_4(s)$, i.e., the free energy of transfer of $RaSO_4$ from a $RaSO_4$ crystal into a $BaSO_4$ crystal. This data, as far as we are aware, is not available. Therefore, as a very crude approximation, we treat the $RaSO_4$-$BaSO_4$ solution as ideal, i.e.,

$$\mu(RaSO_4,ss) = \mu^{o}(RaSO_4,s) + RT\,\ell n(x)$$

where x is the mole fraction of $RaSO_4$ in the solid solution and ss stands for "solid solution". In this approximation, we can calculate the concentration of radium from the equation

$$[Ra^{2+}][SO_4^{2-}] = xK$$

where K is the equilibrium constant for the reaction

$$RaSO_4(s) \rightleftharpoons Ra^{2+} + SO_4^{2-}$$

It is interesting to point out that, for the congruent dissolution model discussed above, the radium concentration is approximately given by

$$[Ra^{2+}][SO_4^{2-}] = xK'$$

where K' is the equilibrium constant of the reaction

$$BaSO_4(s) \rightleftharpoons Ba^{2+} + SO_4^{2-}$$

Since the ideal solution approximation could introduce large errors, we feel that the congruent dissolution model is more reliable for calculating radium concentrations.

3. DISCUSSION

The calculations described in this report show that the selection of values of the Gibbs energies of formation for the calcium arsenates is important in calculating total arsenic solution concentrations in the unsaturated zone. In our database [2], the Gibbs energies were based on the experimental studies of Nishimura et al. [5]. The results of this group agree well with the earlier detailed work of Guerin [7]. The degree of hydration of the solids is strongly dependent on temperature [7]. The Gibbs energies we have used refer to whatever calcium arsenate hydrates are stable in contact with solutions at 25°C, however, we have chosen not to assign a specific hydration number to each solid. Thus, $\Delta_f G^o(Ca_3(AsO_4)_2)$ does not refer to the anhydrous solid of that formula. It should be noted that the value of $\Delta_f G^o(Ca_3(AsO_4)_2)$ in the NBS Tables [3] also probably refers to an unspecified hydrate, as the number appears to be based on the equilibrium solubility study of Chukhlantsev [6].

After adjustment for hydration number, the Gibbs energy we have used for the calcium arsenate with a $CaO{:}As_2O_5$ ratio of 2:1 [2] is approximately 40 $kJ\cdot mol^{-1}$ more positive than was estimated and used for $(CaO)_{2.0}(As_2O_5)_{1.0}(H_2O)_{3.0}$ in a recent report from Knight and Piesold Ltd. [8]. In that report an estimated equilibrium constant of $\log_{10}K = 3.80$ for the reaction

$$(CaO)_2(As_2O_5)\cdot 3H_2O + 4H^+ = 2Ca^{2+} + 2H_3AsO_4 + 2H_2O$$

was proposed. This value leads to very low arsenic solubilities ($\approx 10^{-5}$ $mol\cdot dm^{-3}$) between pH = 7 and pH = 11. It is clear from the work of Guerin [7] and of Nishimura et al. [5] that $(CaO)_2(As_2O_5)\cdot 3H_2O$ is not the stable solid in this range, and is several orders of magnitude less stable than predicted in the report. Our value for the equilibrium constant for the above reaction is $\log_{10}K = 11.3$ (also see below).

To minimize confusion and to reinforce the relationships between the many calcium arsenate solids described in the literature, we list in

Table 2 the simple formulas, together with a correspondence table of formulas based on the elemental oxides.

Under oxidizing conditions, the major equilibrium solid phases in the system are gypsum and dolomite. Nickel remains as β-$Ni(OH)_2$ or is transofrmed to $Ni_3(AsO_4)_2$. Arsenic may remain as $Ca_3(AsO_4)_2$ in the pH range 7 - 9, however, $Mg_3(AsO_4)_2$ and $Ni_3(AsO_4)_2$ can also be formed. Above this pH range $Ca_3(AsO_4)_2 \cdot Ca(OH)_2$ forms, while below pH = 7 the stable alkaline earth arsenates are quite soluble. In the recent report from Knight and Piesold Ltd. [8] it was claimed $(CaO)_2(As_2O_5) \cdot 3H_2O$ was likely to be the stable equilibrium arsenic (V) solid between pH = 6 and pH = 11, and that the equilibrium solubility of arsenic would be limited to $< 10\ mg \cdot dm^{-3}$ in that region by that solid. This is incorrect because their estimate of the Gibbs energy of the solid was inaccurate (as noted above).

TABLE 2.

SOLIDS IN THE CALCIUM/ARSENIC(V)/WATER SYSTEM

Calcium Arsenate Formula	Equivalent Oxide Formula	
$CaH_4(AsO_4)_2$	$(CaO)_{1.0}(As_2O_5)_{1.0}(H_2O)_{2.0}$	(a,b)
2 $CaHAsO_4$	$(CaO)_{2.0}(As_2O_5)_{1.0}(H_2O)_{1.0}$	
2 $CaHAsO_4 \cdot H_2O$	$(CaO)_{2.0}(As_2O_5)_{1.0}(H_2O)_{3.0}$	(a,b)
2 $CaHAsO_4 \cdot 2H_2O$	$(CaO)_{2.0}(As_2O_5)_{1.0}(H_2O)_{5.0}$	(a,b)
2 $CaHAsO_4 \cdot 3H_2O$	$(CaO)_{2.0}(As_2O_5)_{1.0}(H_2O)_{7.0}$	
0.5 $Ca_5H_2(AsO_4)_4$	$(CaO)_{2.5}(As_2O_5)_{1.0}(H_2O)_{0.5}$	
0.5 $Ca_5H_2(AsO_4)_4 \cdot 4H_2O$	$(CaO)_{2.5}(As_2O_5)_{1.0}(H_2O)_{2.5}$	(b)
0.5 $Ca_5H_2(AsO_4)_4 \cdot 9H_2O$	$(CaO)_{2.5}(As_2O_5)_{1.0}(H_2O)_{5.0}$	(a)
$Ca_3(AsO_4)_2$	$(CaO)_{3.0}(As_2O_5)_{1.0}$	
$Ca_3(AsO_4)_2 \cdot 4H_2O$	$(CaO)_{3.0}(As_2O_5)_{1.0}(H_2O)_{4.0}$	(b)
$Ca_3(AsO_4)_2 \cdot 10H_2O$	$(CaO)_{3.0}(As_2O_5)_{1.0}(H_2O)_{10.0}$	(a)
$Ca_3(AsO_4)_2 \cdot Ca(OH)_2$	$(CaO)_{4.0}(As_2O_5)_{1.0}(H_2O)_{1.0}$	(b)
$Ca_3(AsO_4)_2 \cdot Ca(OH)_2 \cdot 4H_2O$	$(CaO)_{4.0}(As_2O_5)_{1.0}(H_2O)_{5.0}$	(a)

(a) Phases identified by Guerin [7] at 17°C.

(b) Phases identified by Guerin [7] at 40°C.

4. CONCLUSIONS

The behaviour of arsenic, nickel and radium was studied in a chemical environment typical of As/Ni rich uranium tailings, using reaction path calculations. The concentrations of arsenic, nickel and radium were calculated and interpreted in the unsaturated and saturated zones.

These calculations show that, based on the currently available thermodynamic data, high concentrations of arsenic will be reached in undiluted, surface tailing ponds, once they reach chemical equilibrium. It seems that the low concentrations sometimes observed are due to non-equilibrium effects (e.g., dilution, kinetics, transport).

Calcium cannot stabilize the arsenic and contain it in solid phases, with concentrations of approximately 10^{-5} M, over the required pH range (i.e., neutral to basic), in particular in presence of CO_2.

Iron (III) cannot suppress arsenic concentrations of approximately 10^{-3} M either (see Section 2.5). The suppressing effect of arsenic concentration by iron (III) reported by Krause and Ettel [9] is probably a short term effect and does not agree with the observations of Robins [10].

A careful study of the geochemical control of arsenic concentration in the tailings is required. This study should include:

- long-term leach studies
- chemical characterization of the solids from which leaching occurs
- well defined field measurements (e.g., to understand the extent of dilution effects)

- site specific environmental modelling, including both source term (i.e., a release model) and contaminant transport. Such a combined model should be able to take into account contaminant release (with either kinetic or thermodynamic control), sorption and dilution effects.

It should be emphasized that the conditions of the field experiments available to us were not well defined. In the future, these studies should carefully define the solids and solution composition at a given location as well as details on the dilution history of the contaminants at that location. The solution composition should include major constituents as well as pH, arsenic and nickel concentrations. As we showed in this report nickel may play an important role in determining arsenic concentrations.

In addition, it would be useful to conduct experiments to test the release model for radium, proposed in this report.

The As/Ni rich tailings are a complex chemical system. The environmental impact of these tailings can only be assessed by a combined effort of field, laboratory and modelling studies. It is important to ensure that the data produced in the field and laboratory experiments is indeed the data required for the assessment calculations. We believe this can be achieved by a close cooperation between the groups involved with each of the studies.

APPENDIX

SPECIES	GIBBS ENERGY OF FORMATION (kJ.mol-1)
H+	0.
H2O	-237.129
OH-	-157.244
CO3-2	-527.81
HCO3-	-586.77
H2CO3	-623.20
Ca+2	-553.58
CaOH+	-718.4
Ca(OH)2(s)	-898.49
CaCO3(aq)	-1081.39
CaHCO3+	-1146.20
CaCO3(s)	-1128.79
As	0.0
As2O3(o)	-585.4
As2O5	-782.3
AsO+	-168.5
HAsO2	-407.4
AsO2-	-354.7
HAsO3-2	-522.6
AsO3-3	-446.1
H3AsO4	-773.8
H2AsO4-	-761.0
HAsO4-2	-721.3
AsO4-3	-655.6
CaH4(AsO4)2	-2069.
CaHAsO4	-1295.
Ca5H2(AsO4)4	-5665.
Ca3(AsO4)2	-3076.
Ca3(AsO4)2.Ca(OH)2	-3990.
Ca(AsO2)2	-1302.
Ca(AsO2)2.Ca(OH)2	-2235.
HS-	12.08
H2S(aq)	-27.83
SO4-2	-744.53
HSO4-	-755.91
S-2	85.8
As2S3	-91.
As4S4(alpha)	-132.
AsS2-	-23.2
H2As2S4	-131.4
HAs2S4-	-101.3
CaSO4.2H2O	-1797.28
Ba+2	-560.77
BaOH+	-730.5
BaSO4(cr)	-1362.2
BaCO3(cr)	-1137.6
Ba3(AsO4)2	-3096.
BaHAsO4	-1314.
Ra+2	-561.5
RaSO4(cr)	-1365.6
Ni+2	-45.6
NiO	-211.7
Ni(OH)2(beta)	-458.1

SPECIES	GIBBS ENERGY OF FORMATION (kJ.mol-1)
NiOH+	-226.4
Ni(OH)2(aq)	-404.
Ni(OH)3-	-591.
Ni4(OH)4+4	-572.6
NiCO3(cr)	-612.5
NiCO3(aq)	-604.
NiS	-85.9
Ni3S2	-212.2
NiSO4.7H2O	-2461.83
NiSO4(aq)	-803.3
Ni3(AsO4)2	-1594.
Ni	0.
MgCO3(s)	-1012.1
MgCO3.3H2O	-1726.1
MgCO3.5H2O	-2199.2
Mg2+	-454.8
Mg3(AsO4)2	-2789.
MgHAsO4	-1194.
CaMg(CO3)2	-2163.4
O2(aq)	16.4
NiAs	-67.89
FeAsO4	-776.
FeHAsO4	-862.
Fe3(AsO4)2	-1781.
NiFe2O4	-973.1
Fe2+	-78.90
Fe3+	-4.7
Fe3O4	-1015.4
Fe(OH)3(cr)	-696.5
Fe(OH)2(cr)	-486.5
FeOH+	-277.4
FeOH+2	-229.41
Fe(OH)2+	-438.0
Fe(OH)3(aq)	-659.3
Fe(OH)3-	-614.9
Fe2O3	-742.2
CO2(g)	-394.359
O2(g)	0.

REFERENCES

1. N.C. Garisto and F. Garisto, "Reaction Path Calculations of Mineral Alteration Products: Application to Nuclear Fuel Waste Management", Nuc. Chem. Waste Management 5, 17-25 (1984).

2. R.J. Lemire, "Chemical Thermodynamic Databases for Nickel and Arsenic", Report submitted to Beak Consultants, January, 1986.

3. D.D. Wagman, W.H. Evans, V.B. Parker, R.H. Schum, I. Halow, S.M. Bailey, K.L. Churney and R.L. Nuttall, J. Phys. Chem. Ref. Data, Vol. 11, Supplement No. 2 (1982).

4. O. Kubaschewski and C.B. Alcock, "Metallurgical Thermochemistry", 5th Edition, Pergamon Press, Oxford (1979).

5. T. Nishimura, C.T. Ito, K. Tozawa and R.G. Robins, "The Calcium - Arsenic - Air System", in Proc. 15th Annual Hydrometallurgical Meeting, Vancouver, 1985, p. 2-1.

6. V.G. Chukhlantsev, "Solubility Products of Arsenates", J. Inorg. Chem. USSR (Eng. transl.) 1, 1975 (1956).

7. H. Guerin, "Sur les Aresenates Alcalino-Terreux, Etude du Systeme As_2O_5-OCa-OH_2", Ann. Chem. 16, 101 (1941).

8. Knight and Piesold Limited, Report submitted to the National Uranium Tailings Program, (1986).

9. E. Krause and V.A. Ettel, "Ferric Arsenate Compounds: Are they Environmentally Safe? Solubilities of Basic Ferric Arsenates" in Proc. 15th Annual Hydrometallurgical Meeting, Vancouver, 1985, p. 5-1.

10. R.G. Robins, "The Aqueous Chemistry of Arsenic in Relation to Hydrometallurgical Processes", ibid p. 1-1.

APPENDIX B

Food Chain and Environmental Transport Parameters

TABLE B5.1.1: ERODIBILITY AND AVERAGE PERCENT BY WEIGHT OF SUSPENDED PARTICLES FOR DIFFERENT SOIL TYPES

Soil Texture	Erodibility Index (tonnes·km^{-2}·a^{-1})[1]	Aggregates <0.05 mm (percent by weight)[2]
Sand	0.98	0.9
Loamy sand	0.60	1.0
Sandy loam	0.38	2.1
Clay	0.38	0.8
Silty clay	0.38	0.8
Loam	0.25	0.6
Sandy clay loam	0.25	4.1*
Sandy clay	0.25	1.0*
Silty loam	0.21	4.1
Clay loam	0.21	2.5*
Silty clay loam	0.17	4.1
Silt	0.17	0.8*

[1] Craig and Turelle (1964).

[2] Chepil (1958).

* Estimated from most similar soil types.

FIGURE B5.1.1: THORNTHWAITE'S ANNUAL PRECIPITATION-EVAPORATION INDEX FOR CANADA (1941-1970) (from NRCC, 1982)

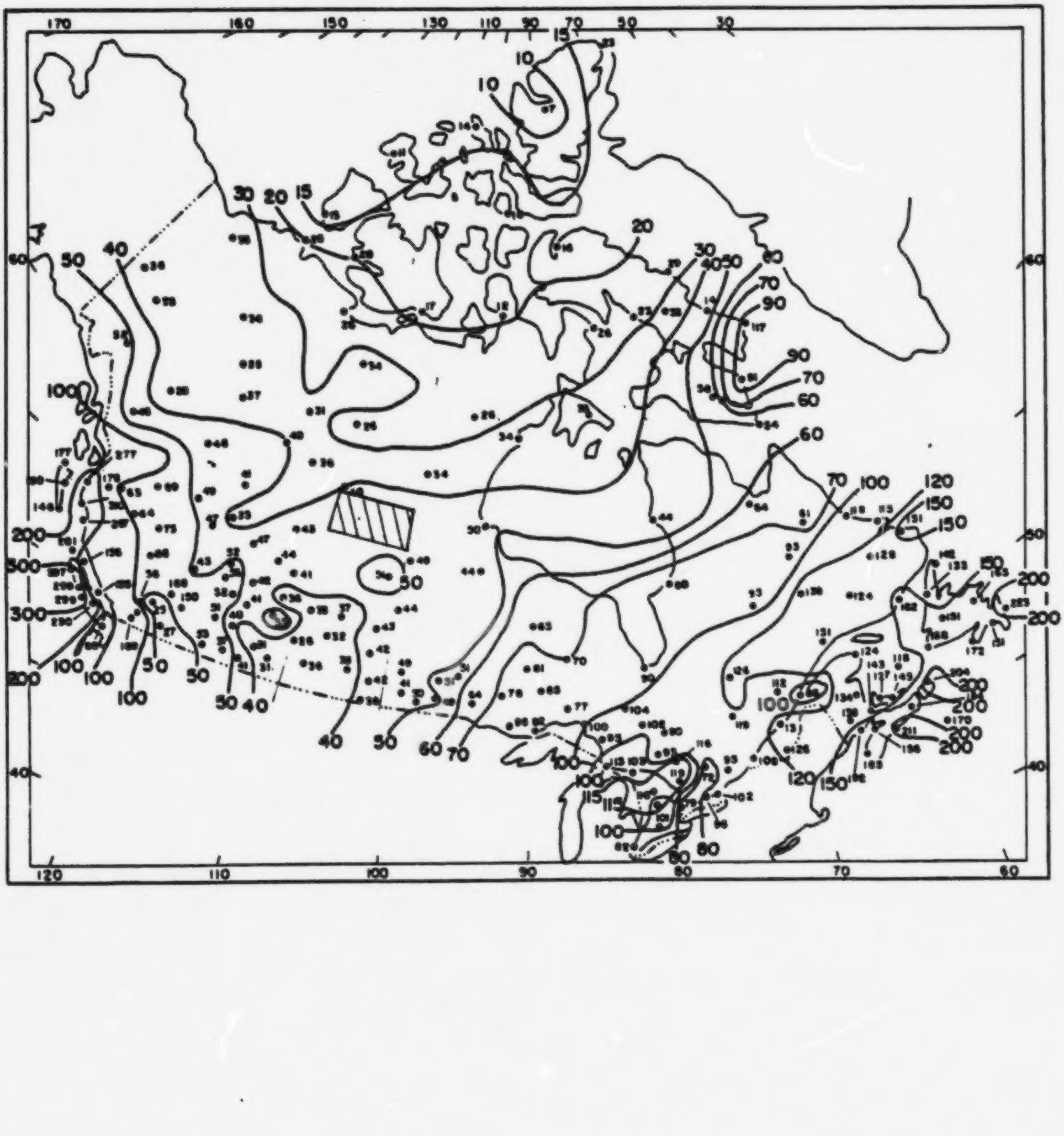
170
160
150
130
110
90
70
50
30
120
110
100
90
80
70
60
40
50
10
15
20
30
40
50
60
70
90
100
120
150
200
300

TABLE B5.5.1: BIOACCUMULATION FACTORS FOR RADIONUCLIDES IN GUNNAR TAILINGS VEGETATION (from data in BEAK, 1986)

Analytical Parameter	Bioaccumulation Factor[1] Typha latifolia Gunnar Main	 Carex aquatilis Frog Pond	 Carex aquatilis Langley Bay
U-238	0.0042	0.0047	< 0.001
Ra-226	0.0025	0.00088	0.0080
Th-232	< 0.016	< 0.011	< 0.011
Th-230	0.00048	< 0.0002	< 0.0004
Th-228	0.029	< 0.0034	0.020
Pb-210	0.0088	0.0075	0.011

---

[1] Wet weight activity ratio of above-ground plant material and associated root zone soils (B_V).

TABLE B5.5.2: SOIL TO PLANT TRANSFER COEFFICIENTS FOR ARSENIC

Species	Plant Concentration (mg/kg) (fresh weight)	Soil Concentration (mg/kg) (dry)	Bv	Reference
Lemon Seedlings				
leaves	0.20*	5	0.04	Liebig et al. (1959)
stems	65*	5	13	
leaves	0.26*	10	0.026	
roots	300*	10	30	
leaves	0.13*	2	0.065	
roots	33*	2	16.5	
leaves	0.14*	5	0.028	
roots	150*	5	30	
Mustard (common)				
tops	L 0.25	92	-	Williams (1940)
roots	8.5		0.092	
Potatoes				
peelings	47.9	321	0.15	Steevens et al. (1972)
flesh	0.3	321	0.0009	
peelings	1.1	25	0.044	
flesh	0.4	25	0.016	
peelings	1.6	14.3	0.11	
flesh	0.2	14.3	0.014	
peelings	0.5	42.9	0.012	
flesh	0.1	42.9	0.0023	
peelings	0.4	21.4	0.019	
flesh	0.2	21.4	0.0093	
peelings	1.6	23.7	0.068	
flesh	0.4	23.7	0.017	
peelings	2.3	21.4	0.11	
flesh	0.1	21.4	0.0047	
peelings	53.7	321	0.17	
flesh	0.6	321	0.002	
peelings	5.2	20	0.26	
flesh	0.1	20	0.005	
flesh	0.6	321	0.002	
peelings	5.2	20	0.26	
flesh	0.1	20	0.005	
Agrostis tennuis				
young leaves	38*	23,200	0.0016	Porter and Peterson (1975)
medium leaves	120*		0.0052	
old leaves	280*		0.012	
stems	40*		0.0017	
inflorescences	130*		0.0056	
seeds	500*		0.022	
Blueberry (lowbush)				
leaves	0.20*	15	0.0133	Anastasia and Kender (1973)
stems	0.068*	15	0.0045	
roots	0.60*	15	0.040	
leaves	0.89*	30	0.030	
stems	0.99*	30	0.033	
roots	13*	30	0.43	
leaves	1.7*	45	0.038	
stems	1.9*	45	0.042	
roots	23*	45	0.51	
leaves	2.0*	60	0.03	
stems	0.17*	60	0.0028	
roots	30*	60	0.5	
Clover Leaves	3*	60	0.05	Williams (1940)
Coastal Bermuda Grass				
foliage	119*	2.0	60	McBee et al. (1967)
	26*		13	
	29*	2.5	12	
	1.3*		0.52	
	480*	2.5	190	
	9.7*		3.9	
Cotton				
new leaves	2.6*	6	0.43	Wilkinson and Handcastle (1969)
old leaves	7.6*	6	1.3	

TABLE B5.5.2: SOIL TO PLANT TRANSFER COEFFICIENTS FOR ARSENIC

Species	Plant Concentration (mg/kg) (fresh weight)	Soil Concentration (mg/kg) (dry)	Bv	Reference
Cottonseed	0.025*	9.8	-	Baker et al. (1976)
	0.025*	20.0	0.0026	
	0.038*	120.0	0.00032	
	3.0*		0.033	
Daisy	3.0*	92	0.033	Williams (1940)
Potato Tubers	0.37	0	-	Baker et al. (1976)
	0.36	9.8	0.037	
	0.41	20	0.021	
	0.70	120	0.0058	
Rhododendron Leaves	2	130	0.015	Williams (1940)
Rice	0.64	0	-	Baker et al. (1976)
	0.68	9.8	0.0704	
	0.69	20	0.035	
	1.16	120	0.0097	
Soybeans	0.15	0	-	Baker et al. (1976)
	0.15	9.8	0.015	
	0.21	20	0.011	
	0.31	120	0.0026	
Spruce (White)				
roots	45	1,780	0.025	Rosehart and Lee (1973)
branch	2.8	1,780	0.0016	
trunk	6.4	1,780	0.0036	
leaves	9.5	1,780	0.0053	
Grass	12*	69	0.17	Ragaini et al. (1977)
	1.2*	93	0.013	
	1.2*	94	0.013	
	1.0*	24	0.042	
	7.5*	110	0.068	
	0.68*	24	0.028	
	0.75*	36	0.021	
	15*	100	0.15	
	4.8*	49	0.098	
Grass (Sporobolus airoides)				
(soil)	-	-	0.0025*	Dreeson et al. (1982)
(tailings)	-	-	0.0011*	
Shrub (Atriplex canescens)				
(soil)	-	-	0.006*	Dreeson et al. (1982)
(tailings)	-	-	0.0038*	

* Calculated from concentrations reported on a dry mass basis, assuming fresh weight = 4 x dry weight.

TABLE B5.5.3: SOIL TO PLANT TRANSFER COEFFICIENTS FOR NICKEL

Species	Plant Concentration (mg/kg) (fresh weight)	Soil Concentration (mg/kg) (dry)	B_v	Reference
Wavy hair-grass (*Deschampsia flexuosa*) (leaves)	150*	1850.7	0.081	Whitby (1974)
	61*	2336.8	0.026	
	33*	1391.8	0.024	
	9.2*	768.7	0.012	
	25*	214.5	0.12	
	3.8*	343.8	0.011	
	9.2*	35.4	0.26	
White birch (leaves)	38*	1850.7	0.021	Whitby (1974)
	24*	1391.8	0.017	
	14*	768.7	0.018	
	14*	214.5	0.065	
	16*	343.8	0.047	
	6.9*	34.9	0.20	
	9.7*	35.4	0.27	
Trembling aspen (leaves)	28*	1850.7	0.015	Whitby (1974)
	35*	2336.8	0.015	
	2.9*	768.7	0.0038	
	24*	214.5	0.11	
	11*	34.9	0.32	
	6.8*	35.4	0.19	
Composite of 10 Pasture Species	0.93*	105	0.0089	Ward *et al.* (1977)
	1.1*	87	0.13	
	0.75*	65	0.012	
	0.65*	60	0.011	
	0.23*	8	0.029	
Blueberry (leaves)	26*	1850.7	0.014	Whitby (1974)
	25*	2336.8	0.011	
	12*	1391.8	0.0086	
	5.9*	768.7	0.0077	
	9.0*	214.5	0.042	
	8.7*	343.8	0.025	
	4.4*	34.9	0.13	
	3.9*	35.4	0.11	

TABLE B5.5.3: SOIL TO PLANT TRANSFER COEFFICIENTS FOR NICKEL

Species	Plant Concentration (mg/kg) (fresh weight)	Soil Concentration (mg/kg) (dry)	B_v	Reference
Red maple (leaves)	26*	1850.7	0.014	Whitby (1974)
	22*	2336.8	0.0094	
	10*	1391.8	0.0072	
	5.7*	768.7	0.0074	
	8.1*	214.5	0.038	
	12*	343.8	0.035	
	4.6*	34.9	0.13	
	3.9*	35.4	0.11	
Horsetail (leaves)	34*	1850.7	0.018	Whitby (1974)
	51*	2336.8	0.022	
	90*	1391.8	0.065	
	3.8*	768.7	0.0049	
	9.5*	343.8	0.028	
Grass (*Sporobolus airoides*)	-	- (soil)	0.015*	Dreeson *et al.* (1982)
	-	- (tailings)	1.7*	
Shrub (*Atriplex canescens*)	-	- (soil)	0.014*	Dreeson *et al.* (1982)
	-	- (tailings)	0.25*	
Buckwheat (roots)	62.5*	1043.4	0.060	Whitby (1974)
	83.8*		0.080	
	128*	1850.7	0.069	
	148*		0.080	
	221*	1391.8	0.159	
	53.3*		0.038	
	22.1*		0.016	
	58.8*	768.7	0.077	
	16.6*		0.022	
	36.0*		0.047	
	225*		0.293	
	73.1*	343.8	0.213	
	88.0*		0.256	
	46.7*		0.136	
	56.5*		0.164	
	319.6*	35.4	9.02	
	27.9*		0.788	

TABLE B5.5.3: SOIL TO PLANT TRANSFER COEFFICIENTS FOR NICKEL

Species	Plant Concentration (mg/kg) (fresh weight)	Soil Concentration (mg/kg) (dry)	B_v	Reference
Radish (roots)	288*	1391.8	0.207	Whitby (1974)
	167*		0.120	
	133*		0.096	
	75*		0.054	
	182*	768.7	0.237	
	37.2*		0.048	
	23.3*		0.030	
	5.5*		0.007	
	107*	214.5	0.499	
	51.5*		0.240	
	48.0*		0.224	
	20.7*		0.097	
	43.1*	343.8	0.108	
	37.3*		0.045	
	15.6*		0.045	
	16.7*	35.4	0.472	
	5.0*		0.141	
	5.0*		0.141	
	40.6*		1.15	

* Calculated assuming dry weight = 0.25 x fresh weight.

TABLE B5.6.1: FISH TISSUE RADIUM BIOACCUMULATION FACTORS (SUPPLEMENTAL)

Location	Species	Tissues Analyzed	Fish Flesh Concentration (Bq/kg) (fresh)	Water Concentration (ug/L)	BF (L/kg)	Reference
Beaverlodge Lake	lake trout	flesh + skin	-	-	3	Swanson (1983)
	lake whitefish	flesh + skin	-	-	20	
	white sucker	flesh + skin	-	-	100	
Gunnar Open Pit	northern pike	flesh	0.22*	0.09, 0.14, 0.13	2	Tones (1982)
			0.22*	$\bar{x}$ = 0.12	2	
			0.44*	(3 samples, 1 m depth)	4	
Fredette Lake	lake whitefish		1.9	LT 0.0037	GT 510	EPS (1978)
	lake whitefish		0.48	(1 sample)	GT 130	
	lake whitefish		0.52		GT 140	
	northern pike		1.2		GT 320	
	northern pike		0.2		GT 50	
	northern pike		0.13		GT 35	
	lake trout		0.22		GT 59	
	lake trout		0.59		GT 160	
Fredette Lake	lake whitefish	flesh	0.1	LT 0.005 (3 samples)	GT 6	Swanson (1982)
			GT 0.6	0.05 (1 sample)	GT 37	
			LT 0.1	$\bar{x}$ = GT 0.016	-	
			0.7		GT 40	
			0.2		GT 13	
			LT 0.1		-	
			0.1		GT 6	
			0.1		GT 6	
			LT 0.1		-	
			4.0		GT 250	
			LT 0.1		-	
			1.3		GT 80	
			LT 0.1		-	
			LT 0.1		-	
			LT 0.1		-	
			9.1		GT 570	
			LT 0.1		-	
Port Hope Harbour	brown bullhead	whole fish	LE 25	LE 0.037	-	BEAK (1985a)
Hidden Bay	white sucker	oil-free muscle	0.6**	0.007	86	John and Dalton (1985)
			0.6**		86	(fish data)
			LT 0.1**		LT 14	BEAK (1985b)
			LT 0.1**		LT 14	(water data)
Quirke Lake	white sucker	flesh	0.2	0.07	2.9	John and Dalton (1985)
			0.3		4.3	(fish data)
			1.2		17	BEAK (1985c)
						(water data)
Langley Bay (Station 3)	lake whitefish	flesh	4.3	0.19	23	D. Waite, EPS, Regina
	northern pike	flesh	0.41		2.2	(pers. comm., February 1986)

* Calculated assuming fresh weight = ash weight/0.011.

** Calculated assuming fresh weight = dry weight/0.2.

TABLE B5.6.2: FISH TISSUE URANIUM BIOACCUMULATION FACTORS

Location	Species	Tissues Analyzed	Fish Flesh Concentration (ug/kg) (fresh)	Water Concentration (ug/L)	BF (L/kg)	Reference
Beaverlodge Lake	lake trout	flesh	-	-	0.3	Lush and Swanson (1981)
		flesh + skin	-	-	0.1	Swanson (1983)
	lake whitefish	flesh	-	-	0.2	
		flesh + skin	-	-	1	
	white sucker	flesh	-	-	0.1	
		flesh + skin	-	-	2	
Gunnar open pit	northern pike	flesh	25*	708, 511, 382	0.046	Tones (1982)
			14*	x̄ = 534	0.026	Tones (1982)
			19*	(3 samples,	0.036	Tones (1982)
				1 m depth)		
Fredette Lake	lake whitefish	flesh	46.8	3 (mean of 4	16	Swanson (1982)
			12.6	samples,	4.2	
			4.6	Stations 1 and 2	1.5	
			LT 0.2		LT 0.07	
			LT 0.2		LT 0.07	
			4.6		1.5	
			10.2		3.4	
			2.9		1.0	
			LT 0.2		LT 0.07	
			10.2		3.4	
			17.6		5.9	
			7.4		2.5	
			1.7		0.6	
			25.5		8.5	
			29.4		9.8	
			3.7		1.2	
			L 0.2		LT 0.07	
			19.1		6.4	
			6.9		2.3	
			5.0		1.7	
			4.7		1.6	
Port Hope Harbour	brown bullhead	whole fish	LT 70	40	LE 1.8	BEAK (1985a)
Hidden Bay		oil-free	6**	3	2	John and Dalton (1985)
		muscle	8**		2.7	(fish data)
			6**		2	
			8**		2.7	BEAK (1985b)
			LT 20**		LT 6.6	(water data)
			LT 20**.		LT 6.6	
			8**		2.7	
			6**		2	
Gunnison National Forest, Colorado						
o Marshall Creek	brown trout	muscle + skin	-	-	5.9	Parkhurst et al. (1984)
			-	-	2.3	
o Tomichi Creek	brown trout	muscle + skin	-	-	0.08	
			-	-	0.33	

---

* Calculated assuming ash weight = 0.011 x fresh weight.

** Calculated assuming dry weight = 0.2 x fresh weight.

TABLE B5.6.3: FISH TISSUE Pb-210 BIOACCUMULATION FACTORS

Location	Species	Tissues Analyzed	Fish Flesh Concentration (Bq/kg) (fresh)	Water Concentration (ug/L)	BF (L/kg)	Reference
Beaverlodge Lake	lake trout	flesh	-	-	18	Lush and Swanson (1981)
		flesh + skin	-	-	10	Swanson (1983)
	lake whitefish	flesh	-	-	18	
		flesh + skin	-	-	140	
	white sucker	flesh	-	-	12	
		flesh + skin	-	-	160	
Gunnar Open Pit	northern pike	flesh	0.66	0.12, 0.05	11	Tones (1982)
			1.5	LT 0.02	25	
			2.2	(3 samples, 1 m depth)	37	
				$\bar{x}$ = 0.06		
Fredette Lake	lake whitefish	flesh	LT 0.2	0.02, 0.03,	GT 10	EPS (1982)
			GT 0.6	LT 0.02, 0.02	GT 30	
			0.5	(2 samples each,	25	
			0.2	Stations 1 and 2)	10	
			0.8	$\bar{x}$ = 0.02	40	
			0.3		15	
			2.9		150	
			LT 1.4		GT 70	
			LT 0.1		GT 5	
			LT 0.2		GT 10	
			0.2		10	
			LT 0.2		GT 10	
			0.4		20	
			0.2		10	
			0.2		10	
			LT 0.2		GT 10	
			LT 0.2		GT 10	
			0.7		35	
			LT 0.2		GT 10	
Hidden Bay	white sucker	oil-free muscle	2.6**	LT 0.02	GT 130	John and Dalton (1985)
			2.4**		GT 120	(fish data)
			LT 6**		GT 300	BEAK (1985b)
			LT 6**		GT 300	(water data)
Langley Bay	lake whitefish	flesh	4.1	LT 0.037	GT 1,100	D. Waite, EPS, Regina
	northern pike	flesh	0.59		GT 16	(pers. comm.,
						February 1986)
Quirke Lake	white sucker	flesh	1.5	0.37, 0.28, 0.087	6	John and Dalton (1985)
			1.3	$\bar{x}$ = 0.25	5.2	(fish data)
			0.66		2.6	BEAK (1985b)
						(water data)

* Calculated assuming fresh weight = ash weight/0.011.

** Calculated assuming fresh weight = dry weight/0.2.

TABLE B5.6.4: FISH TISSUE ARSENIC BIOACCUMULATION FACTORS

Location	Species	Tissues Analyzed	Fish Flesh Concentration (mg/kg) (fresh)	Water Concentration (mg/L)	BF (L/kg)	Reference
Laboratory Bioassay	Green Sunfish	Whole Fish	33.4	100	0.33	Sorenson (1976)
			541.2	500	1.08	
			581.6	1,000	0.58	
Pukaskwa National Park						
o German Lake	White Sucker	Dorsal muscle	0.01	L 0.0005	GT 20	Schiefer and Lush (1984)
o White River	Northern Pike	Dorsal muscle	0.04	0.0005	80	
	White Sucker	Dorsal muscle	0.01	L 0.0005	GT 20	
	White Sucker	Dorsal muscle	0.01	L 0.0005	GT 20	
	White Sucker	Dorsal muscle	0.01	L 0.0005	GT 20	
	White Sucker	Dorsal muscle	0.02	0.001	20	
	Brook Trout	Dorsal muscle	0.01	L 0.0005	GT 20	
	Brook Trout	Dorsal muscle	0.01	0.001	10	
	Shad	Dorsal muscle	0.12	0.0005	240	
	Yellow Walleye	Dorsal muscle	0.02	0.0005	40	
o Widgeon Lake	Brook Trout	Dorsal muscle	0.01	L 0.0005	GT 20	
	White Sucker	Dorsal muscle	0.01	L 0.0005	GT 20	
o Willow Lake	Brook Trout	Dorsal muscle	0.01	L 0.0005	GT 20	
	White Sucker	Dorsal muscle	0.01	L 0.0005	GT 20	
o Berkstrom Lake	Yellow Perch	Whole body	0.01	L 0.0005	GT 20	
o Tagouche Lake	Northern Pike	Dorsal muscle	0.01	L 0.0005	GT 20	
	Yellow Perch	Whole body	0.01	L 0.0005	GT 20	
o Sund Lake	Yellow Perch	Whole body	0.01	0.0005	20	
	Northern Pike	Dorsal muscle	0.01	0.0005	20	
o Buchanan Lake	Lake Trout	Dorsal muscle	0.01	L 0.0005	GT 20	
o Holdoms Lake	Smelt	Whole body	0.01	0.0005	20	
o Gilberts Lake	Yellow Perch	Whole body	0.01	L 0.0005	GT 20	
o Ahdik Lake	Yellow Perch	Whole body	0.02	L 0.0005	GT 40	
o Old Coat Lake	Northern Pike	Dorsal muscle	0.01	L 0.0005	GT 20	
o Lake 6A22	Brook Trout	Dorsal muscle	0.01	L 0.0005	GT 20	
o Beaver Lake	Northern Pike	Dorsal muscle	0.01	0.0005	20	
	Yellow Perch	Whole Body	0.01	0.0005	20	
Outdoor Pool Bioassays	Bluegill	Whole Body - adult	2.61	1.02	2.6	Gilderhus (1966)
		Edible Flesh - adult	1.36	1.02	1.3	
		Whole Body - Immature	2.24	1.02	2.2	
		Whole Body - adult	0.66	0.26	2.5	
		Edible Flesh - adult	0.47	0.26	1.8	
		Whole Body - immature	0.97	0.26	3.7	
		Whole Body - adult	0.39	0.05	7.8	
		Edible Flesh - adult	0.25	0.05	5	
		Whole body - immature	0.52	0.05	10	
		Whole Body - adult	5.49	2.28	2.4	
		Edible Flesh - adult	3.16	2.28	1.4	
		Whole Body - immature	5.60	2.28	2.5	
		Whole Body - adult	1.16	0.61	1.9	
		Edible Flesh - adult	0.67	0.61	1.1	
		Whole Body - immature	1.51	0.61	2.5	
		Whole Body - adult	0.14	0.01	14	
		Edible Flesh - adult	0.19	0.01	19	
		Whole Body - immature	0.12	0.01	12	
		Whole Body - adult	11.6	9.04	1.3	
		Edible Flesh - adult	5.0	9.04	0.6	
		Whole Body - immature	11.7	9.04	1.3	
		Whole Body - adult	1.72	1.74	1.0	
		Edible Flesh - adult	0.76	1.74	0.4	
		Whole Body - immature	1.80	1.74	1.0	
		Whole Body - adult	0.53	0.26	2.0	
		Edible Flesh - adult	0.49	0.26	1.9	
		Whole Body - immature	0.57	0.26	2.2	

TABLE B5.6.4: FISH TISSUE ARSENIC BIOACCUMULATION FACTORS

Location	Species	Tissues Analyzed	Fish Flesh Concentration (mg/kg) (fresh)	Water Concentration (mg/L)	BF (L/kg)	Reference
Baker Creek mouth, Giant Mine, Yellowknife, N.W.T.	Longnose Sucker	Muscle	0.28	0.069	4.1	Falk et al. (1973)
	Whitefish	Muscle	0.22	0.069	3.2	
		Liver	0.87	0.069	13	
	Northern Pike	Muscle	0.31	0.069	4.5	
		Liver	0.70	0.069	10	
Yellowknife Bay	Whitefish	Muscle	L 0.2	0.14	L 1.4	
		Liver	L 0.2	0.14	L 1.4	
	Northern Pike	Liver	0.73	0.14	5.2	
Grace Lake, Yellowknife, N.W.T.	Northern Pike	Muscle	1.69	0.035	48	
		Liver	0.96	0.035	27	
	Walleye	Muscle	0.29	0.035	8.3	
		Liver	1.62	0.035	46	
	Whitefish	Muscle	0.28	0.035	8.0	
		Liver	0.53	0.035	15	
Kam Lake	Whitefish	Muscle	0.28	2.25	0.1	
		Liver	0.80	2.25	0.4	
	Northern Pike	Muscle	3.22	2.25	1.4	
		Liver	2.23	2.25	1.0	
Yellowknife Bay	Northern Pike	Muscle	0.31	0.005	62	Falk et al. (1973)
		Liver	0.32	0.005	64	
	Whitefish	Muscle	L 0.2	0.005	L 40	
		Liver	0.24	0.005	48	
Labine Bay	Lake Cisco	Muscle	0.23	0.019	12	
Ho-Hum Lake	Lake Cisco	Liver	0.48	0.007	69	
	Northern Pike	Muscle	0.34	0.007	49	
Camsell River	Arctic Grayling	Muscle	0.38	0.033	12	
Lake Michigan	Alewife	Whole body	0.59	0.001	590	Copeland et al. (1973)
	Smelt	Whole body	0.49	0.001	490	
	Spottail Shiner	Whole body	0.13	0.001	130	
	Coho Salmon	Muscle	0.18	0.001	180	
	Yellow Perch	Muscle	L 0.02	0.001	L 20	
	Lake Trout	Muscle	0.64	0.001	640	
	Brown Trout	Muscle	0.35	0.001	350	
	Whitefish	Muscle	0.31	0.001	310	
Laboratory Bioassay	Rainbow Trout	Muscle	3.0	2.95	1.0	Dixon and Sprague (1981)

TABLE B3.6.5: FISH TISSUE NICKEL BIOACCUMULATION FACTORS

Location	Species	Tissues Analyzed	Fish Flesh Concentration (mg/kg) (fresh)	Water Concentration (mg/L)	BF (L/kg)	Reference
Laboratory Bioassay	Carp	46-hr-old eggs exposed from time of fertilization	0.35	0.0014	250.0	Blaylock and Frank (1979)
			36.26	3.20	11.3	
			52.63	6.30	8.4	
			61.04	9.70	6.3	
Pukaskwa National Park						
o German Lake	White Sucker	Dorsal muscle	0.08	L 0.001	GT 80	Schiefer and Lush (1984)
o White River	Northern Pike	Dorsal muscle	0.04	L 0.001	GT 40	
	White Sucker	Dorsal muscle	0.10	L 0.001	GT 100	
	White Sucker	Dorsal muscle	0.06	L 0.001	GT 60	
	White Sucker	Dorsal muscle	0.12	L 0.001	GT 120	
	White Sucker	Dorsal muscle	0.10	L 0.001	GT 100	
	White Sucker	Dorsal muscle	0.08	L 0.001	GT 80	
	Brook Trout	Dorsal muscle	0.12	L 0.001	GT 120	
	Brook Trout	Dorsal muscle	0.10	L 0.001	GT 100	
	Shad	Dorsal muscle	0.09	L 0.001	GT 90	
	Yellow Walleye	Dorsal muscle	0.12	L 0.001	GT 120	
o Widgeon Lake	Brook Trout	Dorsal muscle	0.16	L 0.001	GT 160	
	White Sucker	Dorsal muscle	0.08	L 0.001	GT 80	
o Willow Lake	Brook Trout	Dorsal muscle	0.06	L 0.001	GT 60	
	White Sucker	Dorsal muscle	0.14	L 0.001	GT 140	
o Berkstrom Lake	Yellow Perch	Whole body	0.14	L 0.001	GT 140	
o Tagouche Lake	Northern Pike	Dorsal muscle	0.10	L 0.001	GT 100	
	Yellow Perch	Whole body	0.20	L 0.001	GT 200	
o Sund Lake	Yellow Perch	Whole body	0.10	L 0.001	GT 100	
	Northern Pike	Dorsal muscle	0.08	L 0.001	GT 80	
o Buchanan Lake	Lake Trout	Dorsal muscle	0.10	L 0.001	GT 100	
o Holdoms Lake	Smelt	Whole body	0.24	L 0.001	GT 240	
o Gilberts Lake	Yellow Perch	Whole body	0.14	L 0.001	GT 140	
o Ahdik Lake	Yellow Perch	Whole body	0.24	L 0.001	GT 240	
o Old Coat Lake	Northern Pike	Dorsal muscle	0.08	L 0.001	GT 80	
o Lake 6A22	Brook Trout	Dorsal muscle	0.04	L 0.001	GT 40	
o Beaver Lake	Northern Pike	Dorsal muscle	0.10	L 0.001	GT 100	
	Yellow Perch	Whole body	0.24	L 0.001	GT 240	
Michigan Drainage Ditch	Creek Chub	Whole body	1.1	0.005	220	Fitchko (1986)
	Green Sunfish	Whole body	0.7	0.020	35	
	Cyprinid Species	Whole body	0.6	0.020	30	
	Cyprinid Species	Whole body	0.6	0.010	60	
	Cyprinid Species	Whole body	0.5	0.010	50	
	Cyprinid Species	Whole body	0.5	0.010	50	
	Cyprinid Species	Whole body	0.5	L 0.005	GT 100	
Illinois River	Northern Pike	Edible flesh	0.15 (0.08-0.19)	0.002 (0.001-0.005)	75	Mathis and Cummings (1973)
	Largemouth Bass	Edible flesh	0.11 (0.05-0.23)	0.002	55	
	Smallmouth Bass	Edible flesh	0.13 (0.08-0.19)	0.002	65	
	White Bass	Edible flesh	0.08 (0.04-0.12)	0.002	40	
	Spotted Gar	Edible flesh	0.18 (0.07-0.28)	0.002	90	
	Bigmouth Buffalo	Edible flesh	0.10 (0.02-0.18)	0.002	50	
	Gizzard Shad	Edible flesh	0.28 (0.06-0.52)	0.002	140	
	Shorthead Redhorse	Edible flesh	0.14 (0.09-0.22)	0.002	70	
	Quillback	Edible flesh	0.18 (0.15-0.45)	0.002	90	
	Carp	Edible flesh	0.19 (0.04-0.28)	0.002	95	
Black Creek, Virginia	Bluehead Chub	Whole body	2.5 (1.7-15.1)	0.004 (0.001-0.007)	630	Van Hassel et al. (1980)
		Whole body	2.5 (0.2-6.7)	0.003 (0.001-0.005)	830	
		Whole body	2.0 (0.8-3.7)	0.003 (0.001-0.006)	670	
	Blacknose Dace	Whole body	3.0 (0.4-8.8)	0.004	750	
		Whole body	2.9 (0.4-8.8)	0.003	970	
		Whole body	2.0 (0.8-3.7)	0.003	670	
	Fantail Darter	Whole body	5.9 (0.2-15.4)	0.004	1,500	
		Whole body	3.4 (0.2-10.3)	0.003	1,100	
		Whole body	2.9 (0.2-11.8)	0.003	970	

TABLE B5.6.5: FISH TISSUE NICKEL BIOACCUMULATION FACTORS

Location	Species	Tissues Analyzed	Fish Flesh Concentration (mg/kg) (fresh)	Water Concentration (mg/L)	BF (L/kg)	Reference
Wanapitei River	Northern Pike	Muscle	13.3	0.032	420	Hutchinson et al. (1980)
		Liver	15.4	0.032	480	
		Kidney	27.7	0.032	870	
		Gill	17.3	0.032	540	
	Yellow Pickerel	Muscle	13.8	0.032	430	
		Liver	14.4	0.032	450	
		Kidney	51.6	0.032	1,600	
		Gill	16.0	0.032	500	
	Northern Rock Bass	Muscle	12.5	0.032	390	
		Liver	17.0	0.032	530	
		Kidney	17.3	0.032	540	
		Gill	31.7	0.032	990	
	Brown Bullhead	Muscle	9.5	0.032	300	
		Liver	10.7	0.032	330	
		Kidney	11.8	0.032	370	
		Gill	11.1	0.032	350	
	Redhorse Sucker	Muscle	12.9	0.032	400	
		Liver	14.5	0.032	450	
		Kidney	14.1	0.032	440	
		Gill	12.2	0.032	380	
	White Sucker	Muscle	13.2	0.032	410	
		Liver	16.5	0.032	520	
		Kidney	14.0	0.032	440	
		Gill	12.6	0.032	390	

TABLE B5.6.6: FISH TISSUE THORIUM BIOACCUMULATION FACTORS

Location	Species	Tissues Analyzed	Fish Flesh Concentration (Bq/kg) (fresh)	Water Concentration (ug/L)	BF (L/kg)	Reference
Hidden Bay	white sucker	oil-free muscle	0.002*	LT 0.01	GT 0.2	John and Dalton (1985)
			0.002*		GT 0.2	(fish data)
			0.000054*		GT 0.005	BEAK (1985b)
			0.000072*		GT 0.007	(water data)
Quirke Lake	white sucker	flesh	LT 0.0002	LT 0.03 (mean of 3 values)	-	John and Dalton (1985)
			LT 0.0002		-	(fish data)
			LT 0.0002		-	BEAK (1985c)
						(water data)

* Calculated assuming fresh weight = dry weight/0.2.

TABLE B5.6.7: FISH TISSUE Po-210 BIOACCUMULATION FACTORS

Location	Species	Tissues Analyzed	Fish Flesh Concentration (Bq/kg) (fresh)	Water Concentration (ug/L)	BF (L/kg)	Reference
Hidden Bay	white sucker	oil-free	1*	LT 0.02	GT 50	John and Dalton (1985)
		muscle	1.6*		GT 80	(fish data)
			1.4*		GT 70	BEAK (1985b)
			1.6*		GT 80	(water data)
			-	-	50	Thompson et al. (1972)

* Calculated assuming fresh weight = dry weight/0.2.

TABLE B5.6.8: AQUATIC PLANT TISSUE URANIUM BIOACCUMULATION FACTORS

Species	Plant Concentration (mg/kg) (wet)	Water Concentration (mg/L)	BF (L/kg)	Reference
Freshwater Plants	0.7	0.01	70	Dvorak and Lewis (1978)
Cladophora	8.12* one measurement, 1984	$\bar{x}$ 0.065; 34 observations in 1982	120	BEAK (1985d)
Freshwater Plants	-	-	1,000	Thompson *et al.* (1972)
Freshwater Plants	-	-	62-215	Blaylock (1982)
Freshwater Plants	-	-	400	Blaylock (1982)

* Converted from dry weight concentrations; assuming dry weight = 0.1 x wet weight.

TABLE B5.6.9: AQUATIC PLANT TISSUE THORIUM BIOACCUMULATION FACTORS

Species	Plant Concentration (mg/kg) (wet)	Water Concentration (mg/L)	BF (L/kg)	Reference
Freshwater Plants	1.3	0.03	43	Dvorak and Lewis (1978)
Freshwater Plants	-	-	925	Kulikov (1973)
Freshwater Plants	-	-	1,500	Thompson *et al.* (1972)

TABLE B5.6.10: AQUATIC PLANT TISSUE RADIUM BIOACCUMULATION FACTORS

Species	Plant Concentration (Bq/kg) (wet)	Water Concentration (Bq/L)	BF (L/kg)	Reference
Freshwater Plants	-	-	1,500	Thompson *et al.* (1972)
Freshwater Plants	-	-	752-1,200	Blaylock (1982)
Freshwater Plants	-	-	960-6,900	Blaylock (1982)
Cladophora	100 (one measurement, 1984)	LT 0.037	-	BEAK (1985d)
Sagittaria	6.5	0.038	170	BEAK (1985e)

TABLE B5.6.11: AQUATIC PLANT TISSUE LEAD BIOACCUMULATION FACTORS

Species	Plant Tissue	Plant Concentration (Bq* or mg/kg)	Water Concentration (Bq* or mg/L)	BF (L/kg)	Reference
Freshwater Plants*	-	-	-	200	Thompson et al. (1972)
Coontail (Ceratophyllum demersum)	Whole Plant	1.02	0.013	79	Cowgill (1974)
	Whole Plant	0.90	0.015	60	
Pondweed (Potamogeton crispus)	Whole Plant	0.79	0.013	61	Cowgill (1974)
	Buds	0.67	0.013	52	
Pondweed (Potamogeton pradongus)	Whole Plant	0.85	0.013	65	Cowgill (1974)
Yellow Water Lily (Nuphar advena)	Flowers	1.06	0.013	82	Cowgill (1974)
	Flower Stalks	1.02	0.013	79	
	Leaves	1.12	0.013	86	
	Stems	0.82	0.013	63	
Yellow Water Lily (Nuphar advena)	Flowers	1.31	0.015	87	Cowgill (1974)
	Flower Stalks	1.37	0.015	91	
	Leaves	1.41	0.015	94	
	Stems	1.29	0.015	86	
Pickerelweed (Pontederia cordata)	Flowers	1.07	0.013	82	Cowgill (1974)
	Leaves	1.03	0.013	79	
	Stems	0.92	0.013	71	
Pickerelweed (Pontederia cordata)	Flowers	1.19	0.015	79	Cowgill (1974)
	Leaves	1.06	0.015	71	
	Stems	0.92	0.015	61	
Water Lily (Nymphaea odorata)	Flowers	1.04	0.013	80	Cowgill (1974)
	Flower Stalks	1.01	0.013	78	
	Leaves	1.02	0.013	79	
	Stems	0.93	0.013	72	
Water Lily (Nymphaea odorata)	Flowers	1.15	0.015	77	Cowgill (1974)
	Flower Stalks	1.19	0.015	79	
	Leaves	1.26	0.015	84	
	Stems	1.17	0.015	78	
Swamp Loosestrife (Decadon verticillatus)	Leaves	1.06	0.013	82	Cowgill (1974)
	Stems	1.03	0.013	79	
	Roots	0.84	0.013	65	
Swamp Loosestrife (Decadon verticillatus)	Leaves	1.34	0.015	89	Cowgill (1974)
	Stems	1.32	0.015	88	
	Roots	1.22	0.015	81	
Buttercup (Ranunculus fluitans)	Whole Plant (above roots)	-	-	58	Dietz (1973)
Yellow Water Lily (Nuphar luteum)	Whole Plant (above roots)	-	-	10	Dietz (1973)
Water Milfoil (Myriophyllum spicatum)	Whole Plant (above roots)	-	-	18	Dietz (1973)
Duckweed (Lemna minor)	Whole Plant	1.33	0.0157	85	Hutchinson and Czyrska (1975)
Horsetail (Equisetum arvense)	Whole Plant (above ground)	0.23	L 0.005	GT 46	Ray and White (1979)
Pondweed (Potamogeton pectinatus)	Whole Plant	0.24	0.001	240	Abo-Rady (1980)
Pondweed (Potamogeton pectinatus)	Whole Plant	0.68	0.001	680	Abo-Rady (1980)
Horned Pondweed (Zannichellia palustris)	Whole Plant	0.80	0.001	800	Abo-Rady (1980)

* Lead-210 data; other data based on stable lead.

TABLE B5.6.12: AQUATIC PLANT TISSUE POLONIUM BIOACCUMULATION FACTORS

Species	Plant Concentration (Bq/kg)	Water Concentration (Bq/L)	BF (L/kg)	Reference
Freshwater Plants	-	-	2,000	Thompson *et al.* (1972)

TABLE B5.6.13: AQUATIC PLANT TISSUE ARSENIC BIOACCUMULATION FACTORS

Species	Plant Concentration (mg/kg) (wet)	Water Concentration (mg/L)	BF (L/kg)	Reference
Hornwort (*Ceratophyllum demersum*	24* 13*	- -	200* 130*	Hutchinson (1975)
Duckweed (*Lemna perpusilla*)			111 74 34 97 63 37	Rodgers *et al.* (1978)
Freshwater Plants	4.2	0.06	70	Dvork and Lewis (1978)
Hydrophila lacustris	-	-	2	U.S. EPA (1985)
Alligator Weed (*Alternanthera philoxeroides*)	-	-	3	U.S. EPA (1985)
Duckweed (*Lemna minor*)	-	-	5	U.S. EPA (1985)
Water Hyacinth (*Eichhornia crassipes*)	-	-	2	U.S. EPA (1985)
Freshwater Plants	-	-	333	Chapman *et al.* (1968)

* Converted to a wet weight basis, assuming dry weight = 0.1 wet weight.

TABLE B5.6.14: AQUATIC PLANT TISSUE NICKEL BIOACCUMULATION FACTORS

Species	Plant Tissue	Plant Concentration (mg/kg) (wet)*	Water Concentration (mg/L)	BF (L/kg)	Reference
Yellow Water Lily (*Nuphar luteum*)	Whole Plant (above root stock)	-	0.01-0.16	45-64	Dietz (1973)
Arrowhead (*Sagittaria sagittifolia*)	Whole Plant (above root)	-	0.01-0.16	12	Dietz (1973)
Water Milfoil (*Myriophyllum spicatum*)	Whole Plant (above root)	-	0.01-0.16	28.6-35.4	Dietz (1973)
Duckweed (*Lemna valdiviana*)	Whole Plant	4.0	0.01	400	Hutchinson and Czyrska (1975)
		11.2	0.05	224	
		41.9	0.10	419	
		171	0.30	569	
		306.7	0.50	613	
		179.1	1.00	179	
Horsetail (*Equisetum palustre*) (Wanapitei River)	Root	10.1	0.053±0.029	191	Fitchko (1978)
	Stem	2.5	0.053±0.029	47	
	Root	24.6	0.043±0.024	570	
	Stem	3.6	0.043±0.024	84	
	Root	29.1	0.037±0.012	790	
	Stem	9.2	0.037±0.012	250	
	Root	4.1	0.058±0.036	71	
	Stem	2.4	0.058±0.036	41	
	Root	34.4	0.032±0.019	1,075	
	Stem	15.7	0.032±0.019	491	
	Root	18.2	0.028±0.019	650	
	Stem	6.8	0.028±0.019	240	
	Root	26.8	0.030±0.020	890	
	Stem	10.4	0.030±0.020	350	
	Root	28.2	0.021±0.014	1,340	
	Stem	7.1	0.021±0.014	340	
	Root	17.2	0.033±0.018	520	
	Stem	8.6	0.033±0.018	261	
(French River)	Root	10.7	0.015±0.007	710	
	Stem	2.7	0.015±0.007	180	
	Root	9.2	0.020±0.022	460	
	Stem	3.6	0.020±0.022	180	
	Root	2.3	0.005±0.003	460	
	Stem	1.2	0.005±0.003	240	
	Root	2.5	0.004±0.003	625	
	Stem	1.4	0.004±0.003	350	
(Pickerel River)	Root	2.1	0.003±0.003	700	
	Stem	1.5	0.003±0.003	500	
(Badger Lake)	Root	3.1	0.013±0.002	240	
	Stem	1.3	0.013±0.002	100	
Yellow Water Lily (*Nuphar variegatum*) (Wanapetei River)	Root	2.4	0.053±0.029	45	Fitchko (1978)
	Rhizome	1.8	0.053±0.029	34	
	Stem	2.7	0.053±0.029	51	
	Leaf	2.7	0.053±0.029	51	
	Peduncle	2.9	0.053±0.029	55	
	Flower	2.1	0.053±0.029	40	
	Root	5.3	0.032±0.019	170	
	Rhizome	1.9	0.032±0.019	59	
	Stem	3.3	0.032±0.019	100	
	Leaf	4.0	0.032±0.019	125	
	Peduncle	4.0	0.032±0.019	125	
	Flower	2.1	0.032±0.019	66	
	Root	5.3	0.028±0.019	189	
	Rhizome	2.0	0.028±0.019	71	
	Stem	4.6	0.028±0.019	160	
	Leaf	4.6	0.028±0.019	160	
	Peduncle	3.6	0.028±0.019	130	
	Flower	2.3	0.028±0.019	82	
	Root	5.3	0.030±0.0020	180	
	Rhizome	1.3	0.030±0.0020	43	
	Stem	3.9	0.030±0.0020	130	
	Leaf	5.1	0.030±0.0020	170	
	Peduncle	4.2	0.030±0.0020	140	
	Flower	1.7	0.030±0.0020	57	
	Root	2.0	0.021±0.014	95	
	Rhizome	1.6	0.021±0.014	76	
	Stem	2.2	0.021±0.014	100	
	Leaf	3.2	0.021±0.014	150	
	Peduncle	2.8	0.021±0.014	130	
	Flower	2.4	0.021±0.014	110	
	Root	1.5	0.033±0.018	46	
	Rhizome	1.4	0.033±0.018	42	
	Stem	3.0	0.033±0.018	91	
	Leaf	3.9	0.033±0.018	120	
	Peduncle	3.2	0.033±0.018	97	
	Flower	2.1	0.033±0.018	64	

TABLE B5.6.14: AQUATIC PLANT TISSUE NICKEL BIOACCUMULATION FACTORS

Species	Plant Tissue	Plant Concentration (mg/kg) (wet)*	Water Concentration (mg/L)	BF (L/kg)	Reference
Yellow Water Lily	Root	1.1	0.020±0.022	55	Fitchko (1978)
(*Nuphar variegatum*)	Rhizome	0.7	0.020±0.022	35	
(French River)	Stem	1.3	0.020±0.022	65	
	Leaf	1.4	0.020±0.022	70	
	Peduncle	1.2	0.020±0.022	60	
	Flower	1.2	0.020±0.022	60	
	Root	0.9	0.005±0.003	180	
	Rhizome	0.8	0.005±0.003	160	
	Stem	1.2	0.005±0.003	240	
	Leaf	1.2	0.005±0.003	240	
	Peduncle	1.0	0.005±0.003	200	
	Flower	0.7	0.005±0.003	140	
	Root	1.3	0.004±0.003	325	
	Rhizome	0.8	0.004±0.003	200	
	Stem	1.7	0.004±0.003	425	
	Leaf	1.3	0.004±0.003	325	
	Peduncle	1.1	0.004±0.003	275	
	Flower	0.6	0.004±0.003	150	
(Pickerel River)	Root	1.1	0.003±0.003	370	
	Rhizome	1.3	0.003±0.003	430	
	Stem	1.3	0.003±0.003	430	
	Leaf	1.3	0.003±0.003	430	
(Badger Lake)	Root	0.8	0.013±0.002	62	
	Rhizome	0.9	0.013±0.002	69	
	Stem	1.0	0.013±0.002	77	
	Leaf	1.0	0.013±0.002	77	
	Peduncle	0.9	0.013±0.002	69	
	Flower	0.8	0.013±0.002	62	
Water Lily	Root	4.1	0.037±0.012	110	Fitchko (1978)
(*Nymphaea odorata*)	Rhizome	1.8	0.037±0.012	49	
(Wanapetei River)	Stem	3.5	0.037±0.012	95	
	Leaf	5.8	0.037±0.012	160	
	Root	6.2	0.028±0.019	220	
	Rhizome	3.5	0.028±0.019	130	
	Stem	4.3	0.028±0.019	150	
	Leaf	3.6	0.028±0.019	130	
	Root	7.5	0.030±0.020	250	
	Rhizome	4.7	0.030±0.020	160	
	Stem	4.3	0.030±0.020	140	
	Leaf	5.4	0.030±0.020	180	
(French River)	Root	2.1	0.005±0.003	420	
	Rhizome	0.8	0.005±0.003	160	
	Stem	1.3	0.005±0.003	260	
	Leaf	1.2	0.005±0.003	240	
(Pickerel River)	Root	3.7	0.003±0.003	1,200	
	Rhizome	1.5	0.003±0.003	500	
	Stem	1.1	0.003±0.003	370	
	Leaf	1.1	0.003±0.003	370	
(Badger Lake)	Root	1.4	0.013±0.002	110	
	Rhizome	0.8	0.013±0.002	62	
	Stem	1.2	0.013±0.002	92	
	Leaf	1.1	0.013±0.002	85	
Floating Heart	Root	26.6	0.021±0.014	1,300	Fitchko (1978)
(*Nymphoides cordatum*)	Stem	12.5	0.021±0.014	600	
(Wanapetei River)	Leaf	10.8	0.021±0.014	510	
(French River)	Root	15.2	0.015±0.007	1,000	
	Stem	4.0	0.015±0.007	270	
	Leaf	2.5	0.015±0.007	360	
	Root	5.1	9,929±0.022	260	
	Stem	2.9	0.020±0.022	150	
	Leaf	1.4	0.020±0.022	70	
	Root	1.9	0.005±0.003	380	
	Stem	1.7	0.005±0.003	340	
	Leaf	1.9	0.005±0.003	380	
	Stem	1.5	0.004±0.003	380	
	Leaf	1.6	0.004±0.003	400	
(Pickerel River)	Root	3.6	0.003±0.003	1,200	
	Stem	4.4	0.003±0.003	1,500	
	Leaf	1.8	0.003±0.003	600	
(Badger Lake)	Root	5.9	0.013±0.002	450	
	Stem	2.3	0.013±0.002	180	
	Leaf	1.4	0.013±0.002	110	
Pondweed	Whole Plant (?)	9.2	0.0030	310	Abo-Rady (1980)
(*Potamogeton pectinatus*)	Whole Plant	1.58	0.0038	420	
Horned Pondweel	Whole Plant	0.71	0.0030	240	
(*Zannichellia palustris*)	Whole Plant	1.07	0.0038	280	
(River Leine, West Germany)					

TABLE B5.6.14: AQUATIC PLANT TISSUE NICKEL BIOACCUMULATION FACTORS

Species	Plant Tissue	Plant Concentration (mg/kg) (wet)*	Water Concentration (mg/L)	BF (L/kg)	Reference
Pondweed	Stem	6.5	0.037±0.012	180	Fitchko (unpubl. data)
(*Potamogeton* spp.)	Leaf	46	0.037±0.012	1,200	
(Wanapetei River)	Root	30.1	0.037±0.012	800	
	Stem	4.9	0.053±0.029	93	
	Leaf	22.5	0.053±0.029	420	
	Root	10	0.053±0.029	190	
	Stem	3.5	0.012±0.010	290	
	Leaf	10.3	0.012±0.010	460	
	Root	23.1	0.012±0.010	1,900	
	Stem	16.6	0.021±0.014	790	
	Leaf	58.9	0.021±0.014	2,800	
	Root	17.3	0.021±0.014	820	
	Stem	36.0	0.032±0.019	1,100	
	Leaf	59.5	0.032±0.019	1,900	
	Root	22.3	0.032±0.019	700	
	Stem	12.2	0.030±0.020	410	
	Leaf	54.4	0.030±0.020	1,800	
	Root	26.2	0.030±0.020	870	
	Stem	15.7	0.033±0.018	480	
	Leaf	69.5	0.033±0.018	210	
	Root	24.7	0.033±0.018	750	
(French River)	Stem	7.3	0.015±0.007	490	
	Leaf	22.1	0.015±0.007	1,500	
	Stem	2.8	0.020±0.022	140	
	Leaf	7.5	0.020±0.022	380	
	Stem	1.7	0.005±0.003	340	
	Leaf	1.9	0.005±0.003	380	
	Stem	1.7	0.004±0.003	430	
	Leaf	2.1	0.004±0.003	530	
(Pickerel River)	Stem	1.9	0.003±0.003	630	
	Leaf	2.8	0.003±0.003	930	
	Stem	6.1	0.013±0.002	470	
	Root	6.4	0.013±0.002	490	
	Leaf	5.0	0.013±0.002	380	
Yellow Water Lily	Leaf	13.7	1.0	14	Fitchko (unpubl. data)
(*Nuphar* *varigetum*)	Stem	22.3	1.0	22	
(Alice Creek)	Root	12.4	1.0	12	
Horsetail	Stem	31.3	1.0	30	
(*Equisetum* *palustre*)	Root	38.3	1.0	38	
Pondweed	Stem	235.8	1.0	240	
(*Potamogeton* spp.)	Leaf	637.5	1.0	640	
	Root	116.5	1.0	120	
Coontail (*Ceratophyllum* *demersum*)	Whole Plant	0.24	0.00215	110	Cowgill (1974)
Waterweed	Whole Plant	0.14	0.00215	65	
(*Potamogeton* *crispus*)	Buds	0.15	0.00215	70	
Yellow Water Lily	Flowers	0.3	0.00215	140	
(*Nuphar* *advena*)	Flower Stalks	0.19	0.00215	88	
(Linsley Pond, Connecticut)	Leaves	0.24	0.00215	110	
	Stems	0.21	0.00215	98	

* Reported as dry weight plant concentrations. Converted here to wet weight concentrations, assuming dry weight = 0.1 x wet weight.

FIGURE B5.6.1: FREQUENCY OF OCCURRENCE OF FISH SPECIES IN SIX OR MORE LA CLOCHE MOUNTAIN LAKES IN RELATION TO pH. Vertical bar, lowest pH recorded; dashed line, stressed populations; solid line, populations which appear unaffected (from Harvey, 1979)

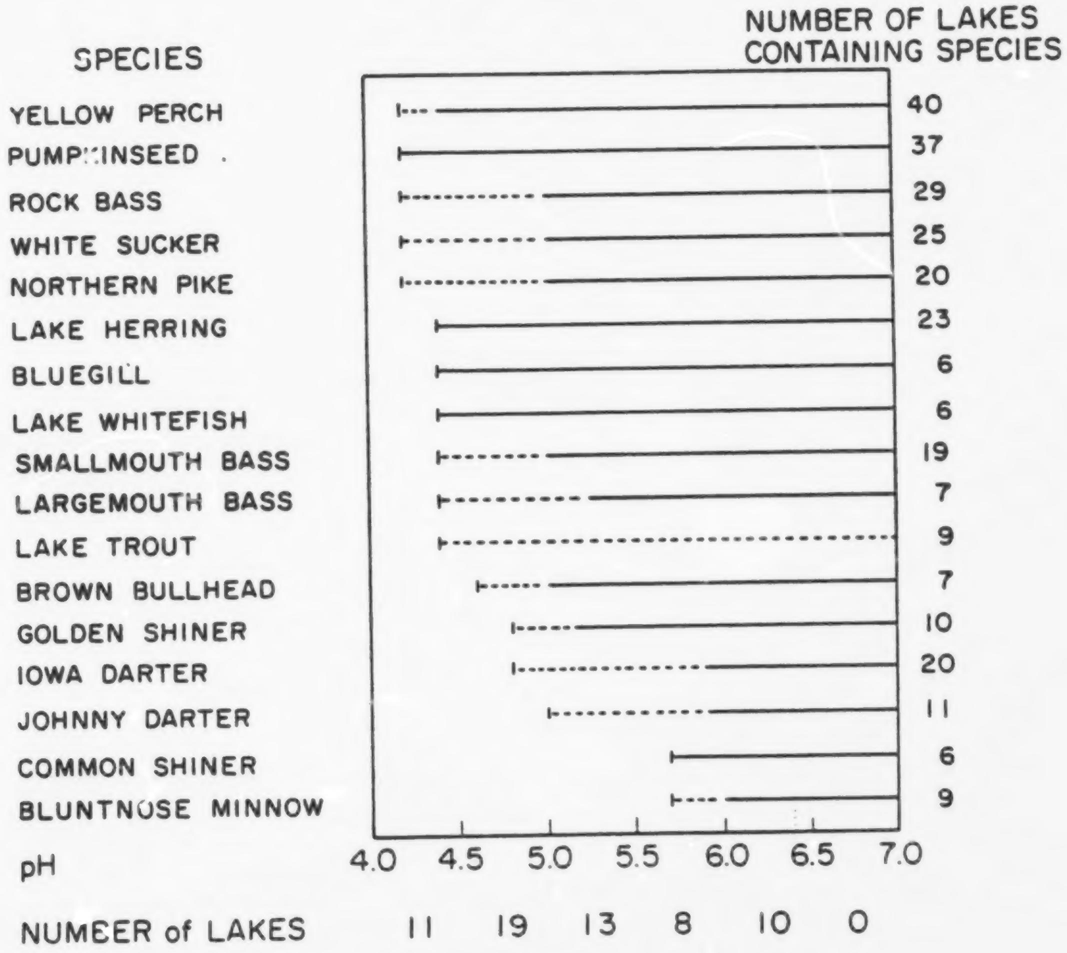

TABLE B5.7.1: WINTER UTILIZATION OF COMMON BROWSE SPECIES BY MOOSE

	Frequency of Occurrence in Moose Rumens (%)[2]		
	Game Harvest Area	Hecla Island	
Species[1]	1979	1978	1979
Willow	16.0	22.6	8.2
Balsam Fir	24.7	16.9	26.1
Dogwood	17.5	25.3	26.5
Mountain Ash	-	-	-
Aspen	29.8	7.5	8.8
Birch	4.9	11.0	3.0
Hazel	-	-	-
Balsam Poplar	2.7	6.9	4.8
Pin Cherry	-	-	-
Maple	2.7	6.6	21.9
Viburnum	-	-	-

[1] Preferred browse species according to Banfield (1974) and Euler (1979).

[2] Data from two Manitoba study areas (Zach et al., 1982).

TABLE B5.7.2: ANNUAL FOOD INTAKE OF MOOSE AND FRACTIONS LOCALLY CONSUMED

V	Food Type	Food Intake Rate (g/yr)		Fraction of Total Intake	
		dry[1]	fresh[2]	all sources (F)[3]	local (Fv)[3]
1	Water	-	1.8E7	0.811	0.405
2	Aquatic Plants	6.0E4	6.0E5	0.027	0.014
3	Browse	1.8E6	3.6E6	0.162	0.081
TOTAL		1.86E6	2.22E7 (Qb)	1.0	0.50

[1] Daily dry weight food intake from Belovsky (1975) converted to an annual value, assuming aquatic plants available for four months each year.

[2] Fresh weights derived from dry weights assuming 10% moisture in aquatic plants (Dietz, 1973) and 50% moisture in browse (Zach and Mayoh, 1982).

[3] Fraction of total fresh weight food intake (F) is adjusted by an occupancy factor to give Fv. The occupancy factor can vary between zero and one. A value of 0.5 is assumed in the table.

TABLE B5.7.3: FEED-TO-MEAT BIOACCUMULATION OF URANIUM SERIES RADIONUCLIDES, ARSENIC AND NICKEL IN RUMINANTS

Feed Contaminant	Ruminant Species	Bioaccumulation Factor[1]			Reference
		Muscle	Kidney	Liver	
U	Moose	0.030	(0.9)	(0.9)	Letourneau (1984)
	Caribou	0.002	(0.06)	(0.06)	
Th	Moose	0.005	(0.15)	(0.15)	Letourneau (1984)
	Caribou	0.0014	(0.042)	(0.042)	
Ra	Moose	0.020	(0.02)	(0.02)	Letourneau (1984)
	Caribou	0.010	(0.01)	(0.01)	
Pb	Moose	0.020	(0.46)	(1.06)	Letourneau (1984)
	Caribou	0.008	0.18	0.42	
	Reindeer	0.0005	0.06	0.1	
Po	Moose	0.300	(5.4)	(4.2)	Letourneau (1984)
	Caribou	0.110	0.6	1.3	
	Reindeer	0.050	0.3	0.5	
As	Beef[3,4]	0.0012	0.0028	0.0104	Peoples (1964)
	Sheep[3]	0.0075	0.1194	0.1157	Calvert (1975)
	Sheep[3]	0.0035	0.0131	0.0117	Lancaster et al. (1971)
Ni	Beef[3,5]	0.001	0.003	0.0004	O'Dell et al. (1971)

[1] Fresh weight meat concentration (ug/g or Bq/g) divided by dry weight feed concentration.

[2] Kidney and liver values in parentheses based on organ:muscle concentration ratios for U, Th (BEAK, 1984), Ra=Ca (Diem and Lentner, 1970), Pb and Po (Persson, 1972).

[3] Computed from mean or median feed and tissue concentrations reported by authors.

[4] Feed intake rate of 5 kg/d (ca 1% of body weight) assumed (see NAS/NRC, 1971).

[5] Tissue moisture assumed to be 70% (see Lloyd et al., 1978).

TABLE B5.7.4: FEED-TO-MEAT TRANSFER FACTORS FOR URANIUM SERIES RADIONUCLIDES, ARSENIC AND NICKEL IN RUMINANTS

Feed Contaminant	Ruminant Species	Transfer Factor (yr/g) Muscle	Kidney[2]	Liver[2]	Reference
U	Moose[1]	1.67E-8	(5.00E-7)	(5.00E-7)	Letourneau (1984)
	Caribou[1]	1.11E-9	(3.33E-8)	(3.33E-8)	
	Beef	9.32E-10	(2.80E-8)	(2.80E-8)	Momeni et al. (1979)
Th	Moose[1]	2.78E-9	(8.33E-8)	(8.33E-8)	Letourneau (1984)
	Caribou[1]	7.78E-10	(2.33E-8)	(2.33E-8)	
	Beef	5.48E-10	(1.64E-8)	(1.64E-8)	Momeni et al. (1979)
Ra	Moose[1]	1.11E-8	(1.11E-8)	(1.11E-8)	Letourneau (1984)
	Caribou[1]	5.56E-9	(5.56E-9)	(5.56E-9)	
	Beef	1.10E-8	(1.10E-8)	(1.10E-8)	Momeni et al. (1979)
	Beef	1.40E-9	(1.10E-8)	(1.10E-8)	NUREG (1980)
Pb	Moose[1]	1.11E-8	(2.56E-7)	(5.89E-7)	Letourneau (1984)
	Caribou[1]	4.44E-9	1.0E-7	2.33E-7	
	Reindeer[1]	2.78E-10	3.33E-8	5.56E-8	
	Beef	2.74E-9	(6.30E-8)	(1.45E-7)	Momeni et al. (1979)
	Beef	1.95E-9	(4.49E-9)	(1.03E-7)	NUREG (1980)
Po	Moose[1]	1.67E-7	(3.0E-6)	(2.3E-6)	Letourneau (1984)
	Caribou[1]	6.11E-8	3.33E-7	7.22E-7	
	Reindeer[1]	2.78E-8	1.67E-7	2.78E-7	
	Beef	3.29E-8	(5.9E-7)	(4.6E-7)	Momeni et al. (1979)
	Reindeer	1.37E-7	(2.5E-6)	(1.9E-6)	Garner (1972)
As	Beef[1]	6.67E-10	1.56E-9	5.78E-9	Peoples (1964)
	Sheep[1]	4.17E-9	6.63E-8	6.43E-8	Calvert (1975)
	Sheep[1]	1.94E-9	7.28E-9	6.50E-9	Lancaster et al. (1971)
Ni	Beef[1]	5.56E-10	1.67E-9	2.22E-10	O'Dell et al. (1971)

[1] Computed from the bioaccumulation factors in Table B5.7.3, divided by dry weight food intake from Table B5.7.2.

[2] Kidney and liver values in parentheses based on organ:muscle concentration ratios for U, Th (BEAK, 1984), Ra=Ca (Diem and Lentner, 1970), Pb and Po (Persson, 1972).

TABLE B5.8.1: COMMITTED EFFECTIVE DOSE EQUIVALENT CONVERSION FACTORS (Sv/Bq)

Radionuclides	Inhalation Class$^+$	Inhalation DCF Adult	Ingestion DCF f_1^+	Ingestion DCF Adult
U-NAT^{++}	Y	1.0E-6	0.05	2.0E-9
Th-230	Y	8.1E-5	0.0002	1.4E-7
Ra-226	W	2.6E-6	0.2	3.2E-7
Pb-210	D	3.5E-6	0.2	1.6E-6
Po-210	W	2.5E-6	0.1	5.3E-7
Rn-222		**	-	-

* For these radionuclides, pathways and age groups, the non-stochastic dose limit for an organ may be limiting. Therefore, a separate calculation using the organ dose conversion factors given in Table ??? should also be made.

** The dose associated with Rn-222 releases results from inhalation of the short-lived daughters. The dose conversion factor for inhalation of radon daughters is given in Section 5.8.3.2.

+ The inhalation class is an indication of the length of time the radioactive material is held in the lungs (D = relatively soluble; material remains in lungs for Days. W = slightly soluble; material remains in lungs for Weeks. Y = insoluble; material remains in lungs for Years). The f_1 value is the fraction of radioactive material reaching body fluids after entry into the gut. Both the inhalation class and the f_1 values depend on the chemical and physical form of the radionuclide. Values listed correspond to the maximum value of the Dose Conversion Factor for each radionuclide.

++ DCF's for U-NAT are in units of $Sv \cdot ug^{-1}$, and are calculated based on the specific activity relationships given in Section ???. U-NAT consists of 99.275 atom % U-238 (includes contributions from Th-234 and Pa-234 m), 0.0054 atom % of U-234, and 0.72 atom % of U-235 (includes contribution from Th-231).

APPENDIX C

Sensitivity Analysis of Radon and Dust Pathway Models

C-8206.195.6

SENSITIVITY ANALYSIS IN THE PROBABILISTIC ASSESSMENT OF URANIUM MILL TAILINGS

Prepared for:

BEAK CONSULTANTS LIMITED

J.R. Walker

Environmental and Safety Assessment Branch
Whiteshell Nuclear Research Establishment
Pinawa, Manitoba ROE 1L0

March 1986

ABSTRACT

A sensitivity analysis of the airborne pathways in the probabilistic assessment of uranium mill tailings is presented.

Three complementary techniques are described that together provide a comprehensive sensitivity analysis of the system under consideration. The three techniques are easily understood, and answer the questions posed by a probabilistic assessment.

The results of the three techniques are compared and contrasted to provide an integrated analysis of the airborne pathways.

1. INTRODUCTION

The National Uranium Tailings Program (NUTP) was established in 1982 to pull together previous work on Canadian mill tailings, to fund additional work where significant gaps were found in understanding or in essential data, and to develop the capability to predict the long-term effects of tailings.

The probabilistic system model has had two phases of development by SENES Consultants of Willowdale, Ontario. Both Phase I and Phase II models have been applied to tailings of pyrite-bearing ore. The methodology is being applied, by BEAK Consultants Ltd., to non-pyritic tailings, rich in arsenic and nickel, which is a second ore type typically found in Canada.

This report details a package of three sensitivity analysis techniques that together form an integrated methodology for sensitivity analysis in probabilistic assessments.

The airborne pathways for As/Ni-Rich tailings are essentially similar to those of the Phase II models. Thus the sensitivity analysis methodology is applied to the airborne pathways of the system model to demonstrate the methodology, and to give a detailed analysis of the importance of parameters in the dust and radon pathways. The same methods can easily be applied to the other pathways of the system model, as required.

2. SENSITIVITY ANALYSIS

In the probabilistic approach adopted by the National Uranium Tailings Program, input parameters of the system model are assigned to probability density functions (pdfs). These pdfs represent the frequency of occurrence of the input parameters in the system model.

The system model is run many times where, in every run, each parameter has a value selected from its associated pdf, and the consequences corresponding to each parameter value set are calculated. Thus each run represents a different Monte Carlo realization of the system. The basic output from such an analysis is a frequency distribution of the possible consequences of the system. A complete account of the method, associated models, and computer code is contained in the Phase II report [1].

Some of the input pdfs represent parameters that are potentially under institutional control, whereas other parameters cannot effectively be influenced by human intervention. An example of a parameter potentially within institutional control might be the distance of the receptor from the tailings site. An example of a parameter effectively outside of institutional control might be the climatic conditions prevalent at the site location.

The aim of sensitivity analysis is to examine how the output consequences are influenced by the input parameter values. The rôle of the sensitivity analysis procedure is to understand the parameter relationships within the system model, so that institutional control or remedial action can be implemented in the most effective manner.

For the purposes of this report it is assumed that the consequence of interest is the radiological detriment to the critical receptor. This report will, therefore, discuss the sensitivity analysis with respect to the annual dose equivalent (H), or annual risk (R) as appropriate, to the critical receptor.

The annual dose equivalent to the critical receptor varies with time [1]. Thus the sensitivity analysis should consider the temporal aspects of the tailings management. The temporal behaviour of the dose rates from the dust and radon pathways are shown in Figures 1 and 2 respectively. From Figures 1 and 2 it can be seen that the mean annual dose equivalent to the critical receptor, from each of the two airborne pathways, is at a maximum at the start of the simulation (T=0). For that reason, the analysis given in this report uses T=0 as its reference time. If required, the analysis could be easily extended to subsequent times.

In order for sensitivity analysis to be useful to the NUTP, the analysis must provide information that will enable tailings management decisions to be made in an effective manner. The information provided by the analysis should indicate the optimum route for any necessary institutional control or remedial action.

From the perspective of a probabilistic assessment methodology, the analysis should provide information, to an acceptable confidence level, in three broad areas:

i) What combination of parameters maximizes (or minimizes) the detriment to the critical receptor?

ii) How is the variability of the dose rate received by the critical receptor influenced by the variability of individual parameters?

iii) How do changes in the value of individual parameters influence the risk to the critical Receptor?

There is no single sensitivity analysis technique that can completely provide the required information in each of these three areas. The following three techniques individually answer one of the three questions, as will be demonstrated in the case of the airborne pathways of the system model. Together the three techniques provide an integrated methodology for sensitivity analysis in probabilistic assessment.

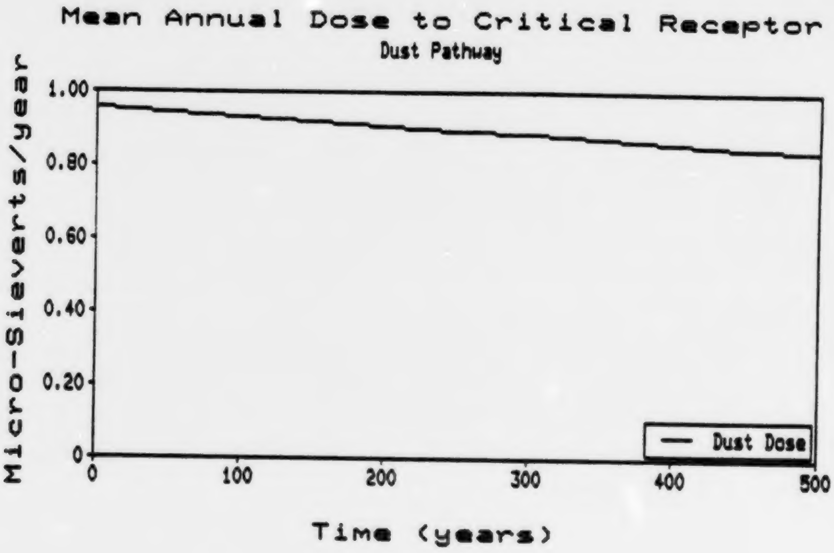

Figure 1

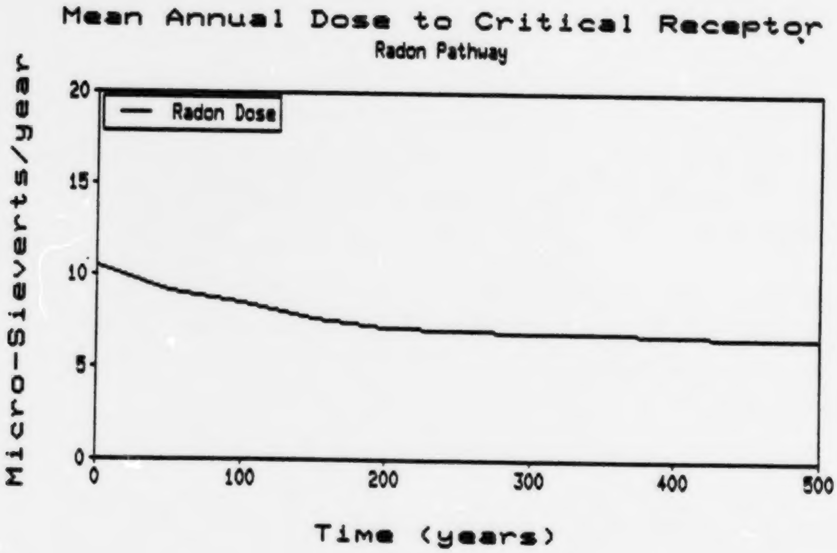

Figure 2

3. DIFFERENTIAL SENSITIVITY ENVELOPES

In first order sensitivity analysis one determines the partial derivative of the output with respect to the input parameters. In the study of complex systems this technique was first proposed by Tomović [2]. This technique is widely used when parameters deviate small amounts from their nominal values.

In the system model for the NUTP the input parameters vary simultaneously over wide ranges, and hence the first order sensitivity methods [3] are inappropriate.

Although first order sensitivity techniques are inappropriate, this does not invalidate the usefulness of the calculation of the partial derivatives. A knowledge of these derivatives is essential in the understanding of how parameters combine to maximize (or minimize) the detriment to the critical receptor.

The procedure is as follows. Each of the (n) input parameters is sampled from its respective pdf. This parameter set defines a particular point in the n-dimensional hyperspace, which has a corresponding dose rate to the critical receptor. At that point in the hyperspace the derivatives of dose rate with respect to each of the input parameters are calculated. The input parameters are again sampled from their pdfs, which defines another point in the hyperspace, and the derivatives are again calculated. This procedure is repeated many times and leads to an envelope (or histogram) of partial derivatives of dose rate with respect to each of the input parameters.

In the analysis given in this report, the partial derivatives are calculated using 1000 points in the hyperspace for both the dust and radon pathways. That is, 1000 realizations ('runs') are performed and the partial derivatives calculated for each realization. An example for the parameter CONCRA in the dust pathway is given in Figure 3.

The utility of calculating the partial differential envelopes is in the understanding of how parameters individually, and in combination, effect the dose rate. From Figure 3 it can be seen that, in the dust pathway, the derivative of dose rate with respect to parameter CONCRA is always positive. Thus an increase in the value of CONCRA will always lead to an increase in the dose rate, irrespective of the values of other parameters. In mathematical terms the dose rate, from the dust pathway, is monotonically increasing (strictly monotonically non-decreasing) with CONCRA.

The envelopes of partial derivatives for parameters that influence dose rate in the dust and radon pathways are given in Tables 1 and 2, respectively. The identities of the parameters of relevance to the airborne pathways is given in the appendix.

TABLE 1

DIFFERENTIAL SENSITIVITY ENVELOPES FOR PARAMETERS THAT INFLUENCE DOSE RATE IN THE DUST PATHWAY

Parameter	$\partial H/\partial$(Parameter) (μSv.a^{-1} for unit increase in Parameter value) minimum	maximum	Monotonicity
FWIND2	2.98	20.98	Increasing
OF	0.47	2.84	Increasing
RAINGP	-2.76	-0.46	Decreasing
UWIND	-0.39	-5.53×10^{-2}	Decreasing
CONCRA	4.27×10^{-2}	0.17	Increasing
FWIND1	8.41×10^{-3}	6.04×10^{-2}	Increasing
VDISP	-3.83×10^{-2}	-4.01×10^{-3}	Decreasing
FPREC	-8.73×10^{-3}	-1.23×10^{-3}	Decreasing
HSRC	-1.91×10^{-3}	-1.23×10^{-4}	Decreasing

TABLE 2

DIFFERENTIAL SENSITIVITY ENVELOPES FOR PARAMETERS THAT INFLUENCE DOSE RATE IN THE RADON PATHWAY

Parameter	$\partial H/\partial$(Parameter) ($\mu Sv.a^{-1}$ for unit increase in Parameter value) minimum	maximum	Monotonicity
FWIND2	5.27	716.56	Increasing
F	1.30	142.82	Increasing
EMANAT	3.81	141.02	Increasing
OF	0.86	91.15	Increasing
UWIND	-13.20	-9.75×10^{-2}	Decreasing
CONCRA	4.02×10^{-2}	6.59	Increasing
MPCH2O	-6.02	-6.02×10^{-2}	Decreasing
VDISP	-1.11	-8.66×10^{-3}	Decreasing
HSRC	-4.49×10^{-2}	-2.27×10^{-4}	Decreasing
RHOTAL	3.74×10^{-7}	5.11×10^{-5}	Increasing

As an example of the use of the above two tables, a unit increase in the value of FWIND2 will cause an increase in dose rate of between 5.27 and 716.56 $\mu Sv.a^{-1}$ from the radon pathway.

All of the parameters, in both the dust and radon pathways, influence the dose rate monotonically. This can be seen in Tables 1 and 2, where $\partial H/\partial$(Parameter) is always either positive (monotonically increasing) or negative (monotonically decreasing). In no case does the partial differential change sign for any of the parameters in either of the airborne pathways.

This is a very useful result since it means that the monotonicity of any individual parameter is independent of the other parameters in the system. Thus, if the value of a parameter that influences the dose rate in a monotonically-increasing manner is increased then the dose rate will always increase, irrespective of the values of the other parameters. Similarly, an increase in any of the parameters that influence the dose rate in a monotonically-decreasing manner will always lead to a decrease in the dose rate.

Since the dose rate behaves monotonically with respect to all of the parameters in the system it is possible to determine the combination of parameters that give rise to the extreme minimum and maximum dose rates. In order to calculate the maximum possible dose rate the parameters that influence the dose rate in a monotonically-increasing manner are fixed at their maximum values, and those parameters that influence the dose rate in a monotonically-decreasing manner are fixed at their minimum values. The calculation of the minimum possible dose rate is determined in the opposite manner. The results of the calculation for the airborne pathways is given in Table 3.

TABLE 3

MINIMUM AND MAXIMUM DOSE RATES POSSIBLE FOR THE AIRBORNE PATHWAYS

Extremum	Dust Pathway	Radon Pathway
Minimum	1.20×10^{-7} Sv.a^{-1}	1.16×10^{-8} Sv.a^{-1}
Maximum	3.60×10^{-6} Sv.a^{-6}	3.15×10^{-4} Sv.a^{-1}

Since none of the parameters influence the dose rate in a non-monotonic manner it is particularly simple to calculate the extreme dose rates. If there had been some non-monotonicity in the system it is still possible to use this method, but the cyclic procedure indicated in Figure 4 must be employed.

In addition to determining the monotonicity of the dose rate relative to the parameters in the system, it is possible to use the partial differentials to produce an estimate of the contribution that each parameter makes to the variability in the dose rate.

If the maximum value of $\partial H/\partial(\text{Parameter})$ (ignoring signs) is multiplied by the total range allowed to the parameter, then this product provides an indication of the variability composition of dose rate caused by the variability of each parameter. The results for the dust and radon pathways are given in Tables 4 and 5.

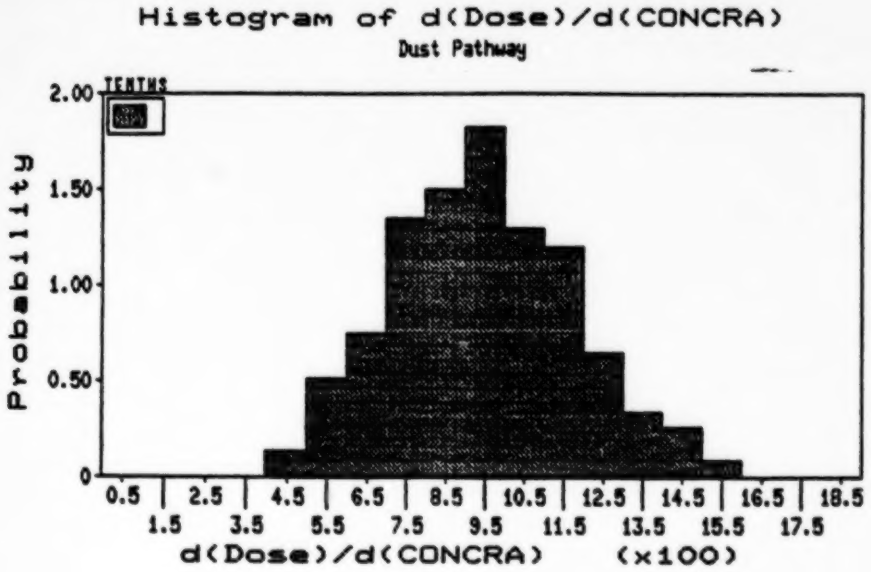

Figure 3

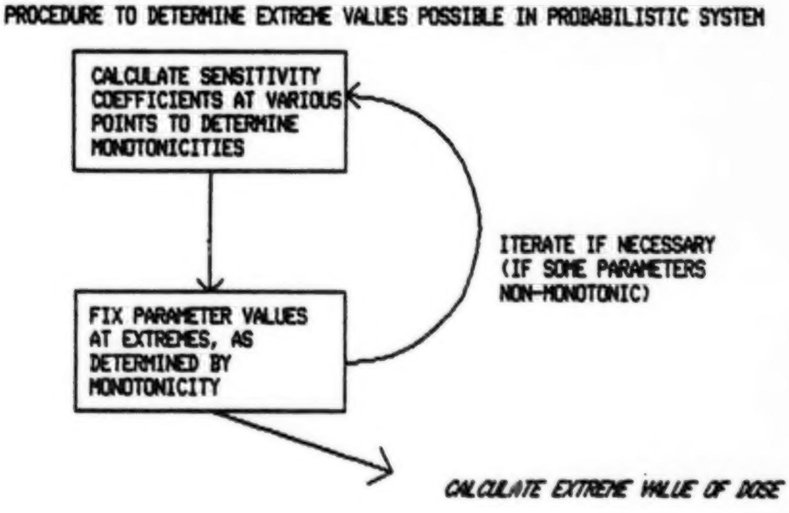
PROCEDURE TO DETERMINE EXTREME VALUES POSSIBLE IN PROBABILISTIC SYSTEM
CALCULATE SENSITIVITY COEFFICIENTS AT VARIOUS POINTS TO DETERMINE MONOTONICITIES
ITERATE IF NECESSARY (IF SOME PARAMETERS NON-MONOTONIC)
FIX PARAMETER VALUES AT EXTREMES, AS DETERMINED BY MONOTONICITY
CALCULATE EXTREME VALUE OF DOSE

Figure 4

TABLE 4

ESTIMATING VARIABILITY COMPOSITION FROM PARTIAL DIFFERENTIALS OF PARAMETERS THAT INFLUENCE DOSE RATE IN THE DUST PATHWAY

Parameter	Maximum value of $\left\|\partial H/\partial(\text{Parameter})\right\|$	Range	Product
CONCRA	0.17	10.0	1.7
RAINGP	2.76	0.55	1.52
OF	2.82	0.5	1.41
VDISP	3.83×10^{-2}	28.1	1.08
FWIND2	20.98	5.7×10^{-3}	0.120
FWIND1	6.04×10^{-2}	1.8	0.109
UWIND	0.39	0.2	0.078
FPREC	8.73×10^{-3}	4.0	0.0349
HSRC	1.91×10^{-3}	2.0	3.82×10^{-3}

TABLE 5

ESTIMATING VARIABILITY COMPOSITION FROM PARTIAL DIFFERENTIALS OF PARAMETERS THAT INFLUENCE DOSE RATE IN THE RADON PATHWAY

Parameter	Maximum value of $\lvert \partial H / \partial(\text{Parameter}) \rvert$	Range	Product
EMANAT	141.02	0.88	124.10
MPCH20	6.02	20.0	120.40
F	142.82	0.5	71.41
CONCRA	6.59	10.0	65.90
OF	91.15	0.5	45.58
VDISP	1.11	28.1	31.19
RHOTAL	5.11×10^{-5}	6.0×10^{5}	30.66
FWIND2	716.56	5.7×10^{-3}	4.08
UWIND	13.20	0.2	2.64
HSRC	4.49×10^{-2}	2.0	0.0898

Although the method given above can give an indication of the variability composition of the dose rate, the results should be used with care since the variability in the values of the partial derivatives is not taken into account. Also no allowance is made for the form of the pdfs assigned to each parameter. That is, the method will not detect differences in variability composition caused by the various types of pdf (uniform, log normal, etc.). A method of calculating the variability composition that does allow for the various distribution types is given in the next section.

3. CORRELATION ANALYSIS

The aim of correlation analysis is to determine how the dose rate is related to the input parameters, and how the variability in the dose rate is related to the variability of the input parameters.

Since we have already determined that, for both airborne pathways, the dose rate is monotonically related to the input parameters, then the appropriate measure of correlation is the rank correlation coefficient of Spearman [4].

Spearman's rank correlation coefficient (ρ) measures the extent to which a consequence is determined by a monotonic relationship to each of the input parameters. The rank correlation coefficient can take values in the range $-1 \leq \rho \leq +1$. Positive values imply that the consequence is related in a monotonically increasing manner to the particular parameter. Negative values imply that the consequence is related in a monotonically decreasing manner. When $|\rho| = 1$ the consequence is entirely determined by the parameter in question. Lesser values of $|\rho|$ imply a lesser degree of correlation between the consequence and the parameter.

One of the advantages of the use of ρ as a statistical measure is that the statistical confidence in the measure is well understood [5]. The standard error in a measured rank correlation coefficient (σ_ρ) is given by $\sigma_\rho = 1/\sqrt{(n-1)}$, where n is the number of data points (in our case the number of Monte Carlo realizations). Since the errors in the statistical measure are known, a parameter importance ranking can be produced with a known level of confidence. This is unlike many other non-parametric measures, where the confidence bounds of a predicted parameter ranking may be unknown.

The analysis presented here is based on 10000 realizations of the system model. Thus $\sigma_\rho = 1/\sqrt{(9999)} \simeq 0.01$. Now, the 95% confidence interval corresponds approximately to ±1.96 standard deviations. Therefore, the rank correlations given in Tables 6 and 7 are accurate to ±0.02 at a 95% confidence level. The ranking and calculation of ρ was performed with the CANAL correlation analysis program [6].

TABLE 6

SPEARMAN'S RANK CORRELATION COEFFICIENT FOR STATISTICALLY SIGNIFICANT PARAMETERS IN THE DUST PATHWAY

PARAMETER	ρ
CONCRA	+0.627
RAINGP	-0.505
OF	+0.493
VDISP	-0.220
FWIND2	+0.024

TABLE 7

SPEARMAN'S RANK CORRELATION COEFFICIENT FOR STATISTICALLY SIGNIFICANT PARAMETERS IN THE RADON PATHWAY

PARAMETER	ρ
EMANAT	+0.657
MPCH2O	-0.587
F	+0.276
CONCRA	+0.235
OF	+0.184
VDISP	-0.081

From the definition of the rank correlation coefficient it can be shown that the square of the correlation coefficient (ρ^2) is the proportion of the total variation in dose rate that is explained by the monotonic relationship between the dose rate and the particular parameter. Hence ρ^2 is termed the coefficient of determination, since it is the proportion of the variation in dose rate that is determined by the variation in the particular parameter. The calculated variability composition for the airborne pathways are given in Figures 5 and 6.

We have seen, therefore, that the rank correlation coefficient is used to determine the variability composition, and hence answer one of the questions required of sensitivity analysis.

There remains the question of how individual parameters can influence the detriment to the critical receptor. This question is answered by the technique demonstrated in the next section.

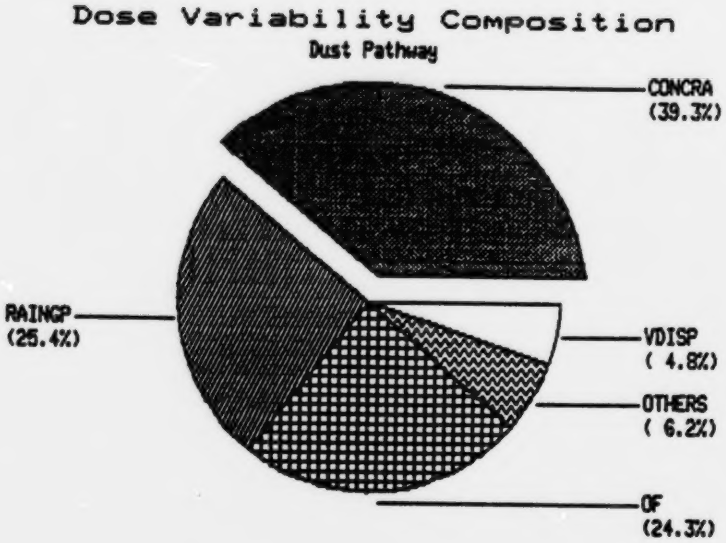

Figure 5

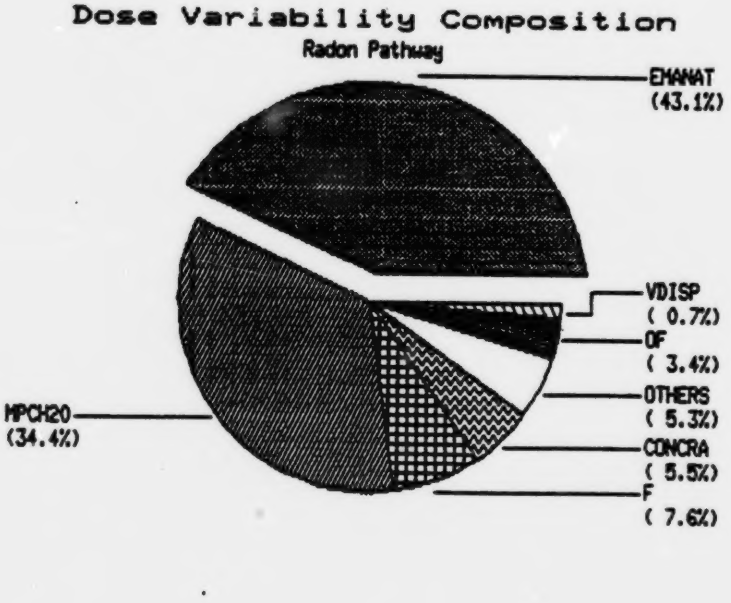

Figure 6

4. INDIVIDUAL PARAMETER RISK ANALYSIS

Of the many parameters in a probabilistic risk assessment, some of the parameters have the potential to be modified by human intervention. This intervention may be in the form of some chemical, or engineering, treatment, or some type of institutional control.

In order that the optimum intervention can be undertaken, it is desirable to understand how modifications to particular parameters can alter the risk to the critical receptor.

At the dose rate levels likely to be encountered in a tailings assessment, the total radiological risk (R) is given by [7] :

$$R = 2\times10^{-2} \int_0^\infty p(H)\, H \; .dH \qquad ,$$

where p(H) is the pdf of annual dose equivalents ($Sv.a^{-1}$).

Now, from the properties of pdfs, the above integral is equal to the expectation value of H (i.e. the mean annual dose H). Thus $R = 2\times10^{-2}H$. The mean annual dose is estimated from $H = \frac{1}{n}\Sigma H_i$, where H_i is the dose rate estimate from the i-th Monte Carlo realization. The error in a calculated value of mean annual dose may be determined by the use of the central limit theorem. The values of H calculated here are typically accurate to ±5%, since they are each based on 1000 realizations of the system.

Therefore, an effective way to determine how an individual parameter may effect the detriment is to fix the parameter at its 'low' value and calculate the mean dose rate (H_{low}) while allowing all other parameters to be sampled from their pdfs. Then fix the parameter under investigation to its 'high' value, and again calculate the mean dose rate (H_{high}), allowing all other parameters to be sampled from their pdfs. The difference ($H_{high} - H_{low}$), when multiplied by 2×10^{-2}, represents the improvement in risk that can be achieved by decreasing the value of the particular parameter from its 'high' to its 'low' value.

This technique has been used previously for a purely graphical representation of sensitivity analysis [8]. An example of the graphical representation of this technique is given in Figure 7. The calculation of the corresponding risks allows quantitative conclusions to be drawn from the available data. The results for statistically significant parameters of the dust and radon pathways are given in Tables 8 and 9 respectively.

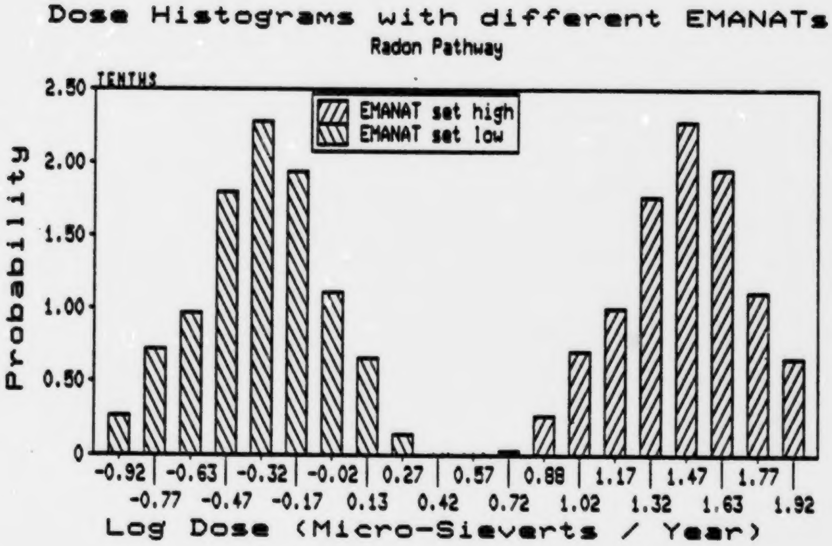
Dose Histograms with different EMANATs
Radon Pathway
TENTHS
2.50
2.00
1.50
1.00
0.50
0
Probability
EMANAT set high
EMANAT set low
-0.92
-0.77
-0.63
-0.47
-0.32
-0.17
-0.02
0.13
0.27
0.42
0.57
0.72
0.88
1.02
1.17
1.32
1.47
1.63
1.77
1.92
Log Dose (Micro-Sieverts / Year)

Figure 7

TABLE 8

RISK ANALYSIS FOR STATISTICALLY SIGNIFICANT PARAMETERS THAT INFLUENCE DOSE RATE IN THE DUST PATHWAY

Parameter	Annual Risk when Parameter set to		Difference
	minimum	maximum	
CONCRA	9.37×10^{-9}	2.81×10^{-8}	1.87×10^{-8}
OF	1.21×10^{-8}	2.73×10^{-8}	1.52×10^{-8}
RAINGP	2.57×10^{-8}	1.08×10^{-8}	-1.49×10^{-8}
VDISP	2.39×10^{-8}	1.50×10^{-8}	-8.85×10^{-9}
FWIND2	1.89×10^{-8}	2.00×10^{-8}	1.11×10^{-9}
FWIND1	1.90×10^{-8}	2.00×10^{-8}	1.00×10^{-9}
UWIND	1.96×10^{-8}	1.89×10^{-8}	-7.28×10^{-10}

TABLE 9

RISK ANALYSIS FOR STATISTICALLY SIGNIFICANT PARAMETERS THAT INFLUENCE DOSE RATE IN THE RADON PATHWAY

Parameter	Annual Risk when Parameter set to		Difference
	minimum	maximum	
EMANAT	1.11×10^{-8}	5.01×10^{-7}	4.90×10^{-7}
MPCH2O	4.98×10^{-7}	5.28×10^{-8}	-4.44×10^{-7}
F	8.99×10^{-8}	3.15×10^{-7}	2.24×10^{-7}
CONCRA	9.77×10^{-8}	2.93×10^{-7}	1.95×10^{-7}
OF	1.23×10^{-7}	2.77×10^{-7}	1.54×10^{-7}
VDISP	2.55×10^{-7}	1.61×10^{-7}	-9.47×10^{-8}
RHOTAL	1.65×10^{-7}	2.55×10^{-7}	9.01×10^{-8}

5. CONCLUSIONS

The techniques described in this report have consistently, and unambiguously, identified the important parameters in each of the airborne pathways. The calculated ranking of important parameters is very similar using each of the techniques. The importance of each parameter can be judged from the numerical results of the assessment techniques.

The techniques provide an integrated methodology for sensitivity analysis in probabilistic assessments. That is:

i) The combinations of parameters that minimize and maximize the dose rate have been identified. The values of the minimum and maximum possible dose rates have been determined.

ii) The variability composition of the dose rate with respect to the input parameters has been calculated.

iii) The effect of changes to individual parameters has been determined.

This sensitivity analysis methodology can be used for any probabilistic assessment sensitivity analysis, and the results are independent of models and pdfs. The use of these techniques provide the information that is essential when options for environmental management are to be considered.

In the context of the Phase II models, the radon pathway is the more important of the airborne pathways, from the viewpoint of detriment to the critical receptor. From Figures 1 and 2, it can be seen that, at all times, the mean dose rate from the radon pathway is approximately one order of magnitude larger than the mean dose rate from the dust pathway.

It may be that the dust source model, and associated data, will be updated to reflect further research on dust dispersion in the climatic conditions of the Canadian shield. If the updated dust source model is not significantly different from the Phase II model, it seems likely that the radon pathway will remain the more important airborne pathway.

In both the dust and radon pathways, relatively few parameters dominate the dose rate to the critical receptor. In the case of the dust pathway, over 85% of the variability in the dose rate is determined by three parameters (CONCRA, RAINGP, and OF). In the case of the radon pathway, approximately 85% of the variability in dose rate is determined by three parameters (EMANAT, MPCH2O, and F). The largest changes in risk can be made by changing these critical parameters from their 'low' to 'high' values. That is, changing CONCRA, RAINGP, and OF most effect the risk in the dust pathway. Similarly, EMANAT, MPCH2O, and F most effect the risk in the radon pathway.

For the dust pathway, CONCRA (initial ^{226}Ra activity in the solid phase of tailings) is not directly under managerial control for historic tailings. Parameter RAINGP (fraction of ^{226}Ra associated with gypsum) is also not under managerial control. Parameter OF (occupation factor) is, however, potentially under institutional control.

For the radon pathway, EMANAT (emanation coefficient) is outside of control in the context of the Phase II models. Similarly, MPCH2O (moisture content of tailings) and F (radon/radon daughters equilibrium factor) are outside of managerial control because they are largely determined by atmospheric conditions. This result is similar to the sensitivity analysis results of the Phase I radon model [9], where the dose rate was also dominated by the emanation coefficient and some climatic parameters.

In addition to parameters explicitly included in the models, it may be necessary to consider additional parameters or treatments, if informed management decisions are to be made. For example, the distance from the reference receptor to the tailings site is fixed at 2km in the reference model. In reality, this distance may vary and may have a profound effect on the annual dose equivalent. Additionally, this distance may be under institutional control.

Another possible treatment, not explicitly considered, is the covering or forced revegetation of the tailings. Cover and/or revegetation may significantly reduce the dose from the airborne pathways.

Parameters or treatments not explicitly included in the models have been excluded from analysis in this report, but indicate areas for further research.

Further study is recommended on the nature of the emanation coefficient, and how sensitive the receptor detriment is to possible cover and revegetation treatments.

ACKNOWLEDGEMENT

The author would like to thank Dr. Nava Garisto, for collaboration during the course of this work, and for helpful comments on the manuscript.

REFERENCES

[1] SENES Consultants Limited, 1985. "Probabilistic model development for the assessment of the long-term effects of uranium mill tailings in Canada - Phase II," Research Report prepared for the National Uranium Tailings Program, CANMET, EMR, under Supply and Services Canada Contract No. 0SQ84-00207

[2] Tomović R., 1963. "Sensitivity Analysis of Dynamic Systems," McGraw-Hill Book Co., Inc., New York.

[3] Tomović R. and Vukobratović M., 1972. "General Sensitivity Theory," American Elsevier Publishing Co., New York.

[4] Spearman, C., 1904. "The Proof and Measurement of Association between Two Things," Amer. J. Psychol. 15, 72.

[5] Kendall,M.G. and Babington-Smith, B., 1939. "The Problem of M Rankings," Ann. Math. Statist. 10, 275.

[6] Walker, J.R., 1986. "Report and User's Guide to the CANAL Correlation Analysis Computer Code," Atomic Energy of Canada Limited Technical Record, TR-370. (In Preparation)

[7] ICRP, 1985. "Radiation Protection Principles for the Disposal of Solid Radioactive Waste," ICRP Publication 46, Pergamon Press, Oxford.

[8] Wuschke, D.M., Rice, A.M., and Gillespie, P.A., 1983. "Environmental Assessment of Sub-Seabed Disposal of Nuclear Wastes: A Demonstration of Probabilistic Systems Analysis," Atomic Energy of Canada Limited Technical Record, TR-206.

[9] Walker, J.R. Unpublished results.

APPENDIX

IDENTITY OF INPUT PARAMETERS RELEVANT TO AIRBORNE PATHWAYS

Parameter	Definition
CONCRA	Initial solid phase activity of ^{226}Ra in tailings ($Bq.g^{-1}$)
EMANAT	Radon emanation coefficient of tailings
F	Equilibrium factor for radon daughters to radon
FPREC	Annual number of days with more than 0.25 mm of precipitation (days)
FWIND1	Percentage of time that the wind speed exceeds 5.1 $m.s^{-1}$ at the mean tailings height
FWIND2	Fraction of time wind blows from the source to receptor
HSRC	Height of the source (m)
MPCH2O	Percent moisture content by weight of tailings
OF	Fraction of year receptor is at reference site
RAINGP	Fraction of total ^{226}Ra associated with gypsum
RHOTAL	Tailings bulk density ($g.m^{-3}$)
UWIND	Mean annual wind speed ($m.s^{-1}$)
VDISP	Vertical dispersion coefficient

APPENDIX D

Output Frequency Distributions
Scenario 1 (Unflooded Tailings)

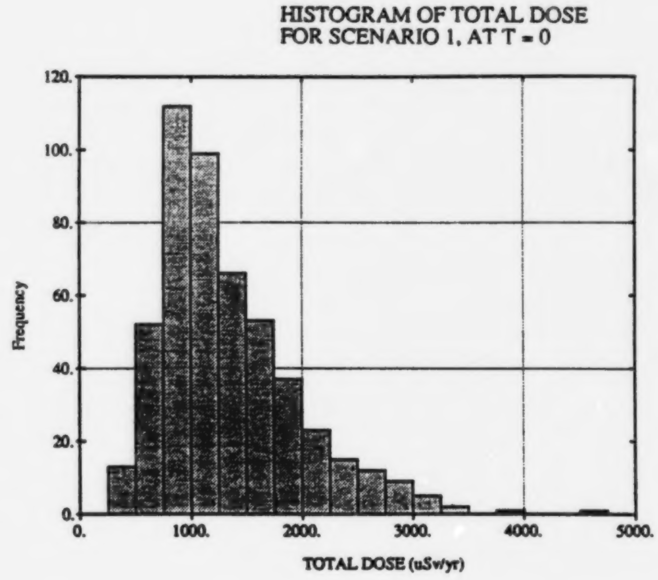

HISTOGRAM OF TOTAL DOSE
FOR SCENARIO 1, AT T = 0

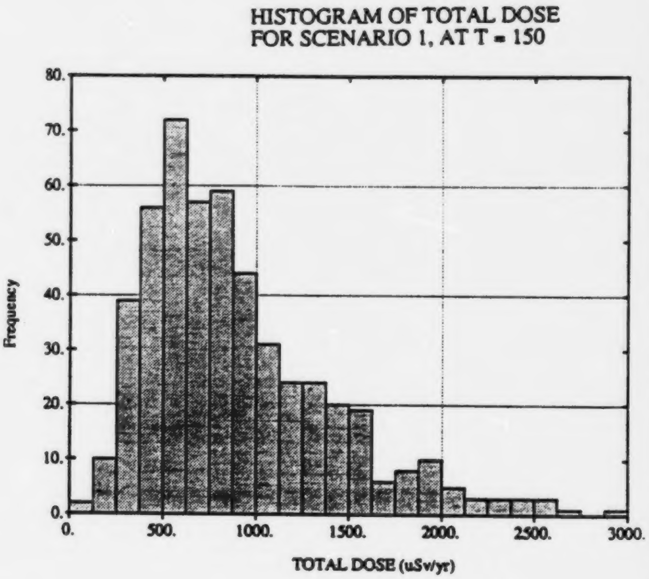

HISTOGRAM OF TOTAL DOSE
FOR SCENARIO 1, AT T = 150

SUMMARY STATISTICS:

MEAN = 0.133e+04
STANDARD DEVIATION = 622.
GEOMETRIC MEAN = 0.121e+04
GEOMETRIC STANDARD DEVIATION = 1.57
MINIMUM = 317.
MAXIMUM = 0.451e+04

SUMMARY STATISTICS:

MEAN = 897.
STANDARD DEVIATION = 499.
GEOMETRIC MEAN = 772.
GEOMETRIC STANDARD DEVIATION = 1.75
MINIMUM = 81.8
MAXIMUM = 0.292e+04

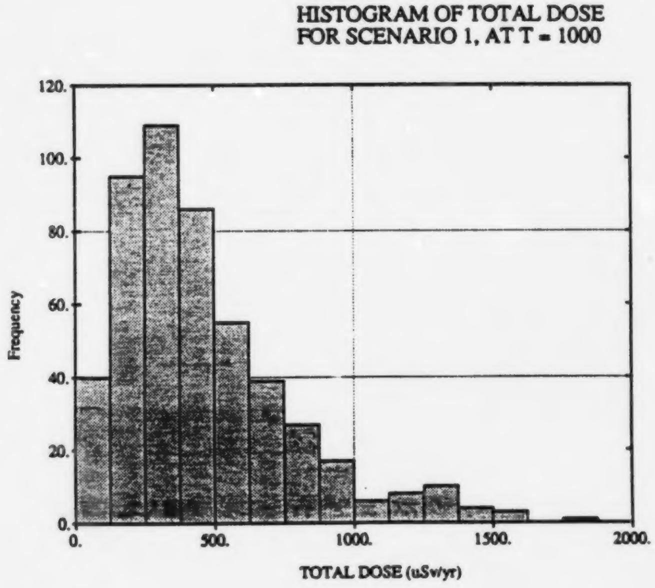

HISTOGRAM OF TOTAL DOSE
FOR SCENARIO 1, AT T = 1000

SUMMARY STATISTICS:

MEAN = 459.
STANDARD DEVIATION = 310.
GEOMETRIC MEAN = 358.
GEOMETRIC STANDARD DEVIATION = 2.27
MINIMUM = 0.494
MAXIMUM = 0.186e+04

HISTOGRAM OF ARSENIC INHALED
FOR SCENARIO 1, AT T = 0

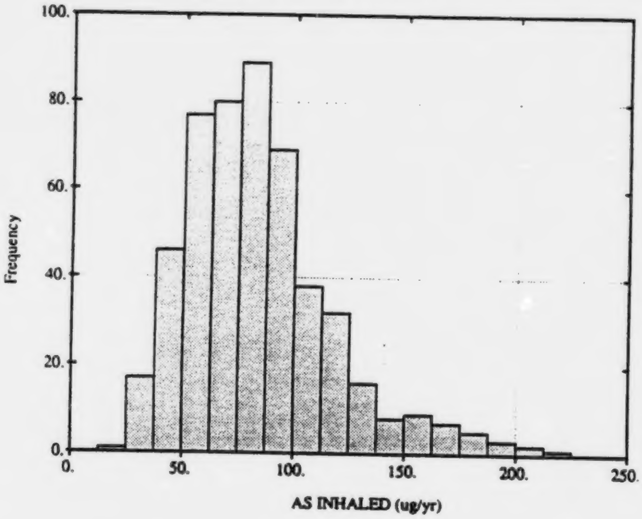

SUMMARY STATISTICS:

MEAN = 83.9
STANDARD DEVIATION = 33.3
GEOMETRIC MEAN = 77.9
GEOMETRIC STANDARD DEVIATION = 1.47
MINIMUM = 24.9
MAXIMUM = 220.

HISTOGRAM OF ARSENIC INHALED
FOR SCENARIO 1, AT T = 150

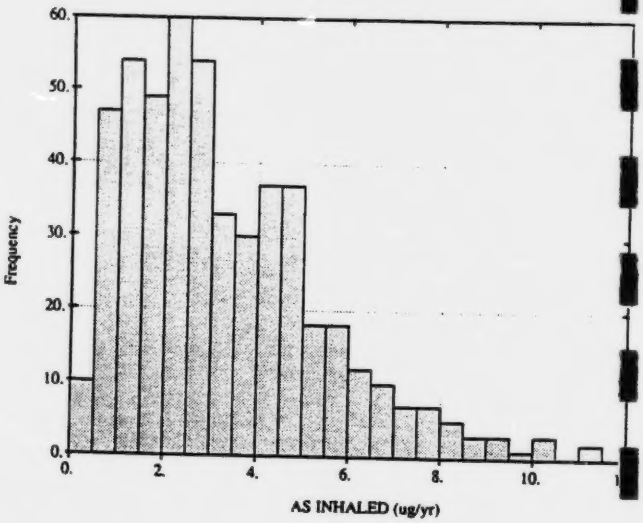

SUMMARY STATISTICS:

MEAN = 3.26
STANDARD DEVIATION = 2.11
GEOMETRIC MEAN = 2.58
GEOMETRIC STANDARD DEVIATION = 2.08
MINIMUM = 0.201
MAXIMUM = 11.4

HISTOGRAM OF ARSENIC INHALED
FOR SCENARIO 1, AT T = 1000

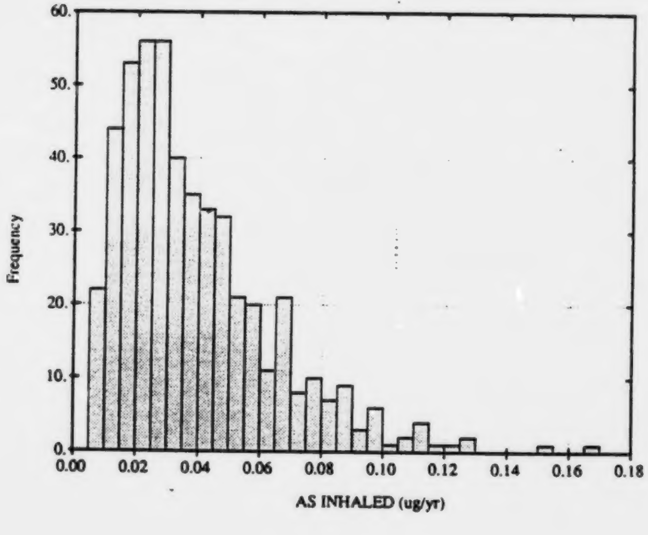

SUMMARY STATISTICS:

MEAN = 0.390e-01
STANDARD DEVIATION = 0.254e-01
GEOMETRIC MEAN = 0.318e-01
GEOMETRIC STANDARD DEVIATION = 1.92
MINIMUM = 0.569e-02
MAXIMUM = 0.168

HISTOGRAM OF ARSENIC INGESTED
FOR SCENARIO 1, AT T = 0

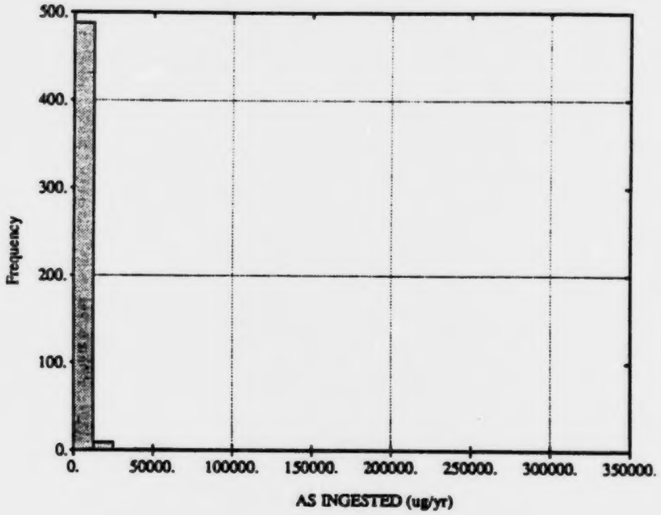

SUMMARY STATISTICS:

MEAN = 0.302e+04
STANDARD DEVIATION = 0.157e+05
GEOMETRIC MEAN = 0.139e+04
GEOMETRIC STANDARD DEVIATION = 2.71
MINIMUM = 91.3
MAXIMUM = 0.342e+06

HISTOGRAM OF ARSENIC INGESTED
FOR SCENARIO 1, AT T = 150

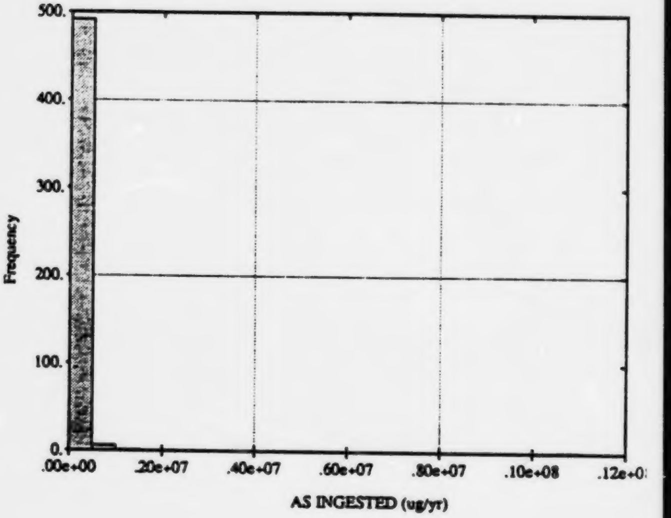

SUMMARY STATISTICS:

MEAN = 0.645e+05
STANDARD DEVIATION = 0.495e+06
GEOMETRIC MEAN = 0.703e+04
GEOMETRIC STANDARD DEVIATION = 7.36
MINIMUM = 41.2
MAXIMUM = 0.108e+08

HISTOGRAM OF ARSENIC INGESTED
FOR SCENARIO 1, AT T = 1000

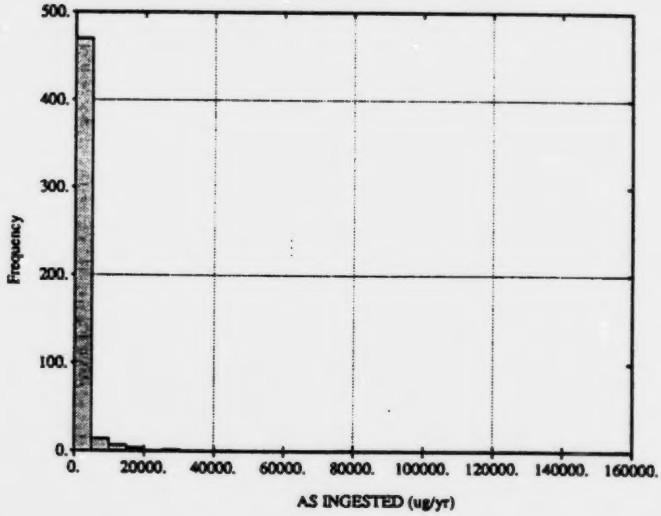

SUMMARY STATISTICS:

MEAN = 0.163e+04
STANDARD DEVIATION = 0.856e+04
GEOMETRIC MEAN = 182.
GEOMETRIC STANDARD DEVIATION = 6.59
MINIMUM = 4.77
MAXIMUM = 0.159e+06

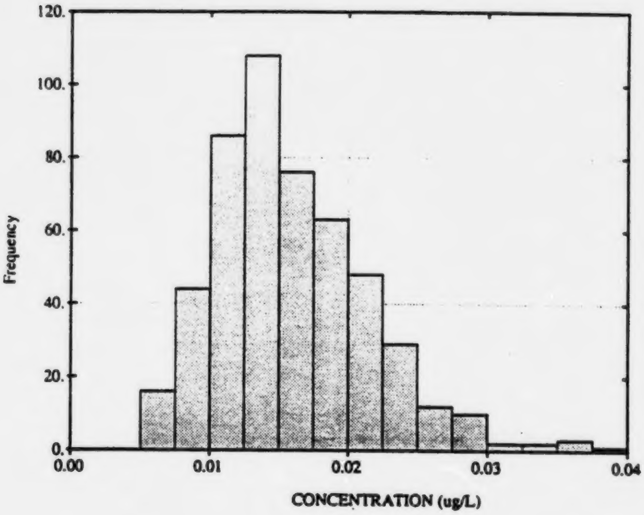

HISTOGRAM OF ARSENIC CONCENTRATION IN AIR
FOR SCENARIO 1, AT T = 0

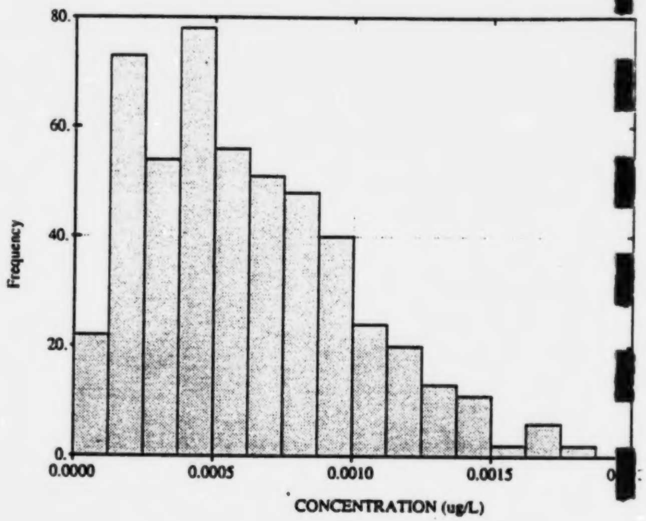

HISTOGRAM OF ARSENIC CONCENTRATION IN AIR
FOR SCENARIO 1, AT T = 150

SUMMARY STATISTICS:

MEAN = 0.159e-01
STANDARD DEVIATION = 0.559e-02
GEOMETRIC MEAN = 0.149e-01
GEOMETRIC STANDARD DEVIATION = 1.42
MINIMUM = 0.557e-02
MAXIMUM = 0.395e-01

SUMMARY STATISTICS:

MEAN = 0.617e-03
STANDARD DEVIATION = 0.374e-03
GEOMETRIC MEAN = 0.495e-03
GEOMETRIC STANDARD DEVIATION = 2.05
MINIMUM = 0.409e-04
MAXIMUM = 0.184e-02

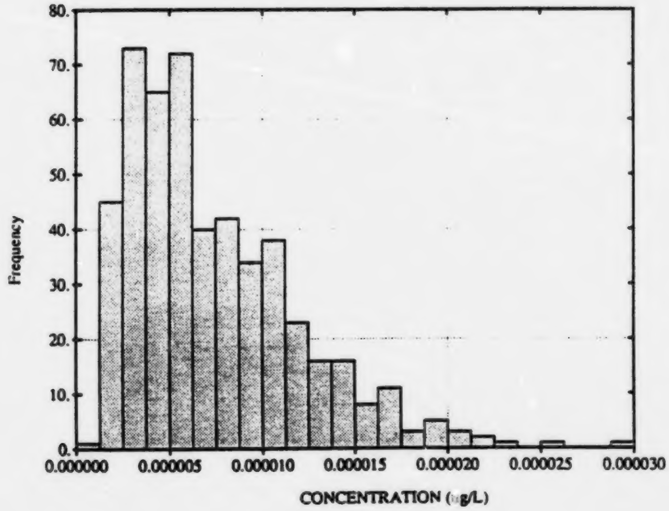

HISTOGRAM OF ARSENIC CONCENTRATION IN AIR
FOR SCENARIO 1, AT T = 1000

SUMMARY STATISTICS:

MEAN = 0.740e-05
STANDARD DEVIATION = 0.458e-05
GEOMETRIC MEAN = 0.611e-05
GEOMETRIC STANDARD DEVIATION = 1.89
MINIMUM = 0.114e-05
MAXIMUM = 0.288e-04

HISTOGRAM OF ARSENIC CONCENTRATION IN LAKE WATER FOR SCENARIO 1, AT T = 0

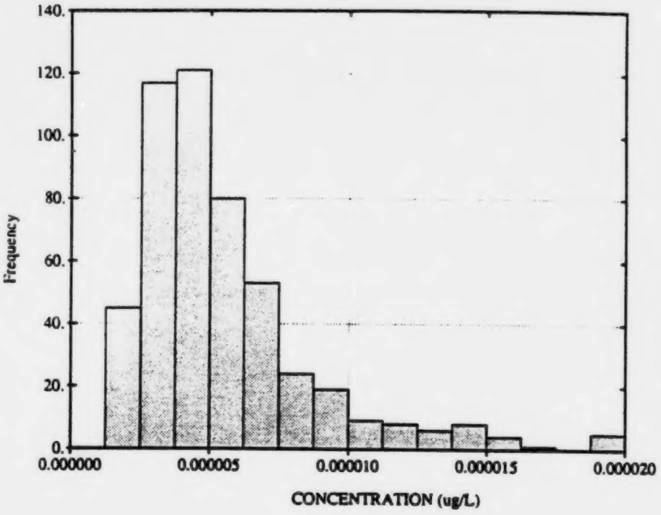

SUMMARY STATISTICS:

MEAN = 0.541e-05
STANDARD DEVIATION = 0.312e-05
GEOMETRIC MEAN = 0.474e-05
GEOMETRIC STANDARD DEVIATION = 1.64
MINIMUM = 0.143e-05
MAXIMUM = 0.194e-04

HISTOGRAM OF ARSENIC CONCENTRATION IN LAKE WATER FOR SCENARIO 1, AT T = 150

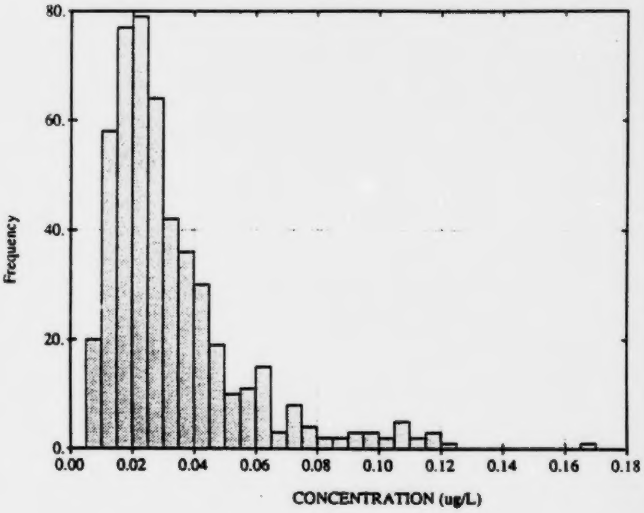

SUMMARY STATISTICS:

MEAN = 0.327e-01
STANDARD DEVIATION = 0.224e-01
GEOMETRIC MEAN = 0.272e-01
GEOMETRIC STANDARD DEVIATION = 1.81
MINIMUM = 0.666e-02
MAXIMUM = 0.168

HISTOGRAM OF ARSENIC CONCENTRATION IN LAKE WATER FOR SCENARIO 1, AT T = 1000

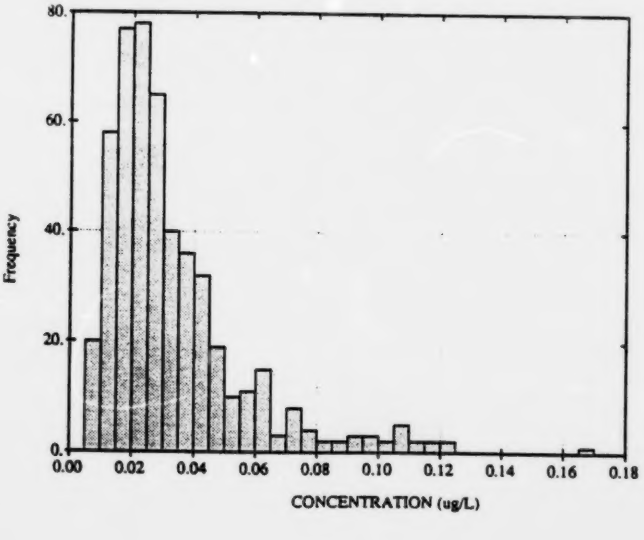

SUMMARY STATISTICS:

MEAN = 0.328e-01
STANDARD DEVIATION = 0.225e-01
GEOMETRIC MEAN = 0.272e-01
GEOMETRIC STANDARD DEVIATION = 1.81
MINIMUM = 0.666e-02
MAXIMUM = 0.169

APPENDIX E

Output Frequency Distributions
Scenario 2 (Flooded Tailings)

HISTOGRAM OF TOTAL DOSE
FOR SCENARIO 2, AT T = 0

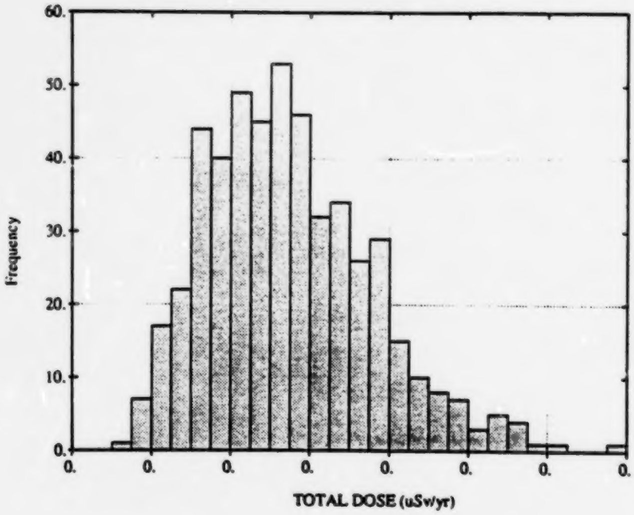

SUMMARY STATISTICS:

MEAN = 0.273
STANDARD DEVIATION = 0.104
GEOMETRIC MEAN = 0.254
GEOMETRIC STANDARD DEVIATION = 1.48
MINIMUM = 0.647e-01
MAXIMUM = 0.697

HISTOGRAM OF TOTAL DOSE
FOR SCENARIO 2, AT T = 150

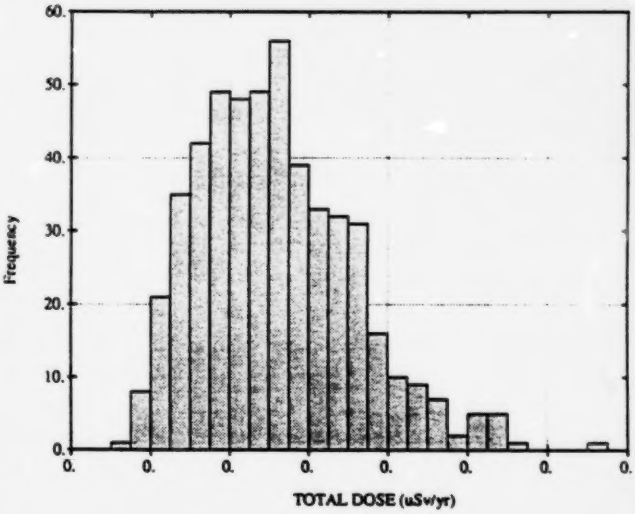

SUMMARY STATISTICS:

MEAN = 0.258
STANDARD DEVIATION = 0.974e-01
GEOMETRIC MEAN = 0.240
GEOMETRIC STANDARD DEVIATION = 1.48
MINIMUM = 0.657e-01
MAXIMUM = 0.657

HISTOGRAM OF TOTAL DOSE
FOR SCENARIO 2, AT T = 1000

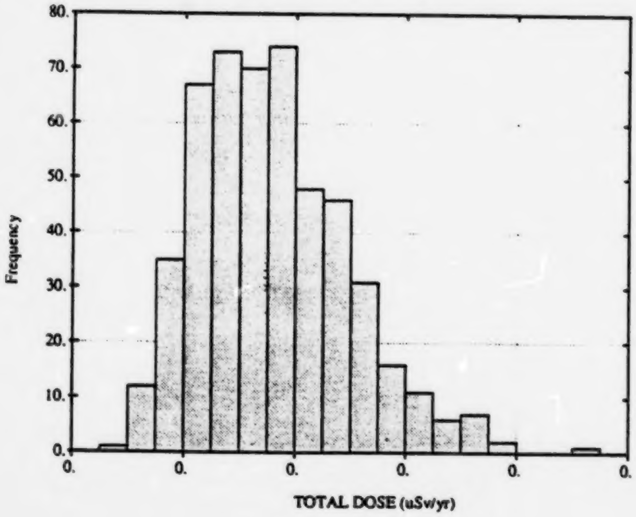

SUMMARY STATISTICS:

MEAN = 0.179
STANDARD DEVIATION = 0.676e-01
GEOMETRIC MEAN = 0.167
GEOMETRIC STANDARD DEVIATION = 1.48
MINIMUM = 0.456e-01
MAXIMUM = 0.456

HISTOGRAM OF ARSENIC INGESTED
FOR SCENARIO 2, AT T = 0

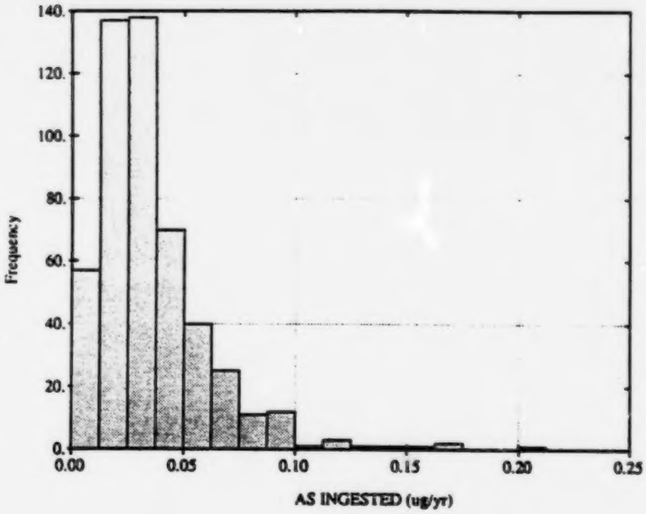

SUMMARY STATISTICS:

MEAN = 0.354e-01
STANDARD DEVIATION = 0.254e-01
GEOMETRIC MEAN = 0.287e-01
GEOMETRIC STANDARD DEVIATION = 1.92
MINIMUM = 0.481e-02
MAXIMUM = 0.208

HISTOGRAM OF ARSENIC INGESTED
FOR SCENARIO 2, AT T = 150

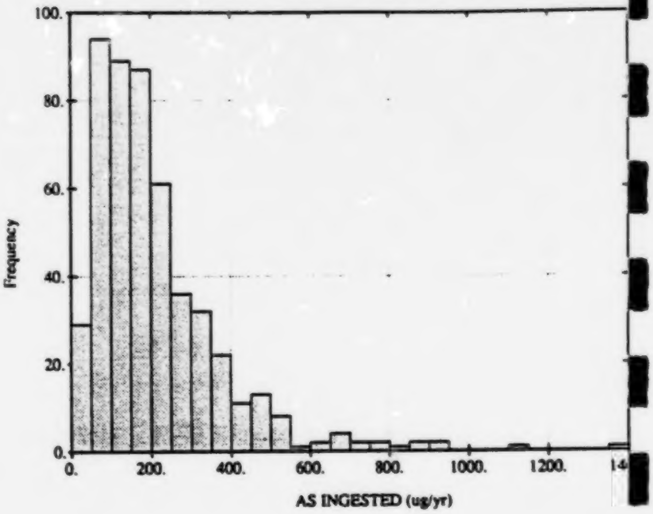

SUMMARY STATISTICS:

MEAN = 212.
STANDARD DEVIATION = 166.
GEOMETRIC MEAN = 164.
GEOMETRIC STANDARD DEVIATION = 2.06
MINIMUM = 20.8
MAXIMUM = 0.137e+04

HISTOGRAM OF ARSENIC INGESTED
FOR SCENARIO 2, AT T = 1000

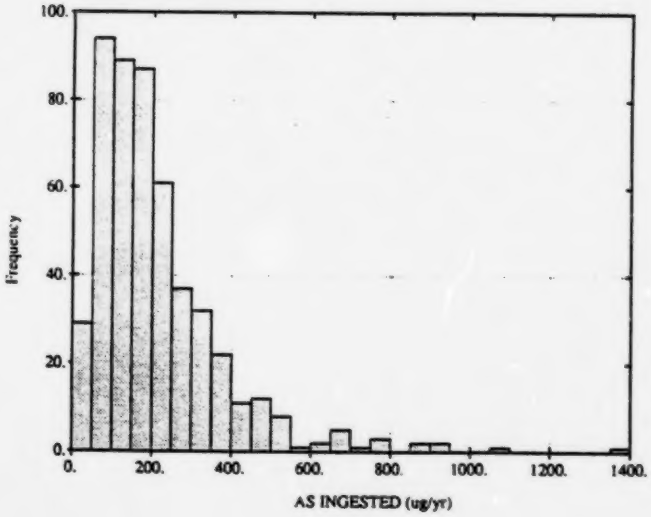

SUMMARY STATISTICS:

MEAN = 211.
STANDARD DEVIATION = 164.
GEOMETRIC MEAN = 164.
GEOMETRIC STANDARD DEVIATION = 2.05
MINIMUM = 20.8
MAXIMUM = 0.135e+04

HISTOGRAM OF ARSENIC CONCENTRATION IN LAKE WATER FOR SCENARIO 2, AT T = 0

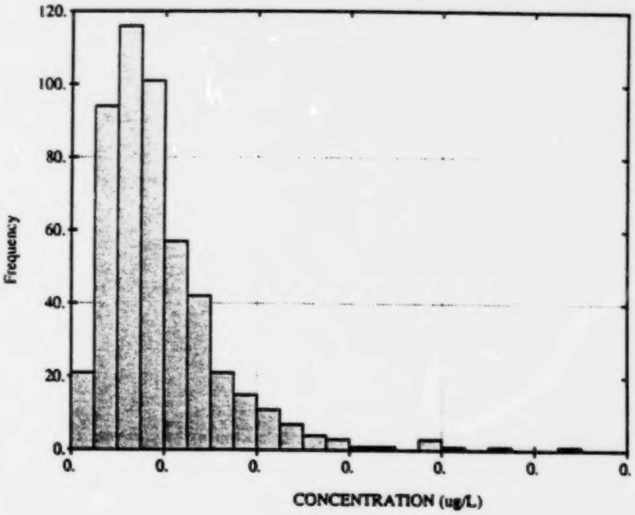

SUMMARY STATISTICS:

MEAN = 0.945e-01
STANDARD DEVIATION = 0.665e-01
GEOMETRIC MEAN = 0.774e-01
GEOMETRIC STANDARD DEVIATION = 1.88
MINIMUM = 0.132e-01
MAXIMUM = 0.534

HISTOGRAM OF ARSENIC CONCENTRATION IN LAKE WATE FOR SCENARIO 2, AT T = 150

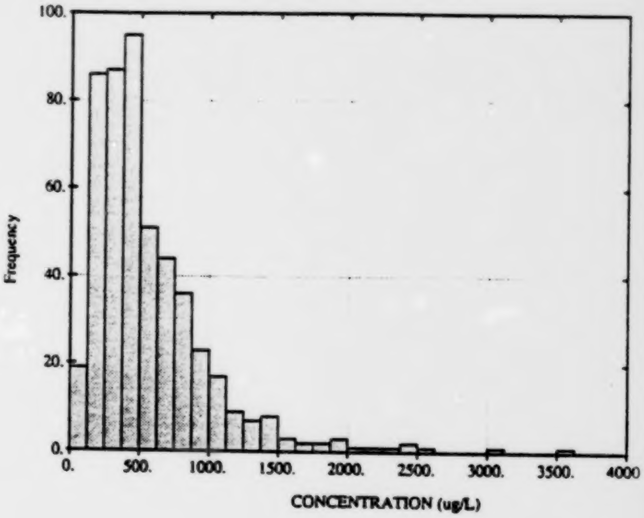

SUMMARY STATISTICS:

MEAN = 565.
STANDARD DEVIATION = 436.
GEOMETRIC MEAN = 443.
GEOMETRIC STANDARD DEVIATION = 2.02
MINIMUM = 56.8
MAXIMUM = 0.356e+04

HISTOGRAM OF ARSENIC CONCENTRATION IN LAKE WATER FOR SCENARIO 2, AT T = 1000

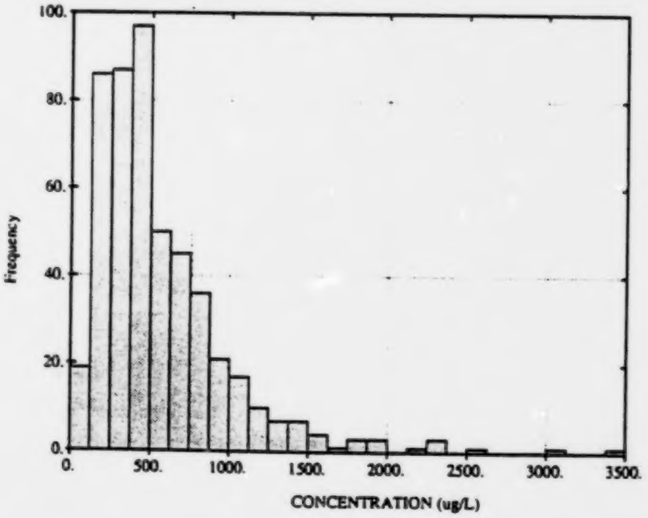

SUMMARY STATISTICS:

MEAN = 562.
STANDARD DEVIATION = 431.
GEOMETRIC MEAN = 442.
GEOMETRIC STANDARD DEVIATION = 2.02
MINIMUM = 56.9
MAXIMUM = 0.349e+04